Mitochondrial ageing in rat brain areas and human fibroblasts

TECHNISCHE UNIVERSITÄT DARMSTADT

Vom Fachbereich Chemie

der Technischen Universität Darmstadt

zur Erlangung des akademischen Grades eines

Doktor rerum naturalis (Dr. rer. nat.)

genehmigte

Dissertation

vorgelegt von

Diplom-Biologin Monika Astrid Frenzel

aus

Königs Wusterhausen

Referent:	Prof. Dr. N.A. Dencher
1. Korreferent:	Prof. Dr. G. Thiel
2. Korreferent:	Prof. Dr. M. Durante
Tag der Einreichung:	1. April 2011
Tag der mündlichen Prüfung:	17. Mai 2011

Darmstadt 2012

D17

Die vorliegende Arbeit wurde unter Leitung von Herrn Prof. Dr. N. A. Dencher in der Zeit vom Oktober 2006 bis Februar 2011 am Clemens-Schöpf-Institut für Organische Chemie und Biochemie, Abteilung Physikalische Biochemie, im Fachbereich Chemie der Technischen Universität Darmstadt angefertigt.

PUBLICATIONS

PARTS OF THIS DOCTORAL THESIS ARE PUBLISHED:

Frenzel M., Rommelspacher H., D. Sugawa M., Dencher N.A. (2010). Ageing alters the supramolecular architecture of OxPhos complexes in rat brain cortex. *Experimental Gerontology* **45**, 563–572.

Wernicke C., Hellmann J., Zieba B., Kuter K., Ossowska K., **Frenzel M.**, Dencher N.A., Rommelspacher H. (2010). 9-Methyl-beta-carboline has restorative effects in an animal model of Parkinson's disease. *Pharmacol Rep*. **62**, 35-53.

Seelert H., Dani D.N., Dante S., Hauss T., Krause F., Schäfer E., **Frenzel M.**, Poetsch A., Rexroth S., Schwassmann H.J., Suhai T., Vonck J., Dencher N.A. (2009) From protons to OXPHOS supercomplexes and Alzheimer's disease: structure-dynamics-function relationships of energy-transducing membranes. *Biochim. Biophys. Acta* **1787**, 657-671.

Dencher N.A., **Frenzel M.**, Reifschneider N.H., Sugawa M., Krause F. (2007). Proteome alterations in rat mitochondria caused by aging. *Ann N Y Acad Sci.* **1100**, 291-298.

NON-REVIEWED PUBLICATIONS:

Frenzel M., Soehn M., Durante M., Fournier C., Ritter S. and Dencher N.A. (2011). Impact of senescence and irradiation on cellular metabolism in human cells. *GSI Sci. Rep. 2010*, in press.

Frenzel M., Durante M., Fournier C., Ritter S., Dencher N.A. (2010). Interplay of irradiation and age on the mitoproteome of human cell cultures. *GSI Sci. Rep. 2009*, 479.

Frenzel M., Dencher N.A., Fournier C., Ritter S., Zahnreich S. (2009). Reactive oxygen species are involved in senescence of human cells independently from irradiation exposure. *GSI Sci. Rep. 2008*, 381.

Zahnreich S., Boukamp P., Colindres M., Dencher N., Durante M., Fournier C., **Frenzel M.**, Krunic D., Ritter S. (2009). Oxidative stress and telomere shortening in normal human fibroblasts after irradiation with X-rays. *GSI Sci. Rep. 2008*, 379.

Colindres M., Fournier C., Ritter S., Zahnreich S., Decker H., Dencher N., **Frenzel M.** (2008). Increase of oxidative stress in normal human fibroblasts after irradiation. *GSI Sci. Rep. 2007*, 356.

MANUSCRIPTS FINISHED OR IN PREPARATION:

Frenzel M., Rommelspacher H., D. Sugawa M., Dencher N.A. (2011). Differential brain ageing quantitated by differential protein profiling of rat mitochondria.

Frenzel M., Fournier C., Melnikova L., Ritter S., Zahnreich S., Dencher N.A. (2011). Long-term effect of X-ray irradiation on the native mitochondrial proteome, ROS generation and physiology in senescent human fibroblasts.

Frenzel M., Fournier C., Melnikova L., Ritter S., Dencher N.A. (2011). Alterations in the mitochondrial proteome of three different human cell lines after X-ray and heavy ion irradiation.

ORAL PRESENTATIONS AT NATIONAL AND INTERNATIONAL SCIENTIFIC CONFERENCES

PHD-workshop 2009/10, Darmstadt, Germany

Title: *Age-dependent changes in mitochondrial protein profile of rat brain*

Heavy Ions in Therapy and Space Symposium, Köln (2009), Germany

Title: *Changes in ROS and mitochondrial proteome during senescence of irradiated human cell lines*

Guest lecture at the Gesellschaft für Schwerionenforschung GSI, Darmstadt (2008), Germany

Title: *Mitochondrial proteome profiling using 2D blue-native/SDS-PAGE*

Symposium "Neuroprotektion von Beta-Carbolinen", Berlin (2008), Germany

Title: *Wirkungen von 9-Methyl-ß-Carbolin auf die Atmungskette einschließlich des Komplex V*

MiMage/LINK-AGE Joint Summer School “Models and Methods in Ageing Research”, Les Diablerets (2007), Switzerland

Title: *Age-dependent alterations in the supramolecular architecture of the oxidative phosphorylation complexes in rat cortex*

3rd Symposium on the Role of Mitochondria in Conserved Mechanisms of Ageing (MiMage), Frankfurt a. M. (2007), Germany

Title: *Age-dependent changes in mitochondrial protein profile and OXPHOS superstructures in rat brain*

17. Jahrestagung der Deutschen Gesellschaft für Alternsforschung, Karlsruhe (2007), Germany

Title: *Comparative studies on age-dependent alterations in the mitochondrial proteome of different brain regions*

POSTER PRESENTATIONS

61. Mosbacher Kolloquium "The Biology of Aging - Mechanisms and Intervention", Mosbach (2010), Germany

Title: *Supramolecular organisation of OxPhos complexes changes during ageing in various regions to a different extent*

11. Jahrestagung der Gesellschaft für Biologische Strahlenforschung (GBS), Tübingen (2008), Germany

Title: *Effect of radiation on the mitochondrial proteome of human cell cultures*

SFRR-Europe Meeting 2008 Berlin, Free radicals and nutrition: Basic mechanisms and clinical application, Berlin (2008), Germany

Title: *The supramolecular organisation of OXPHOS complexes in different rat brain regions changes during ageing*

Joint annual Conference of the Association for General and Applied Microbiology (GBM Tagung), Frankfurt a.M. (2008), Germany

Title: *Age-dependent alterations in the supramolecular organisation of OXPHOS complexes in different brain regions*

Genetics of aging, Annual Conference of the German Genetics Society (GfG), Jena (2007), Germany

Title: *Age-dependent alterations in the supramolecular architecture of the oxidative phosphorylation complexes in rat cortex*

MiMage/LINK-AGE Joint Summer School “Models and Methods in Ageing Research”, Les Diablerets (2007), Switzerland – Poster Awards

Title: *Age-dependent alterations in the supramolecular architecture of the oxidative phosphorylation complexes in rat cortex*

3rd Symposium on the Role of Mitochondria in Conserved Mechanisms of Ageing (MiMage), Frankfurt a.M. (2007), Germany

Title: *Age-dependent changes in mitochondrial protein profile and OXPHOS superstructures in rat brain*

ACKNOWLEDGEMENT OF SCIENTIFIC COLLABORATIONS

I am grateful to the team of the Biophysik group at the "Gesellschaft für Schwerionenforschung" (GSI, Darmstadt, Germany) for their help during my experiments in providing me all facilities for cell culture and irradiation. In particular, I would like to express my graduate to:

Prof. Dr. Marco Durante (head of the department) for giving me the opportunity to work in his group at GSI and for all discussions about my thesis;

Dr. Claudia Fournier, helping me in planning my irradiation experiments, analysis of cell morphology and data discussion;

Dr. Sylvia Ritter for her support in analyzing the apoptotic level and data interpretation;

Dr. Sebastian Zahnreich for performing ROS measurements via FACS;

Larisa Melnikova (Institute JINR, Dubna, Russia) for determination of chromosomal aberrations.

Additionally, I kindly thank Regina Hill for isolation of mitochondria from rat brain areas and for cultivation of HEK-(h)DAT cells.

Furthermore, I am thankful to Prof. Dr. Peter Friedl for his permission of using the cell culture facilities in his lab and to Anke Imrich for her help in the cultivation of BHK21 cells.

The experiments at the Institut Laue-Langevin were enabled and locally supported by Judith Peters (ILL), Joseph Zaccai (ILL), Marion Jasnin (ILL), Dimitrios Skoufias (ILL) and Francoise Lacroix (ILL). Many thanks to Thomas Hauss (Helmholtz-Zentrum Berlin für Materialien und Energie GmbH) for helping me during the second experiment at the ILL and for corrections of my thesis (chapters 1.2.2, 2.7.3 and 4.5) and the physical background included.

Establishment of the OxyBlot assay for analysis of protein carbonylation was done by Tetyana Syzonenko (Forschungspraktikum) and Cathrin Beyer (Diploma thesis), and determination of cellular ATP concentration by Sonja Wendenburg (Bachelor thesis), Beatrice Knab (Forschungspraktikum).

I would like to thank Michaela Söhn for her help during a cell culture experiment and cellular ATP meassurements.

The work was supported by the European consortium, MiMage: ''Role of Mitochondria in Conserved Mechanisms of Ageing", EC FP6 Contact No. LSHM-CT-2004-512020 to NAD, by the German Federal Ministry of Education grant 02S8497 "Genetische Wirkung dicht ionisierender Strahlung" and grant 0315584D "GerontoMitoSys".

DANKSAGUNG

Vielen Dank, Herr Prof. Dr. Norbert A. Dencher, für mittlerweile fünf Jahre wissenschaftliche Zusammenarbeit. Ich habe Ihr aktives Interesse und Ihre stete Diskussionsbereitschaft und Unterstützung immer zu schätzen gewusst. Ihr Vertrauen in meine Arbeit und deren Ergebnisse hat mich immer wieder motiviert.

Weiterhin danke ich Herrn Prof. Dr. Gerhard Thiel für die Übernahme des Korreferats nicht nur für diese Dissertation sondern bereits auch für meine Diplomarbeit.

I am grateful to Prof. Dr. Marco Durante for his kindness, scientific support and his Italian style.

Mein besonderer Dank gilt der gesamten Arbeitsgruppe der Physikalischen Biochemie. Durch Euch wurde jeder Stress und jedes Misslingen im Laboralltag abgefedert. Ich habe eine wundervolle Zeit mit Euch verbracht, die mir sehr fehlen wird. Liebe Eva Schäfer und Sandra Thilmany, lieber Nicolas Heidrich - ein besseres Team als uns kann ich mir nicht vorstellen. Vielen Dank Frau Elisabeth Trapp und Frau Christine Schröpfer, Ihr bildet für mich das Herz der Arbeitsgruppe. Herr Dr. Holger Seelert ist stets mit Rat und Tat zur Stelle, wo immer Hilfe gebraucht wird, und fasziniert durch sein enormes Wissen. Ihr seid mir alle ans Herz gewachsen.

Danke auch an Michaela Söhn, Maria Saager, Manuela Kratochwil, Michael Muschol, Michaela Fröhlich, Gerda Zeising und an alle Diplomanden, Doktoranden, Gastwissenschaftler, Praktikanten und Mitarbeiter der Abteilung, die ich jetzt nicht im Einzelnen genannt habe.

Vielen Dank der Arbeitsgruppe der Biophysik an der GSI für die Hilfe bei meinen Zellkulturexperimenten und während den Strahlzeiten. Mein besonderer Dank gilt dabei Claudia Fournier und Sylvia Ritter für Ihre Unterstützung bei meinen Experimenten in Form von Planung und angeregter Diskussion und Sebastian Zahnreich für seine Unterstützung im Labor.

Unsere gemeinsame Zeit und Zusammenarbeit in Grenoble hat mir sehr viel Spaß gemacht, danke dafür lieber Dr. Thomas Hauß.

Liebe Nataliya Karpenko, Deine Aufmerksamkeit und Freundschaft fängt mich stets auf, wenn mal wieder alles schief läuft.

Thank you Diana Pignalosa for a wonderful time together at GSI. I already miss our days in the small office.

Dear Mira Maalouf our friendship is unlimited despite all distances.

Mein größter Dank gilt meiner Familie, die stets für mich da ist, mich wo es geht unterstützte und besonders in anstrengenden Phasen viel Verständnis für meinen Stress zeigte, mich tröstete und motivierte. Danke für Eure grenzenlose Geduld.

SUMMARY

The aim of this doctoral thesis was, to study the mitochondrial proteome, especially of the oxidative phosphorylation machinery, and its alteration during ageing. Data obtained from protein profiling of rat brain cortex, striatum and hippocampus of two different age states were compared to that of human fibroblasts undergoing senescence and after exposure to X-rays and heavy ions. The focus laid on quantitative analysis of individual Oxidative Phosphorylation (OxPhos) complexes, respiratory chain supercomplexes and ATP synthase oligomers as well as other non-OxPhos proteins that might be involved in the process of ageing, senescence or irradiation response. The most important point was to disclose overall mechanisms (*in vivo* and *in vitro*) to reveal the mostly unknown basic molecular processes involved in both ageing and senescence.

The combination of two-dimensional Blue-native/SDS-PAGE for protein separation, subsequent gel-staining with the fluorescent protein-dye SYPRO Ruby and quantitative analysis of protein spot intensities by 2D-gel image analyzing software was used as powerful tool to analyze not only age-dependent changes in the abundance of individual proteins but also of protein-protein-interactions. In the first step after gentle detergent-solubilisation, single proteins and protein-complexes (homo- and heterooligomers) migrated according to their molecular mass in BN-gels, preserving the structure, activity and all relevant protein-protein interactions. Protein-activity was determined by performing in-gel activity assays. Subsequently, proteins, protein-complexes and supercomplexes were dissociated into their specific subunits after denaturation in the second dimension SDS-PAGE. It was demonstrated that protein quantitation can be performed in both gel dimensions, but the 1D Blue-native gel dimension enables much less resolution power than the second dimension SDS gel.

Essential prerequisites for high quality protein profiling were ascertained. (1) Isolation of mitochondria should be carried out immediately upon dissection of the tissue. Freezing of the tissue (also in liquid nitrogen) reduce the sample quality, visible by a 3-fold reduced protein yield after mitochondrial isolation and reduced solubilization efficiency. (2) Sample storage should take place after mitochondrial isolation. Increased dissociation of protein-protein-interactions, quantitated by an increase of individual complex I, was found in brain tissue after storage at -80°C, but not in frozen mitochondrial fractions. (3) The application of crude mitochondrial fractions not subjected to further purification, in order to preserve also fragile and damaged mitochondria, and of the antioxidant cocktail SCAVEGR, protecting proteins e.g. for oxidative modifications during preparation, are fundamental to obtain samples of high quality. (4) Gentle solubilisation conditions using digitonin as detergent at defined detergent/protein-ratios allow quantitative extraction. In following these four conditions, data were obtained allowing quantitative comparison of protein profiles between e.g. different individuals in one age-group on the one hand and individuals of different age, on the other hand.

In the current investigation it was not only demonstrated that brain mitochondria isolated from young and aged rats show quantitatively different protein pattern but also that ageing occurs

distinct in cortex, striatum and hippocampus. The latter displaying the largest alterations. An observation common for the mitochondria of all three brain areas was that more than 95% of complex I was present in supercomplexes with complex III_2 (I_1III_2) or/and complex III_2 and IV_{1-X} (one to several copies of complex IV). It was emphasized that supercomplex formation follows distinct stoichiometry and optimizes the activity of complexes involved (Frenzel et al., 2010b; Schäfer et al., 2006). The specific activity of complex I increased when assembled to complex III_2 and even more in a supercomplex containing complex III_2 and additionally complex IV ($I_1III_2IV_{1-3}$). The largest specific activity of complex I was found in $I_1III_2IV_1$. An age-associated decrease in supercomplex abundances was always accompanied by an increased proportion of this high active supercomplex $I_1III_2IV_1$ in relation to others. An important new observation was, that the specific activity for each supercomplex was similar in young and aged animals

According to alterations of respiratory chain complexes and supercomplexes during ageing, hippocampus has an exceptional position compared to cortex and striatum. In cortex there was an overall decline in protein abundances of individual and supercomplexes (except III_2IV_1) up to 2.4-fold, while in striatum only minor changes occurred. In contrast, in hippocampus an age-associated pronounced abundance increase of up to 8.3-fold was observed. Although this increase is remarkable, the total protein amount of respiratory chain complexes in hippocampal and striatal mitochondria was smaller than that in cortex especially in young rats. The proportion of respiratory chain complexes assembled in supercomplexes was the highest in cortex.

Also the amount of the ATP synthase (V_1-V_4) was decreased in cortex, unchanged in striatum and increased in hippocampus during ageing. The magnitude of increase or decrease was moderate compared to that of complexes I-IV and was attributed solely to alterations of the complex V monomer (V_1). The absolute amount of ATP synthase oligomers (V_2-V_4) was similar in all three brain areas and unaffected by age. Although changes in the total abundance of the ATP synthase were divergent, an overall age-associated pronounced increase (1.5-4.8-fold) of the unassembled, water soluble F_1-part was found in all three brain areas.

In hippocampus, the pronounced age-associated increase of respiratory chain complexes was accompanied by an increase of the mitochondrial aconitase 2, indicating an enhanced cellular energy level in this brain area in aged animals, possibly to provide the ATP needed by the Na^+/K^+-ATP synthase that also increased in abundance during ageing and utilize about 70% of the cellular energy.

In cortex and striatum the amount of the aconitase was unchanged while that of Na^+/K^+-ATP synthase decreased during ageing, in line with the amount of the mitochondrial heat shock protein 60 (HSP60) that is belonging to the groups of chaperones. The latter remained unchanged in hippocampus.

Contradictory to the “Free Radical Theory of Ageing” postulated by Harman (1956), mitochondrial proteins in rat cortex exhibit less oxidative modifications than those of young rats.

Data obtained from rats (*in vivo* experiments) were compared to that of human fibroblasts (*in vitro* long-term lasting experiments ~240 days; NHDF, WI38, AG1522D), to unravel basic molecular processes involved in both ageing and senescence. It was demonstrated that during cellular senescence the mitochondrial proteome was comparable to that of cortex mitochondria. Comparing young cells and cells after several cell cycles, an overall abundance decline of OxPhos complexes (complex I, III_2, supercomplexes and ATP synthase) and HSP60 occurred during cell ageing. The amount of mitofilin (important for fusion and fission) decreased also while that of prohibitin (cell proliferation and cristae formation) remained constant and that of superoxide dismutase 1 (SOD1) increased. Ageing of cells in culture was additionally accompanied by an increase of chromosomal aberrations and the number of aberrations per cell as well as the level of apoptotic cells and post-mitotic fibroblasts.

Irradiation of normal human dermal fibroblasts with X-rays (8 Gy) resulted in comparable but decelerated senescence-associated alterations of the mitochondrial proteome in progeny of irradiated cells after recovery from irradiation induced chromosomal damages. In contrast to non-irradiated cells, in progeny of irradiated cells (NHDF) a pronounced abundance increase of complex I, supercomplexes and ATP synthase occurred before the age-related decline. The amounts of complex III_2, HSP60, mitofilin and prohibitin were similar at the beginning and at the end of the experiment. Only the abundance of SOD1 increased. The level of chromosomal aberrations, apoptosis and post-mitotic cells increased immediately after irradiation, returned thereafter to the level of progeny of non-irradiated cells and increased also during cellular senescence, but more moderate.

The level of reactive oxygen species (ROS) increased during cellular senescence in both, progeny of non-irradiated and irradiated cells, independent from X-ray exposure, although ROS increased transiently directly upon irradiation (Zahnreich, 2011). No changes in the proportion of different ROS species were observed.

Alterations in the total amount of ATP synthase were correlated to the cellular ATP level. Although in progeny of non-irradiated cells a decrease in the abundance of complex V was observed, the cellular amount of ATP was constant at about 4×10^{-15} mol/cell. After X-ray irradiation, the cellular ATP level was significantly increased at day 15 and 28, decreased thereafter at day 43 first until the ATP-level in non-irradiated cells and later on even there under at day 158.

The decelerated entering in cellular senescence of progeny of irradiated cells may be attributed to a mechanism called hormesis possibly induced by the acute irradiation and/or the irradiation induced increase in ROS.

It was demonstrated the first time that in human fibroblasts (of different origin) two oligomeric states (a heptamer and a smaller form) of homooligomeric mitochondrial HSP60 are present. A shift in the ratio of the two oligomeric states towards the smaller form occurred after irradiation, cellular senescence and after treatment with a Parkinson's disease inducing toxin, and could be correlated with the appearance of an increased level of apoptosis and cell death.

ZUSAMMENFASSUNG

Das Ziel dieser Arbeit war es, das mitochondriale Proteom insbesondere im Hinblick auf die Oxidative Phosphorylierung (OxPhos) und seine Veränderungen im Alter zu untersuchen. Speziell wurden im ersten Schritt drei verschiedene Areale (Cortex, Striatum und Hippocampus) aus Rattenhirn zweier Altersstufen verglichen. Erhaltene Ergebnisse wurden im zweiten Schritt in Bezug gesetzt zu Veränderungen des mitochondrialen Proteoms humaner Fibroblasten beim Eintritt in die Seneszenz und nach Bestrahlung mit Röntgenstrahlen und schweren Ionen. Der Schwerpunkt lag dabei auf der quantitativen Analyse der Atmungskettenkomplexe und ihrer Superkomplexe, sowie dem Auftreten von ATP-Synthase Oligomeren und Nicht-OxPhos-Proteinen, die möglicherweise am Altern, der Seneszenz oder der zellulären Reaktion auf Bestrahlung beteiligt sind. Generelle Mechanismen, die Aufschluss sowohl über den zurzeit noch weitestgehend unverstandenen Prozess des Alterns sowie der zellulären Seneszenz geben, sollten erforscht werden.

Mittels zweidimensionaler Blau-nativer/SDS-Polyacrylamidgelelektrophorese, anschließender Visualisierung der Proteine im Gel mit Hilfe des Fluoreszenzfarbstoffs SYPRO Ruby und abschließender quantitativer Analyse der Proteinfärbung konnten alternsbedingte Veränderungen der Menge einzelner Proteine sowie von Protein-Protein-Wechselwirkungen innerhalb der Mitochondrien untersucht werden. Dazu wurden die Proteine des mitochondrialen Proteoms zunächst mit Hilfe des milden Detergens Digitonin aus den Membranen solubilisiert. Die auf diese Weise nativ extrahierten Proteine und Proteinkomplexe (Hetero- und Homooligomer) wurden mittels Blau-nativer Polyacrylamidgelelektrophorese (BN-PAGE) entsprechend ihrer molekularen Masse aufgetrennt, wobei ihre Struktur, Aktivität und alle relevanten Protein-Protein-Interaktionen erhalten blieben. Die Aktivität der Enzyme wurde über In-Gel-Aktivitätstests nachgewiesen. Die anschließende, denaturierende Tricine-SDS-PAGE diente dazu, Proteine, Proteinkomplexe und Superkomplexe in einer zweiten Dimension in ihre Untereinheiten zu zerlegen. Es wurde gezeigt, dass die Proteinquantifizierung sowohl in der ersten als auch in der zweiten Dimension erfolgen kann, wobei sich die zweite Dimension durch eine bessere Auflösung auszeichnet.

Essentielle Grundvoraussetzungen für die Probenaufbereitung zur späteren hochqualitative Analyse des mitochondrialen Proteoms wurden ermittelt: (1) Die Isolierung der Mitochondrien sollte direkt im Anschluss an die Entnahme der Gewebe erfolgen, da selbst kurzzeitiges Einfrieren die Probenqualität reduziert, was sich in einer 3-fach geringeren Proteinausbeute und verminderten Solubilisierungseffizienz zeigt. (2) Zur längeren Lagerung bei -80°C sollten die Mitochondrien zuvor isoliert werden, da in über einen längeren Zeitraum eingefrorenen Geweben vermehrte Dissoziation von Superkomplexen beobachtet wurde. (3) Die Verwendung des Antioxidantien-Cocktails SCAVEGR schützt die Probe vor oxidativen Schäden während der Isolierung und der Verzicht von weiteren Aufreinigungsschritten verhindert den Verlust defekter oder die Schädigung fragiler Mitochondrien. (4) Milde Solubilisierungsbedingungen mit Digitonin als Detergens bei bestimmtem Detergens-zu-Protein-Verhältnis erlauben quantitative Proteinextraktionen. Unter Berücksichtigung dieser

Bedingungen konnte ein quantitativer Vergleich der Proteinmuster verschiedener Individuen innerhalb einer experimentellen Gruppe und zweier Altersstufen erfolgen.

Im Rahmen dieser Arbeit konnte nicht nur nachgewiesen werden, dass sich das mitochondriale Proteom im Rattenhirn im Laufe des Alterns verändert, sondern zusätzlich, dass Cortex, Striatum und insbesondere Hippocampus unterschiedliche alternsbedingte Veränderungen zeigen. In allen drei Hirnarealen lagen jedoch 95% der Gesamtmenge von Komplex I in Form von Superkomplexen (I_1III_2 und $I_1III_2IV_{1-X}$) vor, wobei diese spezifische Zusammensetzungen aufweisen und die Aktivität der darin beteiligten Komplexe optimieren (Frenzel et al., 2010b; Schäfer et al., 2006). Eine Erhöhung der spezifischen Aktivität von Komplex I zeigte sich nach dem Zusammenschluss mit Komplex III_2 und in noch stärkerem Maße nach zusätzlicher Wechselwirkung mit Komplex IV ($I_1III_2IV_{1-3}$). Die größte Aktivität von Komplex I wurde im Superkomplex $I_1III_2IV_1$ gefunden. Ein alternsbedingter Abfall der Menge an Superkomplexen war stets assoziiert mit einem relativen Anstieg dieses aktiveren Komplexes $I_1III_2IV_1$ im Verhältnis zu den anderen. Eine wichtige Erkenntnis war, dass in jungen und alten Tieren die spezifische Aktivität von Komplex I in den verschiedenen Superkomplexen identisch war.

Alternsbedingte Veränderungen der Atmungskettenkomplexe und –superkomplexe im Hippocampus unterscheiden sich außerordentlich von denen im Cortex und Striatum. Während im Cortex ein allgemeiner, bis zu 2,4-facher Abfall der Proteinmengen von individuellen Komplexen und Superkomplexen (mit Ausnahme von III_2IV_1) erfolgte, wurden im Striatum nur geringe Änderungen beobachtet. Im Gegensatz dazu fand im Hippocampus ein bis zu 8,3-facher alternsbedingter Anstieg der Proteinmengen statt. Trotz dieses extremen Anstiegs war die Gesamtmenge an Atmungskettenkomplexen besonders bei jungen Tieren im Hippocampus und im Striatum kleiner als im Cortex. In Mitochondrien aus dem Cortex lag die größte Menge an Superkomplexen im Verhältnis zu individuellen Komplexen vor.

Die Menge der ATP-Synthase (V_1-V_4) nahm im Cortex im Alter ab, verblieb unverändert im Striatum und stieg im Hippocampus an. Die relativ moderaten Veränderungen der Gesamtmenge konnten dabei der Ab- oder Zunahme der Menge an Komplex V Monomeren zugeschrieben werden. Die Menge der Oligomere (V_1-V_4) war in den drei verschiedenen Hirnarealen gleich und unverändert im Alter. Unabhängig von alternsbedingten, quantitativen Veränderungen der Menge intakter ATP-Synthase stieg in allen Hirnarealen die Menge an freiem, wasserlöslichem F_1-Teil (1,5 - 4,8-fach) an.

Die im Hippocampus beobachtete Mengenzunahme der Atmungskettenkomplexe während des Alterns war begleitet von einer Zunahme der mitochondrialen Aconitase 2, was ein Hinweis auf ein verstärkt vorliegendes zelluläres Energieniveau ist. Es wird angenommen, dass dieses benötigt wird, um die in den Mitochondrien alter Tiere ebenfalls vermehrt vorhandene Na^+/K^+-ATP-Synthase (verbraucht 70% der zellulären Energie in Nervenzellen) mit dem notwenigen ATP zu versorgen.

Die Menge der Aconitase war im Cortex und im Striatum unverändert, während die der Na^+/K^+-ATP-Synthase sich im Laufe des Alterns verringerte, genau wie die des

Hitzeschockproteins HSP60 (Protein der Chaperon-Familie). Im Hippocampus wurden keine Veränderungen des Auftretens von HSP60 beobachtet.

Entgegen der „Freie-Radikale-Theorie des Alterns“, aufgestellt von Harman (1956), wiesen die mitochondrialen Proteine im Cortex älterer Tieren weniger oxidative Modifikationen auf als die von jungen.

Um fundamentale, molekulare Mechanismen allgemeingültig für das Altern von Zellen in Geweben (*in vivo*) und Zellkultur (*in vitro*) aufzudecken, wurden die Daten der mitochondrialen Proteomanalyse der Ratten mit denen von humanen Fibroblasten (NHDF, WI38, AG1522D) verglichen, die sich bis zu 240 Tage in Kultur befanden. Es konnte gezeigt werden, dass das mitochondriale Proteom während der Alterung von Zellkulturen (Seneszenz) vergleichbare Veränderungen aufweist wie im Cortex von Ratten. So wurde ein Absinken der Menge an OxPhos Komplexen (Komplex I, III_2, Superkomplexen und der ATP-Synthase) sowie HSP60 mit fortlaufender Kultivierungsdauer detektiert. Die Menge an Mitofilin (wichtig für Fusion und Fisson von Mitochondrien) fällt ebenso ab, während die von Prohibitin (beteiligt an Zellproliferation und Cristae-Bildung) unverändert bleibt und die der Superoxiddismutase 1 (SOD1) ansteigt. Zudem ist bei zunehmendem Alter der Zellkulturen ein vermehrtes Auftreten chromosomaler Schäden und eine erhöhte Anzahl an Aberrationen pro Zellen sowie ein Anstieg von apoptotischen Zellen und postmitotischen Fibroblasten beobachtet worden.

Nachkommen humaner Fibroblasten zeigten nach Bestrahlung mit Röntgenstrahlen (8 Gy) und dem Überwinden damit verbundener chromosomaler Schäden vergleichbare, aber verzögerte Veränderungen des mitochondrialen Proteoms aufgrund von Seneszenz. Im Gegensatz zu nicht bestrahlten Zellen stieg in Nachkommen bestrahlter NHDF Zellen die Menge an Komplex I, Superkomplexen und der ATP-Synthase an, bevor diese alternsbedingt ein paar Tage später abfiel. Die Anzahl an Komplex III_2, HSP60, Mitofilin und Prohibitin war am Anfang des Experiments vergleichbar mit dem am Ende. Nur die Menge der SOD1 nahm zu. Nach Bestrahlung traten vermehrt chromosomale Schäden, Apoptose und postmitotische Zellen auf, deren Anzahl jedoch nach einigen Tagen auf das Niveau nicht bestrahlter Zellen zurück fiel und erst im Alter im moderaten Ausmaß aufgrund von zellulärer Alterung wieder zunahm.

Das Niveau reaktiver Sauerstoffspezies (ROS) stieg sowohl in Nachkommen nicht bestrahlter sowie bestrahlter Zellen im Laufe der zellulären Alterung an. Dieser Anstieg erfolgte jedoch unabhängig von zuvor durchgeführter Bestrahlung, obwohl direkt im Anschluss an Bestrahlungen bereits erhöhte ROS-Niveau beobachtet wurden (Zahnreich, 2011). Es konnte zudem keine Zu- oder Abnahme einer bestimmten ROS-Spezies beobachtet werden.

Veränderungen der Gesamtmenge der ATP-Synthase wurden in Beziehung gesetzt zur tatsächlichen zellulären ATP-Konzentration. Obwohl in nicht-bestrahlten Zellen ein Absinken der Menge von Komplex V beobachtet wurde, waren konstant 4×10^{-15} mol ATP / Zelle vorhanden. Nach Bestrahlung verdoppelte sich die Menge an zellulärem ATP (Tag 15 und 28), fiel am Tag 43 zunächst zurück auf das Niveau nicht-bestrahlter Zellen und noch weiter

darunter (ab Tag 158), bis sie am Tag 193 nur noch 1/3 der Konzentration in nicht bestrahlten Zellen entsprach.

Das verzögerte Eintreten in die zelluläre Seneszenz in Nachkommen bestrahlter Zellen ist möglicher Weise auf einen Prozess zurückzuführen, der als Hormesis bezeichnet wird. Dieser wiederum könnte Aufgrund der einmaligen Behandlung mit Röntgenstrahlen (akute Dosis von 8 Gy) und/oder dem daraus resultierenden Anstieg an ROS induziert worden sein.

Es konnte zum ersten Mal gezeigt werden, dass in verschiedenen humanen Fibroblasten zwei oligomere Formen (Heptamer und eine kleinere Form) des Homooligomers HSP60 vorliegen. Eine Verschiebung des Verhältnisses der beiden Formen zueinander zum kleineren Oligomer hin wurde nach Bestrahlung, beim Eintreten in die Seneszenz und nach Behandlung mit einem Toxin, das Parkinson auslöst, beobachtet und mit dem Auftreten von erhöhten Mengen apoptotischer Zellen sowie Zelltod in Verbindung gebracht.

Table of contents

1 Introduction

1.1 The mechanism of biological ageing

To date, there is no universally accepted definition of ageing. However, it is postulated that ageing is a progressive, non-reversal process characterized by increased physiological dysfunction causing failure of body/organelle functions and at least death. Currently, there are more than 300 theories of ageing (Vina et al., 2007) and many possible key mechanisms are discussed. But it is questionable if the cause of ageing can be ascribed to a single cause such as accumulation of DNA damage, telomere shortening, and reduced repair or less active defense systems due to reduced enzyme activities and maintenance. It is more likely that ageing is a highly complex process combining all so far discussed damages and alterations, which again are affecting and enhancing themselves. Although there are a lot of factors being involved in ageing are missing, it is possible to form a preliminary solution to the problem, helping to develop new experiments that will increase our understanding of ageing (Borras et al., 2010).

One of the most prominent theories to explain ageing is the “Mitochondrial Theory of Ageing” in combination with the “Free Radical Theory” (Harman, 1956). According to this theory, somatic mutation of mtDNA causes respiratory chain dysfunction leading to the production of oxygen radicals that are inducing damages in macromolecules (Jacobs, 2003). In turn, this is proposed to result in the accumulation of mtDNA mutations. All factors together are leading to tissue dysfunction and degeneration. The mitochondrial theory of ageing has been recently tested in various laboratories and there are many published papers in support of this theory (Vina et al. (2007) and references herein).

The rate of production of oxidants by mitochondria is rather difficult to study. Moreover, although the general agreement is that the ROS level increases with age (as demonstrated also in this study), some laboratories are unable to confirm this fact. Consequently, studying biomarkers of oxidative stress appears more adequate than studying the reactive oxygen species (ROS) production itself.

Malfunction of mitochondria are not representing the final cause for ageing but mitochondria are the cellular organelle being involved the most (Kwong and Sohal, 2000). The study of alterations in the mitochondrial proteome may help to understand age-associated phenomena as it is the case in some age-related diseases. The molecular process of ageing might differ not only between evolutionary distant species but even in the same organism. Especially tissues consisting mostly of post-mitotic cells like brain, muscle or heart are in the focus of ageing studies since age-associated alterations appear more pronounced herein (Kwong and Sohal, 2000).

1.1.1 Mitochondria and their role in ageing and senescence

Mitochondria are double-membrane organelles, playing a critical role in cell signaling, apoptosis, cellular differentiation, cell cycle control, cell growth (McBride et al., 2006) and maintaining the cellular energy status (Gunter et al., 2000). The number of mitochondria varies from only one single (Hecker et al., 1973) up to 1000-2000 per cell dependent on origin (Alberts et al., 1994). In contrast to former opinion, mitochondria show their typical bacterial-like shape only during cell proliferation when being allocated between the daughter cells. The main time of the cell cycle they vary in their shape (e.g. size, elongation, branching) and are forming syncytia, a network out of many mitochondria coalesce controlled via mechanisms called fusion and fission (Bereiter-Hahn and Voth, 1994).

The inner mitochondrial membrane is constituted up to 50% (w/w) of integral membrane proteins, 25% (w/w) of membrane associated peripheral proteins and 25% (w/w) of lipids (Nicholls and Ferguson, 1992). This lipid composition differs compared to other predominant membranes. In mammals, the main component is the phospholipid phosphatidylcholine [27-45% (w/w)]. Compared to other membranes, the amount of phosphatidylethanolamine [(29-39% (w/w)] is increased while that of phosphatidylinositole [2-7% (w/w)] and phosphatidylserine [1% (w/w)] is less. The proportion of cardiolipin (20% of the total lipids) in relation to sterols (cholesterol) and sphingolipids is relatively high (Daum, 1985). Cardiolipin was found to be essential for OxPhos complexes and supercomplex formation (Toescu et al., 2000). Changes in membrane properties, e.g. during the ageing process, may affect the enzyme activity of membrane proteins (Hoch, 1992). Not only may the composition of lipids change but also the type of fatty acid residues. An increase of unsaturated fatty acids e.g. is leading to proton leak across the membrane and higher peroxydative damages of membrane lipids and results in apoptosis (Haripriya et al., 2004; Mattson, 1998).

Contrary to other organelles, mitochondria contain their own circular and double-stranded DNA having no introns that constitutes 0.5-1% of the total DNA in human cells (DiMauro, 2004; Nugent et al., 2010; Taanman, 1999). The mitochondrial DNA is organized in protein-DNA complexes so called mitochondrial nucleoids (mt-nucleoids, in analogy to the bacterial chromosome) (Chen and Butow, 2005; Kuroiwa, 1982; Prachar, 2010). In mammals, mt-nucleoids have a diameter of 0.068 µm. These nucleoids contain in vertebrates typically 5-7 units of the circular mitochondrial genome (Prachar, 2010), which is 16.5 kb long and are associated to the inner mitochondrial membrane (DiMauro, 2004).

The mutation rate in mtDNA is 10-20 times higher compared to nuclear DNA (nDNA), presumably due to its physical closeness to the Oxidative Phosphorylation machinery (OxPhos) embedded in the inner mitochondrial membrane and therewith high level of reactive oxygen species (ROS) produced mainly via the respiratory chain (Ozawa, 1997). Although most proteins of the mitochondrial respiratory chain (80) are encoded by the nDNA, 13 are encoded by mtDNA. Thus, damages of both, mtDNA and nDNA may affect the OxPhos machinery. Hence respiration is the only metabolic pathways under dual control (DiMauro, 2004). The mtDNA harbors 37 genes, i.e. 13 subunits of the respiratory chain

(Fig. 1-1), 2 rRNAs and 22 tRNAs. Damages of the mtDNA affect the cellular maintenance and survival (Nugent et al., 2010).

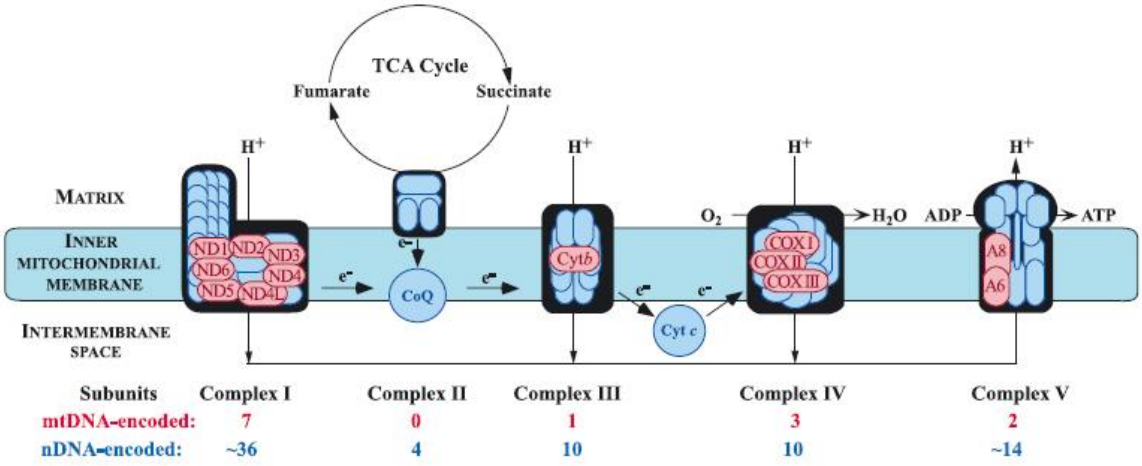

Fig. 1-1. The OxPhos complexes with mtDNA-encoded subunits indicated in red and nDNA-encoded subunits in blue. Complex II is the only complex solely encoded by the nDNA. Electrons (e^-) flow along the respiratory chain and protons (H^+) are translocation from the matrix into the intermembrane space via complexes I, III_2, and IV. The proton gradient is used by complex V to produce ATP. (DiMauro, 2004)

At the respiratory chain, reducing equivalents as $NADH/H^+$ and $FADH_2$, provided by the citric acid cycle, are oxidized by complex I and II, respectively, and respective electrons transferred via the respiratory chain complexes and mobile small electron carriers like coenzym Q (CoQ) and cytochrome c (Cyt c) to the oxygen reduction at complex IV (Fig. 1-1). During this transport protons are translocated across complex I, III_2 and IV from the matrix into the intermembrane space. Free energy thus captured is subsequently used to drive a variety of cellular processes, most prominently the ATP synthesis by the ATP synthase (complex V of OxPhos complexes) (Siegbahn and Blomberg, 2008). The proton gradient (ΔpH, concentration difference over the membrane) and the membrane potential (Δψ) are forming together the proton motive force (Δ*p*) essential for ATP production by the ATP synthase (Nicholls, 2003).

By the OxPhos machinery 90% of the cellular oxygen is consume (Karthikeyan and Resnick, 2005) and ATP generated. The electron transport chain is quite efficient but a small proportion of electrons reduce oxygen before reaching complex IV, leading to the formation of superoxide radical anions. Superoxide radicals are highly reactive and increasing the yield of reactive oxygen (ROS) species [0.2% of the consumed oxygen in mitochondria (Boveris et al., 1972)]. In mitochondria ~90% of the total cellular ROS is produced mostly by respiration (Kim et al., 2006). The intracellular generation of ROS is an inevitable (physiologically important) process (Skulachev, 1996). Mitochondria, which harbor the bulk of oxidative pathways, are packed with various redox-carriers that can potentially leak single electrons to oxygen and convert it into superoxide anion radicals, a progenitor ROS. The majority of ROS are produced at complex III_2 and to a smaller extent at complex I (Andreyev et al., 2005; Dykens, 1994). In fact the source of oxidative stress is not the ROS generation but an imbalance of ROS production and antioxidant defense (Andreyev et al., 2005). To protect

mitochondrial DNA, lipids or proteins from oxidative damages, mitochondria possess numerous antioxidant systems. Nevertheless, mitochondria are the major source and therefore also the major target of ROS (Aquilano et al., 2006).

The main demand of ATP is generated via the OxPhos machinery (up to the body weight per day). Mitochondrial disorders are the reason behind several age-related diseases as Parkinson's or Alzheimer's. Age-associated alterations of the mitochondrial proteome, especially of the OxPhos machinery, have been reported previously for numerous organisms and tissues from e.g. yeast/fungi (Pan and Shadel, 2009), worms/nematodes (Brys et al., 2010), fly/insects (Le Pécheur et al., 2009) and rat and humans (mammals) [(Colindres et al., 2008; Frenzel et al., 2010b; Gómez et al., 2009; Lombardi et al., 2009) and references cited therein]. There are abundance-changes of life sustaining proteins such as ATP synthase, individual respiratory chain complexes, and heat shock proteins as well as changes in protein-protein-interactions like in the assembly of individual complex I, III_2 and IV in respiratory chain supercomplexes or ATP synthase oligomers. It has been demonstrated by Schäfer et al. (2006) that the formation of supercomplexes is increasing the specific enzyme activities of complexes involved and support their assembly and stability. Schäfer et al. (2007) also showed that supercomplex formation is not random as postulated by Hackenbrock et al. (1986) but follows specific stoichiometry that varies in composition between different organisms. They have been found the first time in bacteria (Berry and Trumpower, 1985) and later on in yeast and mammals (Schägger and Pfeiffer, 2000).

The mitochondrial OxPhos machinery can be affected by numerous toxins, as e.g. 1-methyl-4-phenylpyridinium (MPP^+), directly inhibiting specific enzymes of the respiratory chain (Wernicke et al., 2010). Mitochondria are involved in cell death due to their pro-apoptotic role (Budd and Nicholls, 1998) that is e.g. induced by decreased ATP-level (Choi, 1996; Nicholls, 2003), and numerous catabolic and anabolic pathways.

A popular theory of ageing is the "Free Radical Theory of Ageing" established the first time by Harman (1956). According to this, reactive oxygen species (ROS) accumulate within an organism or cell over the time leading to biological damages and malfunction. This is still very controversial due to the fact that, e.g. in the cortex of young rats larger level of ROS-induced oxidative modifications were present than in old (present study, Fig. 4-17 (Hutter et al., 2007)). An age-associated increase of ROS level was found in the brain of rats (Haripriya et al., 2004). ROS are ubiquitary and represent essential intermediates in oxidative metabolism. Nonetheless, when generated in excess, ROS can damage cells by peroxidizing lipids and disrupting structural proteins, enzymes and nucleic acids. Increased amounts of ROS are generated during a variety of cell stresses, including ischemia/reperfusion (Szabados et al., 1999), exposure to ionizing (Zahnreich, 2011) and ultraviolet radiation (Bossi et al., 2008) and/or inflammation (Hakim, 1993). They may contribute to inflammation and tissue damage. The level of oxidative damages of proteins (carbonylation of amino acids as arginine, proline or lysine; oxidation of tryptophan) can be analyzed.

There are several enzymes activated during oxidative stress defending cells against ROS damage such as superoxide dismutases (SOD), catalases, lactoperoxidases, glutathione

peroxidases and peroxiredoxins. Abundance increase of these enzymes prolonged lifespan in *Drosophila* (Parkes et al., 1998) while a knock-down in human fibroblasts induced senescence (Blander et al., 2003). Small antioxidative molecules such as ascorbic acid (vitamin C), tocopherol (vitamin E), uric acid, and glutathione are additionally essential to control ROS levels (Krajcovicova-Kudlackova et al., 2008). In similar manner, polyphenol antioxidants assist in preventing ROS damage by scavenging free radicals (Vladimir-Knezevic et al., 2011). Additionally, cells with damaged mitochondria begin to increase the population of healthy once, to balance the loss of defect cell organelles. Ageing is therefore often accompanied by a larger amount of mtDNA copy number (Toescu et al., 2000).

Harman (1972) also postulated that mitochondria play an important role in ageing since most oxygen is consumed at the respiratory chain and most ROS generated.

1.1.2 Complexity of brain ageing

In all vertebrate and most invertebrate animals, the brain is the center of the nervous system (Shepherd, 1994) and controls voluntary motor function as well as induces secretion of hormones and neurotransmitters allowing fast adaption to outside influences. Except for some basic types of responsiveness like reflexes or simple motor patterns (e.g. swimming or walking) is every body function under centralized control of the brain (Grillner and Wallen, 2002). The major part of the neurons is already present in a new born child. Within the first three years, the number of neuronal connection increases about 6-times. It was assumed until recently that the brain solely consists of post-mitotic cells. Currently it was demonstrated that also in the brain of adults neurogenesis occurs but to a less extent than pre-natal (Greenberg and Jin, 2006).

The organization of the brain is highly complex and its functional principles are only minor understood. The structure of neurons is known and was analyzed in detail, but it still has to be disclosed how the neuronal network enables all brain functions, e.g. cognition. The brain is segmented in distinct brain areas (for vertebrates: medulla, pons, mesencephalon, cerebellum, telencephalon, diencephalon) (Kandel et al., 2000) and consists of two major classes of cells: neurons and glia (Peters, 2007). It is generally assumed that in the human brain contains 10-times more glia cells compared to neurons. But Azevedo et al. (2009) found out that both classes are present in the whole brain of primates and humans to the same extend but that the ratio varies between different brain regions. In the cerebral cortex, e.g., 4-times more glia cells are present compared to neurons (Azevedo et al., 2009). Within the group of neurons and glia cells it can be distinguished additionally between different cell types each characterized by its specific function. Signals are transmitted via the neuronal cells. They are consisting of a cell body containing the nucleus and a neuronal terminus connected by an axon isolated by myelin sheaths. The size of neurons varies. They can be rather small but also several centimeters long, connecting two brain areas (Kandel et al., 2000). Parts of the brain containing high proportions of myelinated axons are called *white matter* and areas with mostly neuronal cell bodies *gray matter*. When analyzing e.g. protein

pattern of different brain areas one has to keep in mind that they are composed of different cells.

Ageing of the brain can be accompanied by neurodegenerative disorders like Alzheimer‘s or Parkinson’s disease. Brain deficiencies affect the quality of life to a large extent. Possible causes are neuronal loss or shrinking of neuronal cells, both leading to reduction of the brain volume (Anderton, 2002). But in some brain areas like hippocampus neurogenesis occur that counterbalance a neuronal loss during e.g. ageing (Galvan and Jin, 2007; Lazarov et al., 2010). Therefore, also other mechanisms (alterations in the metabolic state or energy production) are leading to age-associated diseases or deficits in brain maintenance (Miller and O'Callaghan, 2005).

Besides other reasons, all cell types consume ATP to maintain their transmembrane Na^+ and Ca^{2+}-level due to constant inward leak across membranes. Neuronal cells additionally require a large amount of chemical energy to restore their ion gradients after forwarding electrical signals (Budd and Nicholls, 1998). The recovery is performed mainly via the Na^+/K^+-ATPase and the Ca^{2+}-ATPase. While in normal cells, the Na^+/K^+ ATPase requires 40% of all cellular ATP, in neurons this enzyme is responsible for 2/3 of the cells energy expenditure. The major part of energy (i.e. ATP) needed is provided by mitochondria. Various neurodegenerative disorders (Parkinson’s, Alzheimer’s or Huntington’s diseases) or ageing are accompanied by mal-function of one more respiratory chain complexes or of the ATP synthase. Many diseases are characterized by a decrease in mitochondrial ATP generation (Budd and Nicholls, 1998) and often progressive loss of specific types of neurons. Neuronal cell death is caused therefore mostly by dysfunction in the OxPhos machinery (Henneberry, 1997; Sohal and Sohal, 1991). Additionally, especially the brain is vulnerable to ROS according to its large ATP consumption but minor ability to repair (Ffrench-Constant and Mathews, 1994), also due to less efficient DNA repair system (Gredilla et al., 2008), high amounts of unsaturated fatty acids leading to increased level of peroxydation (Hoch, 1992) and only minor ROS defending mechanisms (antioxidative system) (Stadtman, 2006). In aged animals, abnormalities of the mtDNA and membrane properties observed were combined with depolarised membranes and decreased ATP level (Toescu, 2005). The number as well as size of mitochondria was found to decline during ageing in the brain (Sastre et al., 2003).

The three brain areas often analyzed in e.g. ageing studies are the cortex, striatum and hippocampus.

The **cerebral cortex** (often named as cortex solely) is the largest brain area and involved in memory, attention, perceptual awareness, thought, language and consciousness. This brain structure is forming the outer layer of the cerebrum in mammalian brain. It is quite complex and consists of six layers containing different types of cells (Kandel et al., 2000). *Gray* and *white matter*s are visible in the cortex. The neurons within this large brain region are connected with other areas. In this case, the cell body is located in the cortex but the neuronal terminus in another region. The cortex is characterized by its large surface that is

highly folded. During ageing in some areas a large decrease in the neuronal number was observed in non-human primates (Smith et al., 2004).

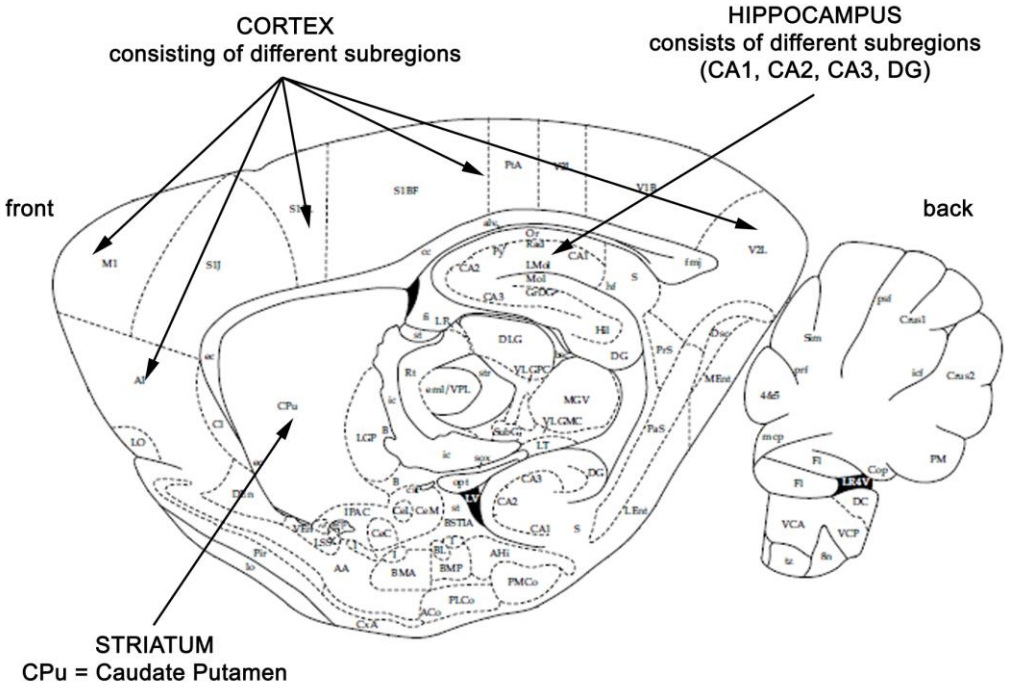

Fig. 1-2 Lateral view of a rat brain. The brain regions cortex, striatum and hippocampus are indicated. [picture modified according to Paxinos and Watson (1998)]

The **striatum** is the main input structure of the basal ganglia (Ferre et al., 2010) and important for planning, modulation and connection of movement, motivation and emotion. Diseases related to impairment of the striatum are e.g. Chorea Huntington's and Parkinson's. The striatum is composed of several neuronal cell types (Yelnik et al., 1997): Medium spiny neurons (96%), Deiters' neurons (2%), cholinergic interneurons (1%), GABAergic parvalbumin expressing interneurons, GABAergic calretinin expressing interneurons and GABAergic somatostatin expressing interneurons.

GABAergic parvalbumin and somatostatin expressing interneurons express dopamine receptors playing an important role in Parkinson's disease and research. While the neuronal cell bodies of dopaminergic cells are mainly in the substantia nigra, the neuronal terminals are located in the striatum.

The **hippocampus** is one of the oldest brain regions and a member of the limbic system located at the inner layer of the cortex. In ageing studies, the hippocampus represents a target of interest due to its almost conserved structure. This brain region is important for learning and memory (conversion from short-term to long-term memory). Postnatal structural development and alterations in hippocampus have been described in several studies (Lavenex et al., 2007). It is extremely vulnerable to psychosocial and environmental chronic adverse stress and ageing (Burger, 2010), leading to diseases such as e.g. Parkinson's and Alzheimer's (Cerqueira et al., 2007; Driscoll and Sutherland, 2005; Miller and O'Callaghan, 2005; Rothman and Mattson). Cortex and hippocampus are interacting to form memory and

during learning processes. Loss of hippocampal activity is accompanied by a loss in memory storage (Nicholson et al., 2004). Restructuring of neuronal circuitry (shortening of dendrites and overall decrease in synapses number) occurs after adverse stress (Sousa et al., 2000) and impairment of hippocampal function during ageing and neurodegenerative processes was demonstrated (Billard, 2006; Laranjinha and Ledo, 2007). If volume-decrease occurs it is always age-related and predominantly due to changes in glia. Therefore, age-dependent decrease in hippocampal function may be related to neurobiological modifications e.g. in signalling, information encoding, electrophysiological or neurochemical properties (Miller and O'Callaghan, 2005) or energy metabolism. Especially in hippocampus, there is a large amount of glucocorticoids receptors. High concentrations of steroids, like e.g. glucocorticoids, involved in cellular stress response, affect the brain function, structure and neurogenesis (Belanoff et al., 2001; Porter and Landfield, 1998). In the hippocampus of adults, contrary to other brain regions, neurogenesis takes place (Altman and Das, 1965; Cameron et al., 1993; Kuhn et al., 1996), enabling recovery and response on external stress as well as maintenance of memory function. Cells are regenerating during life time and the brain area consists of a mixture of cells: young, middle aged as well as old. Neurogenesis in the hippocampus declines with age (Kuhn et al., 1996; Rao et al., 2005; Seki and Arai, 1995) but newly generated neurons at every age state display always same amounts of dendritic spines and afferent glutamatergic connections (Morgenstern et al., 2008). Additionally, in this brain area almost every cell type present within the brain was found and hippocampal cells are characterized by high plasticity (Nicholson et al., 2004).

Ageing of the brain regions is distinct. In the prefrontal cortex as well as in the hippocampus e.g. age-associated neuronal loss was observed (Shankar, 2011) or the *gray matter* of some cortex regions and striatum are more affected than the hippocampus (Mrak et al., 1997). The number of neurons decreased about 30% in a region of the prefrontal cortex in aged non-human primates (Smith et al., 2004). There are also differences in ageing of the brain regions between males and females (Murphy et al., 1996). But it is postulated that neuronal loss is not the only cause of brain ageing, since it occurs only in some areas. Instead it seems to be a result of several alterations affecting the brain function like: combination of altered mitochondrial function, accumulation of ROS and altered cellular calcium homeostasis (Harper et al., 1998). There are possibilities for maintaining the functionality of the brain, e.g. exercising of intellectual and physical activity or caloric restriction (CR) (Miller and O'Callaghan, 2003, 2005).

1.1.3 The process of cellular ageing in vitro - senescence

The smallest unit of all organisms independently from their evolutional level is the cell. Highly developed creatures like mammals consist of numerous different cell types. Each is characterized by its constitution and specific metabolic activity depending on its origin (Yotnda et al., 2010). The shape varies considerably, comparing i.e. neuronal cells with lymphocytes or skin fibroblasts. Cell culture experiments are performed to study general

functions and specializations of each cell type and its response to external stress, like irradiation or chemical treatment. Additionally, interactions between different cell types are studied in multilayer cultures. The results obtained are important to understand biochemical processes and pathways occurring in multicellular organisms. One very complex event affecting and involving all cells and organs is the ageing process. Cellular ageing is also called senescence. Senescent cells are characterized by a loss of ability to divide.

According to Hayflick and Moorhead (1961) there are three growth stages in cell culture: Phase I is the primary culture immediately after extraction of cells from the explants. Phase II represents the period when cells divide in culture. When cells cover the whole surface of a flask, they stop multiplying. For continued cell growth, cells must be subcultivated and transferred into new culture flasks. Since cells divide continuously, further subcultivation is required and has to be repeated within few days. After several cell population doublings and subcultivation, cells start to divide slower marking the beginning of Phase III. Phase III is characterized by a reduced proliferation that may be followed by a cell growth arrest or cell death (Hayflick, 1985, 1994). In cellular or replicative senescence, cells are losing their ability to divide on an average of 50 cell doublings in vitro, known as Hayflick's limit, e.g., induced by increased level of DNA damage or shortened telomeres.

Within the growth stages, cells differentiate showing special morphological shapes (Bayreuther et al., 1988; Fournier et al., 1998). There are four types of proliferating, mitotic active fibroblasts and three types of post-mitotic fibroblasts not able to divide any more. External stress like irradiation or chemical treatment as well as different cultivation conditions (type of medium, additives, regularity of medium change and oxygen conditions) having influence on cell differentiation and may lead to premature senescence (Winter, 2007).

Cell culture experiments may be used as *in vitro* model to unravel basic mechanisms common for both ageing and senescence.

1.2 The biological effect of ionizing radiation

Human cells are continuously exposed to ionizing radiation arising from natural sources on earth (i.e., Radon in rocks and construction materials, ^{40}K in foods) and in space (the sun, supernovae and others sources in the universe), as well as artificial sources as nuclear power plant fallout or nuclear bombs that might have harmful effects on cell survival and maintenance. But the impact of irradiation on cells can be also helpful and used in medical radiation therapy, using photons or heavy ions in tumor therapy.

Ionizing radiation is affecting the cell physiology by inducing DNA damages as single or double strand breaks. The type of radiation differs in their constituents (e.g. neutrons, carbon, nitrogen, protons or electrons) and in their energy. There is photon (X-rays and gamma) and particle radiation (neutrons, electrons, etc). The LET (Linear Energy Transfer, keV/µm) describes the energy in average that is released per distance along the track. Radiation, inducing ionization events densely distributed along their track, like heavy ions

(e.g. carbon) with a minimum LET value of 10 keV/µm, is defined as high-LET radiation. Low-LET radiation (e.g. X-rays or gamma radiation) induces only minor ionizing events along the track that are homogenously distributed in the target. During ionizing events (minimum energy required 10 eV), irradiation induces via Coulomb force the release of valence electrons leading to an opening of chemical bonds (Kraft, 1987).

The physical parameter describing the absorbed dose of ionizing radiation is gray (Gy). One gray is defined as the absorbance of one joule of ionizing radiation by kilogram of matter (e.g. cell tissue, equation 2.1) (Organisation Intergouvernementale de la convention du Mètre, 2006).

$$1\,Gy = 1\,\frac{J}{kg} = 1\,\frac{m^2}{s^2} \qquad (2.1)$$

Gy = gray (SI unit)
J = joule
Kg = kilogram of matter

For both densely and sparsely ionizing radiation the number of the most harmful double strand breaks is comparable (Heilmann et al., 1995), but successful double strand break repair is more likely after low LET than after high LET exposure (Heilmann et al., 1996; Taucher-Scholz et al., 1996). Different spatial distribution of ionizing events characteristic of the radiation type is suggested to influence the ability of the cell to repair these damages.

Dense and sparse ionizing radiations have different biological effects (qualitative and quantitative) when applicated in comparable dose due to their specific deposition of energy (Mehnati et al., 2006).

For the time after irradiation when repair processes occur, cell proliferation is decelerated. If these damages are not repaired or repaired in an incorrect manner, cells undergo growth arrest and/or enter the cascade of cellular death (apoptosis). The relative biological effectiveness (RBE) is describing how specific radiation types affect an organism to different extent. The RBE is defined generally via the ratio of absorbed dose of a reference radiation (mostly X-rays, with 250 kV energy) to the dose of the test radiation type when both showing the same biological effect (equation 2.2) (Krieger, 2007).

$$RBE = \frac{D_X}{D_T} \qquad (2.2)$$

D_X : absorbed dose of reference radiation
D_T : absorbed dose of test radiation type
both leading to same effect

It was demonstrated that, dependent of origin or type, cells show different radiosensitivity. While mainly post-mitotic neuronal cells are characterized by large radioresistence, mucosal cells with high proliferation rate are extremely radiosensitive. The radiosensitivity additionally changes during the cell cycle due to changes in the size of the nucleus and chromatin structure (Sinclair, 1968).

Ionizing radiation is used as a medical tool to cure cancer (Blakely and Kronenberg, 1998; Tsujii et al., 1994; Wachsberger et al., 2003; Weichselbaum et al., 1983). In tumor tissue, the balance between cell division and cell death is disturbed. Cells lost their ability to undergo cell growth arrest and apoptosis and proliferate continuously. Exposure of tumor cells to heavy ions or photons of high-energetic X-ray *Bremsstrahlung* leads to cell death. Tumors located at delicate positions for surgical operation can be often cured by the alternative application of radiation therapy. The effect of radiation on healthy cells still has to be analyzed in detail, since during radiation therapy also healthy tissue surrounding the tumor is exposed to discrete dose amount. In contrast to high-energetic photons, releasing exponentially the energy per unit penetration depth, heavy ions depose their maximal dose at the end range (Bragg peak), whereby the healthy tissue receives relatively small doses.

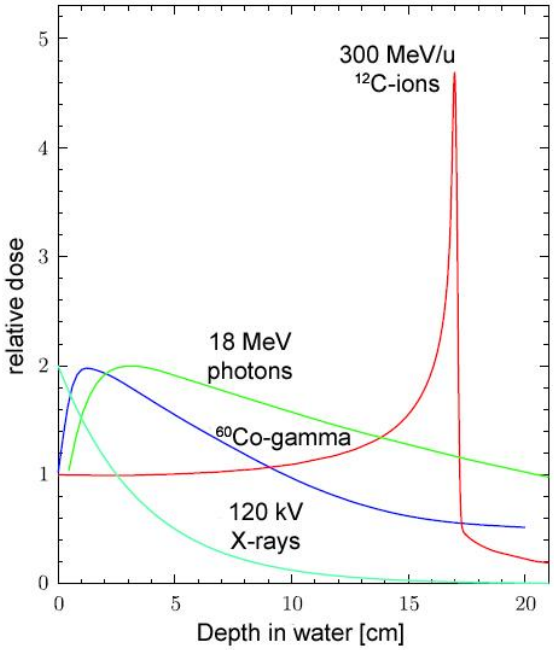

Fig. 1-3. Depth dose curve, showing the absorbed dose deposited by different radiation beams into water on the way of their track. In contrast to photons (18 MeV), Co-γ-radiation and X-rays, the heavy ion radiation decreases only to a small extent until the end of its penetration depth where at the Bragg-maximum high doses are released [figure modified according to Weber (1996)]

Only when applying microbeam, a method allowing targeted irradiation, e.g. one single hit inside the nucleus can be induced. But in general, with X-ray or heavy ion radiation the whole cell (cytoplasm and nucleus) is exposed homogeneously to the ionizing radiation. Proteins in the cytosol are in general present in several numbers and with short half-lifetime of 9.3 days (liver) to 24.4 days (brain) (Menzies and Gold, 1971). Damages can therefore be counterbalanced and defect proteins are replaced. But disruption of DNA affects to a large extent the physiological state of a cell (Munro, 1970). Hence the biological effectiveness results mostly from alterations of the DNA. The majority of studies analyzing the effect of ionizing radiation concentrate solely on damages of chromosomal DNA. But as described in chapter 1.1.1 approximately 1% of the total DNA within a cell is of mitochondrial origin.

Mitochondrial DNA is much more vulnerable to irradiation damages due to its less developed DNA protection and repair system. Mitochondrial dysfunctions are related to several diseases. Therefore, the effect of irradiation on the mtDNA should be analyzed in more detail.

1.2.1 Hormesis

It is known that ionizing radiation is harmful for cells and multicellular organisms (Ina and Sakai, 2004). It is generally assumed that no threshold for the harmful effect of radiation exists. However, following the theory of radiation hormesis (Wolff, 1998), low-dose (Luckey, 1982) and high-dose (Yonezawa et al., 1996; Yonezawa et al., 1990) radiation induce e.g. also enhanced growth rate, prolonged life span (Lorenz et al., 1955) – also after lethal high-dose irradiation (Yonezawa et al., 1996; Yonezawa et al., 1990) – increase function of the immune system (Anderson and Lefkovits, 1979; Liu, 1989; Liu et al., 1987), increased resistance to oxygen toxicity (Lee and Ducoff, 1989). Hormesis as mechanism is unproven right now but there are numerous evidences supporting this theory. Petin et al. (2003) had analyzed the effect of chronic and acute ionizing radiation on the ageing process and cell survival of eukaryotic and prokaryotic cells. An increased lifespan and survival after chronic ionizing radiation was demonstrated for bacteria and yeast after recovery from potentially lethal acute radiation.

The term hormesis is not only used for cellular response on irradiation but also on exposure to toxins or other stressors. According to ageing it is suggested that mild stress is resulting in anti-ageing effects (Rattan, 2008). In several studies, mild stress is induced by e.g. calorie restriction, irradiation or exposure to oxidants (Dani et al., 2009; Gems and Partridge, 2008; Le Bourg and Rattan, 2008; Rattan, 2008).

1.2.2 Neutron scattering experiments

This chapter is based on the research proposal *"Characterisation of functional molecular dynamics in cells under different ageing states"* to obtain neutron beamtime at the neutron spectrometer IN13 at the Institut Laue-Langevin (ILL) in Grenoble (France) and was formulated in cooperation with Thomas Hauss (Helmholtz-Zentrum Berlin für Materialien und Energie GmbH), Judith Peters (ILL), Andreas Stadler (ILL), Joseph Zaccai (ILL) and Marion Jasnin (ILL).

The relevance of molecular dynamics for the understanding of biological activity was established in recent years. Neutron scattering has contributed important experimental information to this research field, a prominent example is the discovery of the "dynamical transition" in protein dynamics (Doster et al., 1989). The method is uniquely sensitive to the appropriate ranges of length and time scales of atomic and molecular motions centered around 1 nm and 1 ps, respectively, with which molecular dynamics simulations can be compared directly. Inelastic neutron scattering experiments specifically probes the motion of

^{1}H atoms because of the exceptional large incoherent neutron cross-section (Sears, 1992) and provide measured values of mean square displacements $<u^2>$. As hydrogen atoms are evenly distributed in biological matter, the method of inelastic neutron spectroscopy gives an average view on structural fluctuations. The systems studied, from biological molecules to cells in different environments, are extremely complex in their structural and dynamic heterogeneity. Their full dynamic description in a purely physics approach is practically impossible.

The usual aim of a study in biology is to understand how systems evolved having different properties fulfilling their specific biological functions. A methodological approach adapted to the complexity of biological systems is based on identifying significant experimental parameters similar in different systems and correlated with their respective functions and activities. Neutron scattering experiments were evolved to reveal such general, overall present parameters (Zaccai, 2000) and applied to analyze the molecular dynamics in cells adapted to extreme environments (Jasnin et al., 2008).

The neutron spectroscopy focuses on internal dynamics in macromolecules, dynamics related to the properties that make a macromolecular structure stable, with the appropriate flexibility to ensure activity. Two parameters are measured: mean fluctuation amplitude related to flexibility and mean force constant related to stability. Because of the way experiments are conducted, samples need not be crystalline or monodisperse. In a complex system the two parameters reflect mean behavior. In experiments on bacteria, the parameters were dominated by the behavior of proteins, and their comparison for bacteria living in various extreme conditions permitted to propose a dynamical interpretation of the adaptation (Tehei et al., 2004). Hence, the proteins in each organism are studied not only in order to be stable under the extreme conditions, but also in order to have the appropriate quantitative flexibility for activity.

Analysis of whole cells is a big challenge, since living cells consists of many different proteins, DNA, membranes and other constituents. It is a priori not clear if a global measurement like neutron spectroscopy is sensitive to dynamical changes in different stages of a cell. Additionally, hydrogen atoms of the cell water and the surrounding buffer increase the ratio of the background to the signal dramatically due to their incoherent contribution during neutron experiments. To decrease background signals cell cultures or the organism of interest (bacteria, yeast, etc) have to be cultivated before in deuterated solutions, that hydrogen atoms are replaced by deuterium. If this is not possible, samples should be washed before the experiment in deuterium oxide.

2 Chemicals, Materials and Analytical Tools

2.1 Chemicals

Chemicals	Manufacturer/Catalogue number
Acetic acid 100% p.a.	Sigma P-2772
Acetonitrile	Roth 4722.1
Activated carbon	Roth 5963
Adenosine triphosphat (ATP)	Sigma A-3377
Annexin-V-Fluos Staining KIT	Roche Diagnostics 11 858 777 001
6-aminohexanoic acid	Fluka 07260
Ammonium bicarbonate	Fluka 09832
Ammonium persulfate (APS)	Fluka 9915
ATP Kit SL	BioThema 144-041
2-[Bis(2-hydroxyethyl)amino]-2-(hydroxymethyl)-1,3-propanediol (Bis-Tris)	Fluka 14880
protein-free T20 (PBS) Blocking Buffer	Thermo Scientific 37573
5-Bromo-4-chloro-3-indolyl phosphate (BCIP)	Roth A155.2
Bromophenol blue	Fluka 18030
BSA (bovine serum albumin)	Sigma A-6003
CASYTON solution	Schärfesystem
Catalase	Sigma C-40
Colcemid (*N*-methyl-*N*-deacetyl-colchicine)	Roche Diagnostics 10295892001
Coomassie® Brilliant Blue G-250	Serva 35050
Coomassie® Brilliant Blue R-250	Fluka 27186
Copper(II) sulfate pentahydrate p.a.	Merck 2790
α-cyano-p-hydroxy cinnamic acid	Sigma C-2020
Cytochrome c (horse heart)	Fluka 30397
3,3'-Diaminobenzidine (DAB)	Sigma D-5637
2‘-7‘-Dichlorodihydrofluorescein diacetate (DCDHF)	Sigma-Aldrich D6883
Digitonin high purity (charg. Nr. B58163)	CalBioChem 300410
Digitonin high purity (charg. Nr. 5H007912)	AppliChem A1905
Dihydroethidium (DHE)	Anaspec 85718
N,N-Dimethylformamide (DMF)	Merck 2937.0500
Disodium hydrogen phosphate	Fluka 71642
1,4-Dithiotreitol (DTT) p.a.	Roth 6908
EDTA-Trypsin-solution (0.05% Trypsin, 0.1% EDTA)	PAN Biotech GmbH P10-027500
EMEM with EBSS (Bio WhittakerTM)	Cambrex Bio Science
Ethanol abolut p.a.	Merck 101986
Ethanol spoilt	Stock of chemistry department
Ethylenediaminetetraacetic acid (EDTA)/Na^+	Sigma 8043.3
Fetal bovine serum (FCS)	Merck
Formaldehyde (35%, aqueous solution)	Roth 7398
Giemsa's azur eosin methylene blue solution	Merck 109204
Glutamine (*N*-acetyl-L-alanyl-L-glutamine)	Biochrom AG K 0302
Glycerol	Roth 7530
Glycine p.A.	Biomol 4943
HEPES (4-(2-hydroxyethyl)-1-piperazineethanesulfonic acid)	Roth 9105.4
HMW Callibration Kit for native gel electrophoresis	Ammersham Bioscience 17-0445-01
Hoechst 33 342	Sigma Aldrich 14533
Imidazole	AppliChem A1073.1000
Iron(III) chloride hexahydrate	Merck 1.03943
LMW Callibration Kid for SDS gel electrophoresis	Ammersham Bioscience 17-0446-01
Magnesium chloride p.a.	Fluka 63068

Chemicals	Manufacturer/Catalogue number
Magnesium sulfate p.a.	Applichem A1037
2-Mercaptoethanol	Sigma M-6250
Methanol spoilt	Stock of chemistry department
Methanol p.a.	Roth
Milk powder blotting grade	Roth T145.3
Potassium acetate	Fluka 60034
Potassium chloride	Merck 104936
Potassium ferrocyanide (III)	Fluka 60299
Sodium carbonate p.a.	Roth 3746
Sodium chloride	Roth 3957.1
Disodium hydrogen phosphate	Fluka 71642
Monosodium phosphate dihydrate	Roth T879.1
Sodium thiosulfate	Fluka 72048
sodium hydroxide solution	Merck 1.05589.0250
Nicotinamide adenine dinucleotide (NAD)	Sigma N4256
Nitro blue tetrazolium chloride (NBT)	Fluka 74032
Oxyblot™ Protein Oxidation Detection Kit	Chemicon S7150
PAGE Blue™ Staining Solution	Fermentas R0579
$PBS^{-/-}$ Dulbecco	Biochrom AG L 182-01/05/10/50
Pefabloc® SC	Biomol 50985
Penicillin/streptomycin (1000U/1000 µg/mL)	Biochrom AG
Bovine serum albumin (BSA) fraction V	Roth 8076.1
Sodium succinate dibasic hexahydrate	Sigma s2378
Protease-Inhibitor-Cocktail	Sigma P-8340
Roti®-Block	Roth A151.2
Rotiblue®	Roth A152.1
Roti®-Block 2A	Roth P037.1
Roti®-Block 2K	Roth P038.1
Roti®-Blue	Roth A152.1
Roti®-Nanoquant	Roth K880.1
Rotiphorese® Gel A	Roth 3037
Rotiphorese® Gel B	Roth 3039
Rotiphorese® Gel 29:1	Roth A515.1
Hydrochloric acid (suprapur)	Merck 9.975
Hydrochloric acid p.a., 37% fuming	Roth 317
D(+)-sucrose	Roth 9286
SCAVEGR®	BrainBitsLLC/USA
Silver nitrate	Roth A1376
Sodium dodecyl sulfate (SDS)	Roth 2326.2
Succinate	Sigma 3/149
SYPRO Ruby® Staining Solution	Bio Rad 170-3125
TEMED (tetramethylethylenediamine)	Roth 4995.1
Trifluoroacetic acid (TFA)	Fluka 91701
Tris(hydroxymethyl)-aminomethan (Tris)	Roth 6977.3
N-(2-Hydroxy-1,1-bis(hydroxymethyl)ethyl)glycine (Tricin)	Roth 5429.3
Trypsin, *Sus scrofa*, sequencing grade, methyliert, TPCK-treated	Promega V5111
Tween® 20	Roth 9127.1
Hydrogen peroxide 30%ig (v/v), aqueous solution	Merck 1.07209.0250

2.2 Antibodies

1. Antibodies (Western Blot)

Antigen	host	Manufacturer	Dilution
mitofilin	rabbit	Novus Biologicals	1:5000
prohibitin	rabbit	Santa Cruz Biotechnology	1:200
superoxide dismutase 1 (internal part)	rabbit	antikörper-online.de	1:1000

2. Antibodies

Antigen	host	type	Manufacturer	Dilution
Rabbit IgG	goat	Alkaline phosphatase	Molecular Probes	1:2000

2.3 Consumables

Consumables	Manufacturer
Blue-Cap-Greiner 15 mL	Greiner
Blue-Cap-Greiner 50 mL	Greiner
Cuvette acryl, slice thickness 1 cm, ½ micro cuvette	Sarstedt
Eppendorf cups	Eppendorf
Kimwipes-Science	Roth
Membrane filter RC 58; 0.2 µm	Roth
96-well-microtiter plate	Millipore
Sequi-Blot™ PVDF membrane (1.5 mm)	BioRad
Rotilabo®-Blotting-Paper	Roth
Zip-Tip, µC18 Tip-size P10	Millipore

2.4 Software and Bioinformatics Tools

Data Explorer, Applied Biosystems
Delta2D Version 3.3 - 3.6, Decodon
Fujifilm LAS-3000, Fuji
GS-800 Calibrated Densitometer, BioRad
Image Reader LAS-3000 2.1, Fuji
ORIGIN 6.0, Origin Lab Corporation
Photoshop 5.1 Service Pack 2, Microsoft
QuantityOne Version 4.4.0 (2000), BioRad
UVProbe Version 1.11 (2000), Shimazu
Office 2007, Microsoft

2.5 Devices

Device	Manufacturer
Balance H 54	Sartorius
Balance R 200 D	Sartorius
Centrifuge rotor F34-6-38	Sorvall
Centrifuge rotor Microliter rotor 24x2 mL Alu	Heraeus
Centrifuge Eppendorf A-4-44	Eppendorf
Centrifuge 5804 R	Eppendorf
Counting chamber Neubauer	Marienfeld
Dosimeter SN4	PTW Freiburg
Dual Gel caster SE 245; Mighty small	Hoefer
Flowcytometer PAS III	Partec
Gel electrophoresis apparatur Hoefer™ SE250; Mighty small	Amersham Biosciences
Gel electrophoresis apparatur Hoefer™ SE400	Amersham Biosciences
Gel electrophoresis double-apparatur Hoefer™ SE600 Ruby™	Amersham Biosciences
Gel preparation apparatur Minipuls 3	Abimed Gilson®
Gel preparation apparatur Minipuls 3	Gilson®
Glass-Teflon-Homogenisator tight fitting, 2 mL (slit width: 45-65 µm)	Braun
Gradient mixer	Mechanics of the chemistry department
Homogenisator prime mover	Braun
Luminescent Image Analyser; LAS-3000	Fuji
Luminometer 1251	BioOrbit
MALDI-MS Voyager-DE Pro	Applied Biosystems
MALDI-sample plate V 700666	Applied Biosystems
pH-elektrode blue line 14 pH	Schott
pH-Meter	Schott
Power Supply EPS 301	Amersham Biosciences
Power Supply EPS 601	Amersham Pharmacia
Power Supply EPS 3501 XL	Amersham Biosciences
Rotilabo Mikropistill	Roth
Scanner GS-800 Calibrated Densitometer	Bio-Rad
Spectrometer Polarstar Galaxy	bmG
Table centrifuge Biofuge Pico	Heraeus
Transblot SD Semi-Dry Transfer cell	BioRad
UV-Vis Spectrometer UV-2401 PC	Shimazu
Water processing system Simplicity	Millipore
X-ray tube isovolt DS1	Seifert

2.6 Animals (*Rattus norvegicus*)

2.6.1 Rat brain areas for ageing studies

Male Wistar rats were obtained from Charles River (Sulzfeld, Germany). They were housed four animals per cage at the Charité Berlin (Prof. Rommelspacher) in an artificial 12-h light–dark cycle with food and water *ad libitum*. Rats were cared and handled in accordance with the guidelines of the European Union Council (86/609 EU) for the use of laboratory animals. The animal housing was performed in a specific artificial surrounding without any contact to common obligate or facultative pathogens (SPF), i.e. exogenous or endogenous parasites, Mycoplasma or Pasteurella. The study was approved by the Animal Care and Use Committee of the Senate of Berlin, Germany (GeschZ. 0273/ 03). Two age-groups

comprising four animals each, were included in this study: 4 to 6 month old (young rats) and 28 month old (aged rats).

The dissection of brain areas – cortex, striatum and hippocampus (each from the right hemisphere) – and immediate isolation of mitochondria from non-frozen tissue was performed by Regina Hill (Technical Assistent of Prof. Rommelspacher, Charité Berlin).

2.6.2 Rat brain striatum as animal model of Parkinson's disease

Male Wistar rats (with an initial body weight of 280–300 g) were obtained from Charles River (Sulzfeld, Germany). The rats were housed under conditions as described in chapter 2.6.1 for at least 7 days until surgery.

Three groups of rats with different treatment were included in this study. All animals received via cannula placement – implanted subcutaneously under anaesthesia – infusions into the anterior part of the left cerebral ventricle via an Alzet® osmotic mini-pump. The first group was treated for 28 days with MPP^+ (0.284 mg/kg/day) and subsequently with 9-me-BC (0.105 mg/kg/day) for 14 days. The second group received MPP^+ for 28 days followed by saline for 14 days. The third group was sham-operated twice at an interval of 28 days. At the end of the 42 day infusion, all animals were killed. Their brains were dissected on ice and divided in two parts at the level of the caudal hypothalamus. Mitochondria have been isolated by Regina Hill (group member of Prof. Rommelspacher, Charité Berlin) from the anterior part containing the striatum immediately upon dissection of brain areas without preceded freezing of tissue.

All experiments were performed in accordance with the National Institutes of Health Guide for the care and use of laboratory animals (Publication no. 85–23, revised in 1985) and were approved by the Animal Care and Use Committee of the Senate of Berlin (Registration no. G-0129/04) (Wernicke et al., 2010).

2.7 Cell cultures

2.7.1 Cell culture as model for Parkinson's disease

The effect of 1-methyl-4-phenylpyridinium (MPP^+) and of the putative neuroprotectant 9-methyl-beta-carboline on the mitochondrial proteome was analyzed on HEK-(h)DAT cells. HEK-(h)DAT cells are human embryonic kidney cells containing the stable transfected human dopamine transporter that is stable expressed (Storch et al., 1999).

Cell culturing of HEK-(h)DAT cells was performed at the Charité Berlin (group of Prof. Rommelspacher) with incubator adjustment of 5% CO_2, 21% atmospheric oxygen, 100% humidity and a temperature of 37°C.

2.7.2 Cell lines applied for long term experiments

The three cell lines (Table 2-1) utilized in this study are normal human dermal fibroblasts of different origin: skin, foreskin and lung. They are non-permanent and characterized by contact inhibition. They undergo biological ageing also referred to senescence.

Table 2-1. Cell lines applied for long term cell culture experiments [normal human dermal fibroblasts (NHDF), human dermal fibroblasts (AG1522D) and fetal lung fibroblasts (WI38)]

Cell line	Tissue	Age of the donor	company	CPD at the beginning of experiments
NHDF	Skin	10 days (postnatal)	Cell Systems (St. Katherinen, BRD	25.8
AG1522D	Foreskin	3 days (postnatal)	Coriell Institute of Medical Research Camden (NJ, USA)	24.4
WI38	Lung	12 weeks (fetal)	Amercian Type Culture Collection (ATCC)	37.2

2.7.3 Cell line applied for neutron scattering experiments

For neutron scattering experiments BHK 21 (Syrian hamster kidney fibroblast) were used. The cells were provided by the lab of Prof. Dr. Peter Friedl at the Technische Universität Darmstadt and pre-cultivated by Anke Imrich. The culture medium (1:1 mixture of Dulbecco's MEM and Ham's F-12) contains 5% NCS (new born calf serum) and 2 mM L-glutamine.

3 Methods

3.1 Cell culture conditions for long term experiments

Employed cell lines of fibroblasts are of human origin and not immortal. They are growing – in contrast to tumour cells – in culture dishes as monolayer and are contact inhibited. Upon contact with neighbour cell, growth arrest is induced followed by cell death (Seluanov et al., 2009). Therefore, cells have to be replaced continuously to ensure continuous cell proliferation.

Cells were cultured in Eagle's MEM (PAN system, Bio-Whittaker) containing 10% foetal calf serum (Biochrom), 1% glutamine and penicillin/streptomycin [pen.: 10^5 U/l; strep.: 0.01% (w/v)]. Incubator adjustment was set to 5% CO_2, 21% atmospheric oxygen and 100% humidity. After irradiation, cells (irradiated cells as well as non-irradiated) were subcultured the first day and then every two weeks until proliferation slowed. Afterwards, passages occurred every three weeks. Passages were done at the beginning or at the end of the week. If the cell splitting was performed e.g. on Monday, a medium change was done on Friday and vice versa. In weeks without cell splitting medium changes occurred on both on Monday and on Friday. During passage, the medium was discarded and the cell layer washed with 1 to 2 mL of Trypsin/EDTA. The cells were detached by adding 2 mL of Trypsin/EDTA for 5 min at 37°C. The separation was controlled with the aid of a microscope and the reaction of Trypsin terminated by addition of twice the volume of the medium. After determining the numbers of cells per milliliter with the cell counter Casy or counting chambers, cells have been seeded again (5 x 10^5 cells per 75 cm^2 culture flask).

At each passage the cumulative population doubling (CPD) was determined according to the mathematical equation (4.1):

$$CPD = CPDs + \frac{ln\frac{A_h}{A_s}}{ln2} \qquad (4.1)$$

A_h = amount of cells harvested
A_s = amount of cells seeded

The calculated amount of cell divisions from seeding until the further cell splitting is always added to the population doubling at the time of seeding (CPDs). The CPD is important to gauge the ageing status of a non-permanent cell culture.

The storage of cell suspension occurred in liquid nitrogen. After detachment with trypsin, separation and counting, cells were frozen suspended in culture medium (20% fetal calf serum and 10% glycerol) at a concentration of 1.8 x 10^6 cells/ml in a specific freezing box with two walls. Isopropyl alcohol was filled between these two walls allowing cooling of suspensions with 1°C/min at -80°C. For longer storage cryo tubes are placed in a liquid nitrogen container the following day. For revitalizing, cells were thawed and transferred to culture flasks with medium that was pre-warmed to 37°C. A change of medium was performed after approx. 4h incubation time. The percentage and number of cells attached after thawing was determined in approximation in advance by counting cells attached to the

bottom of cell culture flasks and unattached cells in the medium. This step is important to calculate the CPD at the further passage

3.2 Irradiation of cell culture

After thawing, the first passage was performed 2 to 3 days later. At the second passage, one week later and approximately ten days before irradiation, cells were seeded with a density of 3000-7000 cells/cm^2. Only confluent cells were exposed to X-rays (250 kV, 16 mA, 8 Gy) or carbon ions (100 MeV/u, 2 Gy, Unilac). Confluency is referred as a state when the ground is completely covered by cells arrested in G0/G1-phase.

Besides irradiated cells, also control cells were used. Controls are treated identically except irradiation, i.e. duration of stay outside the incubator, medium changes with identical medium composition (e.g. lack of foetal calf serum or other additives).

3.2.1 X-ray irradiation

For X-ray irradiation the X-ray tube Isovolt DS1 (Seifert, Bridge Port, USA) with a wolfram anode was used. The voltage was set to 250 kV (1 keV/µm) with a current flow of 16 mA. To exclude longer wavelengths, a filter system consisting of 7 mm beryllium, 1 mm aluminium and 1 mm copper was utilized. To obtain homogeneous irradiation, the distance was adjusted to the size of the cell culture dishes and controlled with the dosimeter SN4 (PTW Freiburg).

During irradiation with a dose of 8 Gy (approx. 1 Gy per min) cell culture flasks (75 cm^2) remained in horizontal position for approximately ten minutes at room temperature and atmospheric conditions. Thereafter, they were immediately returned to the incubator without further medium change. After 24 hours the first passage was performed. As described in chapter 3.1 at the beginning of the experiment cell replacement was done every two weeks and thereafter when cell proliferation slowed down at an interval of three weeks.

3.2.2 UNILAC irradiation

Low-energy irradiation with carbon ions (100 MeV/u, LET 170 keV/µm, 2 Gy) was performed at the UNILAC [Universal Linear Accelerator, Gesellschaft für Schwerionenforschung (GSI), Darmstadt, Germany]. To achieve a specific dose during irradiation, cells are irradiated several times in short intervals with a previously calculated number of pulses.

For carbon ion radiation at the UNILAC cells were seeded 10 days before the experiment with a density of 2000 cells/cm^2 in petri dishes (Ø = 35 mm). Approx. 30 min before irradiation medium was removed and collected (used to refill petri dishes after the experiment) and culture dishes placed in a vertical position in a specific repository filled with medium (without foetal calf serum). The repository was closed, transported in a transport box to the irradiation facilities and opened again under sterile conditions. During irradiation procedure, petri dishes were lifted up automatically one after the other inside the carbon beam and irradiated in this vertical position without being covered by medium as low

energetic carbon ions possess only small penetration depth (approx. 400 µm at 9.8 MeV/u). After irradiation of all petri dishes, the repository was closed again and transported back inside a laminar hood. Cells at the lower edge of the petri dishes had to be removed using sterile Q-tips. These cells were not irradiated due to the small penetration depth of carbon ions, as they were still covered with small amounts of medium that was not emptied out during positioning of the cell culture dish inside the beam. After covering of cells with the medium collected before irradiation petri dished were placed in the incubator for 24 hours. Thereafter, the first passage was performed and cells were seeded for long-term cell culture in 75 cm^2 flasks. Sub-culturing occurred every second week and every three weeks when cells began to slow down in proliferation.

Controls were treated the same way as irradiated cells except for irradiation and the accompanied lifting of petri dishes outside the repository.

3.3 Cell culture experiments with elastic incoherent neutron scattering

The macromolecular dynamics of cells were analysed on Syrian baby hamster kidney cells (BHK 21, chapter 2.7.3), by using elastic incoherent neutron scattering on IN13 (Grenoble, France). BHK cells are characterized by a doubling time of only 10 hours at the maximum growth rate. They were used due to their high proliferation rate and their known sensitivity for apoptosis inducing additives utilized in this experiment.

Two experiments were performed that differs in the way the cells were transported to the experimental facility (IN13, ILL, Grenoble, France). For the first (15.-18.06.2009) experiment, cells were harvested and pelleted via centrifugation (at 800 g, 5 min, RT) one or two days before the experiment in the laboratory at the Technische Universität Darmstadt (Germany) and stored at 4°C until final sample preparation. For the second experiment (26.08.-6.09.2009) cells were transported in cell culture flasks one week before the experiment to France and were harvested immediately before exposure to neutrons. In general, the sample preparation was similar both experiments.

After discarding the medium, remaining medium was removed by washing with 5 mL $PBS^{-/-}$ in D_2O. Cells were removed from the flasks, resuspended in 2 mL $PBS^{-/-}/D_2O$, collected and pelleted by further centrifugation (800 g, 5 min, RT). The cell sediment was washed twice with $PBS^{-/-}/D_2O$. At this stage, cells were stored at 4°C for the transport to ILL in Grenoble (France) for the first experiment. For each measurement, 500-700 mg of this cell pellet was placed in a sterile flat gold-coated sample holder. During the experiment the sample holder was tightly closed. In the first experiment (June 2009), each sample was about 24 hours in the beam and in the second (September 2009) 4 hours – for each temperatures higher than 296 K (300 K, 304 K, 307 K, 315 K) – and until 12 hours for lower temperatures (280 K, 288 K, 296 K). Every lower temperature was also measured for 4 hours but immediately after each other without changing the sample. After exposure to neutrons,

cells were re-cultivated to analyse their survival. Experimental setup was chosen that allowed surviving of control cells to a large extent.

For elastic incoherent neutron scattering experiments, cells were treated with different additives before harvesting to induce distinct metabolic states, e.g. normal and apoptotic. Apoptosis was induced 24 hours before exposure to neutrons in confluent cells, by addition of both the peptide H-RCYVVM-OH in DMSO (0.5 mM, final concentration) and camptothecine (5 µM, final concentration) or solely camptothecin to serum free cell culture medium. The peptide is an activator of the CD47 complex [Cluster of Differentiation 47 (Brown and Frazier, 2001)] while camptothecin prevents DNA re-ligation and therefore causes DNA damage by binding to the topoisomerase type I/DNA complex. This binding prevents DNA re-ligation and is leading to DNA damage and apoptosis (Redinbo et al., 1998).

3.4 Isolation of mitochondria

To ensure isolation of mitochondria from tissue or cell culture in their native state, all buffers are isotonic and ice cooled. To protect proteins from degradation or oxidation protease inhibitor cocktail (PIC) as well as the antioxidant cocktail SCAVEGR® (Brewer et al., 2004) were utilized during homogenization as described in Frenzel (2006). Both are added freshly to the homogenization buffer at the day of preparation. SCAVEGR stock solution consists of superoxide dismutase (2.5 µg/mL), catalase (5 µg/mL), vitamin E (1 µg/mL), vitamin E acetate (1 µg/mL), reduced glutathione (1 µg/mL) und albumin (1 mg/mL). All buffers are sterile-filtered.

3.4.1 Isolation of mitochondria from rat brain

Homogenization buffer
5 mM HEPES/NaOH, pH 7.4
320 mM sucrose
1 mM Na^+/EDTA
in MilliQ water, stored at -20°C

Isolation of mitochondria from rat brain was performed on ice immediately upon dissection of non-frozen tissue. The brain tissue was homogenized in a motor driven, micropistill homogenizer (9 strokes, 600 rpm) with 4 volumes of homogenization buffer (i.e. 1 g tissue/4 mL buffer) containing 0.5% (v/v) protease inhibitor cocktail (Sigma P8340) and 2% (v/v) SCAVEGR (BrainBitsLLC/USA) on ice. After centrifugation at 1300 g (3 min, 4 °C) the supernatant containing the mitochondria was collected. To increase the yield, the pellet was washed twice with homogenization buffer (1500 g, 4 °C, 3 min). To collect the mitochondria, the merged supernatants were centrifuged at 17,000 g (10 min, 4 °C). The pellet was suspended in homogenization buffer (containing 0.5% PIC and 2% SCAVEGR). Aliquots of the mitochondrial fraction were shock-frozen in liquid nitrogen and stored at -80 °C.

3.4.2 Isolation of mitochondria from cell culture

Homogenization buffer

10 mM HEPES/NaOH, pH 7.4
1.1 mM Na^+/EDTA
in MilliQ water, stored at -20°C

Sucrose

2 M sucrose
in MilliQ water, stored at -20°C

$PBS^{-/-}$

140 mM NaCl
8.1 mM Na_2HPO_4
2.7 mM KCl
1.5 mM KH_2PO_4
pH 7.4, in MilliQ water, stored at 4°C

Isolation of mitochondria from cell cultures was performed on ice following a modified protocol by Rickwood et al. (1987). After discarding the medium, flasks were washed with $PBS^{-/-}$ and cells removed after covering with 1 mL homogenisation buffer containing 0.5% protease inhibitor cocktail (Sigma P8340) and 2% (v/v) SCAVEGR (BrainBitsLLC/USA). For mitochondria isolation, cells of 15 to 30 flasks (75 cm^2 each) were collected in centrifugation tubes. Upon centrifugation (700 g, 5 min, 4°C, swing-out rotor) the cell sediment was homogenized in a motor driven, glass/Teflon homogeniser (volume 2 mL, gap distance: 45-65 µm, Braun) with 2 mL homogenization buffer (9 strokes, 800 rpm). To minimise swelling of mitochondria and to retain their function and structure, 2 M sucrose was added immediately to achieve an iso-osmotic final concentration of 0.25 M. The homogenate was sedimented at 1700 g (10 min, 4 °C) and the supernatant containing the mitochondria collected. To increase the yield, the pellet was washed twice with homogenization buffer containing 0.25 M sucrose (1700 g, 4 °C, 10 min). To collect the mitochondria, the merged supernatants were centrifuged at 13,700 g (10 min, 4 °C). The pellet was suspended in homogenization buffer containing 0.25 M sucrose. Aliquots of the mitochondrial fraction were shock-frozen in liquid nitrogen and stored at -80 °C.

To obtain 1 mg of mitochondrial protein approx. 4.4×10^7 cells (determined for NHDF, AG1522D and WI38 cell lines) have to be used.

3.5 Bradford assay

The methodology to determinate protein concentrations via Bradford assay (Bradford, 1976) is described in detail in Frenzel (2006). With Roti®-Nanoquant solution (Fig. 3-1) samples with protein concentrations from 1 ng/µL can be detected (Roti®-Nanoquant manual, Roth, Karlsruhe). To determine protein concentrations from unknown samples, changes in the absorption wavelength of CBB G-250 were compared to bovine serum albumin (BSA) calibration curve.

3.5.1 Protein determination from tissue and cell culture samples

The protein determination was performed in microtiter plates (96 wells) as described by Frenzel (2006). The BSA standard with a stock concentration of 400 µg/mL was diluted in a range of 0 ng/µL-25 ng/µL for calibration curves. Samples were pre-diluted before protein determination (final dilution 10%). Dilutions of samples are shown in Table 3-1.

Table 3-1. Dilution of samples (10-times pre-diluted) for Bradford assay

dilution	V (sample) [µL]	V (MilliQ) [µL]
--	0	50.0
1:20	2.5	47.5
1:10	5.0	45.0
1:7	7.5	42.5
1:4	12.5	37.5
1:2	25.0	25.0

200 µL 1x Roti-Nanoquant working solution was added to 50 µL sample/standard and determination of CBB absorbance was performed with the Microtiter-Reader Polarstar Galaxy (absorption wavelengths: λ = 590 nm and λ = 485 nm) after 25 minutes incubation time at room temperature. MilliQ water was used as blank. The ratio of absorbance (590 nm/485 nm) of the BSA standard was versus the known BSA concentrations to enable determining the unknown protein concentration of samples. Duplicates of each dilution for both standard and sample were prepared. Relative protein concentrations were verified by comparing protein amounts loaded on 1D-SDS gels after staining with colloidal Coomassie Brilliant Blue G-250, gel scanning and quantitation.

3.6 Solubilisation of proteins

The solubilisation of proteins of mitochondrial membranes was described in detail by Frenzel (2006). In the present study the non-ionic detergent digitonin was utilized. It consists of a hydrophobic steroid skeleton and sugar residues as its hydrophilic part (Smith and Pickels, 1940). Digitonin allows gentle solubilisation preserving protein function and protein-protein interactions (Frenzel et al., 2010b; Krause et al., 2005). The optimal detergent to protein ratio for efficient solubilisation has to be determined at the beginning of each experiment. It depends on the type of sample (e.g. originating from tissue or cell culture, as there are variations in the lipid composition of membranes) and detergent (i.e. its molecular properties) (Guillon et al., 1978).

3.6.1 Solubilisation of mitochondrial membranes

Solubilisation buffer (1.11x)

33.33 mM	HEPES/HCl, pH 7.40
166.67 mM	potassium acetate
11.11% (w/v)	glycerol

in MilliQ water, stored at 4°C, sterile filtered

10% digitonin

10% (w/v) digitonin
Dissolve in 9-fold the volume (w/v) of MilliQ water, dissolved for 20 min at 90°C, freshly prepared the day of solubilisation

Pefabloc®-stock solution

0.5 M Pefabloc®
in MilliQ water, stored at -20°C

Solubilisation of mitochondria was performed at 4 °C according to Reifschneider et al. (2006) for 30 minutes using 2, 4 and 8 g digitonin/g protein at a final detergent concentration of 1% (w/v). The digitonin was of high purity and freshly dissolved the day of solubilisation. Crude mitochondrial were thawed and homogenisation buffer removed by adding 800 µL solubilisation buffer and centrifugation (20,800 g, 8 min, 4°C). The sediment containing mitochondria was resuspended in solubilisation buffer containing 0.5 mM Pefabloc (freshly added). Solubilisation was started by adding detergent in the required detergent to protein ratio and final concentration. During solubilisation, the extract was mixed every 5 minutes with a vortexer. Solubilized proteins were separated as detergent mixture (supernatant) from membrane fragments via centrifugation (20,800 g, 4°C, 10 min).

3.7 Polyacrylamide gel electrophoresis

The methodology of polyacrylamide gel electrophoresis (PAGE) was described in detail by Frenzel (2006). In the present study so-called discontinuous gels were utilized (Davis, 1964; Ornstein, 1964). They consist of a stacking gel with larger pores followed by the separating gel with smaller pores. During electrophoresis, samples are first focused in the stacking gel, which leads to increased resolution in protein separation and decreased protein aggregation. Additionally, gradient gels, characterized by a separation gel with continuously decreasing pore size, were used which increases the resolution of protein bands (Seelert and Krause, 2008).

3.7.1 Blue-native polyacrylamide gel electrophoresis (BN-PAGE)

The BN-PAGE allows separation of proteins in their native form due to omitting SDS in buffers. BN-gels are gradient gels composed of a stacking gel with large pores and a separating gel with pores that are gradually decreasing in size. The extent of the gradient can be manipulated (Krause and Seelert, 2008; Seelert and Krause, 2008). In BN-PAGE,

Coomassie Brilliant Blue G-250 is present in the cathode buffer binding to proteins almost proportional to their size. The intrinsic charge of amino acid residues is masked by the negative charge of CBB molecules with minor effects on protein structure or protein-protein interactions. Hence proteins are separated according their molecular mass and enzyme activity can still be determined in in-gel activity tests.

Light BN-PAGE gel buffer (3x)

1.5 M 6-aminohexanoic acid
75 mM imidazole/HCl, pH 7.0
in MilliQ water, stored at 4°C

Heavy BN-PAGE gel buffer (3x)

1.5 M 6-aminohexanoic acid
75 mM imidazole/HCl, pH 7.0
60% (w/v) glycerol
in MilliQ water, stored at 4°C

BN-PAGE sample buffer

50 mM Bis-Tris/HCl, pH 7.0
5% (w/v) Coomassie Brilliant Blue G-250
500 mM 6-aminohexanoic acid
in dest. water, stored at RT in the dark

BN-PAGE anode buffer

25 mM imidazole/HCl, pH 7.0
in bidest. water, stored at 4°C

BN-PAGE cathode buffer

50 mM Tricine
7.5 m imidazole
0.02% (w/v) Coomassie Brilliant Blue G-250
pH 7.0
in bidest. water, stored at RT;
dye is resolved by stirring over night;filtered

10% (w/v) Ammonium persulfate (APS)

in MilliQ water, stored up to 2 months at −20°C. Always used freshly thawed solution.

Linear gradient gels with a total acrylamide concentration of 4–13% overlaid with a 3.5% stacking gel for large gels were used for rat brain cortex, striatum and hippocampus for large gels (Table 3-2) allowing separation of proteins from 100 kDa to 3 MDa (Frenzel et al., 2010b). Protein extracts from cell culture were separated on small BN-gels with a gradient of 3-13% and a stacking gel of 3% (Table 3-3) (Dani and Dencher, 2008; Krause and Seelert, 2008; Neff and Dencher, 1999; Reifschneider et al., 2006).

Table 3-2. Composition of BN polyacrylamide separating and stacking gels (large size: 16 cm x 18 cm x 1.5 mm)

	separating gel T = 4%, C = 3%	**separating gel T = 13%, C = 3%**	**stacking gel T = 3.5%, C = 3%**
Rotiphorese® Gel A	1.9 ml	0.71 mL	1.7 mL
Rotiphorese® Gel B	0.89 mL	--	0.79 mL
Rotiphorese® Gel 29:1	--	4.28 mL	--
Light BN gel buffer (3x)	4.9 mL	--	5.0 mL
Heavy BN gel buffer (3x)	--	4.94 mL	--
MilliQ water	7.0 mL	ad 14.78 mL	7.4 mL
TEMED	6.8 µL	4.1 µL	11.9 µL
APS	86 µL	41 µL	119 µL
Total volume	14.82 mL	14.82 mL	15 mL

Table 3-3. Composition of BN polyacrylamide separating and stacking gels (small size: 10.0 cm x 8.2 cm x 1.5 mm)

	separating gel T = 3%, C = 3%	**separating gel T = 13%, C = 3%**	**stacking gel T = 3%, C = 3%**
Rotiphorese® Gel A	1.44 ml	0.71 mL	1.45 mL
Rotiphorese® Gel B	0.67 mL	--	0.68 mL
Rotiphorese® Gel 29:1	--	4.28 mL	--
Light BN gel buffer (3x)	4.94 mL	--	5.0 mL
Heavy BN gel buffer (3x)	--	4.94 mL	--
MilliQ water	7.6 mL	4.8 mL	7.6 mL
TEMED	6.8 µL	4.1 µL	20 µL
APS	68 µL	41 µL	200 µL
Total volume	14.72 mL	14.77 mL	14,95 mL

The linear gradient of the separating gel was established using a gradient mixer from the bottom up in the gel chamber as described by Krause and Seelert (2008). Separation of rat brain mitochondrial proteins occurred on gels with a size of 16 cm x 18 cm x 1.5 mm. Sample buffer was added immediately before loading of a sample into the well of the gel with a ratio of 2 volumes sample buffer per 1 volume of digitonin in the sample.

Gel electrophoresis of large gels was performed at 4°C. Initially, voltage was set to 100 V and current to 15 mA until the blue-colored front was migrated to the separating gel, indicating that the proteins were completely present in the stacking gel matrix. Thereafter the voltage was set to 500 V. Once 20-25% of the total distance was completed, the cathode buffer containing 0.02% (w/v) CBB G-250 was exchanged for cathode buffer with 0.002% (w/v) CBB G-250 in order to reduce the background staining of the gel matrix. For small gels the exchange step was omitted and only 0.002% (w/v) CBB G-250 cathode buffer and a maximum voltage of 250 V was used. These gels were water-cooled. Electrophoresis was stopped when the dye front has reached the end of the gel.

For mass calibration, high molecular weight (HMW, Table 3-4) protein standard was used. Hence solubilized membrane proteins or protein complexes are surrounded by detergent molecules as well as some residual lipids (both influencing the migration behavior); the HMW (mixture of water soluble proteins) solely helps to estimate the molecular mass of separated membrane proteins.

Table 3-4. Protein mixture of high molecular weight standard

protein	**Molecular mass [kDa]**
thyroglobulin (pork)	669
ferritin (horse)	440
catalase (bovine)	232
lactate dehydrogenase (bovine)	140
bovine serum albumin (bovine)	67

3.7.2 SDS polyacrylamide gel electrophoresis (SDS-PAGE)

SDS-PAGE employs sodium dodecyl sulfate (SDS) an ionic detergent that denature proteins and masks their intrinsic charge [average ratio of 1.4 g SDS per g protein (Lottspeich and Engels, 2006)]. Hence, after addition of a saturating amount of SDS, proteins have identical negative charge per unit mass allowing separation according to apparent mass. The large negative charge also prevents protein aggregation. The distance migrated by proteins in the gel is proportional to the logarithm of the molecular mass over a large range. This is utilized to determine the molecular mass of separated proteins by comparison with a molecular mass standard of water soluble proteins.

3.7.2.1 ***2D-Tricine SDS polyacrylamide gel electrophoresis***

After the native BN-PAGE a denaturing SDS gel electrophoresis can follow (Krause and Seelert, 2008; Schagger and von Jagow, 1987). Lanes from the first dimension BN-PAGE are excised and analyzed by a second dimension SDS–PAGE that allows separation of peptides with a molecular mass of 1-100 kDa. This enables a more detailed analysis of proteins or subunits of protein complexes. Following native BN-PAGE, gels were cut in lanes, incubated in denaturing solution, containing 1% (v/v) mercaptoethanol and 1% (w/v) SDS, for 1h. After incubation, the lanes were embedded in a new gel matrix (5% stacking gel). In 2D-SDS gels, subunits are separated according to their molecular mass in a vertical line below the position of the protein complex in the first dimension (i.e. the BN-PAGE lane). Protein complexes from the first dimension can be identified due to their specific subunit pattern in the second dimension.

Denaturing solution

1% (v/v) β-mercaptoethanol
1% (w/v) SDS
in MilliQ water, stored at -20°C

SDS gel buffer (3x) for stacking gels

3 M Tris/HCl, pH 8.5
0.15% (w/v) SDS
in MilliQ water, stored at RT, sterile-filtered

SDS gel buffer (3x) for separation gels

3 M Tris/HCl, pH 8.5
0.15% (w/v) SDS
30% (w/v) glycerol
in MilliQ water, stored at RT, sterile-filtered

Cathode puffer for 2D-Tricine-SDS gels

100 mM Tris
100 mM Tricine
0.05% (w/v) SDS
pH 8.25, in bidest. water, stored at 4°C

Anode buffer for 2D-Tricine-SDS gels

100 mM Tris/HCl, pH 8.9
in bidest. water, stored at 4°C

Washing of the BN-gel stripes in with MilliQ water after incubation in denaturing solution is crucial because mercaptoethanol affects the polymerization of acrylamide. The BN-gel lane

was positioned on top of a gel chamber. Three gel layers were casted from bottom to top: (1) 13% denaturing separation gel, (2) 5% denaturing stacking gel and (3) 5% native stacking gel (surrounding the BN-gel stripe) The composition of two large (16 cm x 18 cm x 1.5 mm) and four small 2D-SDS (10.0 cm x 10.5 cm x 1.5 mm) gels is shown in Table 3-5.

Table 3-5. Composition of 2D-SDS Tricine gels with 13% separation gel and 5% stacking gels

	separating gel T=13%, C=3%	**stacking gel denat. T=5%, C=3%**	**stacking gel „nativ“ T=5%, C=3%**
Rotiphorese® Gel A	2.6 mL	1.62 mL	1.62 mL
Rotiphorese® Gel B	--	0.75 mL	0.75 mL
Rotiphorese® Gel 29:1	17.6 mL	--	--
SDS gel buffer (3x) with glycerol	20.0 mL	--	--
SDS gel buffer (3x) without glycerol	--	3.30 mL	--
BN gel buffer (3x)	--	--	3.30 mL
20% (w/v) SDS	--	--	100 µL
MilliQ water	19.5 mL	4.28 mL	4.13 mL
TEMED	30 µL	5 µL	7 µL
APS	300 µL	50 µL	70 µL
total volume	60 mL	10 mL	10 mL

For calibration of protein mass and normalization of protein staining for quantitative analysis, low molecular weight (LMW) protein standard (Table 3-6) was applied on each gel in equal amount.

Table 3-6. Protein mixture of low molecular weight standard

protein	**Molekular mass [kDa]**
phosphorylase b	97.0
albumin	66.0
ovalbumin	45.0
carbonic anhydrase	30.0
trypsine inhibitor	20.1
α-lactalbumin	14.4

Gel electrophoresis was performed at 20-50 V, 60 mA, until the dye front entered the separation gel. Then the voltage was increased to 100-130 V. The electrophoresis was stopped when all CBB G-250 left the gel matrix.

3.7.2.2 ***<u>One dimensional SDS polyacrylamide gel electrophoresis (1D-SDS-PAGE)</u>***

One dimensional denaturing SDS-PAGE was performed as described by Frenzel (2006) using a 5% stacking and 13% separation gel (Table 3-7) and Laemmli Tris-HCl/Tris-glycerol buffer system (Laemmli, 1970) allowing high resolution protein separation. Protein-protein interactions as well as the structure of individual proteins were destroyed using high SDS

concentrations and disulfide bonds were broken adding β-mercaptoethanol or dithiothreitol (DTT) in the sample buffer.

In the present study 1D SDS PAGE was used either (1) as a tool to verify protein concentrations determined in preceding Bradford assays after protein staining with colloidal CBB, or (2) to calculate solubilisation efficiency by analyzing the respective amount of protein present in the sediment and detergent extract, respectively, after solubilisation, as well as (3) for further Western Blot/OxyBlot analysis.

Stacking gel buffer
1 M Tris/HCl, pH 6.8
in dest. water, stored at RT

Separation gel buffer
1.5 M Tris/HCl, pH 8.8
in dest. water, stored at RT

5% SDS solution
5% (w/v) SDS
in dest. water, stored at RT

Electrophoresis buffer
400 mM glycerol
50 mM Tricine
0.1% (w/v) SDS
pH 8.5, in dest. water, stored at RT

SDS sample buffer
15% (w/v) sucrose
2.5% (w/v) SDS
0.25% (w/v) sodium carbonate
0.04% (w/v) bromophenol blue
25 mM DTT
in dest. water, stored at -20°C

Before adding SDS, APS and TEMED, the mixture of acrylamide, cross linker, buffer and water was degassed for 10 to 15 minutes to avoid on one hand the formation of air bubbles that may appear during polymerization, especially in thin 1 mm deep gels used in a following Western Blot analysis. On the other hand oxygen affects the polymerization. Thick mini-gels with 1.5 mm depth were utilized for analysis of solubilization efficiency and Bradford control gels.

Table 3-7. Composition of 1D SDS gels with 13% separation gel and 5% stacking gel

	separation gel T=13%, C=4%	**stacking gel T=5%, C=3.3%**
Rotiphorese® Gel A	8.32 mL	--
Rotiphorese® Gel B	5.20 mL	--
Rotiphorese® Gel 29:1	--	1.25 mL
1.5 M separation gel buffer	5.00 mL	--
1 M stacking gel buffer	--	1.25 mL
20% (w/v) SDS	100 µL	50 µL
MilliQ water	1.20 mL	7.34 mL
TEMED	15 µL	10 µL
APS	150 µL	100 µL
total volume	20 mL	10 mL

Before applying the wells, samples were mixed with an equal volume of SDS sample buffer. Protein sediments that were analyzed for determination of solubilization efficiency were solved in 5% (w/v) SDS with 50 µL SDS per 100 µg protein before solubilisation.

Electrophoresis was performed at 50 mA/gel and 100 V until proteins had entered the gel matrix completely. Then the voltage was increased to 130 V.

3.8 In-gel activity assay

3.8.1 NADH coenzyme Q reductase (complex I)

Complex I is visualized in in-gel activity tests in native-gels by the violet color of formazan. Formazan is emerging when NBT (nitro blue tetrazolium chloride) is reduced by electrons released during oxidation of NADH by the NADH coenzyme Q reductase provided that native gel electrophoresis was performed. The activity test was carried out according to Kuonen et al. (1986) and Grandier-Vazeille and Guerin (1996) with modified buffer conditions.

Working buffer for complex I activity assay

100 mM	Tris
768 mM	glycerol
0.04% (w/v)	nitro blue tetrazolium chloride (NBT)
0.1 mM	β-NADH

pH 7.4 (HCl), in MilliQ water, stored at -20°C

The specific procedure for buffer preparation is described by Frenzel (2006). Gels were incubated in the working solution on a shaker for approx. 1h (RT). The reaction was stopped by washing the gel with MilliQ water several times. Gels may be stored after protein fixation using 50% (v/v) methanol and 10% (v/v) acetic acid for 10 min.

3.8.2 Succinate dehydrogenase (complex II)

The in-gel activity test of complex II has been performed in an analoguous manner as the test for complex I with sodium succinate as substrate for succinate dehydrogenase.

Working buffer for complex II activity assay

100 mM	Tris
768 mM	glycerol
0.04% (w/v)	Nitro blue tetrazolium chloride (NBT)
1 mM	Sodium succinate dibasic hexahydrate

pH 7.4 (HCl), in MilliQ water, stored at -20°C

Gels were incubated for approx. 3h until optimal staining. The reaction was stopped by washing the gel several times with MilliQ water. Gels may be stored after protein fixation using 50% (v/v) methanol and 10% (v/v) acetic acid for 10 min.

3.8.3 Cytochrome c oxidase (COX) (complex IV)

Electrons from DAB are utilized in the oxidation of ferrocytochrom c catalyzed by COX. Therefore, complex IV can be detected in in-gel activity tests due to the dark brown color of oxidized DAB, i.e. precipitates of polymeric DAB oxides or DAB indamines. In this thesis, the protocol of Angermüller and Fahimi (1981), modified by Zerbetto et al. (1997), was applied.

Working buffer for complex IV activity assay

50 mM	NaH_2PO_4/Na_2HPO_4/HCl, pH 7.4
25 mg	DAB tetrahydrochloride
25 mg	cytochrome c (horse heart)
0.5 mg	catalase (bovine liver) (20-25 units/mL)
3.75 g	sucrose

in 50 mL MilliQ water, stored at -20°C

Gels were incubated on a shaker for 1 to 1.5 hours until sufficient staining intensity was achieved. The reaction was stopped by washing the gel with MilliQ water several times. Gels may be stored after protein fixation using 50% (v/v) methanol and 10% (v/v) acetic acid for 15 minutes.

3.8.4 ATP synthase (complex V)

Determination of complex V ATPase activity was performed according to Zerbetto et al. (1997). The γ-phosphate released during ATP hydrolysis reacts with the lead ions of the reagent to form insoluble lead phosphate which can be detected as white precipitate in the gel. The hydrolysis reaction is catalyzed by the ß-subunit of the ATP synthase. Therefore, not only complex V monomers or oligomeric forms but also unbound F_1 (the soluble subunit of ATP synthase) is detected.

Working buffer for complex V activity assay

35 mM	Tris/HCl, 7.8
270 mM	glycerol
14 mM	magnesium sulfate
0.8 mM	ATP
0.05% (w/v)	lead(II) nitrate

in MilliQ water, stored at -20°C

ATP was added after adjusting the pH. The reaction was stopped with MilliQ water after 1 to 12 hours.

3.9 Protein staining in gels

3.9.1 Staining with Coomassie Brilliant Blue R-250

Visualization of proteins with CBB R-250 (Fig. 3-1) in gel matrices was devised by Fazekas de St. Groth et al. (1963) the first time. CBB R-250 is binds cationic and hydrophobic amino acid residues semi-quantitatively. Hence proteins containing these residues are stained more efficiently. The detection limit is approximately 0.3 µg protein per lane (Gorg et al., 1978).

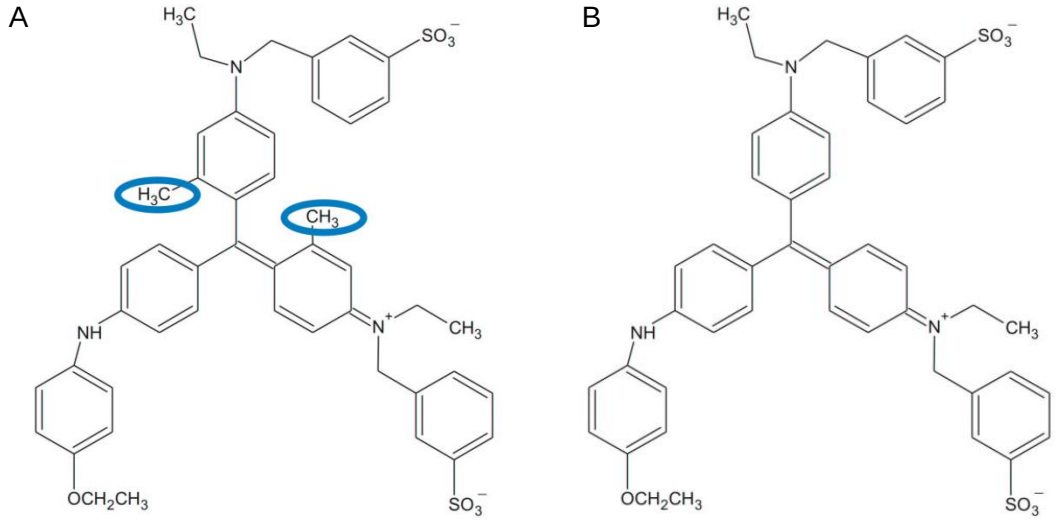

Fig. 3-1. Coomassie Brilliant Blue G-250 (A) und R-250 (B).

In contrast to CBB R-250 (right), CBB G-250 (left) contains two additional methyl groups (indicated in blue). Image source: (Krause, 2004)

Coomassie staining solution

0.5% (w/v)	$Cu^{II}SO_4$*5 H_2O
10% (v/v)	acetic acid p.A.
45% (v/v)	methanol
0.15% (w/v)	Coomassie Brillant Blue R-250

in dest. water, stored at RT

Coomassie destaining solution

0.5% (w/v)	$Cu^{II}SO_4$*5 H_2O
10% (v/v)	acetic acid p.A.
25% (v/v)	methanol

in dest. water, stored at RT

Polyacrylamide gels were incubated in the Coomassie staining solution for 20-40 min (or over-night) with gentle shaking for even exposure. Fixation of proteins occurs in addition caused by methanol and acetic acid. After staining, gels were incubated in destaining solution until proper background contrast was reached.

3.9.2 Colloidal Coomassie staining

Colloidal Coomassie staining enables detection and quantitation of protein amounts at the nanogram-level with low background but high sensitivity.

3.9.2.1 ***Fermentas staining***

The PageBlue™ protein staining solution (Fermentas) with colloidal CBB G-250 allows protein quantitation in 1D SDS gels with a detection limit of 5 ng and a linear dynamic range of 5 ng-500 ng. Small background staining can be removed by several washing steps with MilliQ water. Harmful substances like methanol and acetic acid are not necessary in this protocol (manual Fermentas).

Gels were washed three times in 100 mL MilliQ (for subsequent MALDI-MS analyses) or dest. water to remove residual buffer solution. Fermentas staining solution was added for 60 minutes or over-night (incubation on a shaker). Background and excess staining was removed using water.

3.9.2.2 ***Roti®-Blue staining***

With Roti®-Blue staining solution, proteins separated on polyacrylamide gels can be stained with a detection limit of <30 ng/protein and low background staining (Roti®-Blue manual). The dye also contains colloidal CBB G-250.

Gels were incubated over night (15h) in 1x Roti®-Blue staining solution and then washed in 25% (v/v) methanol (in bidest. water) for 5 minutes.

3.9.3 Silver staining according to Blum

This staining procedure is very sensitive with a detection limit of 1-10 ng, depending on the protocol employed but without a large dynamic range. It is a caveat of this method that silver staining is non-quantitative, due to the fact that every protein is characterized by its own staining intensity and color, and also less reproducible. Application of clean glassware, pure reagents and water of highest purity increases the staining quality.

In the present study the silver staining protocol of Blum (1987) was used, as it allows further identification of proteins by MALDI-MS. The detection limit is 5-30 ng protein per band. For further MALDI-MS analysis MilliQ water and pure reagents have to be used.

Staining protocol:

1.	Fixation 1:	2 x 30 min	
		12% (v/v)	acidic acid
		50% (v/v)	methanol
2.	Fixation 2:	3 x 20 min	
		50% (v/v)	ethanol
3.	Sensitation:	1 x 1 min	
		0.02% (w/v)	$Na_2S_2O_3$•5 H_2O
4.	Washing:	2 x 1 min	
			Dest. H_2O
5.	Silver staining:	20 min	
		0.2% (w/v)	$AgNO_3$
		0.026% (v/v)	formaldehyde (35% stock solution)
6.	Washing:	1 x 1 min	
			Dest. H_2O
7.	Developing:	until sufficient staining intensity	
		6% (w/v)	Na_2CO_3
		0.005‰ (w/v)	$Na_2S_2O_3$•5 H_2O
		0.017% (v/v)	formaldehyde (35% stock solution)
8.	Stop 1:	washing in dest. H_2O for a short time	
9.	Stop 2:	1 x 10 min	
		10% (v/v)	acetic acid
10.	Storage:	max. one day	
		1% (v/v)	acetic acid

3.9.4 SYPRO Ruby® staining

For proteome analysis with protein quantitation in polyacrylamide gels (2D SDS gels in this study, but also applicable for 1D SDS) the fluorescent dye SYPRO Ruby with a large linear quantitation range of 3.3 orders of magnitude and a detection limit of 1 ng protein/spot is used (Wheelock et al., 2006). SYPRO Ruby consists of an organic component and a heavy metal component (ruthenium complex) (SYPRO Ruby manual) with excitation peaks at ~280 nm and ~450 nm and an emission maximum near 610 nm. It binds SDS-protein-complexes with high sensitivity (Soehn, 2009) and without background signals. In contrast to silver staining, proteins are stained quantitatively (i.e. proportional to the protein amount) with SYPRO Ruby. Additionally, proteins difficult to stain using other methods (i.e. glycoproteins, lipoproteins and Ca^+-binding proteins) can be stained with SYPRO Ruby. Nucleic acids, lipopolysaccharides, lipids and glycolipids are not or only to a minor extent visualized.

SYPRO Ruby staining does neither affect further protein staining protocols nor protein identification by MALDI-MS.

Staining protocol:

1.	Fixation:	3-4 h or over night	
		10% (v/v)	methanol
		7% (v/v)	acetic acid
2.	Staining:	3-4 h	
			pure staining solution
3.	Washing:	10 min	
		10% (v/v)	methanol
		7% (v/v)	acetic acid

Gels were placed in bidest water after washing. The SYPRO Ruby signal was analyzed using the Fujifilm LAS-3000 with a CCD camera and the software “Image Reader LAS-3000”. Excitation wavelength was set on 460 nm (blue diode). For detection of the fluorescent signal the filter for 605 nm (band pass) and an iris of F0.85 was utilized.

3.10 Western blot analysis

The protocol for Western blot analysis was developed by the laboratory of George Stark at the Stanford university (Burnette, 1981). The Western blot is a method to detect immunologically specific proteins in a sample from tissue homogenate or extract. After protein separation under both native and denaturizing conditions in polyacrylamide matrices, proteins are transferred to a membrane (e.g. nitrocellulose or PVDF), where they are detected with specific targeted antibodies targeted against a special epitope of the protein of interest (Renart et al., 1979; Towbin et al., 1979).

In the present study Western blotting was utilized to detect specific protein species and proteins with specific posttranslational modifications (e.g. carbonylation). Denaturing 1D-SDS-PAGE was performed using 5% stacking and 13% separation gel (as described in chapter 3.7.2.2) and the Laemmli buffer system (Laemmli, 1970). Protein amounts of 2.5-20 µg were loaded per lane.

3.10.1 Electro-blotting (semi-dry)

Electro-blotting is applied to transfer proteins from a gel onto a membrane using an electric current. During this procedure, proteins are transferred maintaining the sequence they were separated into by PAGE. Electro-blotting (semi-dry) of proteins onto a PVDF membrane was performed as described by Suhai et al. (2008).

Anode transfer buffer

10% (v/v) Roti®-Blot 2A
5% (v/v) methanol p.A.
in MilliQ water, stored at RT

Cathode transfer buffer

10% (v/v) Roti®-Blot 2K
20% (v/v) methanol p.A
in MilliQ water, stored at RT

Following electrophoresis, 1D SDS gels were incubated in electrophoresis buffer for 15 minutes (chapter 3.7.2.2) on a shaker. For blotting, the PVDF membrane was dipped into 100% (v/v) methanol and placed on a Whatman filter paper, wetted with anode transfer buffer and laid on the anode of the blotting device (Fig. 3-2). Next the gel was positioned on the membrane, thereon was put a second layer of Whatman filter paper wetted with cathode transfer buffer and the lid (cathode). During this stacking it was taken care to prevent the formation of air bubbles between the layers.

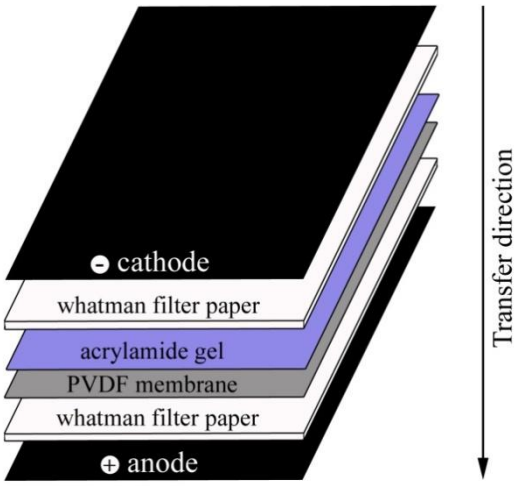

Fig. 3-2. Setup for semi-dry electro-blotting

Blotting occurred at RT for 45 minutes at 25 V and 1 mA/cm^2 membrane. The efficiency of the protein transfer was checked by staining the gels with Roti®-Blue after blotting.

3.10.2 Immunodetection of proteins with alkaline phosphatase

Proteins transferred to PVDF membranes were visualized by antibodies (immunodetection). In the present study all antibodies were diluted in protein-free T20 (PBS) Blocking Buffer (Thermo Scientific).

10x PBS

0.188 M NaH_2PO_4•2 H_2O
0.81 M Na_2HPO_4
1.45 M NaCl
in bidest. water, stored at 4°C

1x PBS-T

10% (v/v) PBS
0.05% (v/v) Tween® 20
in bidest. water, stored at 4°C

Membranes were incubated for 1 hour or overnight (at RT, under gentle agitation) in Roti®-Block blocking buffer to prevent unspecific binding of primary antibodies on the membrane (background staining). In the next step, blocking solution is replaced by the primary antibody (incubation for 1h, at RT, on a shaker), which ideally binds solely its antigenic target protein, i.e. with high specificity. Unbound antibodies are removed by two washing steps using 1x PBS-T at RT, followed by 15 minutes shaking at RT and two final washing steps with 1x PBS and 5 minutes shaking incubation. Membranes were incubated again for 1 hour (at RT, on a shaker) with the secondary antibody that is directed at the species-specific, conserved portion of the primary antibody and was labeled with the enzyme alkaline phosphatase (AP) in the present study.

AP catalyzes the dephosphorylation of 5-bromo-4-chloro-3-indolyl phosphate (BCIP), which then forms dimers. Protons released during dimerization reduce nitroblue tetrazolim (NBT) in a colorimetric reaction that yields an insoluble dark blue diformazan precipitate. Compared to other enzymes, the advantage of alkaline phosphatase is that - due to the fact that its reaction rate remains linear in time - the sensitivity or the staining intensity can be improved simply by allowing the reaction to proceed for a longer time period. The disadvantage is that prolonged AP staining is often accompanied by a high background signal resulting in a low signal-to-noise ratio.

Solution A		**Solution B**	
100 M	Tris	37.5 µL	BCIP [5% (w/v) in bidest water]
10 M	$MgCl_2$	50 µL	NBT [7.7% (w/v) in 70% DMF)
100 M	NaCl	both solutions stored at -20°C, freshly added the day of preparation	
pH 9.5, in bidest. water, stored at 4°C			

The colorimetric reaction was started after adding the mixture of solution A (10 mL) and B to the membrane and stopped by adding water.

3.10.3 OxyBlot

A specific application of Western Blot is the OxyBlot that allows the immunoblot detection of carbonyl groups introduced into proteins by oxidative reactions with reactive oxygen species or ozone or oxides of nitrogen or by metal catalyzed oxidation. With this assay 5 femtomol of carbonyl residues can be detected.
The carbonyl groups are derivatized to 2,4-dinitrophenylhydrazone (DNP) by reaction with 2,4-dinitrophenylhydrazine (DNPH) before protein separation on 1D SDS gels. Two aliquots of each sample were treated (Fig. 3-3). One aliquot was subjected 15 minutes at RT to the derivatizing reaction and the other, as negative control, was treated with the 1x Derivatization-Control Solution instead of the 1x DNPH Solution of the assay kit.

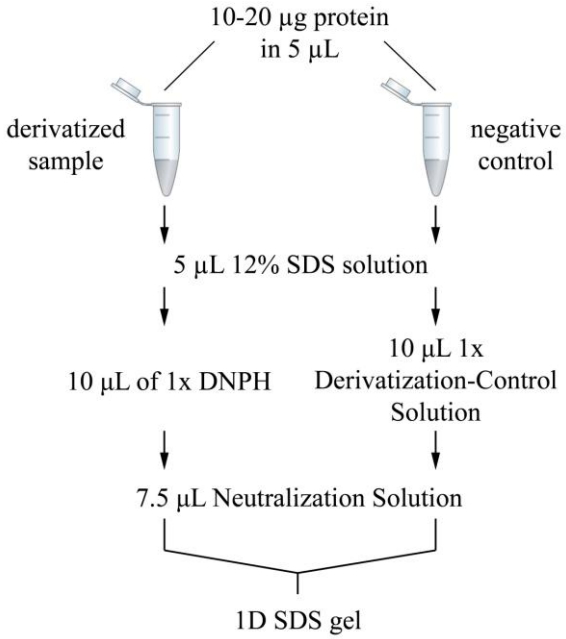

Fig. 3-3. OxyBlot assay

Additionally a positive control was prepared. BSA (Fraktion V) was exposed to highly oxidizing conditions to ensure at least one strong signal for immunodetection. Iron ions serve as catalysts during protein oxidation. From the positive control, also two aliquots were prepared. One aliquot was derivatized and the other treated with the control solution.

Buffer for positive control	
25 mM	HEPES
25 mM	ascorbic acid (Na-salt)
100 µM	$FeCl_3$
pH 7.2, in bidest. water, stored at RT	

Dialysis buffer	
50 mM	HEPES
1 mM	EDTA
in bidest. water, stored at RT	

BSA (10 mg/mL) was incubated for 5h at 37°C in the buffer for positive control. Thereafter, Fe^{3+} ions were removed by dialysis over night with gentle stirring (1 mL oxidized protein solution per 1 L dialysis buffer). The positive control was stored at 4°C.
Protein separation was performed on 1D SDS gels (chapter 3.7.2.2). The procedure of Western Blot is similar to the one as described in chapter 3.10.1 except for the membrane incubation before blotting. Instead of methanol 95% (v/v) ethanol was used. After electro blotting, membranes were blocked with 1% (w/v) BSA in 1x PBS-T. The primary antibody against DNP of the OxyBlot assay was diluted likewise in 1% (w/v) BSA in 1x PBS-T.

3.11 Quantitation of protein abundances

Quantitation of protein bands on 1D BN-gels was performed using a GS-800 calibrated densitometer (BioRad) and Quantity One Software (BioRad, Version 4.4.0). Protein staining intensities of colloidal CBB were expressed at optical density (OD) in figures of data plotted.

Quantitation of protein abundances on 2D BN/SDS gels was performed after visualizing of protein staining with fluorescent SYPRO Ruby using a CCD camera system (LAS-3000, Fuji) and the software Image Reader LAS-3000 with the software Delta2D (Decodon, Greifswald, Germany), as described in detail by Frenzel (2006). All gels included in the analysis were compared directly with each other and the staining intensity (reflecting the protein abundance) indicated in grey units (GU). Gray units represent the sum of pixels belonging to one protein spot. Background subtraction was performed automatically. One black pixel without background represents for an absolute quantity of 1.

3.12 Normalization procedure

To facilitate comparison of different samples, always the same amount of digitonin extract of mitochondria was loaded per lane, e.g., 100 µg or 120 µg protein (before solubilisation) on the first dimension for the 1D- and 2D-BN/SDS-PAGE (large 16 cm x 18 cm x 1.5 mm gels), respectively, and 20 µg or 40 µg protein (before solubilisation) for small 1D-and 2D-BN/SDS-PAGE, respectively.

CBB staining intensities of protein bands on first dimensional BN gels could be compared directly after background subtraction since all samples were separated and stained together on the same gel.

To compensate differences in staining efficiency during quantitation of different 2D BN/SDS gels, a normalization procedure was developed, using low molecular weight protein standards, added in the same amount to each 2D-gel (Frenzel, 2006). For any gel, a correction factor was calculated and applied by considering the SYPRO Ruby fluorescence intensities of four marker bands [phosphorylase b (97 kDa), albumin (66 kDa), ovalbumin (45 kDa) und carbonic anhydrase (30 kDa)]. All measured protein spot intensities were corrected by multiplication with the resulting specific correction factor. Although SYPRO Ruby has a large linear dynamic quantification range (see also chapter 3.9.4) only the spot-intensities of identical proteins can be directly compared since different protein species have different staining behavior, depending on the amino acid composition and the amount of bound SDS. The biological variances as well as technical sources of error were minimized by analyzing four different animals per age group, and – for rat brain cortex – each sample separately in duplicate. Statistical analysis between two age-groups was performed using one-way ANOVA. The significance level was set at $P < 0.05$.

3.13 MALDI mass spectrometry

Protein spots in 2D BN/SDS PA gels were identified by MALDI-TOF-MS analysis, performed as described in detail by Rexroth (Rexroth, 2004) and Reifschneider (2006) or identified according to recent protein profiling of rat brain mitochondria by peptide mass fingerprinting (Reifschneider et al., 2006).

3.14 Measurement of cellular ATP

The cellular ATP level was analyzed by the luciferin/luciferase ATP assay (ATP Kit SL, BioThema) allowing quantitation of ATP over a range of 10^{-12}-10^{-6} mol/L. During ATP consumption by the firefly luciferase reaction light is emitted with a low decay rate (around 0.9% per min) that allows continuous monitoring of ATP level for several minutes.

Tris buffer	**TCA solution**	
50 mM Tris	10% (v/v)	TCA
pH 7.8 adjusted with 20% acetic acid,	4 mM	EDTA
in bidest. water, stored at 4°C	in bidest. water, stored at 4°C	

Cell suspensions containing 8000 cells/µL were incubated for 2 min with an equal volume of TCA solution at room temperature. The reaction was stopped by addition of 50-times the volume of Tris-buffer. From each sample 20 µL cell extract containing 1600 cells, 500 µL Tris-buffer and 12.5 µL ATP Reagent SL (lyophilised reagent containing D-luciferin and luciferase) was employed for ATP determination. ATP concentration of samples was calculated by reference to ATP standards (10^{-9}-10^{-6} mol/L).

3.15 Measurement of intracellular ROS-level

The amount of reactive oxygen species in e.g. cells can be monitored using fluorescence methods. Intracellular ROS-levels were determined by flow cytometry using 2´,7´-dichlorodihydrofluorescein (DCFH, sensitive preferentially for $OH^{\bullet}$ and $ONOO^{-}$) and dihydroethidium (DHE, sensitive predominantly for $O_2^{\bullet-}$) (Halliwell and Gutteridge, 2007).

The conversion of the non-fluorescent DCFH-DA to the highly fluorescent compound 2',7'-dichlorfluorescein (DCF) occurs in several steps. DCFH-DA can enter cells freely but is trapped within the cells after deacetylation by intracellular esterases to form the non-fluorescent 2',7'-dichlorfluorescein (DCFH). DCFH is converted by peroxidases in several reaction steps to green fluorescent DCF^{-} via an intermediate radical $DCF^{\bullet-}$ (Halliwell and Gutteridge, 2007; Owusu-Ansah et al., 2008).

Dihydroethidium (DHE) also freely permeates membranes and is used to monitor superoxide production (Bindokas et al., 1996; Li et al., 2003; Owusu-Ansah et al., 2008; Rivera and Maxwell, 2005). Upon reaction with superoxide radical anions DHE forms a red fluorescent product (2-hydroxyethidium) (Zhao et al., 2005). DHE is highly specific as it detects essentially superoxide radicals, is retained well by cells and even tolerate mild fixation (Owusu-Ansah et al., 2008).

Cells were trypsinized, centrifuged (100 g, 10 min, RT), resuspended in $PBS^{-/-}$ (37°C, recipe see chapter 3.4.2) and again centrifuged (100 g, 10 min, RT). Under dark conditions, $PBS^{-/-}$ (37°C), containing 25 µM DCFH-DA (30 min, 37°C) or 4 µM DHE (10 min, 37°C), was added for final cell concentration of 1×10^5 cells/ml. The fluorescence (DCF: λ_{em} = 515-550 nm;

DHE: λ_{em} = 570-600 nm) of 10^4 cells was measured at room temperature using the flow cytometer PAS III (Partec) with excitation wavelength of λ_{ex} = 488 nm. Only samples analysed with the same freshly prepared DCFH/DHE-solution can be directly compared.

The ROS determinations were performed by Sebastian Zahnreich at the Gesellschaft für Schwerionenforschung (GSI, Darmstadt).

3.16 Giemsa staining of chromosomes

The number of cells showing chromosomal abnormalities, e.g. tetraploidy, loss of chromosomes or mutations in single chromosomes, is increasing during cell senescence, after irradiation or by several diseases. To analyze these aberrations, chromosomes have to be isolated and visualized.

Chromosomal aberrations can be studied only in metaphase chromosomes. To accumulate mitotic cells in cell cultures the microtubule-depolymerizing substance colcemide was added to the medium at a final concentration of 0.1 µg/mL 3 hours before harvesting. (Cells arrest in the metaphase where chromosomes are condensed. The cell cycle cannot be completed.) Thereafter, cells were detached using Trypsin/EDTA. The medium was not discarded but collected together with the cells. The cell suspension was centrifuged (6 min, 800 g, RT). After discarding the supernatant, the cell sediment was resolved and mixed drop by drop with 37°C pre-warmed KCl (0.075 M) for 8 min to achieve swelling of the cells. The KCl solution was removed after the second centrifugation step (8 min, 800 g, RT) and replaced drop by drop by fixative (25% acetic acid, 75% methanol p.A., incubation time 30 min). After further centrifugation (10 min, 1000 g, RT), the last step was repeated. At this time point samples can be stored. Before subsequent fixation of chromosomes, a last centrifugation was performed (10 min, 1000 g, RT). At this time point cells are fixed in their swollen condition. The pelleted cells were slightly diluted with fixative. To open the cytoplasmic membrane and therewith to expose the nucleus, the fixed cells were dropped (approx. 21 µL) on previously water wetted slides. The water enhances the drop spreading and allows thereby a good separation of both mitotic chromosomes and nuclei. Slides were dried over night at RT.

Chromosomes were stained for 10 min in 3% Giemsa diluted in freshly prepared Sörensen buffer pH 6.8 (1x 0.067 M Na_2HPO_4 and 1x 0.067 M KH_2PO_4 in MilliQ water, RT). The slides were washed twice with MilliQ water and dried first with compressed air and thereafter over night at RT and relative room humidity. The next day, slides were sealed and stored in the dark.

3.17 Determination of the apoptotic cell level

The Annexin-V-Fluos Staining KIT (Roche Diagnostics, Mannheim) allows identification and quantitation of apoptotic cells. Annexin V, a phospholipid binding protein, binds Ca^{2+}-dependent with high affinity phosphatidylserine (PS). PS is under physiological conditions

located solely at the inner side of a membrane. But due to the increased loss of plasma membrane asymmetry during apoptosis it is found exposed to the extracellular surrounding in apoptotic and necrotic cells. To differentiate necrotic cells from apoptotic once, necrotic cells are additionally visualized with propidium iodide that stains DNA of leaky necrotic cells only. The construct Annexin-V-fluorescein is excited at 488 nm and showed fluorescence at a wavelength of 518 nm and propidium iodide is excited at 488-540 nm with fluorescence at 617 nm. Hoechst 33 342 is a fluorescent dye that label DNA. It was used to stain all nuclei within a petri dish to determine not only the number of apoptotic cells but also the proportion within a cell population.

To determine the proportion of apoptotic cells within a culture, 30,000 cells were seeded in a small petri dish (Ø 2 cm). Two days later, apoptotic cells were stained by applying the Annexin-V-Fluos staining assay in combination with Hoechst 33 342. In the first step, cells were washed with PBS to remove the medium. A volume of 119 µL staining-solution [Annexin KIT solutions: 100 µL Annexin kit buffer, 2 µL Annexin solution, 2 µL propidium iodide; 15 µL (1.5 µg/mL) Hoechst 33 342] was added and cells were covered with glass to ensure uniform staining. After 15 min incubation at RT the staining solution and the glass was removed. Cells were fixed for 5 min with 8% formaldehyde solution (in PBS), washed with distilled water and dried under dark conditions at RT. Under the fluorescent microscope necrotic cells appear in a red color while apoptotic cells are green.

3.18 Staining procedure for cell differentiation

Hayflick and Moorhead (1961) described three stages of cells growing in cell culture. Phase I represents a primary culture immediately after explanting when cells adapt culture conditions. Phase II represents the period of cells dividing constantly in culture with approximately 50 cell doublings at maximum. Phase III is characterized by a reduced cell population doubling that may be followed by cell growth arrest or cell death (Hayflick, 1985, 1994). Post-mitotic cells after completion phase III are post-mitotic and stop dividing.

Each stage of cell growth is characterized by specific cell shape (Fig. 3-4). An age-associated increase in the volume of the cytoplasm in relation to the volume of the nucleus occurs (Fournier et al., 1998).

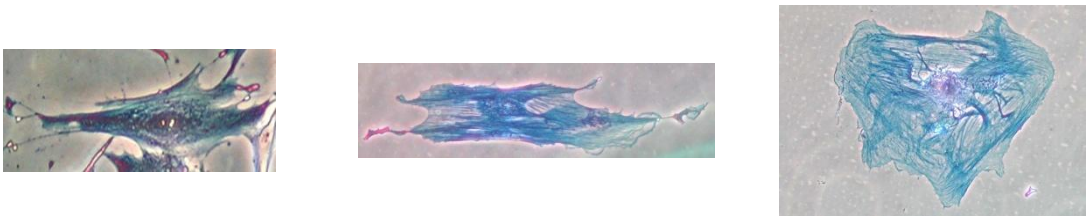

Phase II Phase III Post-mitotic cells

Fig. 3-4. Different cell morphology of NHDF in different ageing stages.

To analyze these morphologic changes, cells were stained in culture dishes with May-Grünwald, Giemsa and Coomassie Brilliant Blue G250. The medium was discarded and cells washed twice with $PBS^{-/-}$ (recipe see chapter 3.4.2). Cells were covered first with undiluted eosin methylene blue dye (May Grünwald) for 5 minutes (RT), secondly for 5 minutes with the same amount of MilliQ water (RT) and washed twice with MilliQ water. Thereafter, 10% Giemsa diluted in Sörensen buffer (1x 0.067 M Na_2HPO_4 and 1x 0.067 M KH_2PO_4 in MilliQ water, RT) was added for 15 minutes and removed with MilliQ water. The blue-violet methylene azure is staining acid cell components (nucleus, cytoplasmic RNA) and the red eosin alkaline parts. Some components are colored by both. Finally, cells were stained for 40 seconds with 2.5% CBB G250 (40% methanol, 7% acetic acid in dest. water) to visualize the whole cell. CBB was diluted with MilliQ water and removed. The cell culture flasks were dried over night in the hood.

4 Results and Discussion

4.1 Sample preparation and storage

Proteome studies especially those with emphasis to analyze proteins in their native state, protein-protein interactions or post-translational modifications, require gentle preparation conditions in order to achieve a sample of high quality that is neither denatured nor artificially modified, e.g. oxidized, carbonylated. This sample has to be stored later on in a proper way remaining its quality. To compare different samples in one experiment, e.g., rats of different age, cells harvested at different time points or irradiated and non-irradiated cells, animals or cells have to be treated the same way and sample preparation as well as storage has to be identical.

4.1.1 Isolation and storage of tissue mitochondria

For proteome profiling of tissue mitochondria, it is important to prove if e.g. for longer time period, if it is better to store the tissue (non-isolated mitochondria) or the isolated mitochondria.

All tissue samples analyzed in this study were provided from Prof. Dr. Hans Rommelspacher, Charité Berlin. The animals were housed and treated (e.g. with MPP^+ see chapter 2.6.2) at the Charité Berlin. The mitochondrial isolation was performed in the non-frozen state immediately after tissue dissection. The importance of this step becomes obvious when comparing the yield of mitochondrial proteins received and the proteome profile of mitochondria isolated from non-frozen rat brain cortex and mitochondria isolated from previously liquid nitrogen-frozen cortex. The yield of mitochondrial proteins from thawed tissue was only 0.76% compared to 2.20% on average from non-frozen tissue. It might be on the one hand that mitochondria are destroyed or damaged during freezing and lost during the isolation procedure. On the other hand after freezing, the tissue is maybe more difficult to homogenize and/or the cell membranes more difficult to disrupt. Additionally, the mitochondrial protein profile from tissue-frozen cortex sample differs compared to non-frozen. In relation to four freshly prepared cortex samples, stored after isolation of mitochondria at -80°C, mitochondria isolated from pre-frozen tissue contained 1.7-fold less intact complex V and 1.8-fold less respiratory chain supercomplexes ($I_1III_2IV_{0-3}$) (Fig. 4-1). The fact that both are decreased to the same extent could be explained by a decrease of solubilisation efficiency. Cell membrane properties may be changed by freezing and thawing of the tissue. From individual complex III_2 and IV and from the unbound F_1 part of complex V same amounts were present in both mitochondria isolated from frozen and non-frozen cortex tissue indicating also, that maybe protein-protein-interactions are less stable after freezing of the tissue and that the stability of proteins complexes, e.g. the ATP synthase or complexes III_2 and IV of the respiratory chain, is affected.

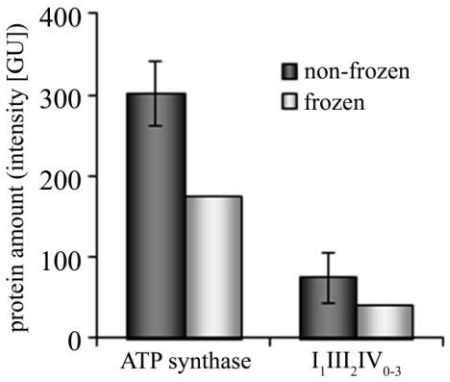

Fig. 4-1. Comparison of total abundances of individual complex V (α-subunit) and supercomplexes ($I_1III_2IV_{0-3}$) in mitochondria isolated from non-frozen (black, average of four individuals) and frozen (grey, n = 1) cortex tissue of aged rats (28 month old).

The importance of the way how samples are stored (tissue or mitochondrial suspension) on the mitochondrial proteome over a long period is unclear. In freshly prepared mitochondria from cortex, striatum and hippocampus after 1 ½ years of storage at -80°C there is only 5% individual complex I present while the major part is assembled together only with complex III_2 (I_1III_2) or complexes III_2 and IV ($I_1III_2IV_{1-X}$) in supercomplexes. In contrast, in whole rat brain stored for 5 years at -80°C 21% (Fig. 4-2) and in cerebellum stored for 4-6 months (Söhn, 2010) up to 17% individual complex I was found.

Concerning all these observations, it is advisable to isolate mitochondria immediately after dissection of the tissue and to freeze solely the mitochondrial suspension. By applying this strategy well preserved mitochondria of high quality will be obtained. It seems also that protein-protein-interactions as well as the stability of individual proteins or protein complexes are better preserved over a long time period by storing the isolated mitochondria.

4.1.2 Cultivating conditions of cell cultures

Cell culture experiments display an *in vitro* model system to analyze molecular processes. They are key elements in research for new vaccines, hormones or anti-cancer substances and to analyze the cell response on external factors, e.g. irradiation (Fournier et al., 2007; Zahnreich et al., 2010). For the majority of cell culture experiments, cultivation conditions with 5% CO_2 and 21% atmospheric oxygen are non physiological. The oxygen delivery of every cell type depends on the metabolic requirement and function of each origin, e.g. organ; therewith each cell line in fact is adapted to and requires unique oxygen level. Carreau et al. (2011) showed that values corresponding to the "physioxia" (physiologic condition) are ranging between 1% and 11% oxygen while current *in vitro* experiments are usually performed in 21% oxygen, an artificial environment as far as oxygen balance is concerned. It is important to note that there is a large discrepancy between *in vitro* cell experiments and *in vivo* oxygen status of tissues and cells which can have detrimental effects on experimental outcomes. *In vitro* cell cultures are traditionally performed in unstirred liquid media at ambient oxygen concentrations in the laboratory, without considering the level of oxygen experienced

by the cells in tissue. These conditions are suitable for many biologic applications but there are other situations in which more attention to oxygenation is appropriate, e.g. in terms of post-translational modification of proteins, substrate transport, metabolic pathways, growth factor signaling and differentiation (Esteban and Maxwell, 2005).

Therefore, cell culture experiments under atmospheric conditions are certainly not reflecting the physiology situation. But nevertheless, it is to date used to analyze basic molecular processes or the cellular response on external effects. For instance, cell culture experiments were fundamental to develop irradiation procedures in cancer therapy by analyzing dose dependent cell survival (Ceriani et al., 1992). In conclusion, for every experiment, cell culture conditions should be chosen to the respective type of question that shall be examined.

In the present study, cell cultivation was performed at 5% CO_2, 21% atmospheric oxygen and 100% humidity at 37°C. Changes in the ROS level were analyzed in long term experiments. The level might be decreased or the response on irradiation stronger in cells cultivated under physioxia but due to the fact that control cells and irradiated cells were exposed to similar conditions, tendencies at least can be described.

Additionally, in long-term cell culture experiments one has to keep in mind that the cell population is inhomogeneous. In the present study, during irradiation cells were confluent and arrested in G0/G1-phase but thereafter due to irradiation induced damages, healthy, post-mitotic, apoptotic cells as well as cells exhibiting genomic variations were present in one culture. For mitochondrial protein profiling approximately 22,000 cells (AG1522D, NHDF, WI38) had to be harvested to obtain 1 µg mitochondrial protein. On 2D BN/SDS gels 20-40 µg proteins were applied (chapter 3.7.1) or for cellular ATP determination 1600 cells were required (chapter 3.14). One confluent 75 cm^2 cell culture flask contained approximately $4x10^6$ cells. Due to the fact that no cell sorting was performed all data in the present study describes the physiology of a heterogeneous cell population.

4.1.3 Purification of mitochondrial samples

Sample purification is an important tool to obtain homogeneous extracts containing solely proteins or organelles of interest. Other cell components, molecules or proteins have to be removed. The purification of rat brain mitochondria by discontinuous sucrose density gradient [three steps: 15%, 23% and 32% (w/v)] ultra centrifugation (Frenzel, 2006) increases significantly the proportion of mitochondrial proteins within a sample. Typical contaminates of rat brain mitochondrial suspensions are myelin proteins (Virchow, 1854). These proteins (mainly myelin basic protein, myelin oligodendrocyte glycoprotein and proteolipid protein; see also Frenzel, 2006 for its position in 2D SDS gels) are forming together with lipids the myelin, a dielectric material that is forming a layer (myelin sheath) isolating neuronal axons. Using discontinuous sucrose gradients reduces the amounts of myelin in the mitochondrial fraction and allows the presence of predominantly mitochondrial proteins. In this way, protein determination, e.g. via Bradford assay, reflect the abundance of mitochondrial proteins more accurate. This is especially important for comparison of different ageing states hence the

amount of myelin proteins itself is changing during ageing (Peters, 2007). Additionally, the solubilisation efficiency is reduced in the presence of myelin proteins (Fig. 4-2) because they bind a proportion of the detergent. The ratio of detergent to mitochondrial proteins has to be increased in non sucrose gradient purified samples to achieve comparable extraction efficiency to gradient samples. Protein separation with 2D BN/SDS PAGE displays less background after purification due to increased solubilisation efficiency by similar detergent to protein ratio of rat brain mitochondrial samples.

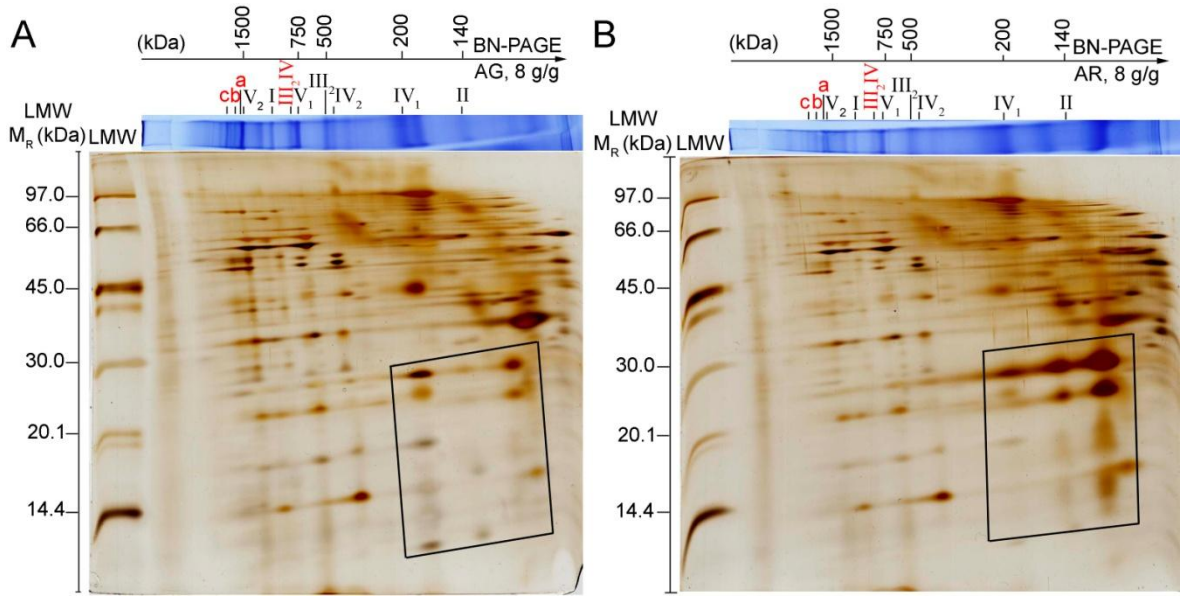

Fig. 4-2. Silver stained 2D BN/SDS gels (BN-PAGE: 3.5% stacking gel, 4-13% separating gel; SDS-gel: 5% stacking gel, 13% separation gel) of solubilized mitochondria (8 g/g digitonin to protein, 120 µg before solubilisation) isolated from whole brain of a 30 month old male Fisher rat (A) after and (B) before discontinuous sucrose gradient. After using of discontinuous sucrose gradient, myelin proteins are less pronounced (see highlighted area) and reduced background staining is present. It shall be noted that whole rat brain is applied and that the tissue was stored approximately 5 years at -80°C before isolation of mitochondria. Abbreviation: AG = 30 month old aged rat, purification of mitochondria via a discontinuous sucrose gradient; AR = 30 month old aged rat, mitochondria without purification; LMW = low molecular weight protein standard.

Although purification of brain mitochondria result in 2D BN/SDS gels with low background and clear protein spot pattern, there are two reasons for omitting this step in the present study for mitochondrial isolation from rat brain and cell culture. Firstly, in crude mitochondrial suspensions fragile and damaged mitochondria, which might be more abundant and more severely affected in aged or irradiated samples, cannot be lost or disrupted during harsh purification steps. Secondly, purification with sucrose gradients is reducing the yield of proteins by about 50%. Some samples as e.g. mitochondrial suspensions of rat brain areas (e.g. hippocampus and striatum) or of cell cultures were characterized by rather small protein amounts. After density purification the protein amount would have been insufficient for proteome analysis.

4.1.4 Use of SCAVEGR during sample preparation

Especially for proteome analysis including determination of posttranslational modifications gentle isolation and solubilisation conditions have to be chosen. One important modification of the mitochondrial proteome important in e.g. ageing studies is the oxidation state of proteins. At every age free oxygen radicals are present in cells but maybe to a different extent. They are important for cellular processes like signaling or for the immune system but they are also harmful when present to a large extent. A relation of protein oxidation and ageing is suggested as one of the main cause (Harman, 1956; Oliver et al., 1987; Smith et al., 1991; Starke-Reed and Oliver, 1989). Harsh homogenizing steps of e.g. tissue may lead to oxidation of the sample, i.e., increased carbonylation of amino acid residues. Determination of oxidative modifications thereafter would not reflect the real (natural) situation within the analyzed tissue or cell.

In this study the anti-oxidant mixture SCAVEGR (BrainBitsLLC, USA) was applied to preserve proteins in their natural oxidative state. SCAVEGR consists of superoxide dismutase (SOD), catalase, vitamin E, vitamin E acetate, reduced glutathione and albumin (Brewer et al., 2004). It was observed previously that SCAVEGR is increasing the sample quality of rat brain mitochondria by preserving respiration. In mitochondria isolated with the anti-oxidant mixture e.g. a 15% higher respiration control ratio and 2-fold increased V_{max} as well as more than 40% less TBARS (ThioBarbituric Acid Reactive Substances, harmful and formed by lipid peroxidation) were found (Brewer et al., 2004).

The formation of lipid radicals and therewith lipid peroxide radicals (lipid peroxydation) are prevented by vitamin E and vitamin E acetate. Target lipids are unsaturated lipids within the cell membrane. The structure of vitamin E (hydrophobic tail) allowing its presence at the side of membrane lipids and membrane proteins, necessary for its role as electron acceptor. Superoxide radicals that may appear during mitochondrial isolation are converted into hydrogen peroxide (H_2O_2) by the SOD. H_2O_2 is removed via the mitochondrial protein glutathione peroxydase that is oxidizing the SCAVEGR component glutathione and via the catalase present in SCAVEGR. The albumin included in the mixture protects mitochondrial proteins from getting oxidized by way of acting as target for oxygen radicals.

According to the product manual 2% (v/v) SCAVEGR was added to buffers (in the present study solely in homogenization buffer, for tests described in this chapter in both homogenization and solubilisation buffer). The effect – positive and negative – of applying the anti-oxidant mixture during mitochondria isolation and protein solubilisation was tested for the first time on rat liver tissue mitochondria (Beyer, 2007). Liver tissue was cut in half. One part was isolated and solubilized in the presence of and the other in the absence of SCAVEGR. In the presence of SCAVEGR protein-protein-interactions were more stable as deduced from the higher protein amounts of the ATP synthase dimer (1.2-fold) and of the supercomplexes III_2IV_1 (1.4-fold), I_1III_2 (1.4-fold) and $I_1III_2IV_2$ (1.7-fold). But, specific enzyme activities of complex I and IV are similar in both samples. The efficiency to act as anti-oxidant was tested by exposing samples to 500 mM H_2O_2 for 10 minutes at RT and determination of the specific activity of complex I and complex IV thereafter. The specific activity of these

enzymes remains unchanged in samples with SCAVEGR as compared to controls in the absence of additionally H_2O_2 while e.g. complex I activity in supercomplex I_1III_2 and $I_1III_2IV_2$ is increased in samples without SCAVEGR. This is a surprising result challenging the “Free Radical Theory of Ageing” of Harman (1956) but going hand in hand with the theory of hormesis (chapter 1.2.1).

Analyses were repeated in a second experiment with BHM tissue with the difference that the distinct effect of SCAVEGR in the homogenization and solubilisation procedure, respectively, was studied (analyses performed by Sandra Thilmany, AG Dencher, Technische Universität Darmstadt). Determination of protein carbonylation by OxyBlot showed that the solubilisation itself represents the critical step whereby the major proportion of protein oxidation occurs. This becomes obvious by comparing the amount of protein modifications of a non-solubilized sample and a sample after solubilisation. When SCAVEGR was used already for homogenization, proteins were protected during further solubilisation without additional adding of the anti-oxidant mixture, i.e. the signal intensity for carbonylation was similar independent of the use of SCAVEGR during solubilisation. The BHM sample homogenized and solubilized without the protection cocktail displayed pronouncedly increased amounts of oxidized proteins. By using SCAVEGR only during solubilisation, the carbonylation was at the level of BHM homogenized with SCAVEGR. The disadvantage of using the anti-oxidant mixture for solubilisation is that all proteins included within the SCAVEGR are separated during electrophoresis together with sample proteins. It is not just that they may mask proteins of interest with similar molecular mass; they additionally affect the quantitation of enzymes present in both sample and SCAVEGR like catalase or SOD.

Based on these data in the present study, SCAVEGR was solely present during homogenization but not protein solubilisation.

4.1.5 Storage of samples for cellular ATP determination

Determination of the cellular ATP level is time consuming, due to the fact, that for every set of measurement an ATP standard has to be prepared freshly the same day. Hence, to facilitate comparative analysis of changes in the ATP level of samples collected over a time range during one experiment, e.g. from a cell culture during long-term cultivation, storage conditions have to be found that are not affecting the ATP content of a sample. In this way, samples belonging to one experiment can be analyzed the same day and at lower costs, i.e. only one standard curve is required (costs of one ATP Kit SL: 316 €). It was demonstrated by Lundin et al. (1986) that the level of cellular ATP is changing when cell culture cells are transferred from 37°C to room temperature.

In an initial experiment (Knab, 2009), the ATP concentration in cells from cell culture was determined immediately after harvesting (sample 1) and after freezing (in liquid nitrogen) and storing of the intact cells at -80°C for 2 hours (sample 1’) in special freezing medium (composition see chapter 2.7.2). A 9.2-fold decrease of cellular ATP concentration was observed between these two states (Fig. 4-3 A, Table 4-1). Both intact cell samples

(sample 1 and 1') and the already TCA treated cells of both samples were frozen and stored at -80°C. Two weeks later, the ATP content was determined. In intact frozen cells (sample 1 and sample 1') compared to TCA incubated cells the ATP level was pronouncedly decreased about 8-fold in sample 1' (Fig. 4-3 B) and more pronounced in sample 1, about 86-fold (Fig. 4-3 C). The ATP content in frozen TCA denaturized samples was approximately

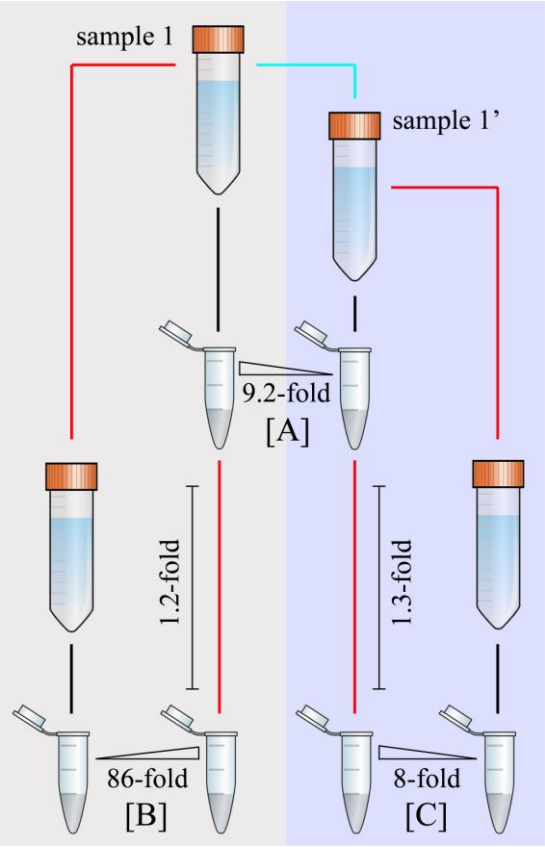

Fig. 4-3. The effect of freezing and storage on the cellular ATP concentration To analyze the effect of freezing on the cellular ATP content, cells (human fibroblasts) freshly prepared (sample 1) and 2h frozen (indicated as blue line) cells (sample 1', in special freezing medium) were compared. Falcon tubes symbolize cell culture suspension and Eppendorf tubes the TCA incubated cells. 2h freezing resulted in a 9-fold decrease in ATP amount (A).

Red lines represent freezing and storage of sample 1 and 1' as well as their respective TCA extracts for 2 weeks at -80°C. After 2 weeks of storage in sample 1 only 1.2% of the initial ATP concentration (86-fold less) was present (B). In sample 1' the ATP concentration decreased about 8-fold (C) compared to the 2h frozen time point and about 78-fold compared to the freshly prepared cells (1.3% of the initial ATP concentration).

In cell extracts incubated with TCA before freezing only small changes (1.2-fold increase for sample 1 and 1.3-fold decrease for sample 1') in the ATP concentration were observed after storage.

identical to the measurement A (1.2-fold increase for sample 1 and 1.3-fold decrease for sample 1'). This small difference might result from sample handling. Multiplication of sample 1' factors, obtained from measurement A and C (2 hours and 2 weeks), of intact

Table 4-1. ATP concentrations [µM] of freshly (sample 1) analyzed cells and of cells frozen for 2h (sample 1') as well as of same cell samples and their respective TCA extracts after 2 weeks of storage at -80°C. Abbreviation: c = concentration [µM], ws = without storage, as = after storage

	Without storage	Storage of intact cells for 2h at -80°C	Storage of intact cells for 2 weeks at -80°C	Storage of TCA extracts 2 weeks at -80°C
Sample	**c_{ws} (ATP) [µM]**	**c_{as} (ATP) [µM]**	**c_{as} (ATP) [µM]**	**c_{as} (ATP) [µM]**
sample 1	0.785		0.011	
				0.948
sample 1'		0.085		
			0.008	
				0.064

frozen cells resulting in an overall factor of 78 that is comparable to that of sample 1 frozen one time for duration of 2 weeks (Fig. 4-3 B). The amount of cellular ATP is decreasing due to the freezing process and during storage at -80°C. These experiments showed that for ATP determination samples should be stored after incubation to TCA to avoid a decrease of the ATP level in the cells.

To approve that the ATP amount remains stable in TCA extracts a second experiment was performed. Cell suspensions of four different previous experiments were analyzed immediately after harvesting of cells and after 5 days storage of TCA extracts at -20°C (Wendenburg, 2010). All samples displayed before and after storage nearly similar ATP amounts (Table 4-2). Variations between both measurements (before and after storage) are small and data reproducibility.

Table 4-2. The ATP amount [mol] in four different samples before and after storage for 5 days at -20°C. Storage occurred in the presence of TCA. Abbreviations: n = amount of substance [mol], ws = without storage, as = after storage

	Without storage	After storage	
Sample	**n_{ws} (ATP) [mol]**	**n_{as} (ATP) [mol]**	**ratio n_{ws}/n_{as}**
A	7.39 E-13	7.51 E-13	0.983
B	1.13 E-12	1.00 E-12	1.132
C	1.48 E-12	1.45 E-12	1.021
D	2.83 E-12	2.86 E-12	0.990

Based in these observations, samples for ATP determination have to be stored at -20°C after incubation with TCA, for analysis of all samples at the same day.

4.2 Age-associated alterations of the mitochondrial proteome of rat brain cortex, striatum and hippocampus

After analyzing changes in the mitochondrial proteome during ageing in whole rat brain (Frenzel, 2006), studies were extended by determining age-associated changes of mitochondrial protein pattern of different brain regions. At first, cortex mitochondria were studied (chapter 4.2.1). The cortex is the largest brain area and the amount of mitochondrial proteins isolated allowed additional analysis of enzyme activity of OxPhos complexes via in-gel activity tests as well as determination of optimal digitonin to protein ratio for high solubilisation efficiency by preserving protein-protein-interactions. Data obtained from protein quantitation were compared to that of mitochondria isolated from hippocampus and striatum, two smaller brain areas (chapter 4.2.2).

4.2.1 Age-associated alterations in the mitochondrial proteome of rat brain cortex

Data described in this chapter have been already published:

Monika Frenzel, Hans Rommelspacher, Michiru D. Sugawa, Norbert A. Dencher (2010). Ageing alters the supramolecular architecture of OxPhos complexes in rat brain cortex. *Experimental Gerontology* **45**, 563–572.

Protein profiling of rat brain cortex mitochondria was performed as described in methods (chapter 3). Crude mitochondrial fractions were isolated freshly immediately after dissection of the brain and stored at -80°C for only a short period (4 months). Mitochondrial proteins were solubilized with 8 g/g digitonin to protein ratio after comparing solubilisation efficiencies using 4 and 8 g/g. The ratio of 8 g/g allowed quantitative extraction of membrane proteins from mitochondria of both young as well as aged animals by preserving protein-protein-interactions. By utilizing 2D-BN/SDS electrophoresis and fluorescent staining with SYPRO Ruby profound changes in the amount of respiratory chain supercomplexes composed of complexes I, III_2, IV as well as of the ATP synthase (complex V) were revealed. Complex I was present solely in supramolecular assemblies with complex I, III_2 and IV. In line with observations described for rat skeletal muscle (Lombardi et al., 2009) but in contrast to rat heart (Gómez et al., 2009) the composition of hetero-supercomplex assemblies in rat cortex changed during ageing towards an enrichment of larger supercomplexes containing complex IV ($I_1III_2IV_{1-3}$, Fig. 4-4). The supercomplex I_1III_2 lacking complex IV was least abundant in aged animals (2.4-fold decline). On the one hand it was possibly more present in larger supercomplexes or on the other hand less present and therefore degraded in individual complexes The supercomplex formation represents a stabilizing mechanism suggested to enhance substrate channeling as well as catalytic enzyme activity and a compensatory effect for the overall abundance-decline of respiratory chain complexes (Silvestri et al., 2011). Protein-activity was demonstrated by performing In-gel activity analysis (Fig. 4-5).

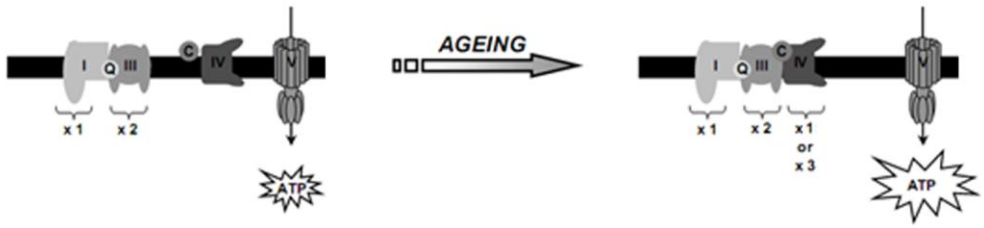

Fig. 4-4. The age-associated shift towards an enrichment of larger supercomplexes containing complex IV as described by Frenzel et al. (2010b) and Lombardi et al. (2009) [modified from Silvestri et al. (2011)]

The specific activities of supercomplexes $I_1III_2IV_{0-3}$ remained unchanged during ageing (Fig. 4-6). The total amount of $I_1III_2IV_{0–3}$ decreased age-associated about 1.6-fold but there is a change in the relative proportion towards supercomplex $I_1III_2IV_1$ displaying the highest specific activity. That complex IV is essential for the activity of complexes I and III_2 was shown by Schäfer et al. (2006) for bovine heart mitochondria. The interconversion of I_1III_2 into $I_1III_2IV_1$ resulted in a higher specific activity of complex I about 2.3-fold that is nearly similar to the 2-fold increase observed for cortex mitochondria of young and aged rats in the present study.

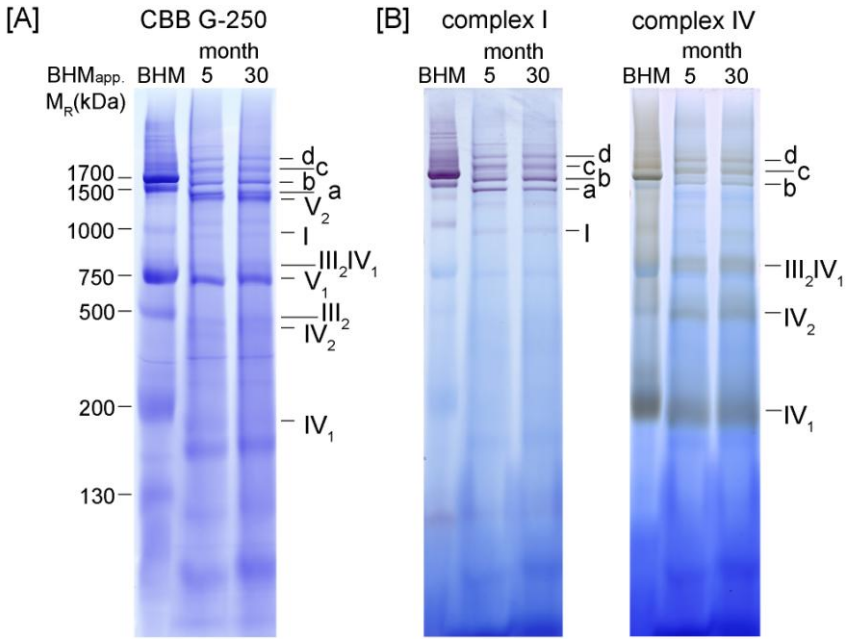

Fig. 4-5. BN-gel (linear 4–13% gradient and 3.5% stacking gel) stained with CBB G-250 (A) and after performing of complex I and complex IV in-gel activity tests (B). Pooled samples of young and aged rats were loaded (100 µg protein before solubilisation, 8 g/g digitonin to protein, mixture of mitochondria of three animals; n = 3). For mass calibration, digitonin solubilized (3 g/g) and well characterized bovine heart mitochondria (BHM) were used. (a = I_1III_2, b = $I_1III_2IV_1$, c = $I_1III_2IV_2$, d = $I_1III_2IV_3$)

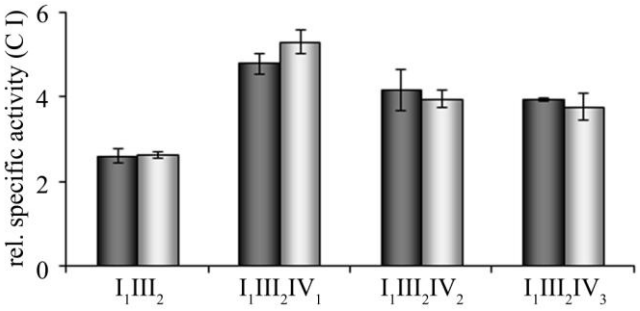

Fig. 4-6. The specific activity of complex I (normalized on the protein amount determined in the second dimension) in supercomplexes $I_1III_2IV_{0-3}$ in young (black) and aged (grey) rat cortex mitochondria. Supercomplex $I_1III_2IV_1$ displayed the highest complex I activity. No age-associated changes in the specific activity were observed. The oxidation of NADH+H^+ via complex I was determined by performing in-gel activity tests in one BN gel [4-13% gradient separating gel, 3.5% stacking gel, 100 µg mitochondrial protein before solubilisation per lane (pool of 3 animals per age group, n = 3)] and quantitation of the staining intensity of the violet formazan.

The ATP synthase (sum of monomer and oligomers) was observed to represent a prominent target of age-associated degradation in rat brain (Frenzel, 2006; Frenzel et al., 2010b), liver (Thilmany, 2008) and other model systems (Groebe et al., 2007). Its total amount decreased about 20% (1.2-fold) in rat brain cortex whereby the largest decline of about 1.5-fold occurred for the monomer. In aged rats a 2.8-fold increase of unbound F_1 was observed that is capable to hydrolyze ATP with high efficiency. The oligomerisation of the ATP synthase increased during ageing. More complex V dimers, trimers and tetramers were found in aged animals.

Young animals of 4-6 month age are named as 5 month old rats and aged rats of 28 month as 30 month old.

Experimental Gerontology 45 (2010) 563–572

Contents lists available at ScienceDirect

Experimental Gerontology

journal homepage: www.elsevier.com/locate/expgero

Ageing alters the supramolecular architecture of OxPhos complexes in rat brain cortex

Monika Frenzel [a,*], Hans Rommelspacher [b], Michiru D. Sugawa [a,b], Norbert A. Dencher [a,*]

[a] Physical Biochemistry, Department of Chemistry, Technische Universität Darmstadt, D-64287 Darmstadt, Germany
[b] Clinical Neurobiology, Department of Psychiatry, CBF, Charité – Universitätsmedizin Berlin, D-14050 Berlin, Germany

ARTICLE INFO

Article history:
Received 28 November 2009
Received in revised form 18 January 2010
Accepted 2 February 2010
Available online 14 February 2010

Keywords:
Ageing
OxPhos supercomplexes
Rat brain
Cortex
Mitochondria
Proteome
Respiratory chain
ATP synthase
Life-span
Native electrophoresis

ABSTRACT

Activity and stability of life-supporting proteins are determined not only by their abundance and by post-translational modifications, but also by specific protein–protein interactions. This holds true both for signal-transduction and energy-converting cascades. For vital processes such as life-span control and senescence, to date predominantly age-dependent alterations in abundance and to lesser extent in post-translational modifications of proteins are examined to elucidate the cause of ageing at the molecular level. In mitochondria of rat cortex, we quantified profound changes in the proportion of supramolecular assemblies (supercomplexes) of the respiratory chain complexes I, III_2, IV as well as of the MF_oF_1 ATP synthase (complex V) by 2D-native/SDS electrophoresis and fluorescent staining. Complex I was present solely in supercomplexes and those lacking complex IV were least stable in aged animals (2.4-fold decline). The ATP synthase was confirmed as a prominent target of age-associated degradation by an overall decline in abundance of 1.5-fold for the monomer and an 2.8-fold increase of unbound F_1. Oligomerisation of the ATP synthase increases during ageing and might modulate the cristae architecture. These data could explain the link between ageing and respiratory control as well as ROS generation.

1. Introduction

Understanding molecular processes underlying ageing still remains a challenge. Besides genetic determinants and the detrimental effects of reactive oxygen species (ROS), age-dependent changes in the abundance and post-translational modification of the cellular proteome are currently considered as targets and even triggers of ageing. In fact, at the protein level numerous alterations in both the abundance (Gómez et al., 2009; Groebe et al., 2007; Lombardi et al., 2009; Poon et al., 2006a,c) and specific post-translational modification (Groebe et al., 2007; Hunzinger et al., 2006; Poon et al., 2006c) have been previously observed for a variety of established ageing models that might represent control determinants of private or evolutionary conserved life- and health-span. Despite this progress on the protein level, the cause and mechanism of ageing is still a secret. The performance of signal cascades as well as of energy-converting pathways is regulated by specific protein–protein interactions too. A wealth of information has been gathered that mitochondria are key targets and mediators of ageing (e.g. reviewed in "Mitochondria and Aging" Biotechnology Journal 3, 701–828, 2008). Therefore, we have analysed the differential protein profile, especially of membrane proteins in the inner mitochondrial membrane, with the emphasis on protein–protein interactions reflecting the architecture of supramolecular OxPhos complex assemblies in cortex mitochondria from young (5 months) and aged (30 months) male rats. (The respiratory chain complexes I [NADH:ubichinone oxidoreductase], III [ubiquinol: cytochrome c oxidoreductase] and IV [cytochrome c oxidase] together with the proton MF_oF_1 ATP synthase [complex V] will be referred to as OxPhos [oxidative phosphorylation] system.) In contrast to the current textbook view, most OxPhos complexes are not residing as individual complexes in the inner mitochondrial membrane but as large supercomplexes with stoichiometric arrangement of the complexes I, III and IV (Fig. 1) (Chance and Williams, 1955; Hackenbrock et al., 1986; Schon and Dencher, 2009; Seelert et al., 2009; Wittig et al., 2006; Wittig and Schägger, 2009) not only in rat brain cortex (Dencher et al., 2007), striatum (Wernicke et al., 2010) and brain (Reifschneider et al., 2006) but also in liver (Dani et al., 2009; Reifschneider et al., 2006), kidney (Reifschneider et al., 2006), skeletal muscle (Lombardi et al., 2009; Reifschneider et al., 2006) and heart tissue (Gómez et al., 2009; Reifschneider et al., 2006) as well as in all evolutionary quite far distant

* Corresponding authors. Address: Technische Universität Darmstadt, Petersen straße 22, D-64287 Darmstadt, Germany. Tel.: +49 6151 16 5275; fax: +49 6151 16 4171.
E-mail addresses: monika.frenzel@physbiochem.tu-darmstadt.de (M. Frenzel), norbert.dencher@physbiochem.tu-darmstadt.de (N.A. Dencher).

0531-5565/$ - see front matter © 2010 Elsevier Inc. All rights reserved.
doi:10.1016/j.exger.2010.02.003

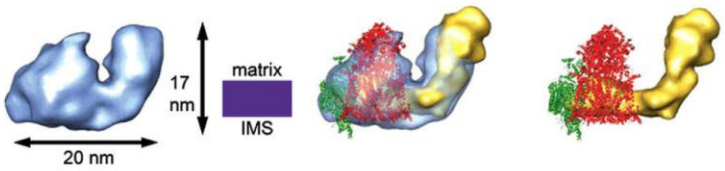

Fig. 1. 3D-structure of supercomplex $I_1III_2IV_1$, with individual complexes highlighted. The left column displays a surface representation in blue of the supercomplex $I_1III_2IV_1$ (1.7 MDa) 3D map, as determined by single particle electron microscopy (Schäfer et al., 2007a). The middle column shows the 3D map with a semitransparent surface and the fitted structures of the individual complexes. The right column displays solely the three individual complexes as they would assemble to form the supercomplex. The electron microscopic 3D map of complex I (Grigorieff, 1998) is shown in yellow, the X-ray structure of complex III_2 [PDB ID 2A06, (Huang et al., 2005)] is displayed in red, and the X-ray structure of complex IV [PDB ID 1OCC, (Tsukihara et al., 1996)] is shown in green. The location of the membrane in a side view is displayed in purple. IMS = intermembrane space. (Adapted from Schäfer et al. (2007) with the permission of the authors.)

organisms studied to date, e.g., fish (Schäfer et al., 2007b), fungi (Krause et al., 2004b; Maas et al., 2009; Marques et al., 2007; Nübel et al., 2009; Schägger and Pfeiffer, 2000), *Caenorhabditis elegans* (Brys et al., submitted for publication), Drosophila (Le Pécheur et al., 2009), bovine heart (Krause, 2007; Reifschneider et al., 2006; Schägger, 2002; Schägger and Pfeiffer, 2001), human skin fibroblast cell culture (Colindres et al., 2007), even in plants (Eubel et al., 2004; Krause et al., 2004a) and bacteria (Krause, 2007; Schägger, 2002; Stroh et al., 2004). Also the MF_oF_1 ATP synthase (complex V) does exist in a large proportion as dimers and homooligomers in these organisms (see also Fig. 2 and 5 for rat cortex) (Krause et al., 2005).

The combination of the powerful techniques employed, e.g., native-PAGE, quantitative evaluation of fluorescent protein spots and mass spectrometry, detected with high sensitivity and accuracy age-associated changes in abundance and assembly of OxPhos complexes and supercomplexes. Notable, complex I is scarcely detectable in rat cortex as individual entity in both age-groups, but assembled with other complexes as supercomplexes (Fig. 2). Its abundance was highly lowered in aged cortex mitochondria (1.6-fold). The observed age-associated decline especially of supercomplexes I_1III_2 (2.4-fold), $I_1III_2IV_1$ (1.4-fold) and $I_1III_2IV_2$ (1.7-fold) as well as of the ATP synthase (1.2–1.5-fold), together with the pronounced increase of unbound F_1 (2.8-fold) will modulate energy conversion and ROS generation.

2. Materials and methods

2.1. Animals

Male Wistar rats were obtained from Charles River, Sulzfeld, Germany. They were housed four animals per cage in an artificial 12-h light–dark cycle with food and water *ad libitum*. Rats were cared and handled in accordance with the guidelines of the European Union Council (86/609 EU) for the use of laboratory animals. The study was approved by the animal care and use committee of the Senate of Berlin, Germany (GeschZ. 0273/ 03).

Two age-groups of male Wistar rats comprising four animals each, were included in this study: 5-month-old (young rats) and 30-month-old (aged rats).

2.2. Isolation of mitochondria

Isolation of mitochondria from rat cortex was performed on ice immediately upon dissection of non-frozen tissue. The brain tissue was minced and homogenised in a motor driven, micropistill homogeniser (9 strokes, 600 rpm) and 4 volumes (1 g tissue/4 mL buffer) of homogenisation buffer (5 mM HEPES/NaOH, 320 mM sucrose, 1 mM Na^+/EDTA, pH 7.4) with 0.5% protease inhibitor cocktail (Sigma P8340) and 2% (v/v) SCAVEGR [BrainBitsLLC/USA; mixture of anti-oxidants; (Brewer et al., 2004)] on ice. After centrifugation at 1300*g* (3 min, 4 °C) the supernatant containing the mitochondria was collected. To increase the yield, the pellet was washed twice with homogenisation buffer (1500*g*, 4 °C, 3 min). To collect the mitochondria, the merged supernatants were centrifuged at 17,000*g* (10 min, 4 °C). The pellet was suspended in homogenisation buffer (containing 0.5 mM Pefabloc SC [Biomol 50985], a serine protease inhibitor). Aliquots of the mitochondrial fraction were shock-frozen in liquid nitrogen and stored at −80 °C. The protein concentration was determined by the Bradford assay (Roth K880.1).

2.3. 2D-BN/SDS–PAGE

Solubilisation of cortex mitochondria was done at 4 °C according to Reifschneider et al. (2006) for 30 min using an 8 g digitonin/g protein ratio at a final detergent concentration of 1% (w/v). The digitonin was of high purity (Calbiochem 300410).

Linear gradient gels with a total acrylamide concentration of 4–13% overlaid with a 3.5% stacking gel were employed for BN-PAGE. Lanes from the first dimension BN-PAGE were excised and analysed by a second dimension SDS–PAGE (5% stacking gel, 13% separation gel) (Dani and Dencher, 2008; Krause and Seelert, 2008; Neff and Dencher, 1999; Reifschneider et al., 2006).

1D-gels were stained with colloidal Coomassie-brilliant-blue G-250 (Rotiblue; Roth A152.1) and 2D-SDS-gels in the first step with fluorescent SYPRO Ruby (Bio Rad 170-3125) for quantitative evaluation and thereafter with silver for visualisation only (Blum et al., 1987).

Mitochondrial proteins were identified by their specific migration behaviour in the first native-PAGE dimension as well as by the characteristic subunit pattern in the 2D SDS–PAGE according to recent protein profiling of rat brain mitochondria by MALDI-TOF-MS peptide mass fingerprinting (Reifschneider et al., 2006).

Quantification of protein bands on 1D BN-gels was performed using a GS-800 calibrated densitometer (BioRad) and Quantity One Software (BioRad, Version 4.4.0). For the second dimension SDS gels, a CCD-camera system (Fuji, Image Reader LAS-3000 2.1) and Delta2D software, Version 3.3, Decodon (Greifswald, Germany) were employed. For quantification of 2D-gels, intensities represent the sum of all pixel gray values belonging to one protein spot.

2.4. Scaling of protein abundance

To facilitate comparison of different samples, always the same amount of digitonin extract of mitochondria was loaded per lane, i.e., 100 μg or 200 μg protein (before solubilisation) on the first dimension for the 1D- and 2D-BN/SDS–PAGE, respectively. To compensate differences in staining efficiency during quantification, a normalisation procedure was developed, using low molecular

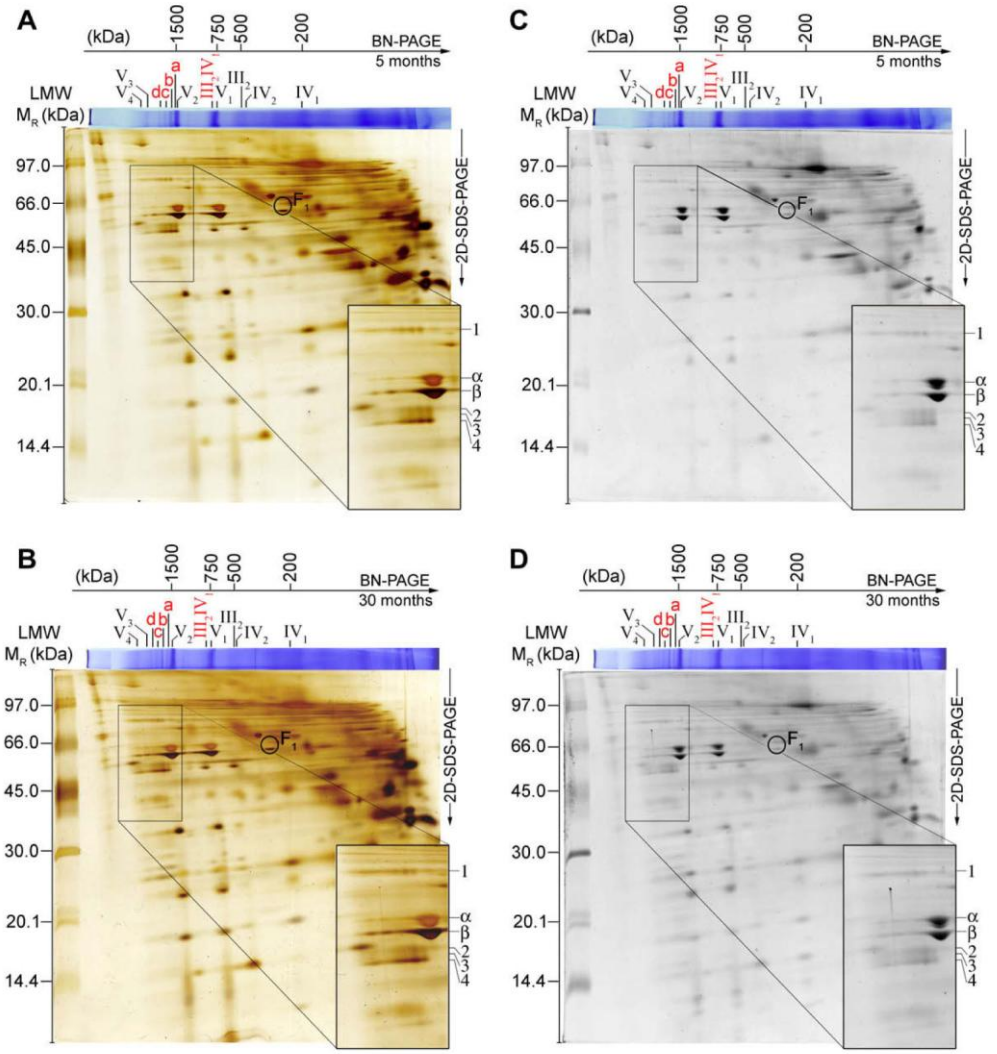

Fig. 2. 2D-BN/SDS–PAGE of digitonin-solubilised (8 g digitonin/g protein) mitochondria isolated from non-frozen rat brain cortex for analysis of age-related changes in the abundance and supramolecular organisation of mitochondrial proteins. In the first dimension, individual proteins, protein complexes and respective supercomplexes are separated in their native state and in second dimension, after denaturation, as subunits in a vertical line according to their position in BN-PAGE. For mass calibration in the first dimension, high molecular weight (HMW) standard respectively digitonin solubilised and well characterised bovine heart mitochondria (BHM) were used: individual complexes I–V (130–1000 kDa), supercomplexes $I_1III_2IV_{0-3}$ (1500–2100 kDa) and ATP synthase oligomers V_{2-4} (1500–3000 kDa). In the second dimensions low molecular weight (LMW) standard was used for mass calibration and standardisation of gels. Characteristic protein patterns of subunits belonging to individual OxPhos complexes I, III_2, IV and V and of their preserved supercomplexes are resolved. 2D-BN/SDS–PAGE from cortex mitochondria stained for visualisation only with silver of young rat (A) and aged rat (B) and with fluorescent SYPRO Ruby for quantification (C + D), respectively. As discussed in Sections 2 and 3, for quantitation of all samples, only the fluorescence readout of the SYPRO Ruby signals was evaluated. In the enlarged inset, protein subunits of supercomplexes $I_1III_2IV_{0-3}$ (numbered from 1–4) and ATP synthase α- and β-subunit are highlighted. [a (I_1III_2), b ($I_1III_2IV_1$), c ($I_1III_2IV_2$), d ($I_1III_2IV_3$), 1 + 2a + 3 (subunits of complex I; 1 = 75 kDa Fe–S subunit; 2a = Fe–S subunit 2; 3 = 51 kDa flavoprotein 1), 2b + 4 (subunits of complex III_2; 2b = core protein I, 4 = core protein II), α (α-subunit of complex V), β (β-subunit of complex V), unbound F_1] [BN-PAGE: linear 4–13% gradient gel with a 3.5% stacking gel, stained with Coomassie-brilliant-blue G-250; 2D-SDS-PAGE: 5% stacking gel, 13% separation gel, silver stained (A + B) and SYPRO Ruby stained (C + D).]

weight (LMW; Amersham Bioscience 17-0445-01) protein standards, added in the same amount to each 2D-gel. For any 2D-gel, a correction factor was applied after considering the SYPRO Ruby fluorescence intensities of four marker bands [phosphorylase b (97 kDa), albumin (66 kDa), ovalbumin (45 kDa) und carbonic anhydrase (30 kDa)]. All measured protein spot intensities for every gel have been corrected by multiplication with the resulting specific correction factor. Although SYPRO Ruby has a large linear dynamic quantification range of about 2000 [detection limit 1 ng protein/spot (Wheelock et al., 2006)] only the spot-intensities of identical proteins can be directly compared due to different staining behaviour, depending on the amino acid composition and the amount of bound SDS.

The biological variances as well as technical sources of error have been minimised by analysing four different animals per age group, each sample separately in duplicate. Mean and standard

deviation of the biological variance are indicated. Statistical analyses between two age-groups have been provided using one-way ANOVA. The significance level was set at $P < 0.05$.

2.5. In-gel complex I activity assay

The NADH dehydrogenase activity of complex I was probed by in-gel formazan precipitation using a modified protocol by Kuonen et al. (1986) and Grandier-Vazeille and Guerin (1996). The in-gel activity tests were performed immediately after BN-PAGE prior fixation of proteins. The gels were incubated for up to 1½ h at room temperature in 100 mM Tris, 768 mM glycine, 0.04% (w/v) 4-nitro blue tetrazolium chloride, and 0.1 mM β-NADH, pH 7.4. Subsequently, the reaction was stopped in 50% (v/v) methanol, 10% (v/v) acetic acid for 10 min. Quantitation of complex I enzyme activity staining in 1D BN-gel was performed using a GS-800 calibrated densitometer and Quantity One Software.

3. Results

3.1. Ageing modulates protein–protein interactions of OxPhos complexes

Contrary to most previous proteome studies reflecting solely changes in the total abundance of proteins or, more recently, in post-translational modifications, utilisation of BN-PAGE enables investigation of age-dependent alterations in the abundance, structure, composition and activity of individual respiratory chain complexes as well as of supercomplexes composed of these complexes. In addition ATP-synthase monomers, dimers and homooligomers are displayed. In the first dimension, proteins are separated as distinct bands in their native, active state, preserving all functional relevant protein–protein interactions (Fig. 2). In the second dimension, the denatured proteins or their dissociated subunits migrate vertically below the respective position of the native protein(complex/supercomplex) in the first dimension. For solubilised cortical rat brain mitochondria individual complexes III_2 (always present as dimer), IV and V as well as ATP synthase (complex V) oligomers (complexes V_2, V_3 and V_4) are visualised on BN-gels. Also the small supercomplex III_2IV_1 containing a complex III dimer and one copy of complex IV as well as large supercomplexes $I_1III_2IV_x$ ($x = 0–3$) containing complex I and complex III dimer and zero to several copies of complex IV (marked in red in Fig. 2) are identified. In contrast to other rat tissues (Dani et al., 2009; Gómez et al., 2009; Reifschneider et al., 2006), in cortex (Fig. 2) and in skeletal muscle (Lombardi et al., 2009) complex I exists almost solely in supramolecular form assembled with other respiratory chain complexes. Complex I is not observed as individual complex neither in young nor in aged animals. The abundance of complex II is not sufficient to detect this complex in first and second dimension. Due to the crude mitochondrial preparation studied, the digitonin-solubilisates exhibit also bands of non-mitochondrial proteins like myeline.

To analyse age-related alterations in the mitochondrial proteome of rat cortex we quantified the amount of protein subunits in the second dimension after staining with SYPRO Ruby, a fluorescent dye with a large linear, dynamic quantification range of 3.3 orders of magnitude (detection limit 1 ng protein/spot, Wheelock et al., 2006) and compared the results with the data obtained for the first dimension. Only for qualitative visualisation silver staining was performed afterwards. To analyse the relative proportion of the respiratory chain complexes as individual complexes or assembled together in supercomplexes on each 2D-gel, no normalisation was necessary. For comparison of different gels, scaling was applied using four protein bands [phosphorylase b (97 kDa), albumin (66 kDa), ovalbumin (45 kDa) and carbonic anhydrase (30 kDa)] as external standard to correct for differences resulting from divergent staining intensities.

3.2. Solubilisation efficiency and membrane properties depend on age

To analyse age-related changes in the protein profile, mitochondria have been isolated immediately upon dissection of the cortex, i.e., from non-frozen tissue. By applying this strategy well preserved mitochondria of high quality have been obtained. Control experiments demonstrated that freezing of cortex tissue in liquid nitrogen before isolation of the mitochondria affects protein–protein interactions and/or detergent solubilisation efficiency (data not shown). The crude mitochondrial fraction obtained by this procedure were not subjected to further purification, in order to preserve the delicate and damaged mitochondria, that might be more abundant and more severely affected in aged samples and possibly lost during harsh purification steps.

The biological variance as well as differences caused by isolation of mitochondria and proteins within each age-group ($n = 4$) are slight as reflected by the small variation in the amount of the α-subunit in complex V for each of the young and aged rats studied separately (Fig. 3). According to these data, in rat cortex there is a highly significant 1.48-fold (32%) age-related decrease in the abundance of the ATP synthase monomer (Fig. 3, α-subunit). The same 1.45-fold age-related decrease is observed if the β-subunit of complex V monomer was analysed instead.

It is important to state that for each sample preparation, i.e., the respective age-state, optimal solubilisation efficiency and preservation of protein–protein interactions have to be determined. Optimal extraction conditions for mitochondrial membrane proteins of rat cortex have been tested using 2, 4 and 8 g detergent/g protein. Quantitative but still gentle solubilisation occurs for both 5 and 30 months mitochondria using a digitonin to protein ratio of 8 g/g. This is demonstrated by comparing e.g. the total amount of ATP synthase extracted with 4 and 8 g digitonin/g protein, respectively [Fig. 4]. Solubilisation of complex V from young rat mitochondria was already quantitative using 4 g/g, since no further increase in the protein abundance occurred upon increasing the ratio to 8 g/g. (Note that the intensities depicted in Fig. 4A and B and Figs. 3 and 5 are a quantitative measure of protein amount.) In contrast, no quantitative extraction of mitochondrial proteins was observed for aged rats when solubilised with less than 8 g/g. Increasing the detergent to protein ratio from 4 g/g (Fig. 4A) to 8 g/g (Fig. 4B) resulted in an apparent 1.53-fold increase of extracted ATP synthase, but only for mitochondria from aged rats.

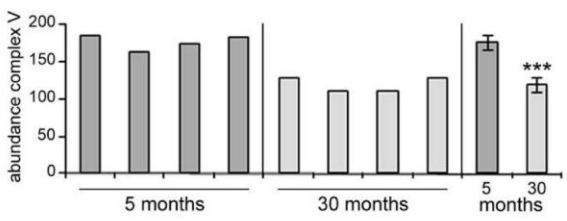

Fig. 3. Age-dependent decline in abundance of monomeric ATP synthase and biological variance within each age-group ($n = 4$). The amount of the α-subunit of ATP synthase monomer of each individual is plotted together with the mean and standard deviation of each age-group. (The data of each individual is the mean of two gel replicates.) At the age of 30 months, the amount of the α-subunit is about 1.5-fold less than at month 5. A very similar age-dependent difference with comparable small biological variance and standard deviation has been obtained for the ATP-synthase monomer β-subunit (data not shown). The ordinate values in Figs. 3–7 represent quantitative measurements of protein amounts. The *P*-value was highly significant: $***P < 0.001$, in comparison to young rats.

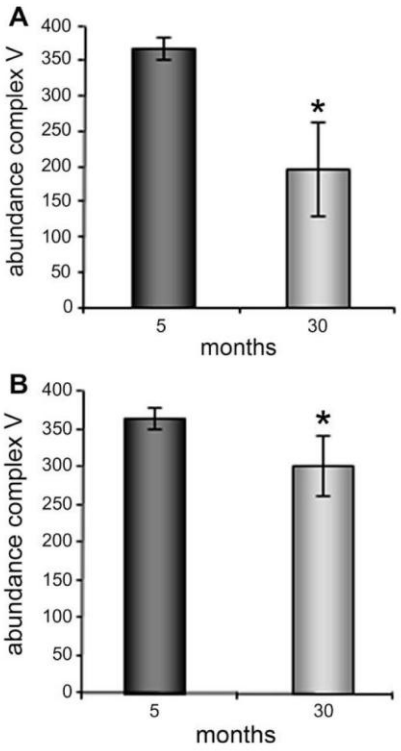

Fig. 4. Age-dependent differences in solubilisation efficiency employing a 4 g/g [A] and 8 g/g [B] digitonin to protein ratio. Protein abundances are shown for the ATP synthase α-subunit in both monomeric and oligomeric complex V. Values displayed are means of four animals per age-group and standard deviation. Only the aged mitochondrial membranes are more resistant to detergent solubilisation and require 8 g/g detergent. The *P*-value was significant: $^{*}0.05 > P > 0.01$, in comparison to young rats.

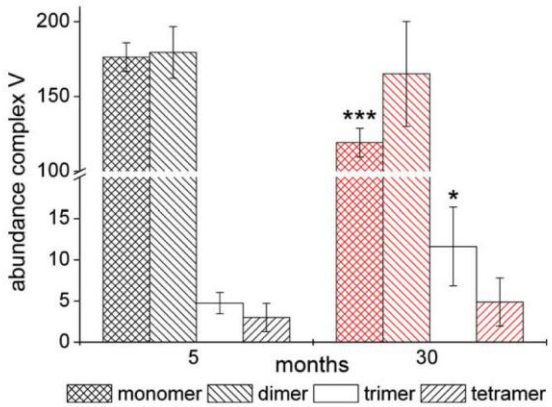

Fig. 5. Ageing enhances the oligomerisation of the ATP synthase. Values presented are mean and standard deviation of ATP synthase α-subunit abundance of four animals per age-group ($n = 4$). The *P*-value was significant: $^{***}P < 0.001$, $^{*}0.05 > P > 0.01$, in comparison to young rats.

Notably this higher detergent amount does not affect the delicate protein–protein interactions of OxPhos supercomplexes. Therefore, besides individual proteins also protein complexes and supercomplexes can be isolated in their native state using digitonin as mild detergent at the applied optimised conditions.

The observations depicted in Fig. 4 demonstrate profound differences in the physico-chemical properties of the lipid phase, i.e., a decrease of the membrane 'fluidity' in the aged state, in line with previous fluorescence polarisation measurements (Eckert et al., 2001; Sugawa et al., 1996).

3.3. Age-related abundance decrease of intact ATP synthase as well as increase of its oligomers and of unbound F_1

Applying quantitative solubilisation conditions (8 g/g digitonin/protein), there is approximately 20% (1.2-fold) less total ATP synthase (sum of complex V monomers and oligomers) present on gels of aged rat cortex mitochondria (Fig. 4B). [If an insufficient amount of detergent is applied, an erroneous apparent age-associated decline of 54% (1.86-fold) would have been deduced (Fig. 4A)]. The abundance of the monomeric form of complex V is even 32% (1.43-fold) less in aged mitochondria (Fig. 3). To analyse and underline the significance of these results, proteins of SDS-solubilised mitochondria of both age-groups have been separated on 1D-SDS-gels allowing quantitation of the total amount of complex V in each sample independent of digitonin solubilisation efficiency. There was also an age-associated 1.2-fold decrease in ATP-synthase abundance detected on 1D-SDS-gels (data not shown).

Noteworthy, the age-associated decrease of the total abundance of complex V is accompanied by an increase of oligomer formation (Fig. 5). On the expense of the monomer, the proportion of the dimeric, trimeric and tetrameric ATP synthase increases. This also explains the differences between the 1.48-fold decrease depicted for the monomer in Fig. 3 as compared to the 1.2-fold decrease for the sum of all complex V assembly states (Fig. 4B).

Besides intact ATP synthase monomer and oligomers (V_2–V_4), also unbound F_1 (catalytic unit of ATP synthase, water soluble) was observed in both age-groups (representing about 9% unbound F_1 in reference to all assembled F_1 in complex V of aged mitochondria, Fig. 6). The total amount of unbound F_1 is independent of the detergent to protein ratio in the tested range of 2–8 g/g (data not shown), demonstrating that the solubilisation conditions do not affect the stability of the ATP synthase. Aged rats feature a 2.8-fold higher amount of unbound F_1 which could be related to an age-dependent instability of ATP-synthase and/or less assembled complex.

3.4. Age-related abundance decrease of complex I comprising supercomplexes

As displayed by the 1D BN-gel and the 2D SDS-gel in Fig. 2, in rat cortex mitochondria, besides the individual respiratory

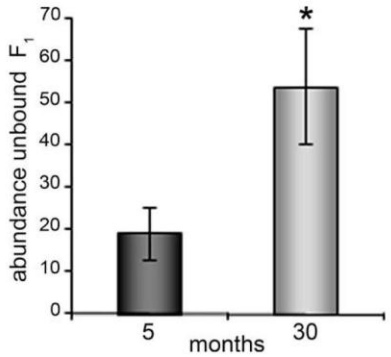

Fig. 6. Ageing increases the abundance of the unbound, water soluble F_1-part of complex V. Combined abundances of α- and β-subunits of unbound F_1 ($n = 4$). The *P*-value was significant: $^{*}0.05 > P > 0.01$, in comparison to young rats.

Table 1
Age-associated abundance decrease of individual OxPhos complexes III_2 and IV and of supercomplexes of different composition in rat cortex mitochondria. Changes in protein abundance are listed in fold as well as in percentage (in brackets; decline of complexes/supercomplexes as related to the abundance in young rats; average of four animals per age-group).

OxPhos		Decrease during ageing
Individual complexes	Complex III_2	1.16 (13.7%)
	Complex IV	1.26 (20.6%)
Supercomplexes	III_2IV_1	1.00 (1.5%)
	I_1III_2	2.38 (58.0%)
	$I_1III_2IV_1$	1.44 (30.8%)
	$I_1III_2IV_2$	1.69 (40.7%)
	$I_1III_2IV_3$	1.16 (13.8%)

complexes III_2 and IV, stoichiometric assemblies with different composition of complexes I, III_2 and IV exist. But contrary to the situation in other rat tissue e.g., liver (Dani et al., 2009; Reifschneider et al., 2006), kidney (Reifschneider et al., 2006), skeletal muscle (Lombardi et al., 2009; Reifschneider et al., 2006), heart (Gómez et al., 2009; Reifschneider et al., 2006) as well as in most organisms studied so far [e.g. the fungi *Neurospora* and *Podospora* (Krause et al., 2004b; Maas et al., 2009; Marques et al., 2007), *C. elegans* (Brys et al., submitted for publication), Drosophila (Le Pécheur et al., 2009), bovine heart (Krause, 2007; Reifschneider et al., 2006; Schäfer et al., 2006, 2007a; Schägger and Pfeiffer, 2001), fish (Schäfer et al., 2007b) complex I is only present in supercomplexes but not as individual complex in rat cortex (this study, Fig. 2), striatum (Wernicke et al., 2010) and skeletal muscle (Lombardi et al., 2009) and human skin fibroblasts (Colindres et al., 2007), respectively.

For individual complex III_2 and IV a small, statistically non-significant decrease in the abundance during ageing (Table 1) occurred. The supercomplex III_2IV_1 composed of complexes III_2 and IV did not change in abundance at all by age (Table 1). Four larger supercomplexes containing complex I (I_1III_2, $I_1III_2IV_1$, $I_1III_2IV_2$ and $I_1III_2IV_3$) could be quantified on the gels (Fig. 2, Table 1). Comparison of young and aged rat mitochondria demonstrates an age-related decrease in abundance of these supercomplexes (a–d) by different extent resulting in a change in the relative proportion of each in the inner mitochondrial membrane, if young and aged organisms are compared. The overall 1.6-fold (40%, Fig. 7A) decline in the sum of all these complex I containing supercomplexes with age is caused to large extent by the pronounced 2.4-fold (58%) abundance decline of the supercomplex I_1III_2 (Fig. 7B).

The proportion of supercomplex $I_1III_2IV_1$ and $I_1III_2IV_2$ also decreases notably during ageing by about 1.4-fold (31%) and 1.7-fold (41%), respectively, whereas the decline of supercomplex $I_1III_2IV_3$ was much smaller, only 1.16-fold (14%) (Table 1). As mentioned before, in rat brain cortex complex I cannot be detected as individual complex. It is almost exclusively assembled as supercomplex. As a consequence, the pronounced decrease of complex I containing supercomplexes $I_1III_2IV_{0-3}$ reflects the large, functional relevant decrease of complex I during ageing by about 1.6-fold (40%, Fig. 7A), which is much larger than that of the individual OxPhos complexes III_2, IV and V (Table 1).

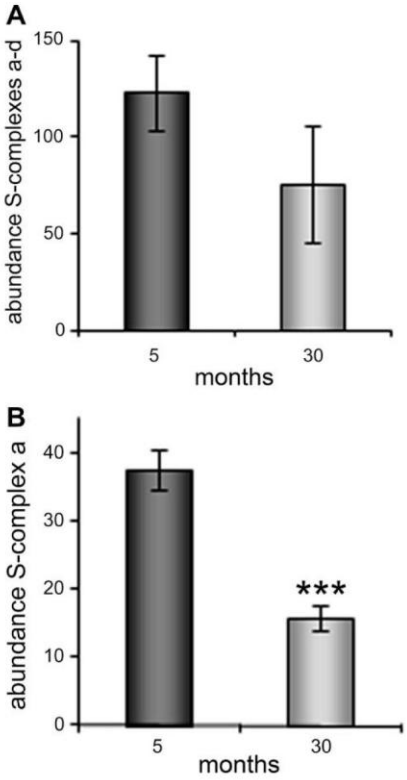

Fig. 7. Age-related decrease in the total abundance of respiratory chain supercomplexes $I_1III_2IV_{0-3}$ (1.6-fold) [A] and of supercomplex I_1III_2 (2.38-fold) [B] in rat cortex mitochondria. The sum of intensities of all quantified complex subunits (1–4, Fig. 2) is shown. Means and ±SD of four animals per age-group. Please note that in the case for the young group of [B] instead of four only three individual are included, since one sample could not be evaluated for these specific data only. The *P*-value was highly significant: $^{***}P < 0.001$, in comparison to young rats.

4. Discussion

Mitochondria are not only prominent targets for ROS-induced impairment but also the major source of ROS. Damages induced in biomolecules like nucleic acids, proteins and lipids are still considered as a root cause in the ageing processes. Therefore, analysis of the protein profile of mitochondria and its age-dependent variation is a promising approach to unravel mechanisms involved in ageing and in age-related diseases.

The brain is especially vulnerable to ROS-attack due to its high level of oxidisable unsaturated fatty acids, high oxygen consumption, high level of free radical-inducing iron, less efficient antioxidant system (Hamilton et al., 2001; Poon et al., 2006c; Tian et al., 1998), less efficient DNA repair system (Gredilla et al., 2008) and being less regenerative (Ffrench-Constant and Mathews, 1994). Age-dependent changes observed for whole brain (cerebrum) (Ekstrom et al., 1980; Groebe et al., 2007; Poon et al., 2006b; Rao et al., 1990) might be difficult to interpret because of regional distinctions in the anatomy, physiology and function. Contrary to most previous studies, we analysed a defined brain area, the cortex, and quantified changes of the mitochondrial proteome not only in respect to the protein abundance but also to protein–protein interactions.

The cortex was selected because having a key role in learning and memory and its important sensory and motor areas. This brain area is prone to neurodegenerative diseases like Alzheimer's, Parkinson's and Huntington's. In addition, the cortex is the largest brain area and therefore easier accessible for proteomic studies.

We quantified changes in the abundances of individual OxPhos complexes (I, III_2, IV and V) and of the respective supercomplexes $I_1III_2IV_{0-3}$ and MF_oF_1 oligomers (V_2–V_4) caused or accompanied by ageing. The importance of proper solubilisation conditions

when analysing the membrane proteome became obvious. Besides the choice of detergent – gentle or harsh –, the application of different detergent to protein ratios shed light on lipid composition and physical state of membranes that may alter during ageing. Presumably the observed different solubilisation behaviour described for ATP synthases in the inner mitochondrial membrane of young and aged rats, respectively, (Fig. 4A and B) results from age-associated changes in composition of the lipid phase. Changes in the lipid membrane are also expressed in the increased anisotropy of the fluorescent probes DPH and TMA-DPH in aged synaptosomal membranes from rat cortex (Sugawa et al., 1996). This age-associated anisotropy increase is indicative of a larger order and/or restricted dynamics of the lipid molecules, which commonly is interpreted as increased viscosity or decreased membrane "fluidity" (Eckert et al., 2001; Sugawa et al., 1996). Therefore, for each sample analysed, dedicated solubilisation conditions have to be determined.

4.1. Age-associated changes in abundance, oligomerisation and stability of MF_oF_1 ATP synthase

As demonstrated in this study, the abundance of mitochondrial ATP synthase (V_1–V_4) is decreasing 1.2-fold during ageing in rat cortex (Fig. 4B) and of the monomer even 1.5-fold (Fig. 3). A similar abundance decrease of complex V has been previously observed in mitochondria of whole rat brain, liver (Dani et al., 2009; Groebe et al., 2007) and skeletal muscle (Lombardi et al., 2009) as well as for the fungus *Podospora anserina* and human cells (Groebe et al., 2007). An age-associated decline in the cellular ATP-level, as previously described for senescent human cells (Stöckl et al., 2006, 2007; Wang et al., 2003; Zwerschke et al., 2003), might be the consequence.

Ageing is accompanied by an 2.8-fold increase of unbound F_1, independent of the detergent to protein ratio employed. However, on an absolute scale, the increase is less than the larger decline of intact ATP synthase (Fig. 6). F_1 was also found in mitochondria of patients with specific mitochondrial disorders (Wittig et al., 2006). Noteworthy, unbound F_1 will hydrolyse ATP in the tissue and in this way even a small population might have a pronounced impact on the ATP level.

To what extent the age-dependent increase of homooligomeric states (V_2–V_4; Fig. 5) on the expense of the monomeric MF_oF_1 influences its activity and with it the cellular energy status is still unknown. To date any differences in specific activity of monomers versus oligomers have not been analysed. In *Chlamydomonas reinhardtii*, the mitochondrial ATP synthase is always present as dimer (V_2), independent of the metabolic state while the monomer to dimer ratio in chloroplasts is influenced by the energy source. In *Chlamydomonas* the MF_oF_1 ATP synthase dimer is the active state while in chloroplasts the monomeric form seems to be more active (Schwassmann et al., 2007). Also in the filamentous fungus *Podospora anserina* almost all of the mitochondrial ATP synthases are arranged in the dimeric state (Krause et al., 2004b). It has to be examined if the observed age-associated increase of ATP synthase oligomerisation in rat cortex mitochondria is accompanied by a shift to a higher specific activity.

In mitochondria, the ATP synthase dimers and homooligomers are involved in cristae formation by inducing curvature of the inner mitochondrial membrane as, e.g. described for yeast (Bornhövd et al., 2006; Gavin et al., 2004; Gilkerson et al., 2003; Giraud et al., 2002; Paumard et al., 2002) and bovine heart (Gilkerson et al., 2003; Minauro-Sanmiguel et al., 2005). The extent of cristae invagination has an effect on distribution of OxPhos complexes (and supercomplexes?) and efficiency of energy conversion in mitochondria (Zick et al., 2009). The magnitude of cristae remodelling by the observed age-associated abundance decrease of ATP synthase (Fig. 4B) and increase in dimerisation/oligomerisation (Fig. 5) is still inexplicit.

4.2. Age-associated decrease of complex I containing supercomplexes is size-dependent

In contrast to common textbook view complexes I, III_2, and IV are not randomly distributed in the inner mitochondrial membrane as individual freely diffusing entities but predominantly assembled in so called supercomplexes of defined stoichiometries (Fig. 1) (Krause, 2007; Schon and Dencher, 2009; Seelert et al., 2009; Wittig et al., 2006; Wittig and Schägger, 2009). Evidence suggests that the assembly of respiratory chain complexes in supercomplex structures is advantageous for efficient substrate channelling and essential for the stability and activity of each complex (Schäfer et al., 2006; Schon and Dencher, 2009; Wittig and Schägger, 2009). Age-related changes in the abundance of these supercomplexes have been reported recently for rat brain (Dencher et al., 2007; Seelert et al., 2009), rat skeletal muscle (Lombardi et al., 2009) and rat heart (Gómez et al., 2009).

For rat brain cortex mitochondria we observed an age-associated abundance decrease of the individual respiratory chain complexes III_2 (1.2-fold) and IV (1.3-fold, Table 1). Individual complex I was not present in 1D BN-gels or in 2D SDS-gels. In addition, we quantified abundance changes in OxPhos supercomplexes, the natural stoichiometric super-assemblies of respiratory complexes I, III_2 and IV (Fig. 1). While the amount of supercomplex III_2IV_1 is not changing in aged rats compared to young, there is a significant apparent loss of complex I containing supercomplexes $I_1III_2IV_{0-3}$ during ageing (1.6-fold, Fig. 7A). The most pronounced decrease occurs for supercomplex I_1III_2 (2.4-fold, Fig. 7B). The proportion of complex IV containing supercomplexes $I_1III_2IV_1$ (1.4-fold) and $I_1III_2IV_2$ (1.7-fold) also declined notably whereas the decrease of supercomplex $I_1III_2IV_3$ (1.2-fold) was smaller (Table 1).

Complex I is almost solely present in supercomplexes and hardly seen as an individual complex. Therefore, the total amount of complex I is decreasing about approximately 40% (1.6-fold, Fig. 7A) during ageing according to the overall decrease of complex I containing supercomplexes. In rat brain cortex mitochondria, complex I displays the most significant age-related decline (Fig. 7A) compared to the other individual OxPhos complexes like complexes III_2 and IV (Table 1).

At a first glance, the simplest explanation of our data is that the observed age-dependent decrease in abundance of the individual complexes III_2 (13.7%, 1.2-fold) and IV (20.6%, 1.3-fold), of complex I (assembled as supercomplex; 40%, 1.6-fold) and of all supercomplexes $I_1III_2IV_{0-3}$ (40%, 1.6-fold) directly results in a pronounced decline in energy conversion via a smaller electrochemical proton gradient generated. Whereas the abundance of supercomplex III_2IV_1 is not affected by age at all, in cortex tissue the most pronounced abundance decrease during ageing occurs for supercomplex I_1III_2. The observed decline of I_1III_2 could be caused by two opposite ways: (1) By an increased interaction with complex IV, forming larger supercomplexes, especially $I_1III_2IV_1$ or (2) by destruction of I_1III_2 via disassembly into its individual complexes. We favour mechanism (1) based on the data depicted in Table 1 and due to the absence of an increase of individual complexes I and III_2 on the gels. (In fact the amount of III_2 decreased in aged mitochondria and individual complex I was not observed. That could only be explained if the supercomplex I_1III_2 would undergo a complete age-associated decomposition directly into its subunits or even into smaller peptides.) Interconversion of I_1III_2 into $I_1III_2IV_1$ will result in a higher activity of both complex I (2.3-fold) and complex III_2 (16.5-fold) as quantified by Schäfer et al. (2006). Complex IV was therefore essential for a boost of the specific

activity of complexes I and III_2 when the activities of I_1III_2 and $I_1III_2IV_1$ were compared (Schäfer et al., 2006). This was directly corroborated by our semi-quantitative in-gel activity determination confirming that $I_1III_2IV_1$ has the highest specific complex I activity of all supercomplexes ($I_1III_2IV_{0-3}$). Furthermore, no age-dependent decline in specific activities of supercomplexes $I_1III_2IV_{0-3}$ occurred (data not shown). Overall supercomplexes $I_1III_2IV_{0-3}$ decrease about 1.6-fold in abundance but there is a change in the relative proportion towards supercomplex $I_1III_2IV_1$ that has the highest specific activity. In conclusion, our results demonstrate that the relative proportion of the various supercomplexes is changing with age. Since the specific activity of supercomplex $I_1III_2IV_1$ is highest and since this supercomplex is increasing in relative proportion as compared to the others, this will in part compensate for the overall abundance-decline in respiratory supercomplexes with age.

Lombardi et al. (2009) also favoured a compensatory mechanism by formation of more active larger supercomplexes to compensate for the reduced level and activity of the MF_oF_1 ATP synthase. This interpretation is supported by their important observation of an increased respiratory control ratio in aged rats, i.e., "of more efficient mitochondrial oxidative phosphorylation in ageing skeletal muscle" (Lombardi et al., 2009). Therefore the energy conversion is presumably less affected by the severe age-dependent decline of supercomplex I_1III_2 abundance (our study).

The fact that with age the amount of the small supercomplex I_1III_2 decreases significantly more as compared to the other, larger complex I containing supercomplexes (with complex IV in addition) (Table 1) supports the notion and previous results that larger supercomplexes are more stable. Consequentially the formation of larger complex IV containing supercomplexes is the most favourably structure for the activity of the assembled complexes, as shown by Schäfer et al. (2006).

Our data for cortex mitochondria are in qualitative and even quantitative agreement with those of Lombardi et al. (2009) for interfibrillar mitochondria of rat skeletal muscle. In rat skeletal muscle a similar significant age-dependent decline of individual complexes III_2, IV, and V as well as of supercomplexes were observed. The major supercomplex bands in aged mitochondria were those representing larger supercomplexes ($I_1III_2IV_{1-4}$) and the majority of complex I was assembled in supercomplexes (Lombardi et al., 2009). Contrary, Gómez et al. (2009) observed in rat heart tissue an age-related deterioration of mainly the larger supercomplexes with a maximal extent of 25% while the amount of individual complexes I, III_2 and IV did not change significantly. Lombardi et al. (2009) (rat skeletal muscle) and our study (cortex) employed Wistar rats as model organism, while Gómez et al. (2009) analysed heart tissue from Fischer rats which might explain, at least in part, the different results. In addition, there is a pronounced tissue specificity of the rat mitochondrial proteome (Reifschneider et al., 2006).

Besides differences in the biological samples, there are also important methodological differences. Lombardi et al. (2009) and Gómez et al. (2009) analysed the protein profile and its age-dependent variation in the 1D blue-native gel dimension only, which has much less resolution power than the second dimension SDS gel we predominantly evaluated (Fig. 2, Table 1). Furthermore, in contrast to Lombardi et al. (2009) and Gómez et al. (2009) the quantification in our study employs the fluorescent dye SYPRO Ruby having a much larger linear dynamic staining range of 2000-fold and sensitivity, as compared to the only 7 to 50-fold dynamic range of classical and colloidal Coomassie-blue G-250 (Berggren et al., 2001; Patton and Beechem, 2001).

By which mechanisms ageing could influence the observed complex to supercomplex transition? It is well documented that cardiolipin is required for supercomplex formation and stability (Brandner et al., 2005; Gohil et al., 2004; Pfeiffer et al., 2003; Wenz et al., 2009; Zhang et al., 2002) as well as can modulate the efficiency of energy conversion (Haines and Dencher, 2002; Mileykovskaya and Dowhan, 2009). In rat heart tissue an age-dependent decline in the cardiolipin content was observed by Paradies et al. (1993, 1997). Reduced levels of cardiolipin in patients with Barth syndrome result in reduced amount of supercomplexes (Brandner et al., 2005; McKenzie et al., 2006).

With our recent knowledge of the 2D and 3D-structures of supercomplexes I_1III_2 and $I_1III_2IV_1$ (Schäfer et al., 2006, 2007a), we aim to understand the age-dependent changes in supramolecular architecture of OxPhos complexes in context to the often described alterations in energy conversion and in ROS generation. From the close spatial arrangement of the respective electron carrier binding sites in supercomplexes as compared to electron transfer by transient encounters of individual complexes I, III_2 and IV with each other and with the mobile electron carriers CoQ and cytochrome c, all laterally diffusing along the inner mitochondrial membrane, less superoxide anion radical formation is expected in supercomplexes to occur (Schäfer et al., 2007a; Vonck and Schäfer, 2009). In line with this postulation, mitochondrial proteins of aged rat brain cortex (Frenzel M. and Syzonenko T., unpublished results) and rat liver (Frenzel M. and Beyer C., unpublished results) displayed a lower amount of carbonyl groups indicative of ROS attack than in young mitochondria, in seeming contradiction to the "Free radical/ROS theory of ageing".

5. Conclusion

Insight into the molecular aspects of ageing was obtained by analysis of the mitochondrial proteome of rat cortex. The observed age-related alterations in the abundance of respiratory chain complexes and supercomplexes may modulate not only free radical/ROS formation but also the magnitude of the electrochemical proton gradient established across the inner mitochondrial membrane that is the driving force for ATP production via the ATP synthase. A second determinant of ATP synthesis is complex V itself which abundance and state of oligomerisation are directly affected by age, as well as the prevalence of unbound ATP-hydrolysing F_1. The age-associated alterations observed for rat cortex mitochondria in abundance and supramolecular architecture of OxPhos complexes I, III_2, IV and V might be an important clue to understand the postulated link between respiration, oxidative stress, and longevity. The data discussed and the methodologies described here are also of high relevance for elucidating the molecular basis of age-related diseases such as Alzheimer's and Parkinson's dementia (Seelert et al., 2009; Wernicke et al., 2010).

Acknowledgements

The work was supported by the European consortium, MiMage: "Role of Mitochondria in Conserved Mechanisms of Ageing", EC FP6 Contact No. LSHM-CT-2004-512020 to NAD. This publication reflects only the authors' views. The EC is not liable for any use that may be made from this information herein. We are grateful to Regine Hill for isolation of mitochondria. This article is part of the doctoral thesis of Monika Frenzel at the Technische Universität Darmstadt.

References

Berggren, K.N., Chernokalskaya, E., Lopez, M.F., Beechem, J.M., Patton, W.F., 2001. Comparison of three different fluorescent visualization strategies for detecting *Escherichia coli* ATP synthase subunits after sodium dodecyl sulfate–polyacrylamide gel electrophoresis. Proteomics 1, 54–65.

Blum, H., Beier, H., Gross, H.J., 1987. Improved silver staining of plant proteins, RNA and DNA in polyacrylamide gels. Electrophoresis 8, 93–99.

Bornhövd, C., Vogel, F., Neupert, W., Reichert, A.S., 2006. Mitochondrial membrane potential is dependent on the oligomeric state of F_1F_0-ATP synthase supracomplexes. J. Biol. Chem. 281, 13990–13998.

Brandner, K., Mick, D.U., Frazier, A.E., Taylor, R.D., Meisinger, C., Rehling, P., 2005. Taz1, an outer mitochondrial membrane protein, affects stability and assembly of inner membrane protein complexes: implications for Barth Syndrome. Mol. Biol. Cell 16, 5202–5214.

Brewer, G.J., Jones, T.T., Wallimann, T., Schlattner, U., 2004. Higher respiratory rates and improved creatine stimulation in brain mitochondria isolated with anti-oxidants. Mitochondrion 4, 49–57.

Brys, K., Castelein, N., Matthijssens, F., Krause, F., Schäfer, E.R., Dencher, N.A., Braeckman, B., Vanfleteren, J.R., submitted for publication. Disruption of insulin signaling preserves bioenergetic competence of mitochondria in aging *Caenorhabditis elegans*.

Chance, B., Williams, G.R., 1955. A method for the localization of sites for oxidative phosphorylation. Nature 176, 250–254.

Colindres, M., Fournier, C., Ritter, S., Zahnreich, S., Decker, H., Dencher, N., Frenzel, M., 2007. Increase of oxidative stress in normal human fibroblasts after irradiation. GSI Sci. Rep. 2007, 356.

Dani, D., Dencher, N.A., 2008. Native-DIGE: a new look at the mitochondrial membrane proteome. Biotechnol. J. 3, 817–822.

Dani, D., Shimokawa, I., Komatsu, T., Higami, Y., Warnken, U., Schokraie, E., Schnölzer, M., Krause, F., Sugawa, M.D., Dencher, N.A., 2009. Modulation of oxidative phosphorylation machinery signifies a prime mode of anti-ageing mechanism of calorie restriction in male rat liver mitochondria. Biogerontology. doi: 10.1007/s10522-10009-19254-y.

Dencher, N.A., Frenzel, M., Reifschneider, N.H., Sugawa, M., Krause, F., 2007. Proteome alterations in rat mitochondria caused by aging. Ann. N. Y. Acad. Sci. 1100, 291–298.

Eckert, G.P., Wood, W.G., Müller, W.E., 2001. Effects of aging and beta-amyloid on the properties of brain synaptic and mitochondrial membranes. J. Neural. Transm. 108, 1051–1064.

Ekstrom, R., Liu, D.S., Richardson, A., 1980. Changes in brain protein synthesis during the life span of male Fischer rats. Gerontology 26, 121–128.

Eubel, H., Heinemeyer, J., Sunderhaus, S., Braun, H.P., 2004. Respiratory chain supercomplexes in plant mitochondria. Plant Physiol. Biochem. 42, 937–942.

Ffrench-Constant, C., Mathews, G.A., 1994. Brain repair: lessons from developmental biology. J. Neurol. 242, S29–32.

Gavin, P.D., Prescott, M., Luff, S.E., Devenish, R.J., 2004. Cross-linking ATP synthase complexes in vivo eliminates mitochondrial cristae. J. Cell. Sci. 117, 2333–2343.

Gilkerson, R.W., Selker, J.M., Capaldi, R.A., 2003. The cristal membrane of mitochondria is the principal site of oxidative phosphorylation. FEBS Lett. 546, 355–358.

Giraud, M.F., Paumard, P., Soubannier, V., Vaillier, J., Arselin, G., Salin, B., Schaeffer, J., Brethes, D., di Rago, J.P., Velours, J., 2002. Is there a relationship between the supramolecular organization of the mitochondrial ATP synthase and the formation of cristae? Biochim. Biophys. Acta 1555, 174–180.

Gohil, V.M., Hayes, P., Matsuyama, S., Schägger, H., Schlame, M., Greenberg, M.L., 2004. Cardiolipin biosynthesis and mitochondrial respiratory chain function are interdependent. J. Biol. Chem. 279, 42612–42618.

Gómez, L.A., Monette, J.S., Chavez, J.D., Maier, C.S., Hagen, T.M., 2009. Supercomplexes of the mitochondrial electron transport chain decline in the aging rat heart. Arch. Biochem. Biophys. 490, 30–35.

Grandier-Vazeille, X., Guerin, M., 1996. Separation by blue native and colorless native polyacrylamide gel electrophoresis of the oxidative phosphorylation complexes of yeast mitochondria solubilized by different detergents: specific staining of the different complexes. Anal. Biochem. 242, 248–254.

Gredilla, R., Garm, C., Holm, R., Bohr, V.A., Stevnsner, T., 2008. Differential age-related changes in mitochondrial DNA repair activities in mouse brain regions. Neurobiol. Aging.

Grigorieff, N., 1998. Three-dimensional structure of bovine NADH:ubiquinone oxidoreductase (complex I) at 22 A in ice. J. Mol. Biol. 277, 1033–1046.

Groebe, K., Krause, F., Kunstmann, B., Unterluggauer, H., Reifschneider, N.H., Scheckhuber, C.Q., Sastri, C., Stegmann, W., Wozny, W., Schwall, G.P., Poznanovic, S., Dencher, N.A., Jansen-Dürr, P., Osiewacz, H.D., Schrattenholz, A., 2007. Differential proteomic profiling of mitochondria from *Podospora anserina*, rat and human reveals distinct patterns of age-related oxidative changes. Exp. Gerontol. 42, 887–898.

Hackenbrock, C.R., Chazotte, B., Gupte, S.S., 1986. The random collision model and a critical-assessment of diffusion and collision in mitochondrial electron-transport. J. Bioenerg. Biomembr. 18, 331–368.

Haines, T.H., Dencher, N.A., 2002. Cardiolipin: a proton trap for oxidative phosphorylation. FEBS Lett. 528, 35–39.

Hamilton, M.L., Van Remmen, H., Drake, J.A., Yang, H., Guo, Z.M., Kewitt, K., Walter, C.A., Richardson, A., 2001. Does oxidative damage to DNA increase with age? Proc. Natl. Acad. Sci. USA 98, 10469–10474.

Huang, L.S., Cobessi, D., Tung, E.Y., Berry, E.A., 2005. Binding of the respiratory chain inhibitor antimycin to the mitochondrial bc1 complex: a new crystal structure reveals an altered intramolecular hydrogen-bonding pattern. J. Mol. Biol. 351, 573–597.

Hunzinger, C., Wozny, W., Schwall, G.P., Poznanovic, S., Stegmann, W., Zengerling, H., Schoepf, R., Groebe, K., Cahill, M.A., Osiewacz, H.D., Jägemann, N., Bloch, M., Dencher, N.A., Krause, F., Schrattenholz, A., 2006. Comparative profiling of the mammalian mitochondrial proteome: multible aconitase-2 isoforms including *N*-formylkynurenine modifications as part of a protein biomarker signature for reactive oxidative Species. J. Proteome Res. 5, 625–633.

Krause, F., Reifschneider, N.H., Vocke, D., Seelert, H., Rexroth, S., Dencher, N.A., 2004a. "Respirasome"-like supercomplexes in green leaf mitochondria of spinach. J. Biol. Chem. 279, 48369–48375.

Krause, F., Scheckhuber, C.Q., Werner, A., Rexroth, S., Reifschneider, N.H., Dencher, N.A., Osiewacz, H.D., 2004b. Supramolecular organization of cytochrome c oxidase- and alternative oxidase-dependent respiratory chains in the filamentous fungus *Podospora anserina*. J. Biol. Chem. 279, 26453–26461.

Krause, F., Reifschneider, N.H., Goto, S., Dencher, N.A., 2005. Active oligomeric ATP synthases in mammalian mitochondria. Biochem. Biophys. Res. Commun. 329, 583–590.

Krause, F., Seelert, H., 2008. Detection and analysis of protein–protein interactions of organellar and prokaryotic proteomes by blue native and colorless native gel electrophoresis. Curr. Protoc. Protein Sci. Chapter 14, Unit 14.11 1–36, republished as Unit 19.18.

Krause, F., 2007. Oxidative phosphorylation supercomplexes in various eukaryotes: A paradigm change gains critical momentum. In: Siso, M.I.G. (Ed.), Transworld Resarch Network, Kerala, India, pp. 179–213.

Kuonen, D.R., Roberts, P.J., Cottingham, I.R., 1986. Purification and analysis of mitochondrial membrane proteins on nondenaturing gradient polyacrylamide gels. Anal. Biochem. 153, 221–226.

Le Pécheur, M., Morrow, G., Kim, H.-J., Schäfer, E., Dencher, N., Tanguay, R.M., 2009. Characterization of OXPHOS complexes in long-lived flies overexpressing Hsp22. Mitochondria in ageing and age-related disease, MiMage final meeting (and LINK-AGE Topic Research) Group Meeting, abstract 16, p. 35.

Lombardi, A., Silvestri, E., Cioffi, F., Senese, R., Lanni, A., Goglia, F., de Lange, P., Moreno, M., 2009. Defining the transcriptomic and proteomic profiles of rat ageing skeletal muscle by the use of a cDNA array, 2D- and Blue native-PAGE approach. J. Proteomics 72, 708–721.

Maas, M.F., Krause, F., Dencher, N.A., Sainsard-Chanet, A., 2009. Respiratory complexes III and IV are not essential for the assembly/stability of complex I in fungi. J. Mol. Biol. 387, 259–269.

Marques, I., Dencher, N.A., Videira, A., Krause, F., 2007. Supramolecular organization of the respiratory chain in *Neurospora crassa* mitochondria. Eukaryot. Cell 6, 2391–2405.

McKenzie, M., Lazarou, M., Thorburn, D.R., Ryan, M.T., 2006. Mitochondrial respiratory chain supercomplexes are destabilized in Barth Syndrome patients. J. Mol. Biol. 361, 462–469.

Mileykovskaya, E., Dowhan, W., 2009. Cardiolipin membrane domains in prokaryotes and eukaryotes. Biochim. Biophys. Acta 1788, 2084–2091.

Minauro-Sanmiguel, F., Wilkens, S., Garcia, J.J., 2005. Structure of dimeric mitochondrial ATP synthase: novel F_0 bridging features and the structural basis of mitochondrial cristae biogenesis. Proc. Natl. Acad. Sci. USA 102, 12356–12358.

Neff, D., Dencher, N.A., 1999. Purification of multisubunit membrane protein complexes: isolation of chloroplast F_oF_1-ATP synthase, CF_o and CF_1 by blue native electrophoresis. Biochem. Biophys. Res. Commun. 259, 569–575.

Nübel, E., Wittig, I., Kerscher, S., Brandt, U., Schägger, H., 2009. Two-dimensional native electrophoretic analysis of respiratory supercomplexes from *Yarrowia lipolytica*. Proteomics 9, 2408–2418.

Paradies, G., Ruggiero, F.M., Petrosillo, G., Quagliariello, E., 1993. Age-dependent decrease in the cytochrome c oxidase activity and changes in phospholipids in rat-heart mitochondria. Arch. Gerontol. Geriatr. 16, 263–272.

Paradies, G., Ruggiero, F.M., Petrosillo, G., Quagliariello, E., 1997. Age-dependent decline in the cytochrome c oxidase activity in rat heart mitochondria: role of cardiolipin. FEBS Lett. 406, 136–138.

Patton, W.F., Beechem, J.M., 2001. Rainbow's end: the question for multiplexed fluorescence quantitative analysis in proteomics. Curr. Opin. Chem. Biol. 6, 63–69.

Paumard, P., Vaillier, J., Coulary, B., Schaeffer, J., Soubannier, V., Mueller, D.M., Brethes, D., di Rago, J.P., Velours, J., 2002. The ATP synthase is involved in generating mitochondrial cristae morphology. EMBO J. 21, 221–230.

Pfeiffer, K., Gohil, V., Stuart, R.A., Hunte, C., Brandt, U., Greenberg, M.L., Schägger, H., 2003. Cardiolipin stabilizes respiratory chain supercomplexes. J. Biol. Chem. 278, 52873–52880.

Poon, H.F., Calabrese, V., Calvani, M., Butterfield, D.A., 2006a. Proteomics analyses of specific protein oxidation and protein expression in aged rat brain and its modulation by L-acetylcarnitine: insights into the mechanisms of action of this proposed therapeutic agent for CNS disorders associated with oxidative stress. Antioxid. Redox Signal. 8, 381–394.

Poon, H.F., Shepherd, H.M., Reed, T.T., Calabrese, V., Stella, A.M., Pennisi, G., Cai, J., Pierce, W.M., Klein, J.B., Butterfield, D.A., 2006b. Proteomics analysis provides insight into caloric restriction mediated oxidation and expression of brain proteins associated with age-related impaired cellular processes: Mitochondrial dysfunction, glutamate dysregulation and impaired protein synthesis. Neurobiol. Aging 27, 1020–1034.

Poon, H.F., Vaishnav, R.A., Getchell, T.V., Getchell, M.L., Butterfield, D.A., 2006c. Quantitative proteomics analysis of differential protein expression and oxidative modification of specific proteins in the brains of old mice. Neurobiol. Aging 27, 1010–1019.

Rao, G., Xia, E., Richardson, A., 1990. Effect of age on the expression of antioxidant enzymes in male Fischer F344 rats. Mech. Ageing Dev. 53, 49–60.

Reifschneider, N.H., Goto, S., Nakamoto, H., Takahashi, R., Sugawa, M., Dencher, N.A., Krause, F., 2006. Defining the mitochondrial proteomes from five rat organs in a physiologically significant context using 2D blue-native/SDS–PAGE. J. Proteome Res. 5, 1117–1132.

Schäfer, E., Seelert, H., Reifschneider, N.H., Krause, F., Dencher, N.A., Vonck, J., 2006. Architecture of active mammalian respiratory chain supercomplexes. J. Biol. Chem. 281, 15370–15375.
Schäfer, E., Dencher, N.A., Vonck, J., Parcej, D.N., 2007a. Three-dimensional structure of the respiratory chain supercomplex $I_1III_2IV_1$ from bovine heart mitochondria. Biochemistry 46, 12579–12585.
Schäfer, E.R., Cellerino, A., Englert, C., Frenzel, M., Terzibasi, E., Dencher, N.A., 2007b. Partial mitochondrial proteome and supramolecular organisation of OXPHOS complexes in the short-lived fish *Nothobranchius furzeri*. Ann. Conf. German Genetic Soc. abstract 43, 38.
Schägger, H., Pfeiffer, K., 2000. Supercomplexes in the respiratory chains of yeast and mammalian mitochondria. EMBO J. 19, 1777–1783.
Schägger, H., Pfeiffer, K., 2001. The ratio of oxidative phosphorylation complexes I–V in bovine heart mitochondria and the composition of respiratory chain supercomplexes. J. Biol. Chem. 276, 37861–37867.
Schägger, H., 2002. Respiratory chain supercomplexes of mitochondria and bacteria. Biochim. Biophys. Acta 1555, 154–159.
Schon, E.A., Dencher, N.A., 2009. Heavy breathing: energy conversion by mitochondrial respiratory supercomplexes. Cell Metab. 9, 1–3.
Schwassmann, H.J., Rexroth, S., Seelert, H., Dencher, N.A., 2007. Metabolism controls dimerization of the chloroplast F_oF_1 ATP synthase in *Chlamydomonas reinhardtii*. FEBS Lett. 581, 1391–1396.
Seelert, H., Dani, D.N., Dante, S., Hauss, T., Krause, F., Schäfer, E., Frenzel, M., Poetsch, A., Rexroth, S., Schwassmann, H.J., Suhai, T., Vonck, J., Dencher, N.A., 2009. From protons to OXPHOS supercomplexes and Alzheimer's disease: structure-dynamics-function relationships of energy-transducing membranes. Biochim. Biophys. Acta 1787, 657–671.
Stöckl, P., Hütter, E., Zwerschke, W., Jansen-Dürr, P., 2006. Sustained inhibition of oxidative phosphorylation impairs cell proliferation and induces premature senescence in human fibroblasts. Exp. Gerontol. 41, 674–682.
Stöckl, P., Zankl, C., Hütter, E., Unterluggauer, H., Laun, P., Heeren, G., Bogengruber, E., Herndler-Brandstetter, D., Breitenbach, M., Jansen-Dürr, P., 2007. Partial uncoupling of oxidative phosphorylation induces premature senescence in human fibroblasts and yeast mother cells. Free Radic. Biol. Med. 43, 947–958.
Stroh, A., Anderka, O., Pfeiffer, K., Yagi, T., Finel, M., Ludwig, B., Schägger, H., 2004. Assembly of respiratory complexes I, III, and IV into NADH oxidase supercomplex stabilizes complex I in *Paracoccus denitrificans*. J. Biol. Chem. 279, 5000–5007.
Sugawa, M., Coper, H., Schulze, G., Yamashina, I., Krause, F., Dencher, N.A., 1996. Impaired plasticity of neurons in aging. Biochemical, biophysical, and behavioral studies. Ann. N. Y. Acad. Sci. 786, 274–282.
Tian, L., Cai, Q., Wei, H., 1998. Alterations of antioxidant enzymes and oxidative damage to macromolecules in different organs of rats during aging. Free Radic. Biol. Med. 24, 1477–1484.
Tsukihara, T., Aoyama, H., Yamashita, E., Tomizaki, T., Yamaguchi, H., Shinzawa-Itoh, K., Nakashima, R., Yaono, R., Yoshikawa, S., 1996. The whole structure of the 13-subunit oxidized cytochrome c oxidase at 2.8 A. Science 272, 1136–1144.
Vonck, J., Schäfer, E., 2009. Supramolecular organization of protein complexes in the mitochondrial inner membrane. Biochim. Biophys. Acta 1793, 117–124.
Wang, W., Yang, X., Lopez de Silanes, I., Carling, D., Gorospe, M., 2003. Increased AMP:ATP ratio and AMP-activated protein kinase activity during cellular senescence linked to reduced HuR function. J. Biol. Chem. 278, 27016–27023.
Wheelock, A.M., Morin, D., Bartosiewicz, M., Buckpitt, A., 2006. Use of a fluorescent internal protein standard to achieve quantitative two-dimensional gel electrophoresis. Proteomics 6, 1385–1398.
Wenz, T., Hielscher, R., Hellwig, P., Schägger, H., Richers, S., Hunte, C., 2009. Role of phospholipids in respiratory cytochrome bc(1) complex catalysis and supercomplex formation. Biochim. Biophys. Acta 1787, 609–616.
Wernicke, C., Hellmann, J., Zięba, B., Kuter, K., Ossowska, K., Frenzel, M., Dencher, N.A., Rommelspacher, H., 2010. 9-Methyl-β-carboline has restorative effects in an animal model of Parkinson's disease. Pharmacological Reports 62 (1).
Wittig, I., Carrozzo, R., Santorelli, F.M., Schägger, H., 2006. Supercomplexes and subcomplexes of mitochondrial oxidative phosphorylation. Biochim. Biophys. Acta 1757, 1066–1072.
Wittig, I., Schägger, H., 2009. Supramolecular organization of ATP synthase and respiratory chain in mitochondrial membranes. Biochim. Biophys. Acta 1787, 672–680.
Zhang, M., Mileykovskaya, E., Dowhan, W., 2002. Gluing the respiratory chain together. Cardiolipin is required for supercomplex formation in the inner mitochondrial membrane. J. Biol. Chem. 277, 43553–43556.
Zick, M., Rabl, R., Reichert, A.S., 2009. Cristae formation-linking ultrastructure and function of mitochondria. Biochim. Biophys. Acta 1793, 5–19.
Zwerschke, W., Mazurek, S., Stöckl, P., Hütter, E., Eigenbrodt, E., Jansen-Dürr, P., 2003. Metabolic analysis of senescent human fibroblasts reveals a role for AMP in cellular senescence. Biochem. J. 376, 403–411.

4.2.2 Differential ageing of mitochondria from cortex, striatum and hippocampus

That ageing in mammals occurs tissue-specific was demonstrated at the DNA level (Meissner et al., 2006), by analyzing enzyme activities (Suzui et al., 1999) and protein expression level (Mizutani et al., 1998). Especially brain mitochondria may be affected by ROS during ageing due to the high oxygen consumption of neuronal cells (chapter 1.1.2). Most studies published so far describing profound age-dependent alterations in the mitochondrial proteome caused by disease (Alzheimer, Parkinson) in whole brain (Ekstrom et al., 1980; Poon et al., 2006b; Rao et al., 1990) disregard the distinct functions, physiology and anatomy of various brain regions. Others focus their analysis on one specific brain area (Butterfield et al., 2006; Navarro et al.; Poon et al., 2006b; Sultana et al., 2006a; Sultana et al., 2006b). To verify if it is adequate to study the whole brain or if ageing occurs different in specific brain areas, age-associated changes in the mitochondrial proteome of rat brain striatum, hippocampus and cortex were analyzed, not only in respect to the protein abundance but also to protein-protein interactions. The data obtained for rat brain cortex, demonstrate an overall decline of OxPhos complexes and respiratory chain supercomplexes, respectively. In contrast to cortex, the mitochondrial proteome of striatum is less affected during ageing or rather characterized by only minor changes. Ageing in hippocampus occurred exceedingly different from cortex and striatum. An overall large increase in the amount of OxPhos complexes and respiratory chain supercomplexes accompanied by an increase of the mitochondrial aconitase (key enzyme of the Krebs cycle) was observed providing a larger cellular energy level required for the Na^+/K^+-ATPase that was also increased in abundance.

4.2.2.1 Gentle solubilisation and 2D-BN/SDS-gels as tools to analyze age-associated changes in OxPhos complexes and supercomplexes

Isolation of mitochondria from striatum and hippocampus was similar to that from cortex (chapter 3.4.1). The crude mitochondrial fractions obtained by this procedure were not subjected to further purification, in order to preserve also fragile and damaged mitochondria that might be more abundant and more severely affected in aged samples and lost during harsh purification steps. For solubilisation, 8 g digitonin per g protein was used, based on the determination of the solubilisation efficiency of cortical membrane proteins (Frenzel et al., 2010b). Separation of proteins occurred by utilizing BN-PAGE (Fig. 4-7) in the first and SDS-PAGE in the second dimension (Fig. 4-8). As discussed in materials and methods, for quantitation of protein abundances of all samples, only the fluorescence signal of the SYPRO Ruby signals was evaluated.

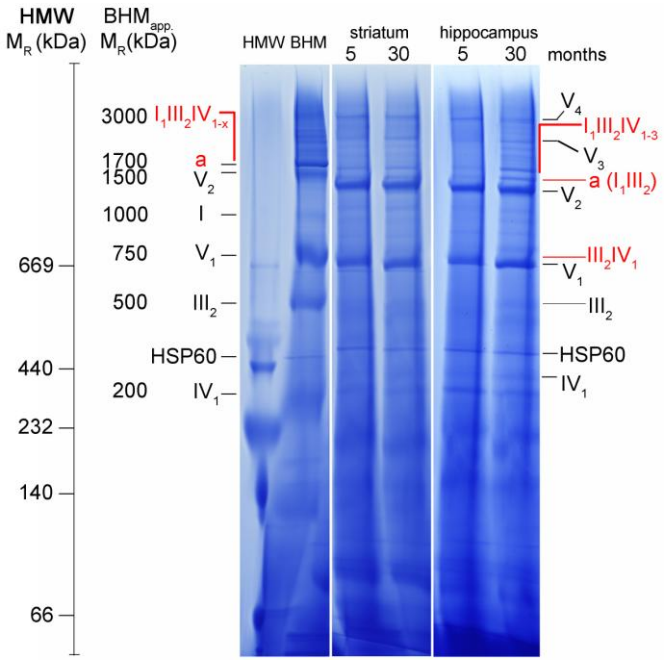

Fig. 4-7. Blue native PAGE of digitonin-solubilized (8 g/g digitonin to protein, 100 µg protein before solubilisation per lane applied) mitochondria isolated from non-frozen rat brain striatum and hippocampus of 5 month old as well as 30 months old animals for analysis of age-related changes in abundance and supramolecular organization of mitochondrial proteins. By applying 1D-BN-PAGE in the first dimension, individual proteins, OxPhos complexes and respective supercomplexes are separated in their native state. For mass calibration, high molecular weight (HMW) protein standards respectively digitonin solubilized and well characterized bovine heart mitochondria (BHM) were used: individual OxPhos complexes I–V (130–1000 kDa), supercomplexes $I_1III_2IV_{0-3}$ (1500–2100 kDa) and ATP synthase oligomers V_{2-4} (1500–3000 kDa). (BN-PAGE: linear 4–13% gradient gel with a 3.5% stacking gel, large gel, stained with CBB G-250)

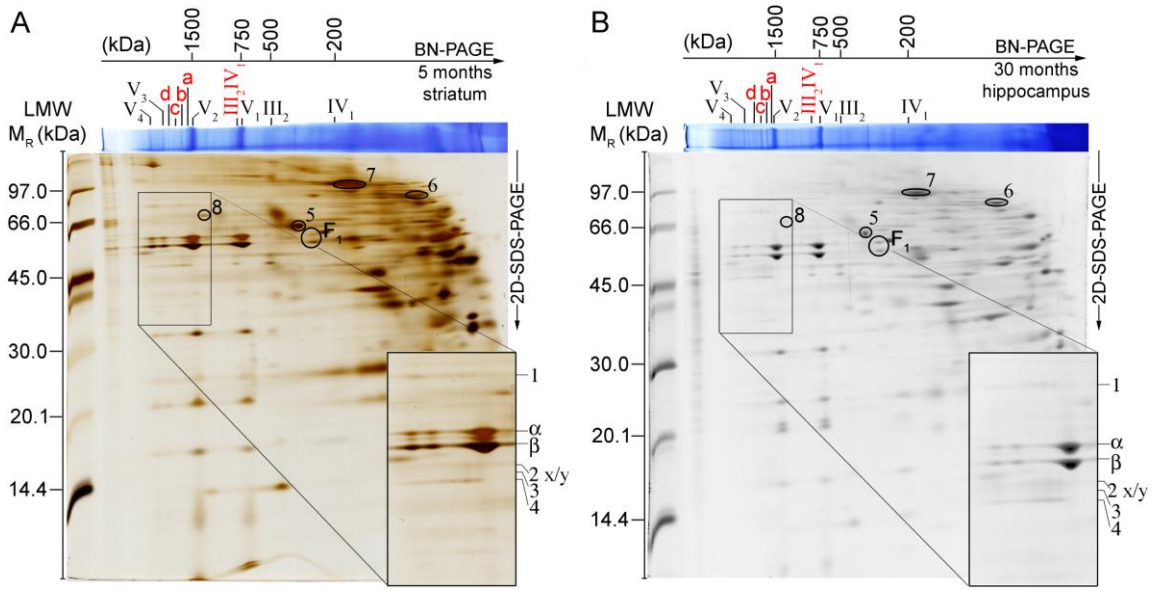

Fig. 4-8. 2D SDS–PAGE of mitochondria from striatum of young rat (5 months) stained for visualization only with silver (A) and from hippocampus of aged rat (30 months) with fluorescent SYPRO Ruby for quantitation (B), respectively. For 2D-SDS gels 120 µg mitochondrial protein before solubilisation was loaded on BN-gels (horizontal blue lane). After denaturation, subunits of protein complexes or supercomplexes are migrating in a vertical line according to their position in BN-PAGE in reference to Reifschneider et al. (2006). Low molecular weight (LMW) protein standards were used for mass calibration of protein spots and standardisation of gels. Characteristic protein patterns of subunits belonging to individual OxPhos complexes I, III_2, IV and V and of their preserved supercomplexes are resolved. The apparent molecular mass of BHM is indicated. In the enlarged inset, protein subunits of supercomplexes $I_1III_2IV_{0-3}$ (numbered 1–4) and ATP synthase α- and β-subunit are highlighted. [a (I_1III_2), b ($I_1III_2IV_1$), c ($I_1III_2IV_2$), d ($I_1III_2IV_3$), 1 + 2x + 3 (subunits of complex I; 1 = 75 kDa Fe–S subunit; 2x = Fe–S subunit 2; 3 = 51 kDa flavoprotein 1), 2y + 4 (subunits of complex III_2; 2y = core protein I, 4 = core protein II), α (α-subunit of complex V), β (β-subunit of complex V), F_1 = unbound F_1 from complex V, 5 = heat shock protein 60, 6 = aconitase 2, 7 = Na^+/K^+-ATP synthase, 8 = V-ATPase] [2D-SDS-PAGE: 5% stacking gel, 13% separation gel

The combination of methods described permits the analysis of age-related changes in protein pattern of the respiratory chain including abundance-changes of individual proteins as well as alterations in the amount and composition of OxPhos-complexes or -supercomplexes and in the formation of ATP-synthase oligomers (dimers, trimers and tetramers). For all three rat brain areas analyzed (cortex, striatum and hippocampus), solubilized mitochondrial suspensions separated on BN-gels generally displayed protein bands with common migration behavior during electrophoresis. Individual complex III_2, complex IV and complex V as well as ATP-synthase (complex V) homooligomers (V_2, V_3 and V_4) were identified according to their position in the gel in reference to Reifschneider et al. (2006). Also the small supercomplex III_2IV_1 containing a complex III dimer and one copy of complex IV and large supercomplexes $I_1III_2IV_{0-3}$ containing complex I, complex III dimer and zero to three copies of complex IV were visualized. As described previously, in contrast to other rat tissues (Dani et al., 2009; Gómez et al., 2009; Reifschneider et al., 2006) no individual complex I was found in cortex (Frenzel et al., 2010b) and skeletal muscle (Lombardi et al., 2009) independent of age. Also in rat brain striatum and hippocampus complex I existed almost solely (>95%) in supramolecular form assembled with other respiratory chain complexes (Fig. 4-7). For rat cortical, striatal and hippocampal tissues complex II of the respiratory chain was not sufficient in abundance for quantitation in both dimensions (1D-BN and 2D-SDS). Also non-mitochondrial proteins like the sodium-potassium ATPase (Na^+/K^+-ATPase) and the vacuolar-type H^+-ATPase were extracted during solubilisation (Fig. 4-8) besides the OxPhos complexes and other mitochondrial proteins like heat shock protein (HSP)60 and aconitase 2 in addition to numerous others yet non-identified proteins, due to utilizing crude mitochondrial fraction.

The biological variances of individual rats as well as differences caused by isolation of mitochondria and proteins within each age-group are relatively small and do not affect interpretation of the data (see also Fig. 3 in Frenzel et al., 2010).

4.2.2.2 Ageing alters the abundance, stability and oligomerisation of ATP synthase differentially in the cortex, striatum and hippocampus

Using quantitative solubilisation conditions (8 g/g digitonin/protein), in cortex an age-associated abundance-decrease in the total amount of ATP synthase (V_1-V_4) of approximately 20% (1.25-fold, Table 4-3, 1.5-fold of monomeric complex V) occurred, while the respective amount increased in striatum (1.11-fold) and hippocampus (1.20-fold). Noteworthy, due to the fact that the abundances of homooligomers (V_2-V_4) in all analyzed rat brain mitochondria remained nearly constant, age-associated abundance-change of complex V mainly resulted from changes in the complex V monomer proportion (Fig. 4-9). In cortex the monomer was decreasing about 1.48-fold during ageing while it was increasing in both, striatum and hippocampus, about 1.26-fold and 1.47-fold, respectively.

Table 4-3. Age-associated abundance changes of individual OxPhos complexes III_2 and IV and of supercomplexes of different composition as well as of ATP synthase [sum of complex V monomer and oligomers (V_2-V_4)] and unbound F_1 in rat cortex, striatum and hippocampus mitochondria. Changes in protein abundance are listed in fold (abundance changes of complexes/supercomplexes as compared to the amount in young rats; average of four (cortex) or three (striatum, hippocampus) individual animals per age-group). Supercomplex $I_1III_2IV_3$ in hippocampus was not detectable in the young group.

OxPhos		Change in respect to young state		
		Cortex	Striatum	Hippocampus
individual complexes	complex III_2	-1.16	1.04	1.38
	complex IV	-1.32	-1.08	1.37
supercomplexes	III_2IV_1	1.00	2.20	7.86
	I_1III_2	-2.38	1.36	8.26
	$I_1III_2IV_1$	-1.44	1.11	6.84
	$I_1III_2IV_2$	-1.69	1.05	8.10
	$I_1III_2IV_3$	-1.16	-1.34	--
complex V	∑ intact complex V	-1.25	1.11	1.20
	unbound F_1	2.81	1.50	4.82

Besides intact ATP synthase (V_1-V_4) also unbound F_1 (water soluble, catalytic unit of ATP synthase, hydrolyzing ATP) was found in mitochondria of all age-groups and all brain areas (Fig. 4-8). In all three brain areas there was an age associated increase in unbound F_1 but to different extent (cortex 2.8-fold, striatum 1.5-fold and hippocampus 4.8-fold, Table 4-3, Fig. 4-10). In the aged animals, in cortex unbound F_1 represented 9%, in striatum 4% and in

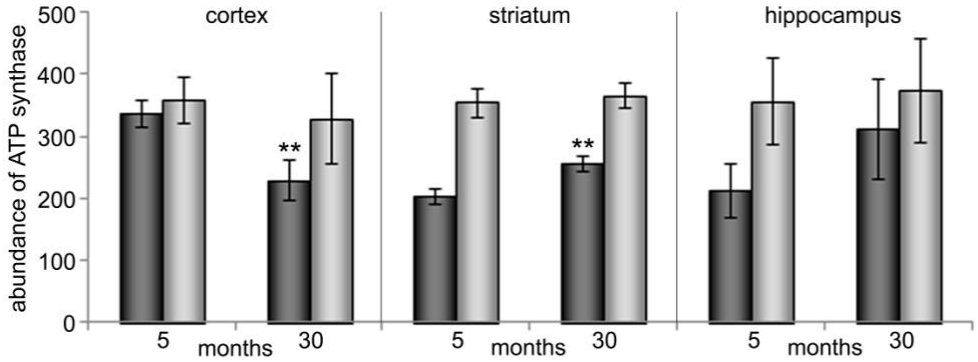

Fig. 4-9. The abundance of ATP synthase oligomers V_2-V_4 in all brain areas is independent of age, contrary to the abundance of monomer [ATP synthase monomer: black column, oligomers (V_2-V_4): grey column]. Values presented are mean and standard deviation of ATP synthase abundance (sum of α- and β-subunit). The ordinate values in Fig. 4-9 and Fig. 4-10 represent quantitative protein amounts. Significant *P*-value: **0.01 > *P* > 0.001 in comparison to young rats.

hippocampus 7% in reference to all assembled F_1 in complex V. As examined for cortex, the total amount of unbound F_1 was independent of the detergent to protein ratio in a range of 4-8 g digitonin / g protein (Frenzel et al., 2010b), demonstrating that the solubilisation conditions do not affect the stability of the ATP synthase. During ageing, the abundance of unbound F_1 in all analyzed brain areas increased but to different extent, with the largest increase in hippocampus, i.e. 4.8-fold (Fig. 4-10). A higher amount of unbound F_1 could be related to an age-dependent instability of ATP-synthase and/or less assembled complex that may lead to a pronounced uncontrolled ATP hydrolysis. (Note that the intensities depicted in Fig. 4-9 and Fig. 4-10 are a quantitative measure of protein amount. They can be compared directly with each other.)

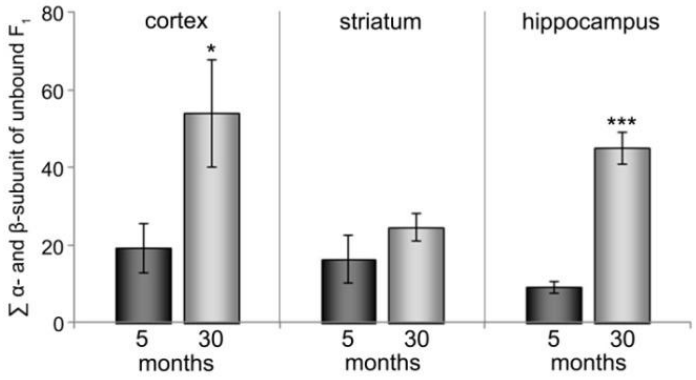

Fig. 4-10. Ageing increases the abundance of the unbound, water soluble F_1-part of complex V in all analyzed brain areas, but to different extent. Combined abundances of α- and β-subunits of unbound F_1. Significant *P*-value: *0.05 > *P* > 0.01, ****P* < 0.001, in comparison to young rats.

4.2.2.3 Differential expression of respiratory chain complexes (I, III_2, IV) and of assembly of supercomplexes in cortex, striatum and hippocampus during ageing

For individual respiratory chain complexes (complex III_2 and complex IV) only minor changes in amount occurred in striatum (Table 4-3). In contrast, in cortex there is a decline in the total amount for both complexes III_2 (1.16-fold) and IV (1.32-fold) while in hippocampus both are increasing in abundance to similar extent (complex III_2: 1.38-fold and complex IV: 1.37-fold). Individual complex I and complex II could not be evaluated due to their small amount (Fig. 4-7).

Four different kinds of respiratory chain supercomplexes were observed in all three brain areas: the smallest supercomplex I_1III_2 containing one complex III dimer (III_2) and a copy of complex IV as well as larger supercomplexes $I_1III_2IV_{0-3}$ consisting each of a copy of complex I, complex III dimer and zero to three copies of complex IV. The abundance of the supercomplex III_2IV_1 remained constant in cortex mitochondria independent during ageing (Fig. 4-11). However, in striatum there was an age-associated significant increase of III_2IV_1 about 2.2-fold that is much larger in hippocampus, 7.9-fold.

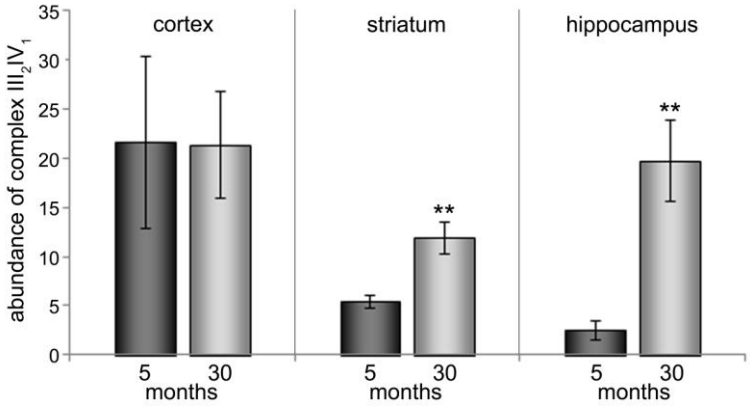

Fig. 4-11. Ageing increases the abundance of the smallest supercomplex III_2IV_1 in striatum and hippocampus, but not in cortex. Significant *P*-value: **0.01 > *P* > 0.001, in comparison to young rats.

The largest difference between the three brain areas emerge when analyzing the abundance of high molecular supercomplexes containing complex I, complex III_2 and complex IV. For cortex an overall age-associated abundance-decrease of about 1.6-fold (40%) of supercomplexes $I_1III_2IV_{0-3}$ (a-d) was described (Fig. 7 A in Frenzel et al. 2010). The largest decline occurred for supercomplex I_1III_2 (2.4-fold, Table 4-3, Fig. 4-12). From all supercomplexes containing complex I, supercomplexes $I_1III_2IV_1$ and $I_1III_2IV_3$ were the most unaffected by age. Supercomplex I_1III_2 (a) featured a 2.38-fold decline compared to only 1.44-fold for supercomplex $I_1III_2IV_1$ (b), 1.69-fold for $I_1III_2IV_2$ and 1.16-fold for $I_1III_2IV_3$. The overall age-associated decline of complex I containing supercomplexes resulted to large extent of the pronounced abundance decline of supercomplex I_1III_2 in cortex mitochondria. As opposed to this, the total amount of supercomplexes ($I_1III_2IV_{0-3}$) in striatal mitochondria remained nearly constant (1.1-fold increase in aged group compared to young animals). Also for striatum the largest abundance changes were observed for supercomplex I_1III_2 (1.36-fold increase, Fig. 4-12). The quantity of supercomplexes $I_1III_2IV_1$ and $I_1III_2IV_2$ were nearly unchanged. The amount of $I_1III_2IV_3$ decreased about 1.34-fold, but its proportion compared to all supercomplexes was small. In hippocampus a significant highly pronounced age-associated increase of all respiratory chain supercomplexes ($I_1III_2IV_{0-3}$) about 8-fold occurred (Table 4-3, Fig. 4-12; I_1III_2: 8.26-fold, $I_1III_2IV_1$: 6.84-fold and $I_1III_2IV_2$: 8.10-fold), demonstrating that ageing is distinct in different brain areas.

As discussed before, complex I was almost exclusively present in supercomplexes and not detected as individual complex. The presence of individual complex I in Fig. 4-2 was due to the fact, that in that case mitochondria were isolated from previously frozen brain tissue, stored for 5 years at -80°C. Therefore, changes in the total amount of complex I are correlated to abundance-changes of supercomplexes containing complex I ($I_1III_2IV_{0-3}$). Compared to individual OxPhos complexes III_2, IV and V, complex I is decreasing by age to a larger extent (1.6-fold) in cortex. In striatum, the amount of supercomplex I_1III_2 increased (1.36-fold) during ageing while no changes were observed for $I_1III_2IV_1$ (1.11-fold) and $I_1III_2IV_2$

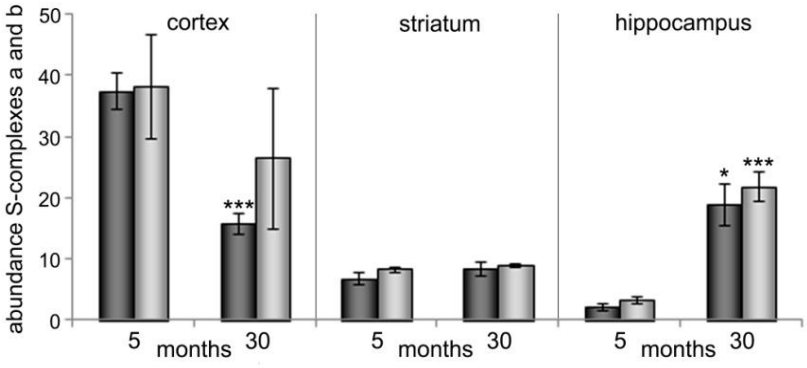

Fig. 4-12. Age-associated abundance changes of supercomplex I_1III_2 (a, black column) and $I_1III_2IV_1$ (b, grey column) in rat cortex, striatum and hippocampus mitochondria. The sum of intensities of all quantified complex subunits (1–4, Fig. 4-8) is depicted. Significant *P*-value: *0.05 > *P* > 0.01, ****P* < 0.001, in comparison to young rats

(1.05-fold) and $I_1III_2IV_3$ decreased (1.34-fold). But compared to cortex and hippocampus these changes were minor due to the fact that in this brain area the total amount of respiratory chain complexes was small in proportion to all proteins solubilized and separated with 2D BN/SDS PAGE. The pronounced increase of the various supercomplexes $I_1III_2IV_{0-3}$ in hippocampus reflected also the large increase for complex I during ageing by about 8-fold, which is much larger than those of individual complexes (III_2, IV and V).

Age-related changes described for supercomplex I_1III_2 and $I_1III_2IV_1$ reflected alterations in the abundance of all large supercomplexes (in sum) since both were more abundant than supercomplex c and d (Table 4-3, the sum of supercomplexes $I_1III_2IV_{0-3}$ is depicted in Fig. 4-13 A). All respiratory chain complexes (sum of individual complexes I, III_2 and IV and supercomplexes) decreased to a small extent in abundance in striatum (1.21-fold) and in cortex (1.13-fold) during ageing while there was a pronounced (1.72-fold) increase observed in hippocampus (Fig. 4-13 B, data obtained by quantitation of protein bands in one BN-gel). Quantitation of proteins in BN-gels is less accuracy than quantitation on 2D SDS-gels but sufficient to study general increase or decrease.

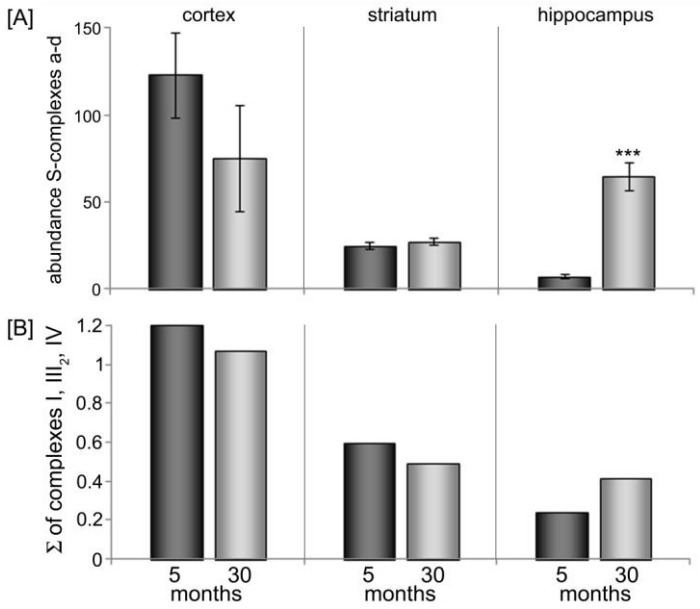

Fig. 4-13. [A] Total amount of large supercomplexes ($I_1III_2IV_{0-3}$; quantitation on 2D-SDS-PAGE, ordinate represents grey units) and [B] sum of all respiratory chain complexes (present in supercomplexes III_2IV_1 and $I_1III_2IV_{0-3}$ and as individual complexes I, III_2 and IV, quantitation in one 1D BN gel, ordinate represents optical density of CBB staining) in both age groups. Significant *P*-value: ***$P < 0.001$, in comparison to young rats.

The proportion of individual complex III_2 to complex III_2 in supercomplexes III_2IV_1 and $I_1III_2IV_{0-3}$ gives a hint on the formation of supercomplexes in both age groups. The proportion of individual complex III_2 slightly increased in cortex (0.20-fold in young and 0.26-fold in aged animals, Fig. 4-14) during ageing due to the more pronounced decline of complex III_2 containing supercomplexes. But in both ageing states, the majority of complex III_2 was present in high molecular assemblies with other respiratory chain complexes. In striatum as

well as in hippocampus different proportions of individual complex III_2 to complex III_2 assembled existed within the age-groups. In mitochondria of young rats in both brain areas the quantity of individual complex III_2 was similar to complex III_2 in supercomplexes (striatum: 0.9-fold, hippocampus: 1:1). In old rats more complex III_2 was assembled in supercomplexes compared to individual complex III_2 resulting in a ratio of 1.4 for striatum and 2.4 for hippocampus. Noteworthy, comparing all three brain areas studied, the cortex had the highest ratio (5) of supercomplexes in relation to individual complex III_2. The increase of supercomplexes in striatum during ageing occurred mainly due to an increase of III_2IV_1 abundance. Also on the absolute scale, the inner mitochondrial membrane in cortex showed the highest abundance of supercomplexes. Only in the aged state, both cortex and hippocampus had comparable amounts, much more than in striatum.

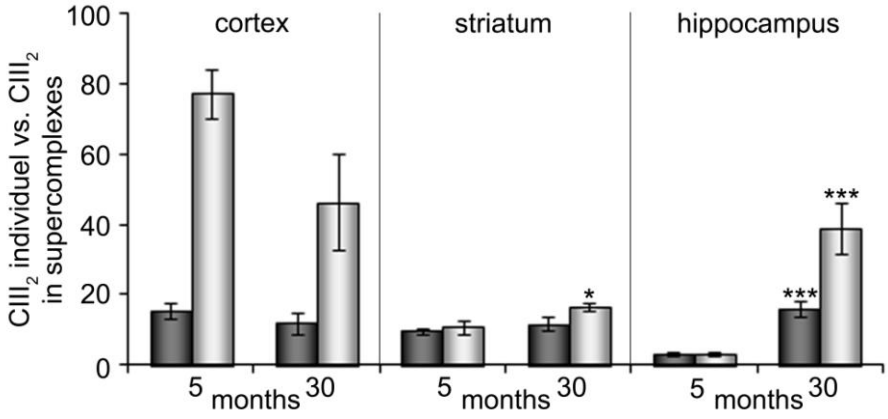

Fig. 4-14. Complex III dimer as individual complex III_2 (black column) and complex III_2 assembled in supercomplexes ($I_1III_2IV_{0-3}$) in young and aged rats of cortex, striatum and hippocampus. Significant *P*-value: *0.05 > *P* > 0.01, ****P* < 0.001, in comparison to young rats.

4.2.2.4 Age-associated abundance-changes of non-OxPhos proteins

Besides OxPhos complexes and supercomplexes there are numerous mitochondrial and non-mitochondrial proteins separated on gels by PAGE that are involved in or affected by ageing. For the mitochondrial aconitase 2 (ACO2) in both, cortical and striatal mitochondria, no age-related alterations in protein abundance occurred (Fig. 4-15). However, in hippocampus there was a 1.7-fold abundance increase during ageing. In all three brain areas comparable amounts of ACO2 were present.

During ageing, in rat brain cortex and striatum the amount of the mitochondrial heat shock protein (HSP)60 decreased (Fig. 4-15, cortex: 2.1-fold, striatum: 1.8-fold). Contrary, in hippocampus no significant age-associated alteration occurred. Whereas in cortex and hippocampus comparable amounts of HSP60 were present, in striatum only half that amount was found.

The amount of the Na^+/K^+-ATPase is decreased about 1.7-fold and 2.4-fold, respectively, in the cortex and striatum of aged rats (Fig. 4-15). In hippocampus a pronounced age-

associated increase about 3.3-fold occurred. The relative proportion of the Na^+/K^+- ATPase in the crude mitochondrial preparations was by far the highest in cortex.

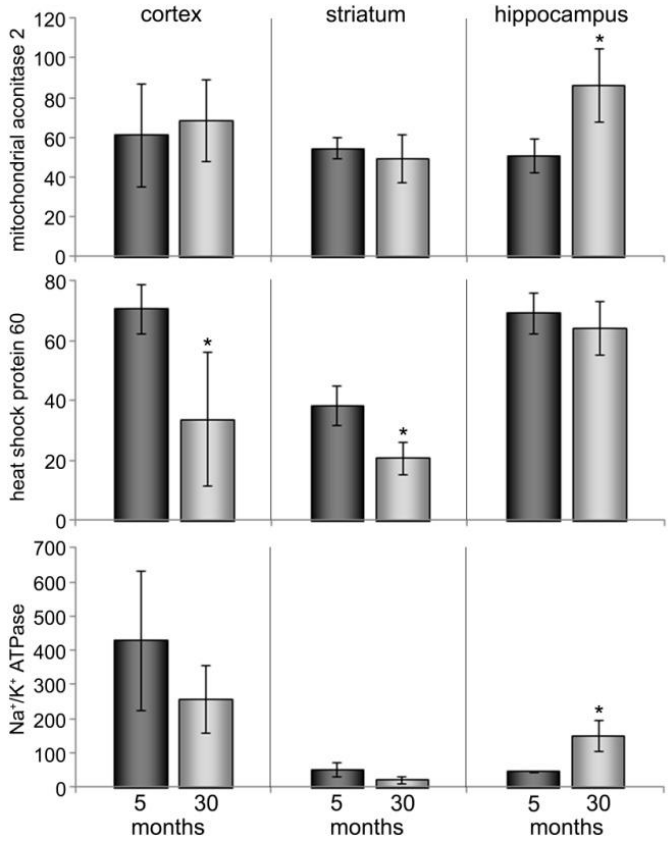

Fig. 4-15. Age-associated abundance changes of non-OxPhos mitochondrial and non-mitochondrial proteins: mitochondrial aconitase 2, mitochondrial heat shock protein (HSP)60 and sodium-potassium ATPase. Significant *P*-value: *0.05 > *P* > 0.01, in comparison to young rats.

The abundance of the vacuolar H^+-ATPase (V-ATPase) is not changing during ageing in all brain areas studied (Fig. 4-16). Moreover, the total amount is comparably in cortex, striatum and hippocampus.

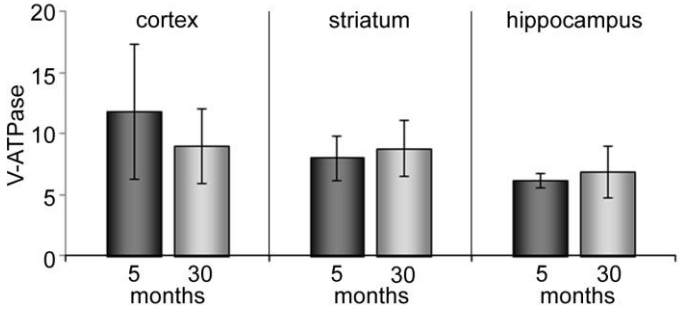

Fig. 4-16. Abundance of the vacuolar H^+-ATPase is not changing during ageing in all brain areas analyzed with comparable amount in cortex, striatum and hippocampus.

4.2.2.5 Summary

To disclose the nature of brain ageing and of ageing-accompanied neurodegenerative disorders like Alzheimer‘s or Parkinson’s, the mitochondrial proteome of three brain areas (cortex, striatum and hippocampus) was analyzed. Variations in abundances of mitochondrial proteins, especially belonging to the oxidative phosphorylation machinery, may help to understand the process of ageing or to find causes for the appearance of age-associated diseases. There is evidence for age-related alterations in the whole brain (Ekstrom et al., 1980; Frenzel, 2006; Groebe et al., 2007; Poon et al., 2006b; Rao et al., 1990), but the organ is extremely complex due to the fact it is composed of divergent brain areas exhibiting individual anatomy, physiology, metabolism and function. The mitochondrial proteome of the three different brain areas cortex, striatum and hippocampus was compared to discover age-associated changes in protein abundances as well as protein-protein-interactions. Mitochondria isolation from non-frozen tissue and efficient protein solubilisation were essential for this analysis to ensure quantitative comparison of the protein profiles of these three brain areas in two age groups.

Considering all data obtained, ageing occurs different in cortex, striatum and hippocampus in respect to changes in the mitochondrial proteome. The overall age-associated decrease in protein abundances of OxPhos complexes and supercomplexes and non-OxPhos proteins (HSP60, Na^+/K^+-ATPases) observed for cortex is comparable to that of whole rat brain (Frenzel, 2006; Groebe et al., 2007). This is not surprising since the cortex represents the largest brain region. In striatum only minor changes (except an increase in abundance of supercomplexes III_2IV_1, I_1III_2 and a decrease in $I_1III_2IV_3$) occurred and in contrast to cortex, the protein abundances were slightly increased by trend. Therefore, the metabolic performance of this brain area seemed to be unaffected during the ageing process. Pronounced age-associated alterations were found in hippocampus. All OxPhos complexes and non-OxPhos proteins analyzed increased in abundance (besides HSP60 and H^+-ATPase) – and some to a large extent up to 8-fold. The results will be itemised below in detail.

Divergent alterations in the oligomeric state but convergent loss in stability of ATP synthase in cortex, striatum and hippocampus

Changes in the amount of ATP synthase should have an impact on the overall energy supply of a cell. There is evidence for decreased metabolic energy (ATP, $NADH+H^+$) generated in neurons during ageing (Rothman and Mattson). Three conditions may change during ageing concerning the ATP synthase: (1) decrease or increase in protein abundances (V_1-V_4), (2) variations in the ratio of ATP synthase monomer (V_1) to oligomeric state (V_{2-4}) and (3) level of non-assembled enzyme (soluble F_1).

The total amount of mitochondrial ATP synthase (sum of V_1-V_4) in cortex, striatum and hippocampus was comparable (Fig. 4-9). Its 1.25-fold decrease in abundance in cortex (Frenzel et al., 2010b; Seelert et al., 2009) was previously described for whole rat brain (Groebe et al., 2007), liver (Dani et al., 2009) and skeletal muscle (Lombardi et al., 2009) as

well as for the fungus *Podospora anserina* and human cells (Groebe et al., 2007). While in striatum no age-associated change in the protein abundance of complex V occurred (1.1-fold increase), there was a comparable 1.2-fold increase of complex V in hippocampus. These changes in abundance have to be related to the enzyme activity and the cellular ATP content for all brain regions and ageing states in future.

In cortex, striatum and hippocampus the amount of ATP synthase oligomers (V_2-V_4) remained constant. Only complex V monomer changed in abundances. In both, striatum and hippocampus there was an increase of complex V monomer about 1.3-fold and 1.5-fold, respectively (Fig. 4-9). In contrast, in cortex the monomer was decreased in abundance about 1.5-fold. It has to be determined, if oligomerisation of the ATP synthase modulates its specific activity. In *Chlamydomonas reinhartii*, the mitochondrial F_OF_1 ATP synthase is only present as dimer (Schwassmann et al., 2007). The importance of complex V dimerization is becoming apparent since ATP synthase oligomers are involved in cristae formation by inducing curvature of the inner mitochondrial membrane as, e.g. described for yeast (Bornhövd et al., 2006; Gavin et al., 2004; Gilkerson et al., 2003; Giraud et al., 2002; Paumard et al., 2002) and bovine heart (Gilkerson et al., 2003; Minauro-Sanmiguel et al., 2005). Cristae themselves are important for the localization of OxPhos complexes and therewith the efficiency of energy conversion (Zick et al., 2009). The overall relatively constant level of complex V oligomers observed may give a hint for their essential role in maintaining the spatial structure of the inner mitochondrial membrane and optimal energy supply.

Individual F_1 (not assembled with F_O) was found to represent a reliable ageing marker in all three brain areas, cortex, striatum and hippocampus, because of its 1.5 to 4.8-fold age-associated abundance increase that will have a large impact on the cellular ATP concentration. In all three brain areas studied, ageing was accompanied by an increase of the water soluble F_1-part (Fig. 4-10, Table 4-3) that represent at maximum in the cortex of aged rats 9% of the total F_1. An increased amount of unbound F_1 could be indicative of an age-associated instability of ATP-synthase and/or less assembled complex resulting in pronounced uncontrolled ATP hydrolysis. This observed increase of unbound F_1 might lead to an increase of ATP hydrolysis and to a severe decline of the cellular ATP-pool, especially pronounced in cortex (highest amount of unbound F_1 compared to the total F_1) and hippocampus (largest age-associated increase of unbound F_1).

Antidromic age-related abundances-changes of respiratory chain complexes and supercomplexes in cortex and hippocampus

The individual respiratory chain complexes I, III_2 and IV are not randomly distributed in the inner mitochondrial membrane but naturally assembled in so called supercomplexes of specific stoichiometries (Krause, 2007; Schäfer et al., 2006; Schägger and Pfeiffer, 2000; Schon and Dencher, 2009; Seelert et al., 2009). They were isolated reliably from mitochondrial membranes using gentle solubilisation conditions (Fig. 4-7). The supercomplex formation permits efficient substrate channelling and is essential for the stability and activity

of the interacting complexes (Fig. 4-6) (Schäfer et al., 2006; Schägger and Pfeiffer, 2000; Schon and Dencher, 2009). Efficient substrate channelling reduces ROS generation. While complex III_2 and complex IV were also present as individual complexes (Table 4-3), complex I was almost solely assembled as supercomplexes in rat brain cortex, striatum and hippocampus. In contrast, individual complex I was found in mitochondria from rat skeletal muscle (Lombardi et al., 2009), rat heart (Gómez et al., 2009) and rat liver (Dani et al., 2009). In rat cortex, striatum and hippocampus complex I total abundance was reflected by the amount of complex I containing supercomplexes. Both, complex I as well as complex III_2 require supercomplex formation together with complex IV ($I_1III_2IV_{1-X}$) for optimal specific enzyme activity [(Frenzel et al., 2010b; Schäfer et al., 2006) and present study Fig. 4-6]. The abundances of individual complex III_2 and complex IV altered distinct during ageing in all three analyzed brain areas (Table 4-3). During ageing, the abundance of both enzymes decreased in cortex while it remained mainly constant in striatum but increased in hippocampus.

The supercomplex formation was analyzed by comparing the proportion of individual complex III_2 to complex III_2 assembled in supercomplexes (III_2IV_1 and $I_1III_2IV_{0-3}$, Fig. 4-14). It was demonstrated in the present study (Fig. 4-6, Fig. 4-20) as well as by Schäfer et al. (2006), that the assembly of complex I and III_2 with one or more copies of complex IV is leading to an increased specific activity of both complexes I and III_2. Alterations in the supercomplex formation in cortex, striatum and hippocampus are distinct.

(1) In cortex the total amount of all respiratory chain complexes present (as individual complexes as well as in supramolecular assemblies) was slightly decreased about 1.13-fold in aged rats (Fig. 4-13 B). The pronounced decrease of the complex I containing supercomplexes $I_1III_2IV_{0-3}$ was not accompanied by an increase in the amount of the smaller supercomplex III_2IV_1 (remaining unchanged) or of the individual complex III_2 or IV. But the individual complex III_2 compared to complex III_2 assembled with other respiratory chain complexes increased in proportion. That in mitochondria of aged rats less formation of complex I containing supercomplexes occurred was indicated by two observations: Firstly, the relative increase of individual complex III_2 in relation to supercomplexes and secondly the unchanged ratio of III_2IV_1 by a general decline of individual respiratory chain complexes and larger supercomplexes. To minimize changes in the energy status, the relative proportion of supercomplexes containing complex IV, characterized by higher complex I and III_2 activity, increased (Table 4-3), also discussed by Silvestri et al. (2011) for rat brain and skeletal muscle. Supercomplex I_1III_2 decreased about 2.4-fold and supercomplex $I_1III_2IV_1$ about 1.4-fold. Since no individual complex I was observed in both ageing states, its expression was down regulated or the enzyme disassembled into its subunits. In cortex, the decline in respiratory chain complexes was accompanied by an overall decrease of the ATP synthase (1.2-fold). The detrimental decrease of ATP that might result may be counter balanced by the observed age-associated increase in the relative proportion of supercomplexes $I_1III_2IV_1$ and $I_1III_2IV_{2-3}$ showing the highest specific activity of complex I and III_2 as described for rat skeletal muscle (Silvestri et al., 2011). Supercomplex b is the most pronounced supercomplex in all brain regions and in all ageing states. As pointed out in chapter 4.2.1, the

highest activity of complex I was found especially in this supercomplex (Fig. 4-6). Also Schäfer et al. (2006) described an increase of complex I (2.3-fold) and complex III_2 (16.5-fold) activity after binding one copy of complex IV to supercomplex I_1III_2 forming $I_1III_2IV_1$. Comparative results were described for whole rat brain (Frenzel, 2006) and rat skeletal muscle (Lombardi et al., 2009). The cortex is essential for cognitive functions (learning and memory). Most learning and memory processes take place in young individuals at the beginning of the life time. Later on, aged individuals may solely use already learned skills and less memory and learning processes are performed compared to young. This might explain the decrease of proteins belonging to the oxidative phosphorylation machinery as well as in the proportion of supramolecular assemblies during ageing. The cortex is susceptible for neurodegenerative diseases like Alzheimer's, Parkinson's and Huntington's. The neuronal number in the part of the cortex important for memory processes and in the hippocampus in non-human primate decreased the most (up to 30%) (Smith et al., 2004). Therefore, animals lost a lot of brain functions (memory) due to the malfunction of these regions (McIntyre and Craik, 1987; Spencer and Raz, 1995). In general, the cortex seems to have the largest energy demand of all three brain areas studied. According to the results presented in Fig. 4-12, Fig. 4-13 and Fig. 4-14, in mitochondrial membranes all respiratory chain complexes were more abundant in cortex than in striatum and hippocampus.

(2) In line with the data described for cortex, in striatum the abundances of all respiratory chain complexes (individual and assembled as supercomplexes) decreased about 1.2-fold (Fig. 4-13 B) during ageing. But in contrast to cortex, formation of supercomplexes (III_2IV_1 and $I_1III_2IV_{0-3}$) increased to a small extent. While in mitochondria of young rats nearly the same ratio of individual complex III_2 to complex III_2 in supercomplexes was found (1.1-fold), the proportion of assembled complex III_2 increased (1.4-fold) in aged rats. This increase was mainly caused by an increase of the smaller supercomplex III_2IV_1 (2.2-fold, Fig. 4-11) while the larger supercomplexes $I_1III_2IV_{0-3}$ were unaffected by age (Fig. 4-13 A). Generally, striatal membranes contained up to 7-fold less supercomplexes in the inner mitochondrial membranes than cortex (Fig. 4-11, Fig. 4-12). Additionally, all changes are rather small (except for III_2IV_1) compared to those in cortex and hippocampus, including alterations in the amount of the ATP-synthase and the soluble F_1-part. The striatum is the main input structure of the basal ganglia (Ferre et al., 2010) and important for planning, modulation and connection of movement, motivation and emotion. Aged rats are characterized by reduced movement but they are able to move until they die. Therefore, no pronounced age associated changes of the mitochondrial proteome occurred in this brain area. Diseases developing by mal-function of striatum are e.g. Chorea Huntington, tremor and Parkinson's.

(3) In the present study, it was demonstrated that ageing occurs antidromic in the hippocampus of rats. In hippocampus, a pronounced age-associated increase in protein abundance was found for all individual respiratory chain complexes (1.38-fold for complex III_2, 1.37-fold for complex IV) and especially for supercomplexes (III_2IV_1 and $I_1III_2IV_{0-3}$) up to 8-fold (Fig. 4-11, Fig. 4-12, Fig. 4-13, Table 4-3). In the inner membrane of hippocampal mitochondria of young rats even less respiratory chain complexes were present that in striatum. Therefore, even though this pronounced 8-fold increase in the abundance of

respiratory chain complexes in hippocampus during ageing is remarkable, the total protein amount was still smaller than that in cortex. In aged rats additionally there was more supercomplex formation. Approximately 71% of all complex III_2 present was assembled with other respiratory chain complexes but to a less extent than in cortex (79%). The increase of individual respiratory chain complexes and supercomplexes was accompanied by an increase of the ATP synthase (1.2-fold). In hippocampus of aged animals a higher energy level seems to exist according to these data. The hippocampus is evolutionally one of the oldest brain regions and important for learning and memory (conversion from short-term to long-term memory). It is extremely vulnerable to psychosocial and environmental chronic adverse stress, e.g. Parkinson's and Alzheimer's disease (Cerqueira et al., 2007; Driscoll and Sutherland, 2005; Miller and O'Callaghan, 2005; Rothman and Mattson). Cortex and hippocampus are interacting to form memory and during learning processes. Loss of hippocampal activity is accompanied by a loss in memory storage. In ageing studies, this brain area represents a target of interest due to its almost evolutionally conserved structure. No overall age-associated loss of cells or synapses were observed in this brain area although a reduction in the volumes was observed in non-human primates (Smith et al., 2004). In contrast to the other brain regions, in hippocampus of also adults neurogenesis takes place, enabling recovery and response on external stress as well as maintenance of memory function. Cells are regenerating during life time and this brain area consists of a mixture of cells: young, middle aged as well as old. Additionally, in hippocampus almost every cell type occurring within the brain was found and hippocampal cells are characterized by high plasticity.

To conclude, ageing in the three brain areas examined occurs by different alterations in the protein profiles, as demonstrated in this study. Therefore, it is necessary to perform discrete assays for each brain area. If the whole brain is analyzed, data of proteome studies reflect mainly the situation in the cortex, the largest brain area (Frenzel, 2006). The cortex, striatum and hippocampus are characterized each by specific function and also by specific composition of cell types with different metabolic emphasis. They contain the same proteins but expressed to a cell-specific demand.

Age-associated changes of mitochondrial non-OxPhos and non-mitochondrial proteins

The mitochondrial aconitase 2 (ACO2), a key enzyme of the citric acid cycle (Krebs cycle) with additionally new functions (metabolic signaling and maintenance of mtDNA), is playing an important role in mitochondrial ageing (Hunzinger et al., 2006 and references cited therein). It is a soluble enzyme located in the mitochondrial matrix and catalyzes the stereo-specific isomerization of citrate to iso-citrate in the tricarbonic acid cycle (Beinert and Kennedy, 1993). The enzyme is known to be vulnerable to posttranslational modifications like oxidation, influencing cell death and survival and resulting in several pathologies. Due to posttranslational modification 14 different isoforms have been observed that might influence the activity of the enzyme (Hunzinger et al., 2006; Yan et al., 1997). There are modifications

known to enhance the function of the aconitase (*N*-formylkynurenine) as well as modifications (carbonylation) affecting it (Yan et al., 1997). Carbonylation leads to decreased ACO2 activity in housefly. The posttranslational modification being most abundant for proteins in rat brain mitochondria is carbonylation (Prokai et al., 2007). The connection between reduced aconitase 2 activity combined with increased oxidative modification and simultaneous reduction of life span was demonstrated for brain and kidney of mammals and for insects (Carney et al., 1991; Yarian et al., 2005; Yarian and Sohal, 2005). The aconitase is a water soluble protein. Its protein abundance on 2D-SDS gels is independent of solubilisation efficiency. In cortex and striatum no age-associated abundance changes occurred in line with data from *Podospora anserine*, human cells (Groebe et al., 2007) and insects (Yarian et al., 2005; Yarian and Sohal, 2005). However in rat brain hippocampus an increased amount of ACO2 was found in aged rats (1.7-fold, Fig. 4-15) accompanied with enlarged protein abundances of OxPhos complexes indicating a higher metabolic activity in this brain area (Fig. 4-11 and Fig. 4-12). Since the tri carbon acid cycle and respiratory chain have to work in concert for optimal and efficient energy conversion (aconitase is supplying the latter with most of the required electron carrier as e.g. NADH + H^+), the age-associated increase in abundance of the aconitase 2 and the increase in abundance of individual respiratory chain complexes and supercomplexes as well as ATP synthase observed in hippocampus fulfill that requirement.

The mitochondrial heat shock protein 60 (HSP60) is located in the mitochondrial matrix and acts as chaperone for proteins transferred into the mitochondria. Chaperones are highly conserved proteins, essential for protein-folding and cognition of misfolded or damaged proteins. They are involved in intracellular signaling, protein transport and apoptosis. Several chaperones are known to have an impact on cellular senescence (Di Felice et al., 2005) and in maintaining mitochondrial functions in the brain (Shankar, 2011). Mitochondrial HSP60 is known to feature proapoptotic functions as opposed to the cytoplasmic form (Arya et al., 2007; Di Felice et al., 2005). In cortex and striatum an age-associated decrease in HSP60 abundance was observed about 2.1-fold and 1.8-fold, respectively (Fig. 4-15). The amount of HSP60 in the hippocampus was comparable in both ageing states. It was similar in abundance to that of cortex in young rats. In striatum there was the smallest amount of HSP60. Unchanged level of mitochondrial HSP60 in hippocampus indicates a higher amount of misfolded and damaged proteins compared to cortex and striatum possibly induced by the increased metabolism suggested for hippocampus that may lead to increased ROS production and oxidative damage of proteins. For cells in culture distinct age-related abundance-changes of HSP60 have been described. Di Felice et al. (2005) postulated an overall increase in HSP60 abundance when entering the senescence stage, suggesting a regulatory effect of HSP60 on cell cycle and cytoskeleton remodeling. Lee et al. (2009) found no age-related or oxidative stress induced changes in the protein amount of cytoplasmic and mitochondrial HSP60 in sum. But after oxidative stress, the mitochondrial HSP60 was transferred to the cytosol suggesting a regulatory effect on apoptosis. In mollusks as well as in rat heart and liver the amount of mitochondrial HSP60 decreases during ageing (Colotti et

al., 2005; Ivanina et al., 2008) while in rat skeletal muscle there is an increase (Chung and Ng, 2006) indicating tissue specific changes.

Na^+/K^+-ATPases are integral membrane enzymes of high molecular mass. They are necessary to maintain the ionic imbalance across membranes required for neuronal function (Ashmore et al., 2009; Scherer et al., 2009) with a large consumption of ATP to restore the ion gradients (membrane potential) after transmitting electrical signals (Budd and Nicholls, 1998). The Na^+/K^+-ATPase as transmembrane protein is residing in plasma membranes. It is ubiquitously expressed and essential for the generation and maintenance of the electrochemical gradient by transferring three Na^+ out of the cell in exchange to two K^+ taken in. This transport is driven by hydrolyzing one ATP molecule. The enzyme is highly evolutionarily conserved, essential for normal brain function and the predominant consumer of cellular ATP especially in neural cells (Ashmore et al., 2009; Blanco and Mercer, 1998). While in other cell types, the Na^+/K^+-ATPase utilizes 40% of all cellular ATP, in neurons this enzyme is responsible for 2/3 of the cells energy. In brain, the expression and activity of Na^+/K^+-ATPase is especially high (Attwell and Laughlin, 2001; Beal et al., 1993; Erecinska and Dagani, 1990). To maintain ionic gradients, they are present with multiple proteins in large complexes additionally involved in cell adhesion, polarity, signaling and endocytosis (Ashmore et al., 2009; Cai et al., 2008; Cereijido et al., 2008). In the present study, in cortex and striatum the abundance of the Na^+/K^+-ATPase declined with age about 1.7-fold and 2.4-fold, respectively (Fig. 4-15). In rat brain an age-associated reduction in activity of about 20% has been observed in general in line with my results from cortex and striatum. In other studies, that decrease was accompanied additionally by a 20-70% decrease in protein abundance (Arivazhagan and Panneerselvam, 2004; Haynes et al., 2010; Kaur et al., 2001). The specific activity for the exchange of Na^+ and K^+ remained mainly constant but the ATPase activity was decreased about 40%, whereas more ATP was required for maintaining full Na^+/K^+-ATPase activity (Haynes et al., 2010). The enzyme is known to be sensitive to the lipid composition (Arivazhagan and Panneerselvam, 2004) that is changing during ageing. Of all brain areas, the largest amount was found in cortex. The 3.3-fold abundance increase of Na^+/K^+-ATPase, the major ATP consumer (2/3 of all ATP in neuronal cells), in hippocampus indicates pronounced changes in the cellular energy requirement. The higher required energy demand is compensated in aged animals by the increase of proteins belonging to the oxidative phosphorylation machinery (respiratory chain complexes and supercomplexes as well as ATP synthase) and of the aconitase (Fig. 4-13, Fig. 4-15), indicating a larger turnover supplying the necessary reduction equivalent of the Krebs cycle. This again underlines differences in metabolic conditions of the three brain regions analyzed.

The protein abundance of the vacuolar H^+-ATPase (V-ATPase) was comparable in all three brain areas and in both ageing states (Fig. 4-16). This non-mitochondrial enzyme represents one of the most essential proteins in nature that exclusively acts as ATP-dependent proton pump. V-ATPases have a key role in the brain for neuronal transmission at neuronal terminals. They represent the major constituent of brain synaptic vesicles (20% of total membrane proteins) and generate the electrochemical gradient of protons across the membranes of vesicles used as driving force for transmitter import (Moriyama and Futai,

1990; Moriyama et al., 1992). V-ATPases of plants and animals show the same structure and essentially the same subunit composition (Moriyama and Nelson, 1989a, b). They are found also in membranes of several organelles (e.g. Golgi complex, lysosomes) as well as in plasma membranes and in mitochondria-rich cells (Harvey, 1992). Mitochondria have been found to localize next to membranes containing V-ATPases and even to migrate towards these membranes, when ion transport processes are induced (Bradley and Satir, 1981). Therewith, ATP is directly available to power these H^+-transporting processes.

The quest for *"housekeeping"* proteins

For quantitative analysis of age-related alterations in the proteome of e.g. tissues or cell organelles, normalization factors are essential to compare different samples. Proteins present in constant amount, not affected by the cellular response to be studied, e.g. from the metabolic status, ageing or development of the cell, are referred to *housekeeping* proteins. *Housekeeping* proteins may differ between different types of model organism, tissues and even cell types due to the fact, that these proteins are involved in basic cellular functions as e.g. major metabolic pathways (Butte et al., 2001; Eisenberg and Levanon, 2003). In the current study, several proteins were studied for their ability to serve as *housekeeping* protein. Most proteins analyzed were membrane proteins. Hence, to fulfil the requirement for the present study, *housekeeping* proteins should belong to the class of integrated membrane proteins. This would allow, to use them as normalization factors for alterations in the solubilisation efficiency during ageing. Ideally for the present study the *housekepping* proteins should reside in membranes, however also water soluble housekeeping proteins might be useful.

In cortex and striatum no age-associated changes of the mitochondrial aconitase occurred in line with data from *Podospora anserine*, human cells (Groebe et al., 2007) and insects (Yarian et al., 2005; Yarian and Sohal, 2005). Hence, it was thought to be able to serve as *housekeeping* protein. However, in rat brain hippocampus an increased amount of ACO2 was found in aged rats (1.7-fold, Fig. 4-15). Therefore, for the present study, the mitochondrial aconitase does not fulfill the qualification of a *housekeeping* protein to compare all three brain areas due to the fact that it is present to a different extent. But it can be used to compare solely cortex and striatum.

In contrast to the mitochondrial aconitase 2, HSP60 cannot be used as *housekeeping* protein in rat cortex and striatum, due to the age-associated decrease, but for hippocampus (Fig. 4-15). In the hippocampus the amount of HSP60 was comparable in both ageing states and represents therefore a *housekeeping* protein only for this brain area.

In the three brain areas studied here, cortex, striatum and hippocampus, the abundance of the Na^+/K^+-ATPase changed differently during ageing (Fig. 4-15). Therefore, also this enzyme was not qualified as *housekeeping* protein.

The only enzyme having constant protein abundances in all three brain areas and for both ageing states was the vacuolar H^+-ATPase (V-ATPase, Fig. 4-16). Hence, it might be applied

as *housekeeping* protein. That V-ATPases function as *housekeeping* gene with constitutive expression was already described for *Neurospora crassa* (Wechser and Bowman, 1995). There are similarities in the structure of genes and promoter elements with other mammalian *housekeeping* genes. V-ATPases as membrane proteins have to be solubilized for further analysis on PAGE and depict therefore all properties a *housekeeping* protein should fulfill in the present study.

4.2.3 Mitochondrial proteins of cortex from aged rats are less carbonylated

Determination of oxidative modifications was performed by the OxyBlot assay (chapter 3.10.3) to analyze the level of carbonylation in cortex mitochondria isolated from rats of different age (Fig. 4-17). Of each age group two animals were included in the study.

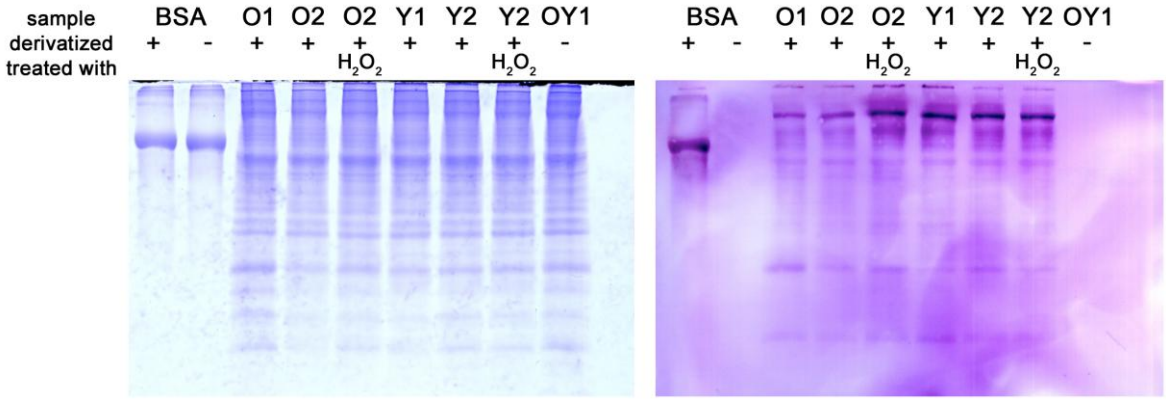

Fig. 4-17. Determination of the level of carbonylation in cortex mitochondria of each two young (Y1 and Y2) and aged (O1 and O2) rats by OxyBlot [right, visualization with alkaline phosphatase, PVDF membranes] after separation of mitochondrial proteins (30 µg) on 1D SDS gels [left, 5% stacking gel and 13% separation gel, stained with Fermentas after blotting]. As control and mass standard, bovine serum albumin (BSA, 5 µg, 60 kDa) was loaded. As negative control for immuno-binding a non-derivatized mixture of young and aged mitochondrial proteins (OY1, each 15 µg) and BSA was used. As positive control one sample of each age group was incubated previously with H_2O_2.

As depicted in Fig. 4-17, the protein transfer during blotting was mostly homogeneous and the immuno-binding specific. No signal was obtained from non-derivatized samples. Larger amounts of carbonyl-groups were present in mitochondrial proteins of high molecular mass of young rats (Y1 and Y2) compared to aged (O1 and O2). It seems that both young samples analyzed were maximal oxidized since the intensity of the immuno-signal was similar compared to the sample of young rats treated with hydrogen peroxide (H_2O_2) before derivatization. In the mitochondria of aged rats, less carbonylation of proteins occurred. The level of oxidative modified protein residues in aged rats (O1 and O2) was less than that of the H_2O_2-exposed aged rat sample for the high molecular mass band. The signal intensity of the latter was similar to that of young rat samples (untreated and oxidized). Noteworthy, the level of carbonylation was comparable in each age group. The amount of oxidative post-translational modification of proteins was much less in mitochondria of aged rats than in young.

Referring to the „Free Radical Theory of Ageing“ (Harman, 1956), according to which ROS accumulate during ageing and lead to increased oxidative damages of proteins, especially

within the mitochondria, an age-associated increase of oxidative modifications was suggested. This postulation cannot be confirmed by the present data, at least not for mitochondrial proteins of rat cortex. Hutter et al. (2007) found higher levels of ROS production in young compared to aged human skeletal muscle and no increase in oxidative modification of mitochondrial proteins in muscles from elderly donors.

4.3 The effect of MPP^+ and 9-methyl-β-carboline on the OxPhos complexes *in vivo* and *in vitro*

Data described in this chapter have been already published:

Wernicke C., Hellmann J., Zieba B., Kuter K., Ossowska K., **Frenzel M.**, Dencher N.A., Rommelspacher H. (2010). 9-Methyl-beta-carboline has restorative effects in an animal model of Parkinson's disease. *Pharmacol. Rep*. **62**, 35-53.

Ageing is often accompanied by neurodegenerative disorders like Alzheimer‘s or Parkinson’s. Brain deficiencies affect the quality of life to a large extent. Possible causes are neuronal loss or shrinking of neuronal cells, both leading to reduction of the brain volume. But in some brain areas like hippocampus the number of neurons remains nearly constant during ageing. Therefore, also other mechanisms (alterations in the metabolic state or energy production) are leading to age-associated diseases or deficits in brain maintenance (Miller and O'Callaghan, 2005).

1-Methyl-4-phenylpyridinium (MPP^+) is an active neurotoxic metabolite of 1-methyl-4-phenyl-1,2,3,6-tetrahydropyridine (MPTP). It was used as herbicide. In the brain, MPTP is converted by the enzyme monoamine oxidase B to MPP^+ (Sonsalla et al., 2010). The compound reduces dopamine levels within the brain by inducing mitochondrial dysfunctions, that itself lead to the loss of dopaminergic neurons in the substantia nigra. In Parkinson’s disease (PD) similar alterations occur. Hence treatment with MPP^+ is widely used (e.g. in rodent and cell models) to elicit neurochemical alterations associated with PD (Petit-Paitel et al., 2009). The neurotoxin is a selective inhibitor of the mitochondrial OxPhos complex I and induces depletion of ATP concentration and induces neuronal apoptosis.

9-Methyl-β-carboline (9-me-BC) has neuroprotective properties. It protects cells from death and reverses the effect of MPP^+ (Wernicke et al., 2010).

The restorative effect of 9-methyl-beta-carboline was studied *in vivo* in an animal model (Wistar rats) and *in vitro* on HEK cells. The abundance of OxPhos (super)complexes and activity and mitochondrial HSP60 was analyzed after treatment with only MPP^+ and MPP^+ together with 9-me-BC.

4.3.1 9-Methyl-β-carboline has restorative effects on the OxPhos machinery in an animal model of Parkinson's disease

The rat model used has been reported by Yazdani and coworkers (2006). It is based on the damage of dopaminergic neurons due to chronic delivery of the neurotoxin MPP^+ into the left cerebral ventricle. MPP^+ delivery to rats over a four-week period followed by a two-week period of vehicle infusion provides a chronic model of mitochondrial dysfunction without mortality and low inter-animal variability with regard to the degree of neuropathology. As described in chapter 2.6.2, three groups of rats with different treatment were included in this

study. All animals received subcutaneously infusions into the left cerebral ventricle. The first group was treated for 28 days with MPP^+ (0.284 mg/kg/day) and subsequently with 9-me-BC (0.105 mg/kg/day) for 14 days. The second group received MPP^+ for 28 days followed by saline for 14 days. The third group was sham-operated twice at an interval of 28 days. At the end of the 42 day infusion, all animals were killed and the mitochondria isolated from both left and right striatum immediately upon dissection of brain areas without preceded freezing of tissue.

The delivery of 0.284 mg/kg/day MPP^+ for 28 days followed by delivery of saline for 14 days caused an approximately 50% reduction in the dopamine levels in the left striatum ($p < 0.001$ compared with both the sham-operated rats and with the right striatum), while the levels in the right striatum were in the range of sham-operated rats (5.1 ± 0.8 ng/mg of the tissue, $n = 6$). In rats treated with MPP^+ and 9-me-BC, the dopaminergic level of the left striatal side was similar to those of the right (Fig. 1 in Wernicke et al., 2010). Therefore, 9-me-BC was restoring the effect of MPP^+.

It has been reported that some β-carbolines bind to complex I of the respiratory chain in mitochondria. This finding suggested that 9-me-BC might affect the respiratory chain as well. In search of an explanation for the restorative effect of 9-methyl-beta-carboline, changes in the abundance and activity of OxPhos (super)complexes and mitochondrial HSP60 were analyzed in striatum. Mitochondrial proteins were solubilized with digitonin as described in chapter 3.6.1 with a detergent to protein ratio of 8 g/g and separated using 2D BN/SDS PAGE.

In summary, the overall composition of OxPhos complexes remained unchanged but the activity of complex I was increased by approximately 80% in mitochondria from rats treated with MPP^+ and 9-methyl-*β*-carboline compared to MPP^+ and saline and to sham-operated rats, as determined by measurements of nicotinamide adenine dinucleotide dehydrogenase activity by in-gel activity tests. The findings demonstrate restorative effects of 9-methyl-β-carboline in an animal model of Parkinson's disease that improve the effectiveness of the respiratory chain. A control showing solely the effect of 9-me-BC on the striatum was missing.

4.3.1.1 No alterations in the abundance of OxPhos (super)complexes but in complex I activity of supercomplex $I_1III_2IV_2$

The rat model employed produces selective, progressive loss of nigrostriatal dopaminergic cells through perturbation of mitochondrial function (Yazdani et al., 2006). Considering that the dose of MPP^+ used in the experiment caused only a 50% reduction in DA levels, it represents a model corresponding to an early stage of PD. Dysfunction of mitochondria could reveal key mechanism of the neurotoxic process and of PD. Therefore, the mitochondrial proteome of striatal tissue was analyzed with emphasis on the composition, abundance, protein-protein-interactions, and activity of membrane proteins and their modulation by consecutive treatment with MPP^+ and saline and with MPP^+ and 9-me-BC, respectively. By

application of BN-PAGE separating proteins in their native, active state and preserving all functional relevant protein-protein interactions, distinct protein bands containing either the individual complexes or the supercomplexes with a defined complex stoichiometry were identified (Fig. 4-18). Presented are the findings from mitochondria of the left and right striata

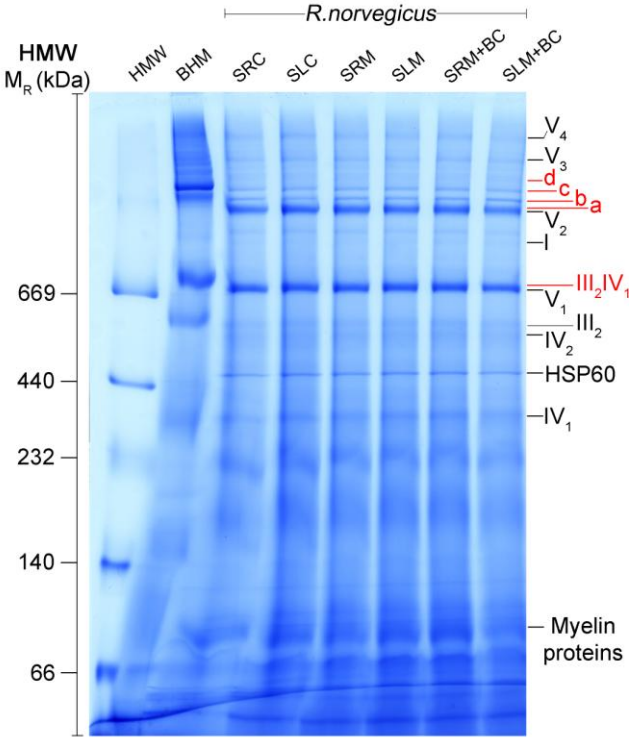

Fig. 4-18. Analysis of the abundance and the supramolecular organization of mitochondrial proteins extracted from rat striatum. Rats were treated with MPP^+ (28 days) and then saline and 9-me-BC, respectively (14 days), delivered into the left ventricle. BN-PAGE (linear 4–13% gradient gel with a 3.5% stacking gel, stained with CBB G-250) of digitonin solubilized rat mitochondria. For mass calibration, high molecular weight (HMW) protein standard and digitonin-solubilized bovine heart mitochondria (BHM, 3 g/g) were used: individual complexes I–IV (130–1000 kDa) and supercomplexes a–d ($I_1III_2IV_{0-3}$, 1500–2100 kDa). Membranes were solubilized with 8 g digitonin/g protein. The characteristic bands of the individual OxPhos complexes I, III_2, IV, IV_2 and V and their preserved supercomplexes are recognizable. In addition, heat shock protein HSP60 and myelin proteins [Myelin basic protein isoform 5, lipophilin (proteolipid protein)] are indicated. Abbreviations: striatum left sham-operated control (SLC); striatum right, sham-operated control (SRC); striatum left, MPP^+ and subsequently saline (SLM); striatum right, MPP^+ and subsequently saline (SRM); striatum left, MPP^+ and subsequently 9-me-BC (SLM+BC); striatum right, MPP^+ and subsequently 9-me-BC (SRM+BC)

from single rats, either sham-operated twice, treated with MPP^+ and saline, or treated with MPP^+ and 9-me-BC. The composition, abundance and proportion of respiratory chain complexes and respective supercomplexes as well as monomeric versus oligomeric (dimers, trimers, tetramers) assembly of the MF_OF_1 ATP synthase were comparable in all 6 samples (Fig. 4-19). The unaltered amount of proteins is in line with a previous study analyzing the dopaminergic system of PD patients (Schagger, 1995). Moreover, no abundance changes of the mitochondrial HSP60 (Fig. 4-19, description and role of HSP60 see also chapter 4.2.2.5) were observed. The specific activity of individual complex I and complex I in supercomplexes (sum of individual complex I and all complex I containing supercomplexes) was similar in all striata except in the striatum treated with 9-me-BC (Fig. 4-20 A). The activity of the left striatum from the rat treated with MPP^+ and 9-me-BC was approximately 80% higher than that from the sham-operated rat and 75% higher than in the rat treated with MPP^+ and saline. In this respect it is worth mentioning that about 90% of all complex I was found in various supercomplexes; only the remaining 10% were present as individual complexes. Therefore, we measured the complex I activity of the different supercomplexes. The specific activity of supercomplex $I_1III_2IV_2$ was approximately 3-fold higher in the left striatum of the rat with the combined treatment as compared to both the sham-operated rat and the rat treated with

MPP^+ and saline (Fig. 4-20 B). The specific activity of individual complex I was 2-fold less than that of I_1III_2 and 3-fold compared to $I_1III_2IV_1$.

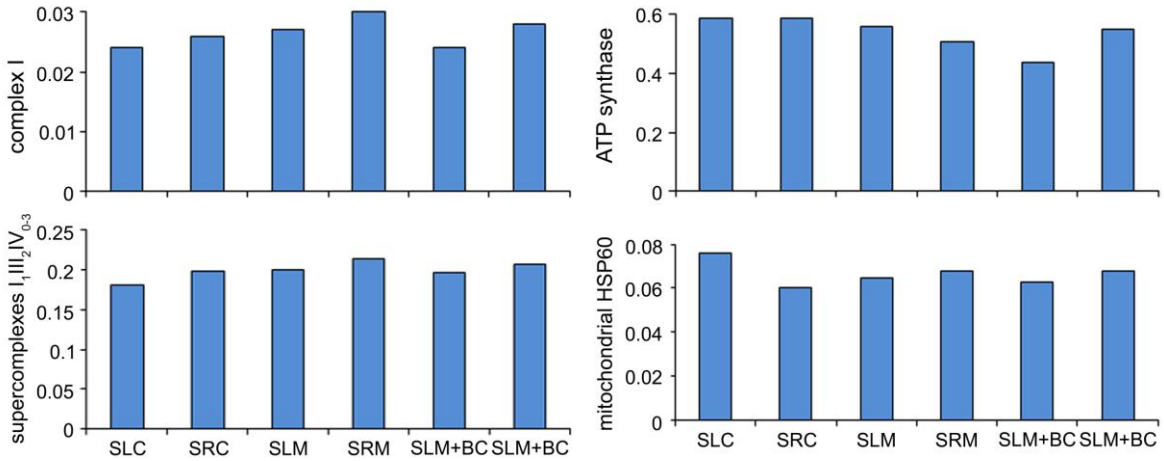

Fig. 4-19. No significant changes in the abundance of complex I, complex I containing supercomplexes $I_1III_2IV_{0-3}$, complex V (sum of ATP synthase monomer and dimer) as well as HSP60 were observed in all rats and respective right and left striata. [Data were obtained from quantitation of protein band separated on one 1D BN gel stained with CBB G-250 (n = 1).] Abbreviations: see legend of Fig. 4-18.

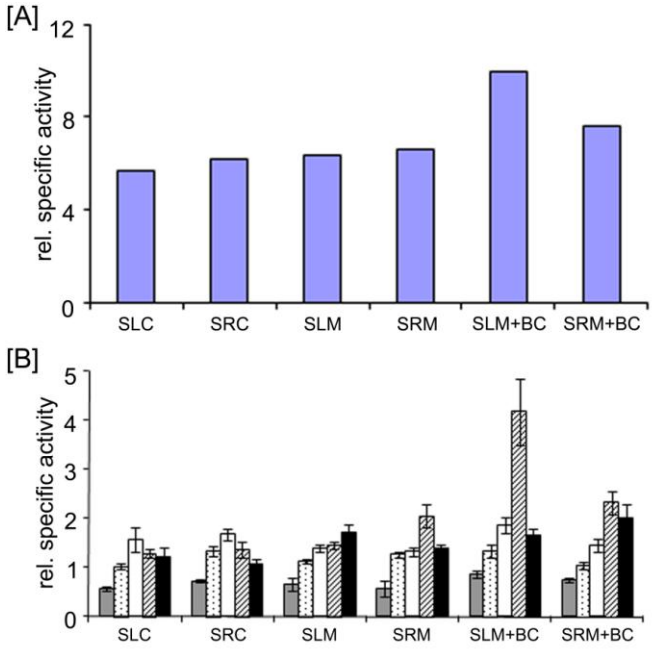

Fig. 4-20. Specific NADH dehydrogenase activity (in relative units) of complex I in striatal mitochondria determined in 1D BN gels. (A) Enzymatic activity of all protein bands containing complex I, i.e., individual complex I and supercomplexes containing complex I, one copy of the complex III dimer and 0–3 copies of complex IV. About 90% of all complex I was assembled in the various supercomplex species. (B) NADH dehydrogenase activity of individual complex I (gray), supercomplex I_1III_2 (dotted), $I_1III_2IV_1$ (open column), $I_1III_2IV_2$ (hatched), and $I_1III_2IV_3$ (black). Abbreviations: see legend of Fig. 4-18.

The amount of mitochondrial HSP60 was determined as a non-membrane and non-OxPhos protein. The heat shock protein provides protection against intracellular dysfunction and cell death by maintaining the structure of mitochondrial proteins e.g. involved in oxidative

phosphorylation (Veereshwarayya et al., 2006). HSP60 abundance in the striata did not differ between the various treatment conditions. Noteworthy MPP^+ does not affect the abundance of complex I, supercomplexes, complex V and HSP60.

4.3.1.2 Summary

As described in Wernicke et al. (2010), a single injection of MPP^+ into the striatum of rats already induced retrograde damage of dopaminergic neurons in the substancia nigra, together with extensive oxidative stress (Miwa et al., 2004). In rats infused with MPP^+ for several days, progressive changes in the behavior and neuronal alterations appeared correlated with typical syndromes of Parkinson's disease (Fornai et al., 2005). The restorative effect of 9-me-BC after treatment with MPP^+ was demonstrated in cell culture and for rats, e.g. rescue of damaged dopaminergic neurons (Wernicke et al., 2010).

The loss of nigrostriatal dopaminergic cells after MPP^+-infusion occurred due to perturbation of mitochondrial function induced by the inhibition of complex I (Nicklas et al., 1985). The degree of perturbation might be reflected by the amount of complex I expressed, the abundance of supercomplexes and specific enzyme activity. However, the protein patterns of substancia nigra from control individuals and patients with Parkinson's disease did not differ (Schapira et al., 1990a; Schapira et al., 1990b). In mitochondria from frontal cortex of PD patients the 8 kDa subunit of complex I was decreased in abundance by 34% and the proteins comprising the catalytically active core of complex I were oxidative damaged (Keeney et al., 2006). In the present study, separation of OxPhos complexes and supercomplexes as well as in-gel activity tests was performed in BN-PAGE (Fig. 4-18) and determination of the subunit pattern of denatured complexes and supercomplexes in a subsequent SDS-PAGE. No changes in the abundance of OxPhos complexes or supercomplexes containing complex I (a finding not investigated by others) was observed in striatal mitochondria of rats treated with MPP^+ (Fig. 4-19). Reduced catalytic activity of complex I in frontal cortex and substancia nigra, respectively, was reported for PD patients (Keeney et al., 2006; Schapira et al., 1990b) but not confirmed by others (Schagger, 1995). In the present study, no changes in the catalytic activity of isolated complex I and of supercomplexes were observed upon treatment with MPP^+ possibly due to the fact that solely 50% reduction of the dopaminergic cells was observed while more than 80% is characteristic for PD. The In-gel measurement of complex I activity demonstrated that 9-me-BC stimulated the enzyme activity of complex I in rats pre-treated with MPP^+ by 80% (Fig. 4-20 A). This increase was mainly caused by supercomplex ($I_1III_2IV_2$), which activity increased by 3-fold (Fig. 4-20 B). In the control rat, in line with cortex shown in chapter 4.2.1, the supercomplex $I_1III_2IV_1$ had the highest specific activity of all complex I containing supercomplexes and compared to individual complex I. The protein amount of individual complex I was rather small (approximately 5% of the total complex I). In both striata of animals treated with MPP^+ or MPP^+ and 9-me-BC, the specific activity of supercomplexes I_1III_2 decreased while it increased for $I_1III_2IV_2$ and $I_1III_2IV_3$. It is tempting to speculate that 9-me-BC specifically interacts with the dimer of IV in $I_1III_2IV_2$.

One has to keep in mind that MPP^+ is suggested to kill predominantly neurons containing dopaminergic transporter. In the striatum or substantia nigra, there are several cell types present next to dopaminergic cells. While the neuronal cell bodies of dopaminergic cells are mainly in the substancia nigra, the neuronal terminals are located in the striatum. After 4 weeks of exposure to MPP^+ mainly dopaminergic cells are affected. These are suggested to die. Therefore, data obtained in the present study from analysis of the striatum are showing the mitochondrial protein profile of dopaminergic cells that may survived the MPP^+ treatment or of those that entered already in the dying process as well as of healthy unaffected other cells. Additionally, 9-me-BC was added after the 4 week treatment with MPP^+. Cells were therefore not protected during the MPP^+ treatment. Only those, having only minor damages and survived the exposure to MPP^+, might recover with the help of the neuronal protectant.

4.3.2 The effect of MPP^+ and 9-me-BC on the mitochondrial proteome of HEK-(h)DAT cells

In parallel to the animal experiments on rat substancia nigra described in chapter 4.3.1, the effect of 1-methyl-4-phenylpyridinium (MPP^+) and the putative neuroprotectant 9-methyl-beta-carboline on the mitochondrial proteome of human embryonic kidney cells (HEK-293) was analyzed. HEK-(h)DAT cells are stable transfected with human dopamine transporter (hDAT) gene (Storch et al., 1999). These cells are used to study the impact of the Parkinson-inducing toxin MPP^+ on mitochondrial OxPhos complexes and especially on complex I that was found to be inhibited by MPP^+. The dopamine transporter is transporting MPP^+ within the cells. The level of ATP is reduced in cells incubated with this neurotoxin (Storch et al., 1999). As described in chapter 4.3, 9-me-BC acts as neuroprotectant in rat. It has an enhancing effect on the specific activity of complex I in the respiratory supercomplex $I_1III_2IV_2$ (Fig. 4-20).

HEK-(h)DAT cells were seeded with $5x10^5$ cells per 75 cm^2 culture flask by Regina Hill (Technical Assistent of Prof. Rommelspacher, Charité Berlin, Fig. 4-21). After 48 hours MPP^+ was added to the medium at a final concentration of 2 µM (sample 1-4). At the same time, sample 2 additionally received 9-me-BC at a final concentration of 100 µM. At day 5 (48h after adding of substances), sample 1 and 2 were harvested and isolation of mitochondria was performed immediately. The same day, for remaining cell samples a medium change was performed. Sample 3 and 5 received medium without any further additive, while to the fresh medium in sample 4 additionally 9-me-BC (100 µM) was added. Then after 48 hours cells were harvested and mitochondria isolated. The mitochondrial suspensions were frozen in liquid nitrogen and stored at -80°C.

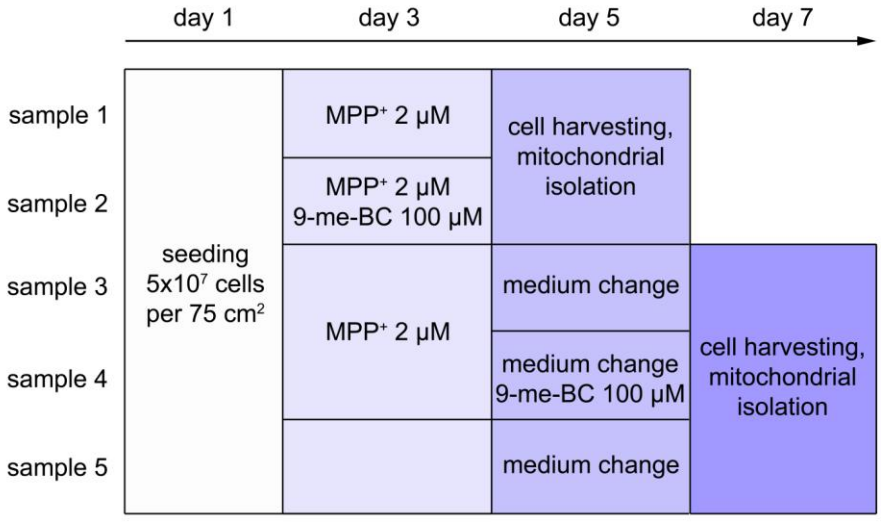

Fig. 4-21. Experimental setup to analyze the effect of MPP^+ and MPP^+ in combination with 9-me-BC on the mitochondrial proteome of HEK-(h)DAT cells. Of sample 1-4 two 75 cm^2 cell culture flasks were combined while of sample 5 one 175 cm^2 cell culture flask was used for isolation of mitochondria. The experiment was performed only once by Wernicke.

Mitochondrial proteins were solubilized with 8 g/g digitonin to protein and separated on 2D BN/SDS gels. In the first dimension, the respiratory chain supercomplexes I_1III_2 (a) and $I_1III_2IV_1$ (b) as well as complex V (ATP synthase) monomer (V_1) and dimer (V_2) were observed (Fig. 4-22 A). The individual respiratory chain complex IV was only visible in the

second dimension (Fig. 4-22 B). Additionally, the characteristic protein band of the mitochondrial heptameric HSP60 was present in the BN gel nearby a second band suggested to represent a smaller assembly state of this homooligomer (here referred to HSP60*). According to its position in the BN gel, it may possibly be a hexameric form of the homooligomer. But it cannot be excluded that it represents the heptamer and the upper band is a heptamer assembled with another protein. Such a double band of HSP60 was neither observed in rat brain (Frenzel, 2006; Frenzel et al., 2010b), skeletal muscle (Lombardi et al., 2009; Reifschneider et al., 2006), liver (Dani et al., 2009; Thilmany, 2008) and heart (Reifschneider et al., 2006) or bovine heart (Frenzel, 2006; Reifschneider et al., 2006) nor in fungi (Krause et al., 2004b) or plants (Krause et al., 2004a) but in fibroblasts (chapter 4.4.1). Like in the rat brain cortex (Frenzel et al., 2010b), striatum and hippocampus (chapter 4.2) or rat skeletal muscle (Lombardi et al., 2009), complex I was almost solely present in high molecular supercomplexes assembled with only complex III_2 (I_1III_2) as well as complex III_2 and IV ($I_1III_2IV_{1-X}$). No individual complexes I, II and III_2 were found in the first (Fig. 4-22 A) as well as the second dimension (Fig. 4-22 B).

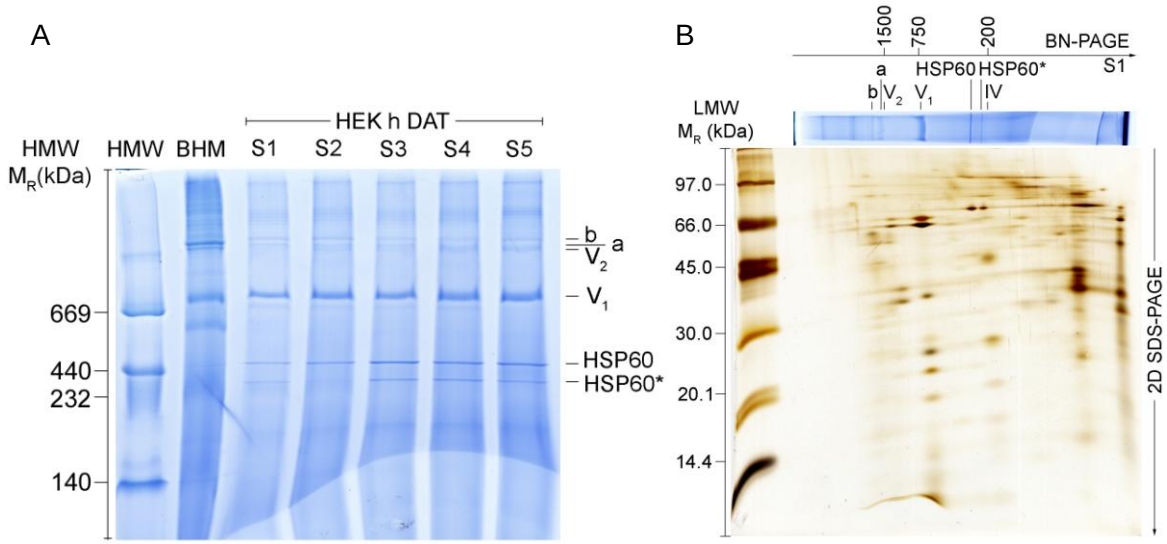

Fig. 4-22. Analysis of the abundance and the supramolecular organization of mitochondrial proteins isolated from HEK-(h)DAT cells. (A) BN-PAGE (small gel, linear 4–13% gradient gel with a 3% stacking gel, stained with CBB G-250) and (B) 2D SDS-PAGE (13% separating gel and 3% stacking gel, silver stained) of 8 g/g digitonin solubilized HEK-(h)DAT mitochondria of sample 1 (S1, incubated for 48h with 2 µM MPP^+, 40 µg protein before solubilisation). For mass calibration in the first dimension, high molecular weight (HMW) protein standard and digitonin-solubilized bovine heart mitochondria (BHM, 3 g/g) were used: supercomplexes a and b ($I_1III_2IV_{0+1}$, 1500–1700 kDa). The ATP synthase monomer and dimer are recognizable in both dimensions. In addition, the mitochondrial heptameric HSP60 and a suggested hexameric HSP60 form (HSP60*) are indicated.

The amount of respiratory chain supercomplexes I_1III_2 and $I_1III_2IV_1$ (Fig. 4-23 A) in cells incubated only with MPP^+ for 48h (sample 1) remained unchanged compared to cells without any treatment (sample 5), while incubation for the same time additionally with 9-me-BC was leading to an 1.2-fold increase (sample 2) compared to sample 1 and 5. If cells received a medium change after 48 hours treatment with MPP^+ (sample 3) the amount of supercomplexes was decreased about 1.4-fold and even 2.3-fold in cells that were treated additionally thereafter for 48 hours with 9-me-BC after a medium change (sample 4).

Incubation of cells with MPP^+ changed the ratio of supercomplex I_1III_2 to supercomplex $I_1III_2IV_1$. In all samples I_1III_2 is more present. While in sample 2 and 5 the overall amount of supercomplexes was unchanged, $I_1III_2IV_1$ is in average 3.4-fold less abundant than I_1III_2 (data not shown). In sample 1 (incubation with only MPP^+ for 48h) and sample 3 and 4 there was a shift towards the smaller supercomplex. $I_1III_2IV_1$ was 3.9-fold (sample 1) and 4.5-fold (sample 3 and 4) less abundant. The amount of the ATP synthase (sum of monomer and dimer, Fig. 4-23 B) remained nearly unchanged in all samples. Only in sample 1 and 3 solely treated with MPP^+ there was a slightly small decrease about 1.16-fold. The ATP synthase monomer was approximately 4.8-fold more pronounced in abundance than the dimer (Fig. 4-22 A).

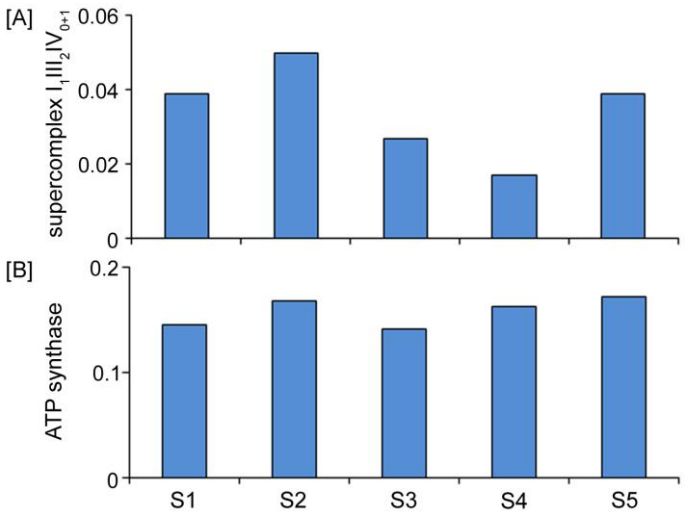

Fig. 4-23. Changes in the total amount of (A) supercomplexes $I_1III_2IV_{0+1}$ and (B) ATP synthase (sum of monomer and dimer) after exposure to 2 µM MPP^+ for 48h (S1, sample 1) and the same time to 100 µM 9-me-BC (S2, sample 2) or after incubation for 48h to MPP^+ followed by a medium change (S3, sample 3) or 48h incubation to 9-me-BC without removing of the neurotoxin with a medium change (S4, sample 4), respectively. Sample 5 (S5) was cultivated the same time period as sample 3 and 4 and used as control, but without any additives. Quantitative data were obtained from gel shown in Fig. 4-22 A.

The abundance of the mitochondrial HSP60 (sum of HSP60 and HSP60*, Fig. 4-24 A) was dependent on the duration of cultivation but not affected by MPP^+ or 9-me-BC. The smaller HSP60* species is in all samples less abundant than the larger form, suggested to represent the heptamer. In the mitochondria of cells incubated only to MPP^+ (sample 1 and 3) there is a slightly shift to the smaller HSP60*. The heptameric HSP60 was approximately 1.6-fold more abundant while in samples 2 and 4 (MPP^+ + 9-me-BC) as well as sample 5 (no additive) the ratio between HSP60/HSP60* was around 2.3-fold.

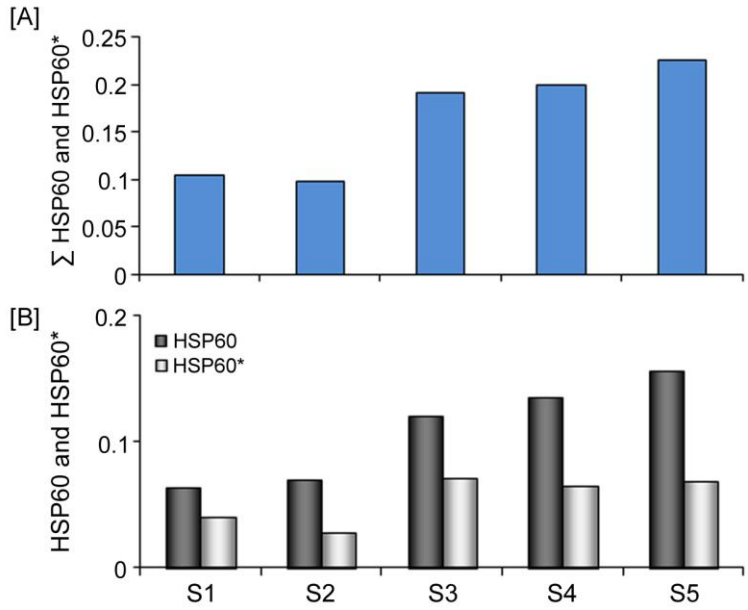

Fig. 4-24. Amount of the heptameric mitochondrial HSP60 and the suggested hexameric HSP60* sum (A) and as individual species (B). The total abundance increases during the time after seeding (A) and is unaffected by MPP^+ or 9-me-BC while the ratio between both oligomeric forms shifts towards HSP60* after incubation with only MPP^+. Quantitation from gel Fig. 4-22 A. Abbreviations: see legend of Fig. 4-23.

4.3.2.1 Summary

The effect of 1-methyl-4-phenylpyridinium (MPP^+) and the putative neuroprotectant 9-methyl-β-carboline on the mitochondrial proteome was analyzed *in vitro* in human embryonic kidney cells with a stable transfected human dopamine transporter (HEK-(h)DAT). It has been demonstrated by Storch et al. (1999) that the mitochondrial respiratory chain complex I is inhibited in HEK-(h)DAT cells after incubation with MPP^+. In the present study no individual complex I was found in mitochondria of HEK-(h)DAT cells since almost all complex I was present in respiratory chain supercomplexes as described for rat striatal mitochondria (chapter 4.3.1 and Wernicke et al., 2010). The total amount of supercomplexes was decreased in sample 3 after 48 hours MPP^+-incubation although a medium change was performed (Fig. 4-23). The decrease may result from disassembly of complex I. However, no increase of individual complex III_2 and IV was observed.

As described in chapter 4.3, 9-me-BC may feature neuroprotective functions. The simultaneous addition of 9-me-BC and MPP^+ the same time seems to nullify the effect of the toxin (sample 2) and even to increase the amount of supercomplexes while the addition of the neuroprotectant after 48 hours MPP^+-incubation had no regenerative effect (sample 4). Not only supercomplex abundance was affected by MPP^+, but additionally the proportion of the larger supercomplex containing one copy of complex IV. The ratio of $I_1III_2IV_1$ to I_1III_2 was shifted towards the smaller supercomplex after treatment only to MPP^+ (sample 1) or incubation additionally to the neuroprotectant after 48 hours (Fig. 4-23 A). Due to the fact that the decrease of supercomplex abundance was not accompanied by an increase of individual respiratory chain complexes I, III_2 and IV, possibly all respiratory chain complexes were affected in HEK-(h)DAT cells by MPP^+ treatment. In line with rat striatum (chapter 4.3.1),

where selective, progressive loss of nigrostriatal dopaminergic cells occurred after MPP^+ treatment, mitochondrial functions seem to be perturbated by MPP^+ in HEK-(h)-DAT cells (Yazdani et al., 2006).

Wernicke et al. (2010) described a decline in the cellular ATP concentration after incubation with the neurotoxin MPP^+. The amount of complex V in HEK-(h)DAT cells was unaffected by MPP^+ treatment (Fig. 4-23 B). A rather small decrease may occur in cells treated only with MPP^+ (sample 1 and 3) as compared to sample 5. Therefore, the toxin was affecting solely the abundance of respiratory chain complexes. In a mesencephalic cell culture, the treatment with 9-me-BC was leading to increased level of ATP (Wernicke et al., 2010). As demonstrated in chapter 4.4.2, changes in the amount of ATP can be balanced by an increased ATP synthase activity without an increase in its protein abundance.

The total amount of HSP60 (sum of both oligomeric forms) seemed to be unaffected by additives but increased with time after seeding (Fig. 4-24 A, a respective control for day 5 is missing). All samples harvested at day 7 contained 2-fold more HSP60 that samples harvested at day 5. In mitochondria isolated from cell culture, two HSP60 oligomeric forms seem to exist (see also chapter 4.4.1.5). The larger form is suggested to represent the heptameric one, while the smaller form may be a hexamer. A second possibility is, that HSP60* is a heptamer and the larger form (named as HSP60) a heptamer assembled in a complex with another protein. Protein-protein-interactions were preserved during solubilisation and separation in the first dimension. Further analysis has to be performed to answer this question. In any case, incubation of cells to solely MPP^+ was leading to a shift towards the smaller HSP60* form (sample 1 and 3, Fig. 4-24 B). These two oligomeric HSP60 forms as well as a comparable shift towards the smaller HSP60 oligomer were observed in mitochondria isolated from fibroblasts in cultures after irradiation with heavy ions (carbon) or X-rays and when aged cell entered the phase with reduced cell proliferation rate before senescence (Frenzel et al., 2010a). The shift from the larger to the smaller oligomeric form of HSP60 could represent a kind of stress response.

The addition of MPP^+ (2 µM) to the cell culture medium was leading after 48 hours to a decline of respiratory chain complexes and to a shift towards the smaller supercomplex I_1III_2 missing complex IV. The supercomplex formation and/or the supercomplex stability were affected with MPP^+. If only complex I expression, stability or activity changed or those of complex III_2 and IV has still to be proven. The fact that no individual complex I, III_2 or an increase of individual complex IV was observed, although supercomplexes disassembled or decreased in total amount give a hint, that the expression of all three complexes was decreased. A decrease in the number and composition of supercomplexes is leading to mitochondrial dysfunction. Evidence that MPP^+ was harmful for cells was given by the altered ratio of the heptameric HSP60 towards the suggested hexameric HSP60* after incubation with the toxin. The same shift was described for HSP60 and HSP60* in human dermal fibroblasts in cell culture exposed to ionizing radiation or X-rays (chapter 4.4.1.5). The reason for that observation should be analyzed in future and may disclose the role of mitochondrial HSP60 in stress response or apoptosis.

Due to the fact that a control for analyzing the effect of 9-me-BC as well as a control for sample 1 and 2 harvested at day 5 are missing it can only be suggested, that the treatment with both MPP^+ and 9-me-BC the same time (sample 2) was not only nullifying the effect of MPP^+ but even increasing the amount of supercomplexes. But if 9-me-BC was given in the medium 48 hours after MPP^+ was added, no restorative effect was observed any more (sample 4). There was even a larger decrease compared to sample 3 were MPP^+ was removed by performing a medium change after 48 hours of incubation to the neurotoxin.

The abundance of the ATP synthase remained unchanged possibly due to the fact that this enzyme seems to be able to modulate its specific activity to supply the cellular energy level required without an increase of its total abundance as demonstrated in chapter 4.4.1.5 (Fig. 4-38).

This experiment is only giving preliminary data describing the effect of MPP^+ and 9-me-BC on HEK-(h)DAT cells. The control for the short duration treatment (48h) with MPP^+ and MPP^+ together with 9-me-BC is missing as well as a sample to determine if only 9-me-BC has an effect on the mitochondrial proteome. Additionally, it would have been interesting to know, if the cell shape, number or cell proliferation rate differs between cells incubated with MPP^+ or MPP^+ and 9-me-BC. These data are not known.

4.4 Long-term effect of X-ray and heavy ion irradiation on the native mitochondrial proteome, ROS generation and physiology in senescent human fibroblast

Data described in this chapter have been already published:

Frenzel M., Soehn M., Durante M., Fournier C., Ritter S. and Dencher N.A. (2010). Impact of senescence and irradiation on cellular metabolism in human cells. *GSI Sci. Rep.*, in press.

Frenzel M., Durante M., Fournier C., Ritter S., Dencher N.A. (2009). Interplay of irradiation and age on the mitoproteome of human cell cultures. *GSI Sci. Rep.*, 479.

Frenzel M., Dencher N.A., Fournier C., Ritter S., Zahnreich S. (2008). Reactive oxygen species are involved in senescence of human cells independently from irradiation exposure. *GSI Sci. Rep.*, 381.

Zahnreich S., Boukamp P., Colindres M., Dencher N., Durante M., Fournier C., **Frenzel M.**, Krunic D., Ritter S. (2008). Oxidative stress and telomere shortening in normal human fibroblasts after irradiation with X-rays. *GSI Sci. Rep.*, 379.

Colindres M., Fournier C., Ritter S., Zahnreich S., Decker H., Dencher N., **Frenzel M.** (2007). Increase of oxidative stress in normal human fibroblasts after irradiation. *GSI Sci. Rep.*, 356.

Human cells are continuously exposed to ionising radiation arising from natural sources as space or earth radiation that might have harmful effects on cell survival and maintenance. But the impact of irradiation on cells is also helpful and used in medical radiation therapy – like X-ray irradiation in tumour therapy – and an experimental tool e.g. electron diffraction or neutron scattering.

In the present study, the effect of X-ray irradiation on the cellular ageing of human fibroblasts was analyzed and will be discussed in this chapter. Senescence and the process of biological ageing of tissue are discriminative but cell culture models can disclose basic molecular processes involved in both ageing and senescence.

Cultured cells undergo biological ageing called senescence (see also chapter 1.1.3). At first, senescence associated alterations of the mitochondrial proteome were studied. In cellular (replicative) senescence, human fibroblasts are losing their ability to divide on an average of 50 cell doublings *in vitro* – known as Hayflick's limit – induced e.g. by increased level of DNA damage or shortened telomeres. In the present study it was analyzed, if long-term cell culture experiments with cells undergoing senescence turn out to be an approach to study the ageing process *in vitro*, e.g., to unravel basic mechanisms common for both ageing and senescence. Results obtained for senescence-associated alterations in the mitochondrial proteome will be compared to those obtained from ageing studies on rats (chapter 4.2). Furthermore, it is known that irradiation with X-rays or heavy ions transiently increase the ROS-level (Zahnreich, 2011). The increase of ROS, often assumed to accompany ageing as suggested by the Free Radical Theory of ageing (Harman, 1956), is mimicked. As a

consequence, progeny of these cells are supposed to undergo premature ageing due to increased ROS-induced damages. To reveal the effect of irradiation on mitochondria and their role in the ageing-process, normal human dermal fibroblasts (NHDF), human fetal lung fibroblasts (WI38) and human dermal fibroblasts (AG1522D) were irradiated with X-rays (8 Gy) and AG1522D and NHDF in parallel experiments with carbon ions (2 Gy, 100 MeV/u, Unilac) and nitrogen (2 Gy, 100 MeV/u, LET 70 keV/µm, SIS), respectively, and subcultured afterwards for more than 230 days. Analysis of the mitochondrial proteome was performed using digitonin (8 g detergent/g protein) for gentle solubilisation followed by two-dimensional blue-native/SDS gel electrophoresis (2D BN/SDS-PAGE). Changes in the mitochondrial protein profile were analyzed. There are abundance-changes of life sustaining proteins such as ATP synthase, individual respiratory chain complexes, and heat shock proteins as well as changes in protein-protein-interactions (e.g. assembly of individual complex I, III_2 and IV in respiratory chain supercomplexes). Data from native proteome studies were compared with chromosomal aberration number, ROS generation, the amount of apoptotic cells and the differentiation pattern.

4.4.1 Alterations in the mitochondrial proteome of NHDF during senescence and after irradiation with X-rays

The mitochondrial proteome of normal human dermal fibroblasts (NHDF) was analyzed during a long-term experiment to reveal senescence and irradiation induced changes in the protein pattern. Cells were irradiated with X-rays (8 Gy) and compared to non-irradiated cells (in the following referred to as control). Data obtained from cell cultures were compared to that of rat brain to reveal, if there are similar alterations in ageing of tissue and senescence of fibroblasts in cell cultures.

4.4.1.1 The effect of senescence and irradiation on cell proliferation, differentiation, number of chromosomal aberrations and apoptosis

Upon irradiation with X-ray and/or during senescence different types of damages – oxidation of lipids and proteins, missfolding of proteins, and DNA aberrations – can appear. In the case these damages are beyond repair, they are leading to growth arrest or apoptosis. During subculturing, these cells are lost or overgrown by normal dividing cells. Insufficient repair may affect the cell cycle control mechanisms resulting as consequence in uncontrolled cell growth.

For fibroblasts in non permanent cell cultures, the time required for cell doubling is increasing during cultivation time and gives a hint on the ageing status of the cell. Cellular senescence that is theoretically achieved at CPD50 (Hayflick, 1985) was not reached in our study. At day 240 a portion of cells were still proliferating, especially in non-irradiated cells. Nevertheless, data obtained from day 240 will be defined as senescent time with senescent cells.

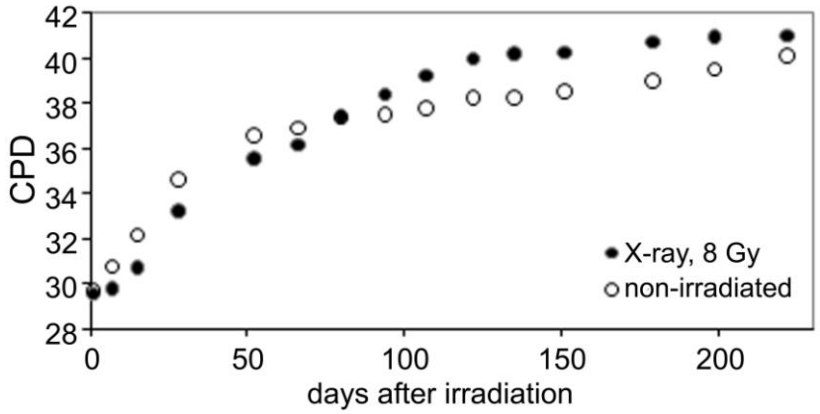

Fig. 4-25. Growth curve of normal human dermal fibroblasts exposed to X-rays (8 Gy, closed circle) at day 0 and respective non-irradiated cells (open circle). The number of cumulative population doublings (CPD) after X-ray exposure during this long-term experiment is plotted.

As shown by the growth curves, non-irradiated cells enter a phase of reduced cell proliferation approximately at day 80 while at that time point the cell doubling in progeny of irradiated cells reveal reinitiated proliferation (Fig. 4-25). Until day 20 after X-ray irradiation cell doubling is decelerated accompanied by an increase of phase III and post-mitotic cells

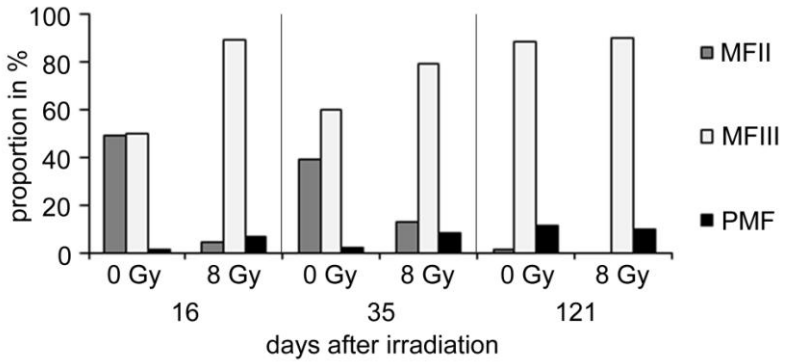

Fig. 4-26. Analysis of the differentiation pattern of NHDF upon and without irradiation. An increase of post-mitotic fibroblasts (PMF) and mitotic fibroblasts in the phase III (MFIII) together with a decrease of phase II mitotic fibroblasts occurred during the first 35 days after exposure to X-rays (8 Gy). After 121 days, in irradiated and in non-irradiated cells the abundance of PMFs and MFIII were similar.

(Fig. 4-26) and increased numbers of chromosomal aberrations due to X-ray radiation (Fig. 4-27 A) as well as increased number of aberrations per aberrant cell (up to 3 per cell, Fig. 4-27 B). The number of aberrations per diploid cell after X-ray exposure returned at the level of non-irradiated cells at day 17 and remained there until the end of the experiment, but the proportion of aberrant cells was always (Fig. 4-27 B, except day 109 and 245) higher. Considering cell differentiation, 121 days after irradiation comparable proportions of mitotic fibroblasts in phase III and post-mitotic fibroblasts in both irradiated and non-irradiated cells were found. Only a small number (1%) of mitotic fibroblasts in phase II remained. At approximately day 60, when non-irradiated cells showed reduced cell growth (indication for early senescence) a transient increase of aberrant cells (Fig. 4-27 A) as well as of aberrations per cell (Fig. 4-27 B) were found. Additionally, already at day 30, cells with twice the set of chromosomes (4n) appeared in non-irradiated cells (Fig. 4-27 C). The number of chromosomal aberrations in these cells (4n) remained at the same amount except day 137 where it was decreased. At day 245 non-irradiated cells contained more aberrant metaphases than progeny of irradiated cells. The latter showed reduced growth with a delay of four cell population doublings or 50 days compared to controls, respectively, that is accompanied, in line with non-irradiated cells, with an increase of aberrant cells and the appearance of 4n metaphases. In contrast to non-irradiated cells, the number of aberrations per cell in 2n was unchanged while that in 4n increased. Noteworthy, at day 68, shortly before progeny of non-irradiated cells showed enlarged cell proliferation, an increased amount of aberrant cells was observed.

In non-irradiated cells, from day 9, a time point of constant proliferation, until the time cell proliferation slowed down at day 68, a slightly increased amount of apoptotic cells from 6.2% up to 8.2% was found (Fig. 4-28). At day 94 it was decreased to 5.5% to increase thereafter about 3.6-fold up to 20%. At day 151 the apoptotic level was still large (20.3%) but decreased compared to day 124. After exposure to X-rays, there was an increase in the apoptotic cell level around 10% in progeny of irradiated cells until day 17. Later on, it was at the level of controls until day 82 and increased again to a lesser extent than in non-irradiated cells at day 94 and 124 up to 10.5%. A value for day 151 was missing.

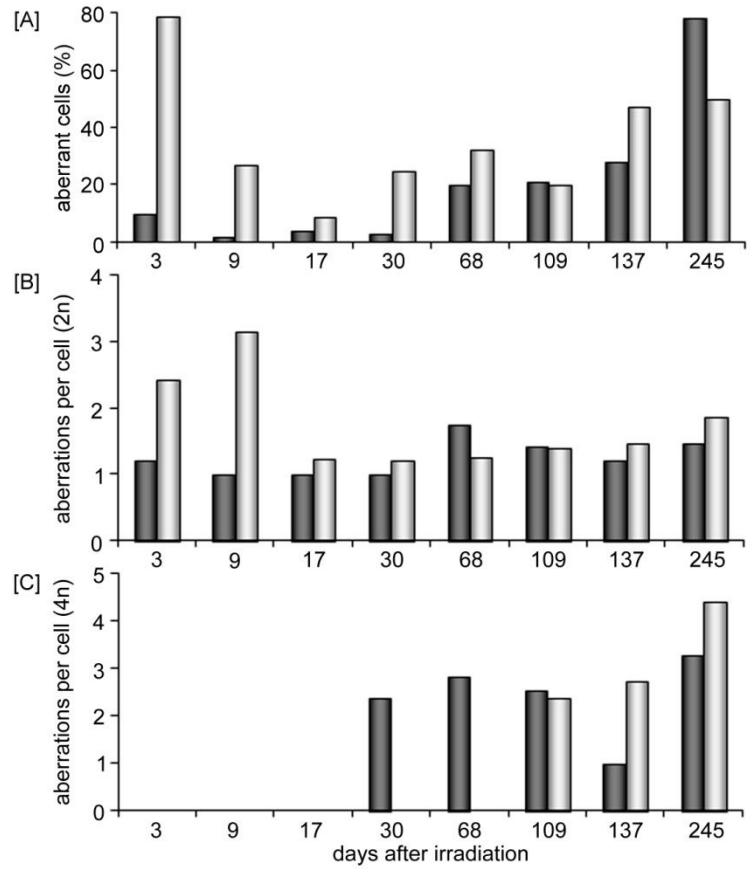

Fig. 4-27. [A] Proportion of aberrant cells (with normal chromosomal number, 2n) in percent and [B] number of aberrations per aberrant cell (2n) in progeny of non-irradiated (black) and irradiated cells (gray). The number of aberrations was divided by the amount of aberrant cells. Cells with twice a set of chromosomes [4n] appeared in non-irradiated cells at day 30 and in irradiated at day 109. Considering amount of chromosomes per cell, two aberrations per aberrant cell in 4n [C] are equal to one aberration for 2n.

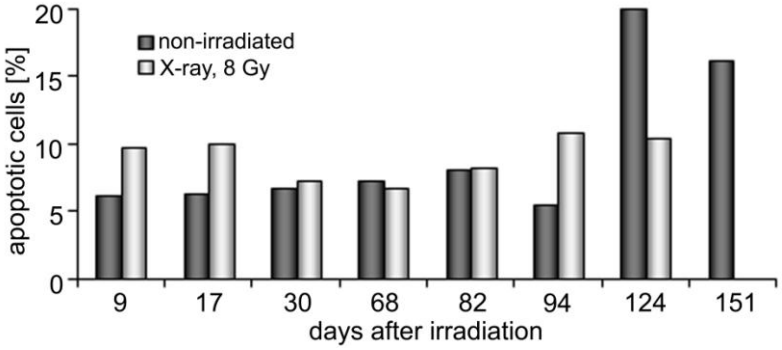

Fig. 4-28. Determination of the apoptotic cell level in progeny of non-irradiated (black) and irradiated (X-ray, 8 Gy, gray) cells. In average, 600 cells were counted in each sample at each time point. The determination of the apoptotic level was performed by Sylvia Ritter (GSI, Darmstadt).

4.4.1.2 *Age-related increase of ROS is independent of irradiation*

After irradiation with X-rays, the intracellular ROS-level of different human cell lines increased dose dependent with a maximum between day 3 to day 6 after exposure and declines thereafter to the level of non-irradiated cells (Zahnreich, 2011). To study the long-term effect of irradiation, ROS-levels in progeny of irradiated cells were compared to those of non-irradiated cells at day 66 and day 151 (Fig. 4-29 A, sum of DCF and DHE fluorescence, normalized to non-irradiated cells, ROS measurements were performed by S. Zahnreich). No pronounced irradiation dependent changes were observed at these late time points, except a decrease 4% at day 151. But compared to non-irradiated young (CPD10) cells, in aged progeny of irradiated (8 Gy, CPD40) and non-irradiated (CPD39, 151 days in culture) cells an age-associated 2.8-fold increase of ROS was observed that was independent of radiation exposure (Fig. 4-29 B, comparison of fluorescent signals). Irradiated cells displayed an even slightly less elevated ROS level.

As described in chapter 3.15, DCF and DHE are sensitive for different intracellular ROS-species. While DCFH is known to be sensitive preferentially for $OH^{\bullet}$ and $ONOO^{-}$, with DHE predominantly $O_2^{\bullet-}$ is detected (Halliwell and Gutteridge, 2007). The determination of the ROS level in the present study was not quantitative due to the fact, that the results of samples were not compared to a standard or to a certain amount of reactive oxygen species as e.g. H_2O_2. But for every measurement the same concentration was used for each dye. Therefore, the comparison of the fluorescent signals of both dyes allows a statement if $OH^{\bullet}$ and $ONOO^{-}$ or $O_2^{\bullet-}$ are relatively increasing or decreasing compared to each other occurred. The ratio of DCF and DHE fluorescent signals remained unchanged (Fig. 4-29 B). This indicates that the same proportion of different reactive oxygen species were generated in the offspring of both non-irradiated and irradiated cells, independent of irradiation and age.

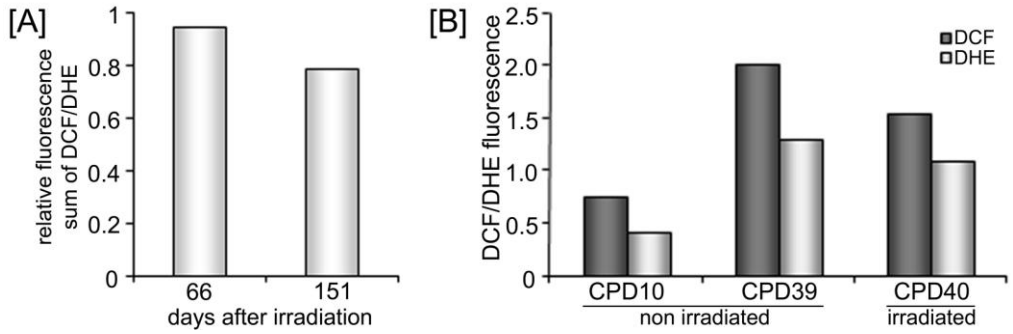

Fig. 4-29. (A) Relative intracellular ROS-level (sum of DCF and DHE fluorescence signal) in NHDF at day 66 and day 151 after irradiation with X-rays (8 Gy) normalized to non-irradiated cells. (B) ROS induced fluorescence signal of DHE and DCF in non-irradiated young (CPD10) cells and in progeny of irradiated (8 Gy, CPD40) and non-irradiated (CPD39) cells after several cell population doublings determined the same day. The same freshly prepared DCF and DHE solution was used for all three samples allowing direct comparison of the different fluorescence signals. Young NHDF cells (CPD10) were freshly thaw and cultivated for 14 days before ROS determination.

4.4.1.3 *Conditions for mitochondrial isolation, protein solubilisation and protein separation for NHDF*

The mitochondrial fractions obtained from NDHFs were not subjected to further purification, in order to preserve also fragile and damaged mitochondria that might be more abundant and more severely affected in senescent cells and/or upon X-ray exposure and possibly lost during harsh purification steps. Optimal gentle solubilisation conditions for mitochondria from cell culture were tested with digitonin as detergent to obtain quantitative and reproducible protein extraction by preservation of protein-protein interactions. With a detergent to protein ratio of 8 g/g, protein extraction was attained allowing detection of individual OxPhos complexes and respiratory chain supercomplexes as well as ATP synthase oligomers (Fig. 5-30). Digitonin to protein ratio of about 4 g/g was not sufficient (Fig. 4-30) for quantitative solubilisation of proteins. Individual proteins and protein-complexes were separated using 2D BN/SDS PAGE.

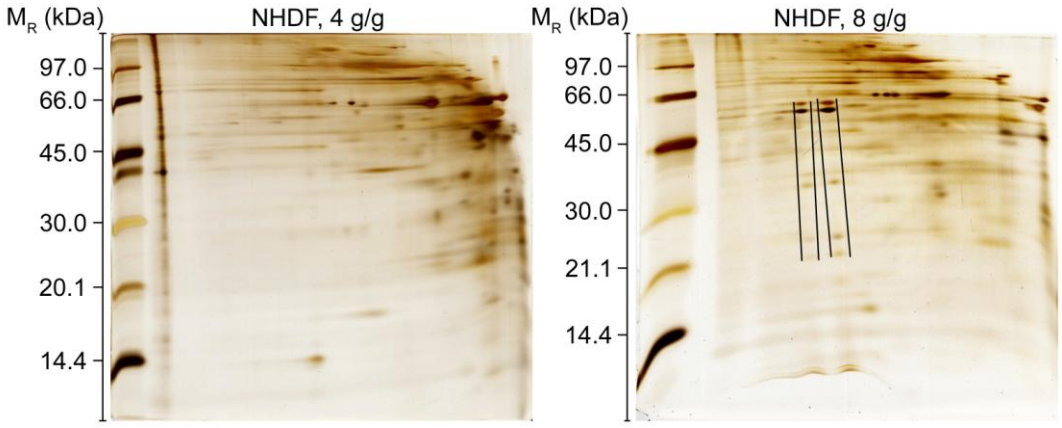

Fig. 4-30. Different extraction efficiency for mitochondria isolated from NHDF cells using 4 g/g (left) and 8 g/g (right) digitonin/protein ratio. The total abundance of isolated ATP synthase monomer and dimer (indicated in the right gel) increased when using 8 g/g while for 4 g/g only small amounts were solubilized.

The combination of methods described permits analysis of irradiation induced and/or senescence-related changes in protein pattern of the OxPhos machinery including abundance-changes of individual proteins as well as alterations in the amount and composition of respiratory chain complexes or supercomplexes and of ATP synthase oligomers. Individual complex I, III_2 (always present as dimer), complex IV and complex V as well as ATP-synthase homodimers (V_2) were identified. Large supercomplexes $I_1III_2IV_{0-3}$ containing complex I, complex III dimer and zero to three copies of complex IV were visualized. For mitochondria of NHDF complex II of the respiratory chain were not sufficient in abundance to be detected in both dimensions (BN and 2D-SDS-PAGE). Besides the OxPhos complexes other mitochondrial proteins like heat shock protein (HSP)60 are extracted during solubilisation (Fig. 4-35, Fig. 4-36).

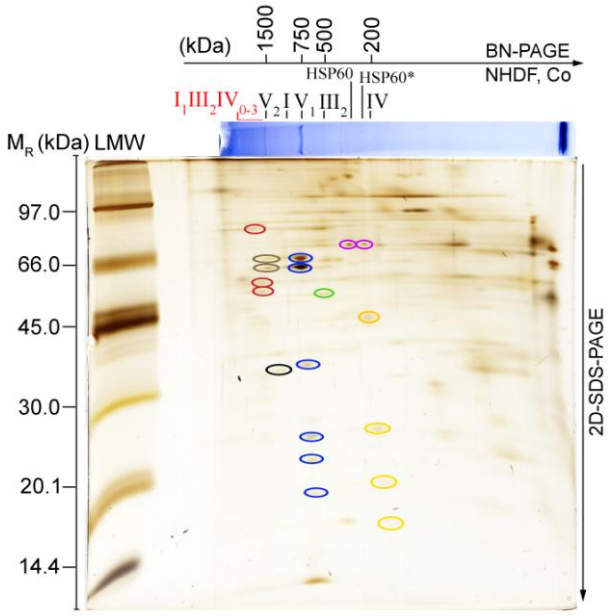

Fig. 4-31. 2D-BN/SDS–PAGE of digitonin-solubilized (8 g digitonin/g protein) mitochondrial proteins from NHDF cell culture (non-irradiated, referred as control) 80 days after the start of the experiment. In the first dimension (BN-PAGE), individual proteins, protein complexes and respective supercomplexes are separated in their native state. In the second dimension (SDS-PAGE), subunits are separated in a vertical line according to their position in BN-PAGE. For mass calibration in the first dimension, high molecular weight (HMW) protein standards respectively digitonin solubilised and well characterised bovine heart mitochondria (BHM) were used: individual complexes I, III_2 and V (130–1000 kDa), supercomplexes $I_1III_2IV_{0–3}$ (1500–2100 kDa) and ATP synthase dimer V_2 (1500 kDa). In the second dimensions a low molecular weight (LMW) protein standard was used for mass calibration and standardisation of gels. Characteristic protein patterns of subunits belonging to individual OxPhos complexes I (black), III_2 (green), IV (yellow) and of their preserved supercomplexes (red) and of complex V monomer (blue) and dimer (brown) are resolved. Furthermore, two oligomeric forms of heat shock protein 60 (violet) – HSP60 and HSP60* suggested to represent a heptamer and hexamer, respectively –are indicated. [BN-PAGE: linear 3–13% gradient gel with a 3% stacking gel, stained with CBB G-250; 2D-SDS-PAGE: 5% stacking gel, 13% separation gel, silver stained.]

4.4.1.4 Different abundances of OxPhos complexes and supercomplexes in progeny of non-irradiated and irradiated cells

The ATP synthase (complex V) is the terminal complex of the OxPhos machinery. Its total amount (sum of V_1 and V_2) declined in non-irradiated cells at day 21 (1.48-fold) and returned at day 80 again to the level at day 14 (Fig. 4-32 A). At day 240, when cell proliferation was slowed down, the level of ATP synthase was decreased about 2-fold. In the offspring of irradiated cells, complex V abundances were comparable during the first 21 days. At day 80 there was a 2-fold increase that slightly (1.3-fold) declined at day 240. Comparing senescent controls and progeny of irradiated cells at day 240, in irradiated cells 3.3-fold more ATP synthase was found.

Individual complex I is only present in a small amount (Fig. 4-32 B). Irradiated cells contained 1.4-fold less complex I at day 14 compared to non-irradiated cells. In both, there was a pronounced decrease in complex I abundance from day 14 to day 21 that was smaller after irradiation, 3.5-fold vs. 2.5-fold. At day 80 there was an increase about 2.5-fold in controls but much larger (8-fold) in the offspring of irradiated cells. Senescent cells at day 240 exhibited,

compared to day 80, a decrease in protein abundances of about 1.7-fold in controls and 2-fold in irradiated cells.

In non-irradiated cells, the amount of complex III_2 decreased about 1.7-fold at day 21 and recovered again thereafter at day 80 (Fig. 4-32 C). At day 240, similar to complex I and V, a pronounced decrease in the protein amount occurred (9-fold) in non-irradiated cells. In the offspring of irradiated cells, the level of complex III_2 was comparable at days 14, 21 and 240. Only at day 80, there was a 1.4-fold abundance decrease.

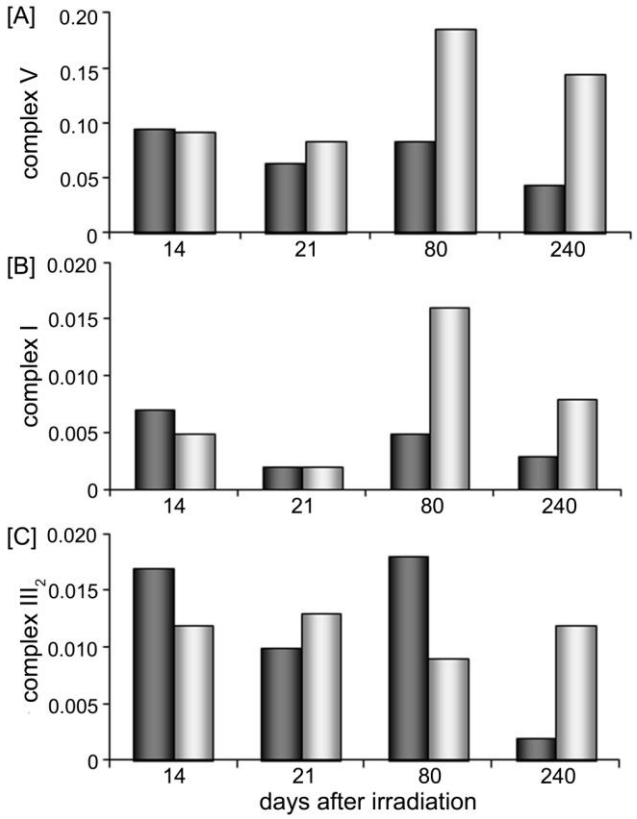

Fig. 4-32. Changes in the total amount of ATP synthase (sum of monomer and dimer), of individual complexes I and III_2 in progeny of non-irradiated (dark) and irradiated cells (gray). Quantitation occurred in the first dimension after CBB G-250 staining of proteins.

Changes in the protein abundance of respiratory chain supercomplexes $I_1III_2IV_{0-3}$ (depicted as sum of all supercomplex species in Fig. 4-33) were analogous to complex I with a decrease in the protein amount at day 21 and day 240 interrupted by a recovery at day 80 for non-irradiated and irradiated cells. In progeny of irradiated cells the decrease at day 21 was smaller. At day 80 compared to day 21 there was a 4.3-fold increase in the supercomplex level. This boost at day 80 as well as the reduced protein level of supercomplexes $I_1III_2IV_{0-3}$ in senescent (240 days) cells was also observed for complex I and the ATP synthase.

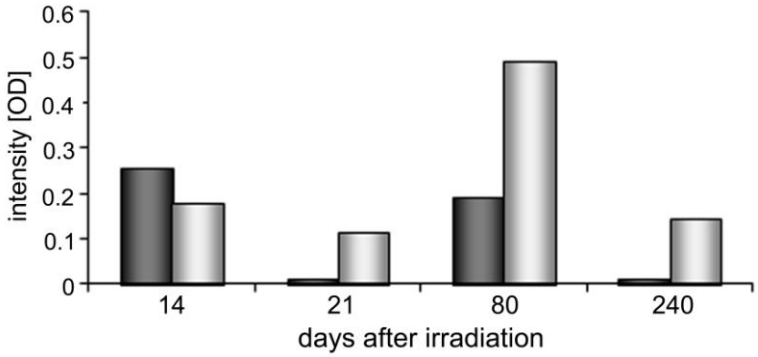

Fig. 4-33. Alterations in the abundance of supercomplexes (sum of $I_1III_2IV_{0-3}$) in progeny of non-irradiated (dark) and irradiated cells (gray). Quantitation occurred in the first dimension after CBB G-250 staining of proteins.

4.4.1.5 Abundance changes of non-OxPhos proteins and cytoplasmatic SOD1 caused by senescence and irradiation

Besides OxPhos complexes and supercomplexes the protein abundances of other mitochondrial proteins (HSP60, prohibitin and mitofilin) as well as the cytoplasmic SOD1 were analyzed. Contrary to mitochondria from rat brain (Frenzel et al., 2010b; Reifschneider et al., 2006), liver (Dani et al., 2009; Reifschneider et al., 2006), kidney (Reifschneider et al., 2006), heart (Gómez et al., 2009; Reifschneider et al., 2006) and skeletal muscle (Lombardi et al., 2009; Reifschneider et al., 2006) in mitochondria of cell cultures two forms of HSP60 can be separated (Fig. 4-31, Fig. 4-34, chapter 4.3.2). As described in chapter 4.3.2 the mitochondrial HSP60 is commonly present as heptamer (Cheng et al., 1990). According to the molecular mass, the larger HSP60 form could be the heptamer (Fig. 4-31). The second form with smaller molecular mass might represent a hexamer (referred to as HSP60*). At day 14 after X-ray exposure the total amount of HSP60 (sum of both oligomeric states) was 1.2-fold less than in non-irradiated cells (Fig. 4-35 A). An increase of HSP60 occurred at day 21 about 1.3-fold in non-irradiated cells and 2.2-fold in irradiated cells. Henceforward, in progeny of irradiated cells the protein level remained mainly unchanged while in progeny of non-irradiated cells a gradual decline about 1.3-fold and 1.2-fold occurred until day 240.

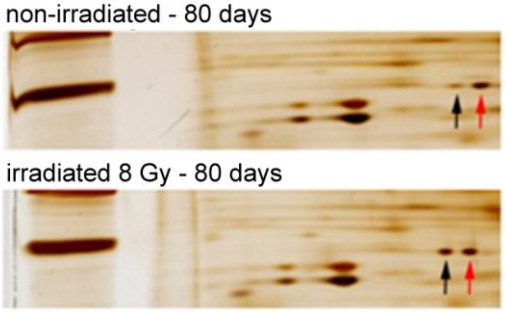

Fig. 4-34. Silver stained 2D-BN/SDS gels of mitochondrial fractions at day 80. Protein spots of HSP60 heptamer (black arrow) and the smaller form (red arrow) are highlighted.

Both, senescence and radiation influence the proportion of the two HSP60 forms (Fig. 4-35 B). Two weeks after irradiation the smaller HSP60 exceeded the heptamer by 1.8-fold and thereafter both species are present in equal quantities. In controls there was a

pronounced shift in the ratio towards the smaller form of HSP60 when cells enter senescence at day 80 that in part returns at day 240.

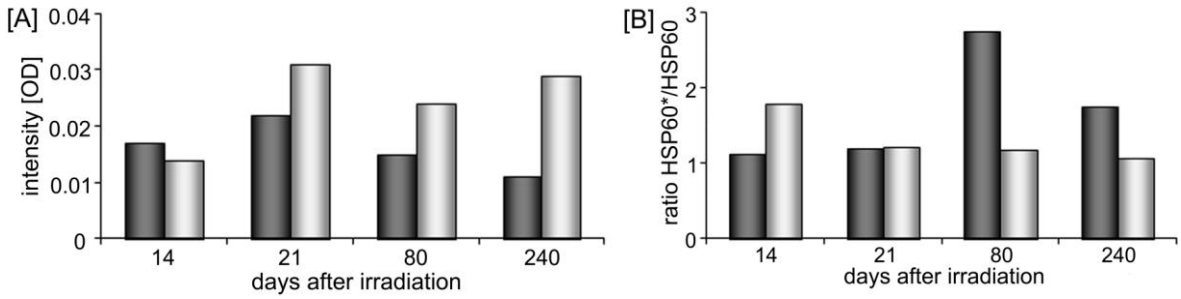

Fig. 4-35. (A) Total amount of heat shock protein 60 (sum of both oligomeric forms) and (B) the ratio of HSP60* and HSP60 in progeny of non-irradiated (black) and irradiated (gray) cells. Quantitation occurred in the first dimension after CBB G-250 staining of proteins.

In progeny of irradiated cells less mitofilin (important for fusion and fission of mitochondria) was found at day 14, 21 and 80 compared to non-irradiated cells (Fig. 4-36). The amount was comparable at day 14 and day 80, but decreased to a small extent at day 21 and an increase at day 240. In non-irradiated cells there was a pronounced decrease in mitofilin abundance at days 240. While in non-irradiated cells the level of prohibitin (involved in cell proliferation) increased at day 21 and decrease strongly at day 80 to recover again to the level of day 14 at day 240, in the progeny of irradiated cells it remains nearly constant. In both, non-irradiated and irradiated cells the cytoplasmatic SOD1 (essential in ROS defence) amount increased during senescence but more pronounced in non-irradiated cells interrupted by a small decrease at day 80 in non-irradiated cells.

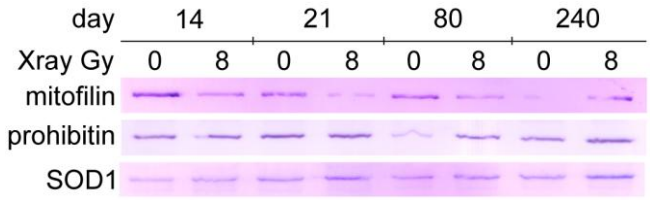

Fig. 4-36. Abundance changes of mitofilin, prohibitin and SOD1 in irradiated and non-irradiated cells during senescence. (Immunodetection of proteins after Western blot on PVDF membranes using alkaline phosphatase reaction for visualization.)

4.4.1.6 Ageing in progeny of non-irradiated and irradiated cells

It was demonstrated that the level of ROS increase the first days after ionizing irradiation (Zahnreich, 2011). Before starting the experiment, it was therefore assumed that, progeny of cells exposed to X-rays enter senescence earlier than non-irradiated in respect to the “Free Radical Theory of Ageing” from Harman (1956). But according to the growth curves, progeny of non-irradiated cells entered cellular ageing, characterized by decreased cell proliferation, earlier than irradiated cells. The comparison of changes in the cell physiology like cell differentiation, chromosomal aberrations or the level of apoptotic cells as well as

determination of the cellular ROS level after several cell population doublings and analysis of alterations in the mitochondrial proteome may reveal the reason for this observation.

In the first step, alterations in the mitochondrial proteome of NHDF cells in non-irradiated cells during cellular ageing were compared to those of rat tissue and in the second step, to those obtained from progeny of irradiated NHDF cells. Quantitation of protein abundances was performed in a gel of the first dimension after CBB G-250 staining. This step is less time consuming than analyzing a second dimensional gel but in comparison to the second dimension, quantitations of protein abundances in the first dimension are less precise and only larger alterations represent indications for changes at the protein level.

4.4.1.7 Ageing in non-irradiated cells is similar to those of rat brain cortex and liver mitochondria

According to the growth curve (Fig. 4-25), during the first 50 days non-irradiated cells showed exponential growth behavior. Afterwards, the time required for cell division increased and cumulative cell population doubling was slowed. In line with the model of cellular senescence described by Hayflick (1985), ageing of the cell culture was accompanied by a decrease in the number of phase II cells and an increase of phase III cells. The latter were characterized by a reduced cell proliferation and represent antecedents of post-mitotic fibroblasts that themselves increased in amount too (Fig. 4-26). Additionally, at the chromosomal level, aberrations increased in progeny of non-irradiated cells during cellular ageing at day 68 up to 20% (2n) aberrant cells until 80% at day 245 (Fig. 4-27 A). Already at day 30 the first cells containing twice the set of chromosomes and additionally chromosomal aberrations appear (Fig. 4-27 C). An overall cell growth arrest was not attained since from day 170 to day 240 small but constant cell proliferation occurs. As described by Hayflick (1985), after passing phase III, cells stop proliferation, enter senescence and die. This correlates with the pronounced increase of the apoptotic level in aged cells beginning at day 124 (Fig. 4-28).

At the mitochondrial protein level, cellular ageing of non-irradiated human fibroblasts in cell culture was accompanied by a decrease in protein abundances of individual OxPhos complexes (complex I: 1.7-fold, III_2: 9-fold and V: 3.3-fold) as well as the sum of respective supercomplexes (16-fold) at day 240 compared to day 80. An overall decline in protein amount occurred also at day 21 followed by a recovery for complex III_2 and complex V and to a lesser extent for complex I and supercomplexes. The decrease in protein abundances at day 21 was smaller for complex III_2 and V compared to that from day 80 to day 240 where cells entered already phase III characterised by reduced cell population doubling or differentiated post-mitotic cells undergoing apoptosis (Hayflick, 1985). The protein amount of mitochondrial HSP60 decreased continuously until days 240 and that of mitofilin pronouncedly at day 240 (Fig. 4-35 A and B, Fig. 4-36). The ratio of HSP60* to HSP60 were comparable until day 80. Thereafter, the smaller oligomeric form HSP60* was more pronounced until day 240. Prohibitin abundances were comparable at day 14 and 240 but

increased at day 21 and decreased day 80. The SOD1 is the only enzyme that slightly increased during cell ageing in progeny of non-irradiated cells (Fig. 4-36).

For various established ageing models from fungi to rat, used for evaluation of fundamental mechanisms controlling life-span, changes in the protein abundances (Gómez et al., 2009; Groebe et al., 2007; Lombardi et al., 2009; Poon et al., 2006a; Poon et al., 2006b) and post-translational modifications (Groebe et al., 2007; Hunzinger et al., 2006; Poon et al., 2006c) have been previously described. Age-related alterations in the native mitochondria profile were described for rat brain (Frenzel et al., 2010b), liver (Dani et al., 2009), skeletal muscle (Lombardi et al., 2009) and heart (Gómez et al., 2009). Rat skeletal muscle (Lombardi et al., 2009) and rat brain cortex (Frenzel et al., 2010b) show comparable age-associated changes in protein abundance of OxPhos complexes and supercomplexes as observed for NHDF. In both, tissue and cell culture, there is a decrease in complex I, III_2 and V abundance as well as in supercomplexes. OxPhos complexes are essential for the energy status. Variations in their amount may give a hint on the metabolic activity and ROS level within a cell. Inhibited oxygen uptake by mitochondria is harmful for cells, due to the fact that 90% of the cellular oxygen is consumed by the respiratory chain (Karthikeyan and Resnick, 2005). Whether the observed declined ATP synthase amount in senescent cells is followed as consequence by an age-associated decrease in the cellular ATP-level, as already described for senescent human cells (Stöckl et al., 2006; Stöckl et al., 2007; Wang et al., 2003; Zwerschke et al., 2003), will be discussed in chapter 4.4.2.

The level of HSP60 declines during ageing in molluscs and rat heart, brain and liver (chapter 4.2.2.4, Fig. 4-15) (Colotti et al., 2005; Haak et al., 2009; Ivanina et al., 2008). A remarkable difference to all rat tissues types studied so far is the presence of two oligomeric forms of mitochondrial HSP60 in NHDF cells (Fig. 4-31, Fig. 4-35 B). It seems to be a phenomenon typical for cell cultures since the same observations were made in HEK-(h)DAT cells (chapter 4.3.2, Fig. 4-24). The amount of the oligomeric forms was equal at day 14 and 21. At day 80 the ratio increased to a value of 3, indicating an pronounced increase in the relative proportion of the smaller HSP60* form. As described in chapter 4.3.2, the larger HSP60 form seems to represent the mitochondrial heptameric state while HSP60* might be a hexamer. Another possibility is that the smaller form is the heptamer and the other a heptamer associated with another protein. This still has to be analyzed. Since the mitochondrial HSP60 has a proapoptotic role, and since the level of apoptotic cells increased with larger CPD and cultivation time this shift in the ratio towards HSP60* may represent a mechanism to induce programmed cell death. Also in HEK-(h)DAT cells after treatment with the toxin MPP^+, inducing mitochondrial dysfunctions by affecting complex I, the proportion of HSP60* increased compared to the larger oligomeric form, underlining the putative proapoptotic function of HSP60*. That the smaller HSP60* form was not described in tissue may arise from a permanent higher oxidative environment cell cultures are exposed to (21% atmospheric oxygen).

An additional hint for mitochondrial dysfunction is given by the observed decrease in mitofilin abundances during senescence (Fig. 4-36). Mitofilin represents a transmembrane protein of the inner mitochondrial membrane. It is essential for cristae formation and determines

mitochondrial morphology as well as fusion and fission (John et al., 2005). Decreased cellular proliferation and increase in the apoptotic level are found in HeLa cells after down regulation of mitofilin utilising small interfering RNAs. The decrease of mitofilin in the present study may also induce apoptosis in NHDF cells with increased CPD after long-term cultivation. Low level of mitofilin may lead to abnormal mitochondrial function possibly due to impaired cristae formation, resulting in increased reactive oxygen species production. John et al. (2005) postulated that despite the enlarged metabolic flux induced by mitofilin deficiency, mitochondrial oxidative phosphorylation was not increased accordingly. One explanation may be an additional general decrease in abundance of OxPhos complexes.

Prohibitin abundance was, except for day 80, slightly increased (Fig. 4-36). Prohibitin is a transmembrane protein of the inner mitochondrial membrane, evolutional conserved and ubiquitously expressed, involved in cell proliferation, cristae formation and therewith also important for mitochondrial maintenance (Merkwirth and Langer, 2009). Additionally it is postulated to act as chaperone for the respiratory chain complexes (Nijtmans et al., 2000). The abundance of prohibitin is possibly increased to decrease the amount of misfolded respiratory chain complexes.

The slight increase of SOD1 abundance can be correlated with the observed increase of ROS during ageing (Fig. 4-36) that is underlining the suggestion that during ageing there is an increase of reactive oxygen species (Harman, 1956). The cytosolic superoxide dismutase 1 is a prominent member of the cellular antioxidative protection system, important for ROS defence in catalyzing the dismutation of superoxide radical anions into oxygen and hydrogen peroxide. It is predominantly found in cytoplasm but to 1% in the intermembrane space of mitochondria (Kloppel et al.; Li et al.). Slightly reduced SOD1 abundance causes already increased level of superoxide. Decrease in SOD1 amount affects the mitochondrial transmembrane potential and ATP production. SODs are also important for protein import, e.g. of complex I (Aquilano et al., 2006).

Noteworthy, alterations in the mitochondrial proteome in human fibroblasts in cell culture during senescence – demonstrated here for NHDF are comparable to those described for tissue. Therefore, overall appropriate basic molecular processes involved in both ageing and senescence may be disclosed with this cell culture model.

4.4.1.8 X-ray radiation induced increase in protein abundances of ATP synthase, individual OxPhos complexes and supercomplexes enable prolonged proliferation

X-ray application was used as a tool to (1) study the effect of ionizing radiation on the proteome and on mitochondrial functions, (2) to trigger ROS-generation and to analyze the long-term effect of ROS in progeny of irradiated cells, (3) to induce DNA modification and (4) to compare our data with the “Free Radical Theory of Ageing” (Harman, 1956) to reveal basic mechanisms of ageing. Oxidative stress is an indirect effect of X-ray radiation. The relatively high dose of 8 Gy was chosen to induce pronounced effects on protein expression and interaction. In the cell response to X-ray irradiation, several proteins are involved belonging

e.g. to the DNA-repair systems. Also during senescence, cellular damage accumulates, leading to impaired functions. In this part of the study, alterations in abundances of proteins involved in stress response, such as the chaperone HSP60 and in antioxidative systems like SOD1 will be correlated to damages in nDNA, cell differentiation, ROS level and the amount of apoptotic cells. But also changes in the level of the mitochondrial proteins prohibitin and mitofilin provide evidence about mitochondrial maintenance and survival.

In progeny of irradiated cells until day 20 after exposure to X-ray the cell doubling seemed to stagnate (Fig. 4-25). There are two explanations for this observation:

(1) Irreversible irradiation-induced damages may cause apoptosis or cell growth arrest. Growth-arrested cells are not dividing anymore and get lost during further passages or are diluted by cells still undergoing cell doubling, respectively.

(2) Small irradiation induced damages can be repaired by the cellular repair system. During rectification of these damages cell growth and division are decelerated. After recovery, normal cell division is regained.

Exposure to X-rays induced not only high number of chromosomal aberrations but additionally increased numbers of aberrations per cell. Hence, an increase of the apoptotic level was observed after irradiation (Fig. 4-28) as well as an increase of phase III fibroblasts and post-mitotic cells (Fig. 4-26). Therefore, reduced cumulative population doubling was observed (Fig. 4-25). After damage repair the offspring of irradiated cells exhibits prolonged ability to proliferate.

At day 80, when non-irradiated cells entered phase III, progeny of irradiated cells exhibited an increased cell division. At day 30, the proportion of cells with chromosomal aberrations was already increased, but even larger at day 68 short before the increased proliferation frequency. At day 94, a higher number of apoptotic cells was observed, possibly due to the appearance of aberrant cells containing twice the set of chromosomes (4n). Progeny of irradiated NHDFs entered reduced cell proliferation later approximately at day 140, accompanied by an additional increase of cells containing chromosomal aberrations (2n) at day 137. Further question arise: Why undergo progeny of irradiated cells cellular senescence later than non-irradiated?

In cellular ageing, alterations in the mitochondrial proteome are different in progeny of X-ray irradiated cells compared to non-irradiated cells. Considering protein analysis at day 80, when cell proliferation was increased, there was a significant large abundance increase of individual complex I (8-fold), V (2.2-fold) and of the respiratory chain supercomplexes $I_1III_2IV_{0-3}$ (4.3-fold) after exposure to X-rays (Fig. 4-32, Fig. 4-33). Complex I of the respiratory chain allocates the major part of electrons provided for oxygen reduction. It requires supercomplex formation with complex III_2 and IV for its optimum stability and activity (Fig. 4-6) (Schäfer et al., 2007). Complex I and supercomplexes were less abundant compared to non-irradiated cells 14 days after irradiation and decreased thereafter at day 21 before the pronounced increase at day 80. Nugent et al. (2010) found a decrease in the activity of OxPhos complexes in cell cultures 4 hours after γ-radiation with a recovery 12-

96 hours after irradiation. But the level of complex V in progeny of irradiated cells was similar to non-irradiated cells and remained constant until the increase at day 80. The only enzyme of the respiratory chain behaving differently is complex III_2. The abundance of complex III_2 was decreased after irradiation compared to non-irradiated cells, but remained unchanged until day 240 with a small decrease at day 80. The slight decrease at day 80 may result from supercomplex assembly.

Increased abundances of respiratory chain complexes and supercomplexes upon X-ray exposure might indicate high oxygen consumption and therewith enlarged membrane potential used by the ATP synthase, whose abundance also increased. This may explain the observed increased cell proliferation rate at day 80 in progeny of irradiated cells (Fig. 4-25). A correlation of ATP synthase abundances to the level of cellular ATP is described in chapter 4.4.2. The flattened growth curve at day 130, typical for the phase with reduced cell proliferation shortly before senescence, demonstrates that for the majority of cells the proliferation was still regulated by cell cycle control proteins. Irradiation was not inducing those mutation or deliberate modification leading to immortalized cells proliferating indefinitely. At day 240 also progeny of irradiated cells showed indication for early senescence due to slowed cell proliferation. At this time, in line with progeny of non-irradiated cells as well as rat striatum and liver, the total abundance of the individual OxPhos complexes – except complex III_2 – and supercomplexes was decreased. This supports the notion that these alterations in protein abundance are commonly present in both ageing and senescence.

The expression level of HSP60, mitofilin and SOD1 altered after X-ray irradiation. At day 14 the total amount of HSP60 amount (sum of both oligomeric states) was comparable in progeny of irradiated and non-irradiated cells (Fig. 4-35 A). While there was a transient decline thereafter in non-irradiated cells, at day 21 the total amount of HSP60 (Fig. 4-35 A) was increasing in progeny of irradiated cells about 2.2-fold and afterwards remains at a comparable level without showing senescence-related decrease at day 240. HSP60 works as chaperone and has proapoptotic functions. An increase in its protein abundance after irradiation may be correlated with to the presence of larger numbers of damaged proteins or/and induction of apoptosis. Since the amount of HSP60 was not enlarged before day 21 after exposure to X-rays, the protein response on this external stress appeared delayed. In contrast to non-irradiated cells, the ratio of both oligomeric forms was also unaffected by cellular ageing but transiently changed after irradiation (Fig. 4-35 B). At day 14 there was more HSP60* present (1.8-fold). At the same time, the amount of apoptotic cells was increased. Later on, after several cell population doublings the level of HSP60* and HSP60 was similar. Additionally, the level of apoptotic cells only minor increased. This underlines the role of the smaller oligomeric state (HSP60*) in induction of apoptosis as suggested already in chapter 4.4.1.7.

Protein abundances of mitofilin in progeny of irradiated cells were less until day 80 compared to non-irradiated cells, but remained at the same level until day 240 (Fig. 4-36), while in non-irradiated cells there was an age-associated decrease. Mitofilin is important to maintain mitochondrial functions (fusion and fission as well as cristae formation).

The total amount of SOD1 increased transiently with increased CDP and to a larger extent in senescent progeny of irradiated cells than in non-irradiated (Fig. 4-36). Considering the ROS level, in progeny of non-irradiated cells and irradiated cells, the ROS-level is similar at day 66 but slightly lower in progeny of irradiated cells at day 151 (Fig. 4-29 A), possibly due to the increase abundance of this antioxidant enzyme. The suggestion that progeny of irradiated cells depicts constantly increased ROS level larger than that of non-irradiated cells is refuted by the data obtained (Fig. 4-29). An increase of reactive oxygen species occurred as a immediate response on irradiation as described by Zahnreich (2011). Afterwards progeny of X-ray exposed cells exhibit ROS level similar to non-irradiated cells. The irradiation induced increase of ROS about 1.5-fold [for X-rays, (Zahnreich, 2011)] is relatively small compared to the significant age-associated increase of ROS about 2- to 3-fold (Fig. 4-29 B).

The ROS level increased during ageing, in line with the “Free Radical Theory of Ageing” by Harman (1956) independently of radiation exposure. Furthermore, no prevalence of a predominant reactive oxygen species such as superoxide radicals was observed as indicated by the comparable ratio of DCF and DHE signals in young, aged and irradiated cells (Fig. 4-29 B). It is proven that small amounts of ROS are essential for the immune system or signalling processes (Chew and Park, 2004). Immoderate increased levels of ROS lead to damage of nucleic acids, lipids and proteins and results in less efficient antioxidant system and in turn to more ROS. It would be interesting to correlate the level of ROS to the amount of mitochondria per cell (Lee et al., 2005; Limoli et al., 2003; Spodnik et al., 2002). The number of mitochondria per cell was not analyzed.

An increase in protein abundances of SOD1 and HSP60 as well as constant level of mitofilin were accompanied by a prolonged ability of progeny of irradiated cells to proliferate. It is known that ionizing radiation is harmful for cells and multicellular organisms (Ina and Sakai, 2004). But following the theory of radiation hormesis (Wolff, 1998), low-dose (Luckey, 1982) and high-dose (Yonezawa et al., 1996; Yonezawa et al., 1990) radiation induce e.g. also enhanced growth rate, prolonged life span (Lorenz et al., 1955) – also after lethal high-dose irradiation (Yonezawa et al., 1996; Yonezawa et al., 1990) – increased function of the immune system (Anderson and Lefkovits, 1979; Liu, 1989; Liu et al., 1987), increased resistance to oxygen toxicity (Lee and Ducoff, 1989). In the present long-term cell culture experiment, X-ray irradiation with a dose of 8 Gy stimulates the expression of antioxidants as well as stress response proteins as chaperones. Therefore, cells may be more protected for later stress as e.g. ROS increase. Also acute doses of oxidative substances (e.g. ROS) are postulated to increase the cellular protection against further oxidative stress and therewith lifespan. Therefore, irradiated NHDF cells were exposed to two acute stresses that may both induce prolonged cell survival due to increased stress response system in progeny of cells that were able to recover.

The abundance of prohibitin constantly increased until day 240 and was slightly larger in progeny of irradiated cells compared to non-irradiated. Prohibitin is known to enhance cell proliferation (Langer et al., 2006) as observed in this experiment for progeny of irradiated cells.

4.4.1.9 Summary

In the present study, it was discovered that ageing of NHDF cells was characterized by comparable alterations of the mitochondrial proteome as observed previously for rat brain cortex (Dencher et al., 2007; Frenzel et al., 2010b) and skeletal muscle (Lombardi et al., 2009). Progeny of non-irradiated cells exhibiting a pronounced decrease in protein abundances of individual OxPhos complexes I, III_2 and V and supercomplexes as well as mitofilin and HSP60 when cells entered the phase of reduced cell growth (pre-stage of cellular senescence). Prohibitin and SOD1 increased until day 240. Cellular ageing was accompanied by increase in the level of phase III and post-mitotic cells as well as by cells with chromosomal aberrations, number of aberrations per cell, increased amount of aberrant cells with twice the set of chromosomes and by cells undergoing apoptosis. Additionally, the "Free Radical Theory of Ageing" by Harman (1956) was supported, at least for cells in culture.

Progeny of cells irradiated with X-rays maintained their ability to proliferate for a longer time. Immediately after X-ray exposure, cells provided increased numbers of aberrant cells and chromosomal aberrations per cell, respectively, apoptotic cells as well as phase III and post-mitotic fibroblasts that returned to the control level after cell recovery. Increased cell division was observed at day 80, possibly enabled by the pronounced abundance increase of complex I, V and of respiratory chain supercomplexes. Thereafter, also progeny of irradiated cells exhibit reduced cell proliferation and therewith a decrease in complex I, V and supercomplex abundances as observed also for progeny of non-irradiated cells. Increased amount of HSP60 and SOD1 as well as stable level of mitofilin may enable additionally the prolonged proliferation ability in progeny of non-irradiated cells. Prohibitin (except for day 21) and SOD1 are increasing in abundance after irradiation and during cell ageing until day 240 to larger extent compared to non-irradiated cells. ROS-level increased independent from irradiation exposure in progeny of irradiated and non-irradiated cells. The present experiments confirm the suggestion made in chapter 4.3.2 that two oligomeric forms of HSP60 are present in human cell cultures. It is described for the first time that a shift towards the smaller oligomeric state (HSP60*) may lead to an induction of the apoptotic pathway.

4.4.2 Changes of the cellular ATP level during ageing and after X-ray irradiation in NHDFs

Changes in the amount of the ATP synthase could affect the cellular ATP level (ATP generation versus consumption). Additionally, increased demand of ATP, possibly needed after external stress like irradiation, has to be provided by complex V. In the present study, in NHDF a decline in the amount of ATP synthase was observed in progeny of irradiated and non-irradiated cells at the time point cell proliferation slowed down (Fig. 4-32 A). Less ATP synthase, due to its role as main ATP generating enzyme, may have a direct impact on the overall energy status of the cell. For ATP determination, as demonstrated in chapter 4.1.5, cells have to be analyzed immediate after harvesting or after storage with TCA that was added immediately after harvesting and before freezing to cells, to ensure no destruction of ATP during the time of storage. For the experiment described in chapter 4.4.1 (Fig. 4-25), no ATP determination had been performed. To reveal if the observed decline in protein abundance of the ATP synthase was accompanied by a decline in the ATP level of a cell, the experiment was repeated with NHDF cells using the same conditions for X-ray irradiation and cell culturing to study the effect of senescence and X-ray irradiation on the cellular ATP level. NHDF were subcultured for 193 days (Fig. 4-37). Determination of the cellular ATP amount was performed as described in chapter 3.14. At every subcultivation, cells were incubated with TCA and stored at -20°C until ATP determination.

In the present experiment, progeny of irradiated and non-irradiated cells entered the phase of reduced cell proliferation around a CPD of 49 that is quite near to the Hayflick limit of 50 cell population doublings (Hayflick, 1985). In the initial experiment (chapter 4.4.1), cells entered the phase of reduced cell proliferation around a CPD of 37 (Fig. 4-25). Additionally, in contrast to the first experiment, in progeny of irradiated cells cell doubling was decelerated later between day 15 and day 28 possibly due to irradiation induced damages (Fig. 4-27). At day 92 both irradiated and non-irradiated cells completed again the same population

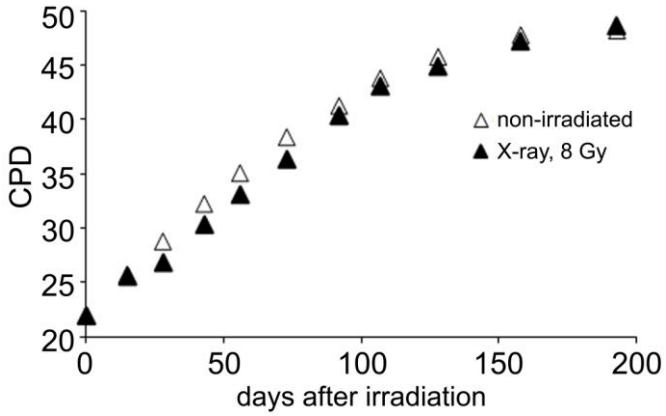

Fig. 4-37. Growth curve of normal human dermal fibroblasts (NHDF) exposed to X-rays (8 Gy, filled triangle) at day 0 and respective non-irradiated cells (open triangle). Repetition of the first experiment in Fig. 4-25. The number of cumulative population doublings (CPD) after X-ray exposure during this long-term experiment is plotted.

doublings. Thereafter, progeny of irradiated and non-irradiated cells showed similar proliferation frequency and entered the phase of reduced cell proliferation after 128 days.

The cellular amount of ATP in progeny of non-irradiated NHDF was quite constant at about 4 x 10^{-15} mol/cell, independent of the age (Fig. 4-38). The amount of ATP per cell according to present literature is 10^{-15} mol ATP or more (BioThema, ATP Biomass Kit HS). At day 15 and 28 after X-ray irradiation, the abundance of cellular ATP was strongly increased by a factor of about 2 compared to controls, followed by a sharp decrease between day 28 and day 43, reaching the level of non-irradiated cells and remained there until day 128. Thereafter, it declined continuously until day 193. At this time point, the cellular ATP level in progeny of X-ray irradiated cells was 1/3 of the level in the respective controls.

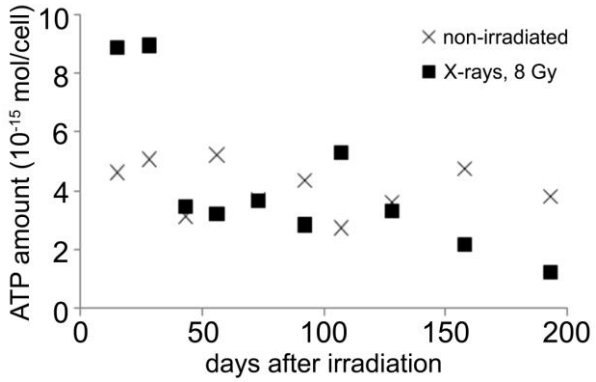

Fig. 4-38. Changes in the cellular ATP level in progeny of X-ray (8 Gy) irradiated and non-irradiated cells. The ATP amount was determined for 1600 cells. It is noteworthy to mention that cell shape and cell volume, respectively, show significant changes during ageing. The ATP level is normalized to the number of cells and not on their volume.

The senescence-associated decrease in ATP synthase abundance observed in the initial experiment (Fig. 4-32 A) in non-irradiated cells was possibly not accompanied by a simultaneous decline in ATP amount. There are two possible explanations: (1) the specific activity of ATP synthase increases during senescence or/and (2) senescent cells consume less ATP and the observed reduced amount of ATP synthase is sufficient to maintain the cellular energy status of a senescent cell.

In progeny of irradiated cells (X-rays and nitrogen ions), there was a pronounced transient increase of cellular ATP level at day 15 and day 28 (Fig. 4-38). At the protein level, no corresponding radiation-induced increase of the ATP synthase amount was observed in the initial experiment (Fig. 4-32 A), indicating that complex V can provide the higher ATP energy level required by increased specific activity. But the senescence-associated decline of ATP synthase in irradiated cells seems to be accompanied by a decrease in ATP amount. This may demonstrate a late-effect of X-ray radiation on the ATP synthase that is reflected by a loss of ability to further increase its specific activity.

To explain these data and their molecular interpretation in more detail, enzyme activity tests have to be performed to determine the specific activity of the ATP synthase and its dependence on X-ray exposure and age.

4.4.3 Comparison of alterations in the mitochondrial proteome of NHDF, WI38 and AG1522D fibroblasts during senescence and after irradiation with X-rays and carbon ions

The human body consists of different cell types like neuronal cells, lymphocytes or fibroblasts, only to name some of them. As introduced in chapter 1.1.3, each is characterized by its morphology and specific metabolic activity depending on its origin. Additionally, according to their origin (e.g. liver, lung or skin) and energy demand (oxygen consumption), they are exposed to different levels of oxygen. Oxidative damages, induced by increased amounts of ROS, are postulated to play an important role in ageing and senescence (Harman, 1956). Hence, it can be assumed, that ageing occurs distinct in different cell types, e.g. detectable by different age-associated alterations of the mitochondrial proteome. The cellular oxygen level was also found to influence the radiosensitivity. Cells in several solid tumors under hypoxic conditions are extremely resistant to irradiation therapy (Yotnda et al., 2010).

In the present study, confluent human foetal lung fibroblasts (WI38) and human dermal fibroblasts (AG1522D), the latter isolated from the foreskin of newborns (chapter 2.7.2, Table 2-1), were irradiated with X-rays (8 Gy) and AG1522D in a parallel experiment with carbon ions too (100 MeV/u, Unilac) and subcultured until cell proliferation slowed down due to entering phase III and/or senescence. Sample-analysis focused on two aims: (1) Age-related changes of the mitochondrial proteome, (2) interplay of irradiation- and age-dependent changes and (3) effect of different irradiation (X-ray and heavy ions). Data obtained for WI38 and AG1522D are compared to that of normal human dermal fibroblasts (NHDF) (chapter 4.4.1).

4.4.3.1 Changes in cell proliferation and the number of chromosomal aberrations of AG1522D and WI38 during cellular ageing and after X-ray/heavy ion irradiation

Non-irradiated WI38 cells entered phase III of cell growth at CPD46 and were senescent at day 52 (CPD47) showing no cell division any more (Fig. 4-39). Cellular ageing was accompanied by an increase of chromosomal aberrations (6-fold) at day 66 (unchanged thereafter until the end of the experiment, Fig. 4-40 A). The number of aberrations per diploid cell increased transiently at day 28 (Fig. 4-40 B) and that of tetraploid cells at day 66 and even more at day 107 (Fig. 4-40 C). After X-ray irradiation, at day 1 the number of WI38 cells exhibiting chromosomal aberrations as well as the number of aberrations per cell (2n and 4n) was increased to a large extent (Fig. 4-40) and the cell proliferation was slowed down dramatically (Fig. 4-39) until recovery at day 52 (similar level as non-irradiated cells). Progeny of irradiated cells entered senescence after less CPD (45) than non-irradiated but later at day 66. Thereafter, in line with non-irradiated cells, no or only minor cell proliferation was observed. While a constant increase of chromosomal aberrations was counted already at day 66 until day 107 that was larger than in progeny of non-irradiated cells, the number of aberrations per cell was unchanged until day 107,

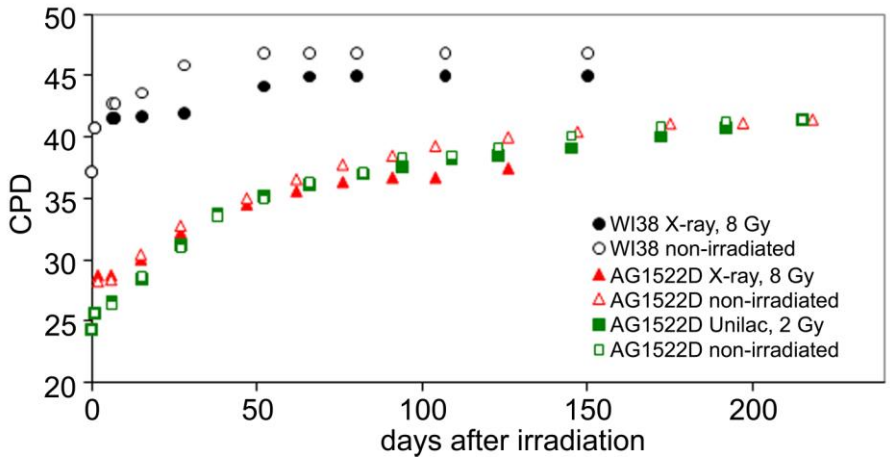

Fig. 4-39. Growth curve of WI38 (black) and AG1522D (green and red) exposed to X-rays (8 Gy) and carbon ions (2 Gy) at day 0 and respective non-irradiated cells (empty symbols). The number of cumulative population doublings (CPD) after X-ray exposure during this long-term experiment is plotted.

According to previous experiments at GSI, an application of a dose of 2 Gy with heavy ion (carbon) irradiation at the Unilac (GSI) is inducing an equivalent relative biological effect (RBE, see also chapter 1.2) as a dose of 8 Gy X-rays. Cell proliferation was unaffected of exposure to carbon ions in AG1522D cells (Fig. 4-39). Only at day 91, cell population

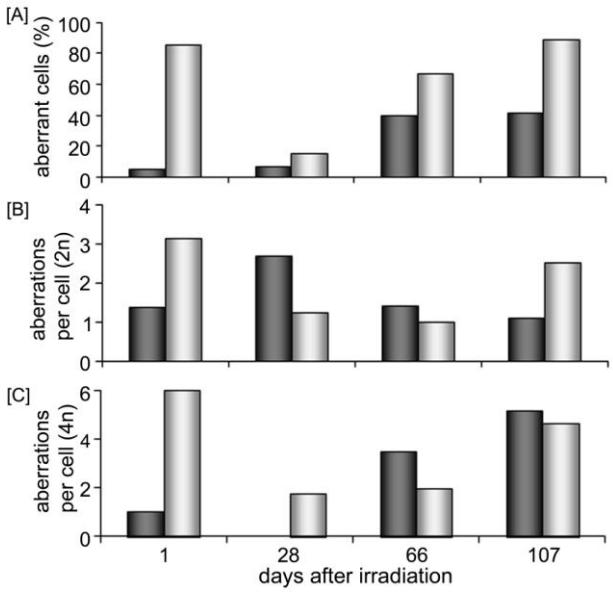

Fig. 4-40. [A] Proportion of aberrant cells (with normal chromosomal number, 2n) in percent, [B] number of aberrations per diploid cell (2n) and [C] tetraploid in progeny of non-irradiated (black) and irradiated (gray) WI38 cells. The number of aberrations was divided through the amount of aberrant cells.

doubling was slightly decelerated, but thereafter similar to non-irradiated cells. Also after X-ray irradiation, no immediate effect on cell proliferation was observed, but in contrast to heavy ions, a pronounced decrease in cell population doubling occurred, beginning at day 62

and at a CPD of 35.5. The subcultivation of AG1522D cells exposed to X-rays was stopped already at day 126 due to an experimental error. Cell doubling of progeny of non-irradiated and heavy ion irradiated cells also slightly decelerated at day 62/66.

In progeny of non-irradiated AG1522D cells, the amount of aberrant cells increased during cellular ageing from max. 20% (most times 4-8%) in young cells up to 80% when entering phase III of growth (Fig. 4-41 A1, B1). The number of aberrations increased only to a small extent (Fig. 4-41 A2, B2). The appearance of cells with twice the set of chromosomes differs in both experiments (Fig. 4-41 A3, B3). While in non-irradiated cells cultivated in parallel to the Unilac-experiment (Fig. 4-41 A3) tetraploid cells appear at day 82 with increased number of aberrations per cell during cellular ageing, in non-irradiated cells from the X-ray-experiment already at day 6 aberrant cells with twice the set of chromosomes (4n) were found whose number of aberrations increased until day 147 and decreased thereafter again until day 249.

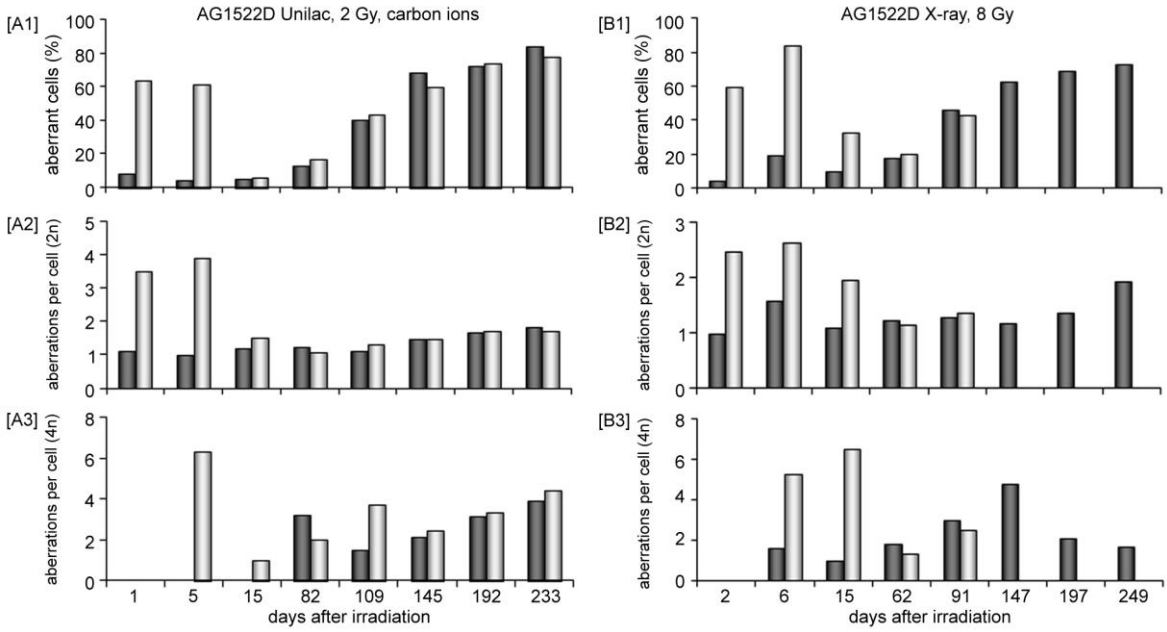

Fig. 4-41. [A1, B1] Proportion of aberrant cells (2n) in percent and number of aberrations per aberrant cell in diploid (2n, A2, B2) and tetraploid (4n, B3, B3) progeny of non-irradiated (black) and irradiated (gray) AG1522D cells.

The number of aberrant cells for AG1522D was increased after both carbon ion and X-rays irradiation, respectively (Fig. 4-41 A1, B1). After exposed to carbon ions maximal 60% of the cells had chromosomal aberrations at day 1 and 5. The amount of damaged cells was at the level of non-irradiated cells already at day 15. In contrast, X-ray irradiation resulted in up to 80% aberrant cells (at day 5) and still increased level at day 15 before reaching the level of non-irradiated cells. Thereafter, the number of aberrant cells was similar to that of non-irradiated until the end of the experiment. The amount of chromosomal damages after carbon ion irradiation was up to 4 per cell until day 1 and 5 (Fig. 4-41 A2). Thereafter it returned to the level of non-irradiated cells. Exposure to X-ray also led to an increase of aberrations per cell, but to a less extent (Fig. 4-41 B2) and still increased at day 15 before reaching normal

level. These observations were comparable to the amount of damages in tetraploid cells that were increased after heavy ion irradiation only at day 5 while after exposure to X-rays it was still high at day 15 (Fig. 4-41 A3, B3). In both experiments it returned to the level of non-irradiated cells thereafter and increased during cellular ageing with a small transient increase at day 109 in carbon ion irradiated cells.

4.4.3.2 Alterations in the mitochondrial proteome of AG1522D after X-ray and heavy ion irradiation

In progeny of non-irradiated cells (both controls for X-ray and carbon ion irradiation) an age-associated decrease in ATP synthase, complex I and complex III abundances occurred between day 117 and day 208 as well as day 90 and day 216, respectively (Fig. 4-42). Only in non-irradiated cells, representing the control for heavy ion radiation, the protein amount of the ATP synthase increased constantly until day 117 and of complex I and complex III_2 transiently at day 98 and day 117, respectively, before the overall decrease (Fig. 4-42 A).

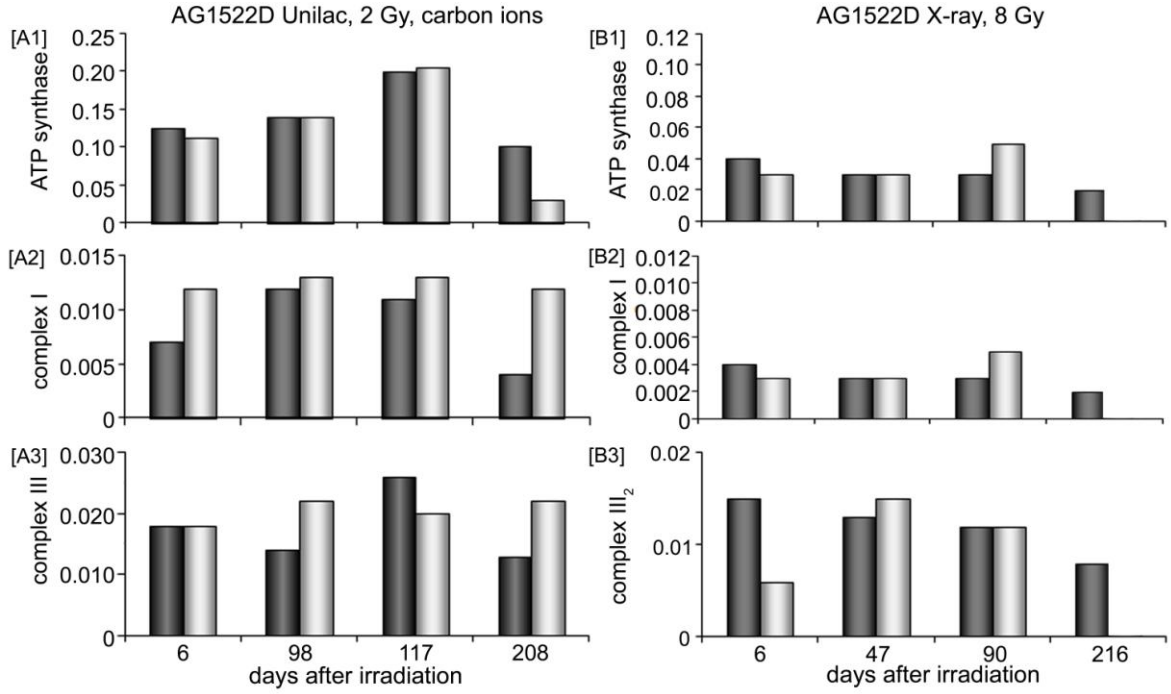

Fig. 4-42. Changes in the total amount of ATP synthase (sum of monomer and dimer) as well as of individual complexes I and III_2 in progeny of non-irradiated (dark) and irradiated (gray) AG1522D cells after exposure to heavy ions and X-rays. Quantitation occurred in the first dimension after CBB G-250 staining of proteins.

In progeny of X-ray irradiated cells, the protein abundance of ATP synthase and complex I was always at the level of non-irradiated cells until day 47 (Fig. 4-42 B). Thereafter it increased slightly at day 90.Complex III_2 was less present at day 6, increased up to the level in non-irradiated cells at day 47 and decreased again at day 90. In progeny of AG1522D cells exposed to heavy ions the ATP synthase amount increased in line with the level of non-

irradiated cells until day 117 but decreased to a larger extent at day 208. Complex I and complex III_2 showed only minor alterations in abundance and were more pronounced in aged cells at day 208.

The sum of supercomplexes ($I_1III_2IV_{0-X}$) changed in abundance in non-irradiated cells (in controls for both X-ray and heavy ion irradiation) comparable to that of individual complex III_2 in the respective experiments (Fig. 4-43). While the amount transiently decreased from day 98 in controls of carbon ion irradiated cells (Fig. 4-43 A) before the age-associated decrease from day 98 to day 208, in controls of X-ray irradiated cells (Fig. 4-43 B) the abundance remained constant after the pronounced decrease at day 47.

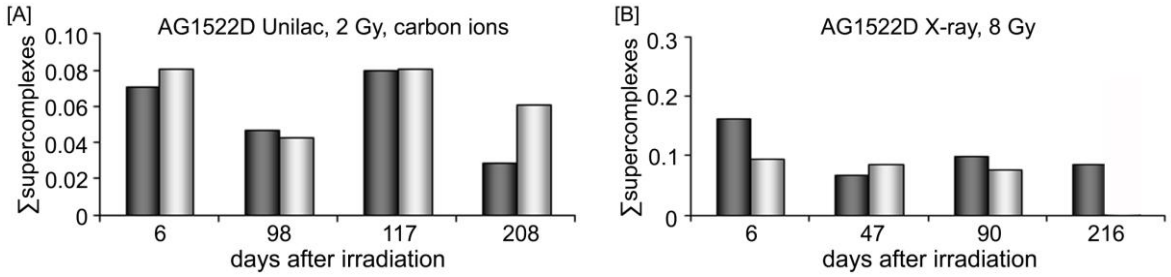

Fig. 4-43. Alterations in the abundance of supercomplexes (sum of $I_1III_2IV_{0-3}$) in progeny of non-irradiated (dark) and irradiated (gray) AG1522D cells after exposure to heavy ions and X-rays. Quantitation occurred in the first dimension after CBB G-250 staining of proteins.

The total amount of mitochondrial HSP60 (sum of both oligomeric forms) changed in abundance in irradiated AG1522D cells comparable to non-irradiated independent of X-ray and carbon ion irradiation (Fig. 4-44 A and Fig. 4-45 A). But an increase of HSP60 occurred in irradiated and non-irradiated cells in the carbon ion experiment at day 98 followed by an age-associated decline in protein abundance until day 208 (Fig. 4-44 A) while in the parallel X-ray experiment, the level of HSP60 was nearly unchanged during the whole time of cultivation in progeny of non-irradiated and irradiated cells (Fig. 4-45 A).

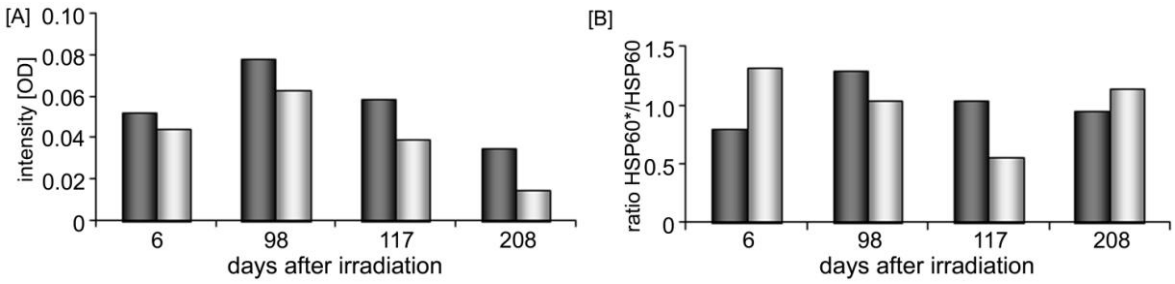

Fig. 4-44. (A) Total amount of heat shock protein 60 (sum of both oligomeric forms) after exposure to carbon ions and (B) the ratio of HSP60* to HSP60 in progeny of non-irradiated (black) and irradiated (gray, 2 Gy, carbon ions, Unilac) AG1522D cells. Quantitation occurred in the first dimension after CBB G-250 staining of proteins.

In line with HEK-(h)DAT cells (chapters 4.3.2) and NHDF (chapter 4.4.1.8) two oligomeric forms of the mitochondrial HSP60 were present also in AG1522D cells. In progeny of non-irradiated AG1522D cells, the ratio of the two oligomeric forms was shifted towards the smaller HSP60* form during cellular ageing but at different times. While in Fig. 4-44 B the proportion of HSP60* was already relatively increased at day 98 followed by a slightly decrease thereafter until day 208, in Fig. 4-45 B a small decrease occurred at day 47 compared to day 6 but increased later on constantly until day 216.

As observed already for NHDF, also in AG1522D cells a shift towards the smaller oligomeric form (HSP60*) was found after irradiation, that was decelerated at day 47 in X-ray exposed cells (Fig. 4-45 B) compared to day 6 for heavy ions (Fig. 4-44 B). In both experiments the proportion of the larger HSP60 increased thereafter again. After irradiation to heavy ions, a change of the ratio of HSP60* to HSP60 occurred again at day 208.

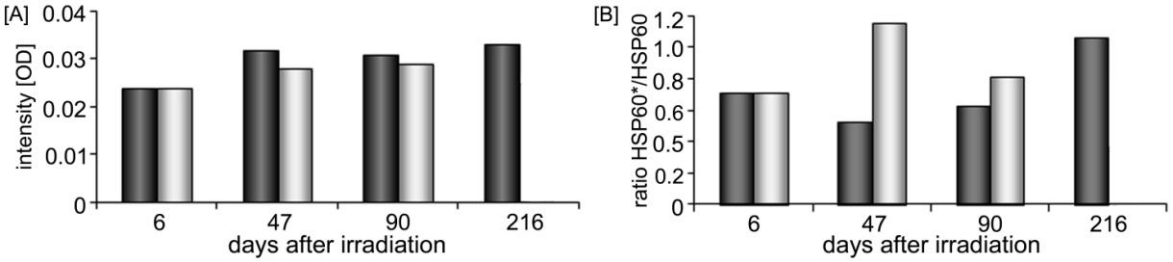

Fig. 4-45. (A) Total amount of heat shock protein 60 (sum of both oligomeric forms) after exposure to X-rays and (B) the ratio of HSP60* to HSP60 in progeny of non-irradiated (black) and irradiated (gray, 8 Gy, X-ray) AG1522D cells. Quantitation occurred in the first dimension after CBB G-250 staining of proteins.

4.4.3.3 Alterations in the mitochondrial proteome of WI38 after X-ray irradiation

From progeny of non-irradiated WI38 cells at day 66 not enough cells were present for the isolation of mitochondria since cells stopped proliferation. The abundance of the ATP synthase (Fig. 4-46 A) and complex I (Fig. 4-46 B) was unchanged until day 52 and day 35, respectively, and decreased thereafter until day 66. Individual complex III_2 decreased transiently at day 35 but returned to the level of day 15 at day 52 (Fig. 4-46 C). The abundance of respiratory chain supercomplexes ($I_1III_2IV_{0-3}$) even increased during cellular ageing at day 52 (Fig. 4-46 D). Irradiation to X-rays was accompanied by a pronounced increase of complex III_2 at day 15. While the protein abundance of ATP synthase, complex I and complex III_2 was declined at day 66 (complex I already at day 52) due to senescence, the amount of supercomplexes remained unchanged except the transient decline at day 35.

In non-irradiated cells, the mitochondrial HSP60 was slightly reduced in abundance between day 35 and day 52 in non-irradiated WI38 cells during cellular ageing but accompanied by a shift in the ratio of HSP60* to HSP60. This observation is contrary to NHDF and AG1522D (Fig. 4-47 A). In progeny of irradiated cells, the HSP60 abundance increased constantly until day 52 followed by a decrease until day 66. After exposure to X-rays the proportion of the

smaller HSP60* was enlarged in relation to HSP60 at day 35 but returned to the ratio of day 15 at day 52 and 66 (Fig. 4-47 B).

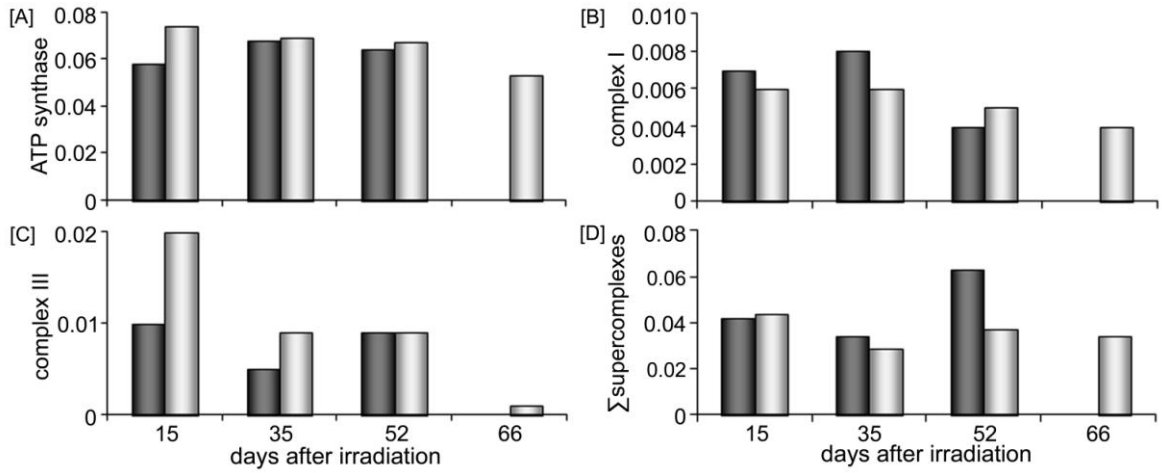

Fig. 4-46. Changes in the total amount of (A) ATP synthase (sum of monomer and dimer), (B) of individual complexes I and (C) III_2 as well as (D) sum of supercomplexes ($I_1III_2IV_{0-3}$) in progeny of non-irradiated (dark) and irradiated (gray) WI38 cells after exposure to X-rays. Quantitation occurred in the first dimension after CBB G-250 staining of proteins.

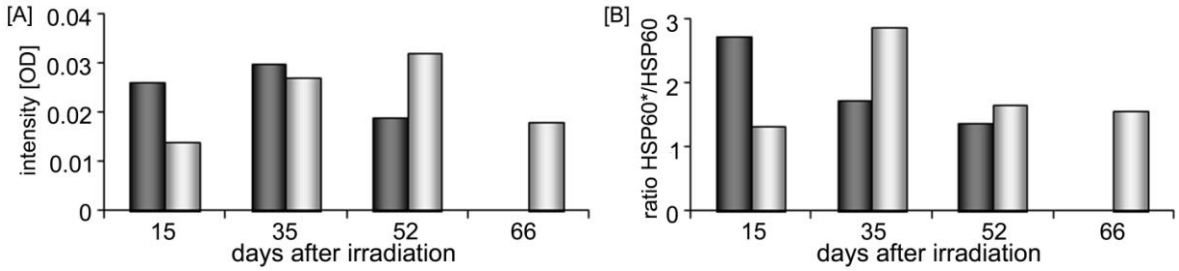

Fig. 4-47. (A) Total amount of heat shock protein 60 (sum of both oligomeric forms) and (B) the ratio of HSP60* to HSP60 in progeny of non-irradiated (black) and irradiated (gray, 8 Gy, X-ray) WI38 cells. Quantitation occurred in the first dimension after CBB G-250 staining of proteins.

4.4.3.4 *Short term and doses effect of irradiation with X-rays on the mitochondrial proteome of WI38*

To analyze the short-term effect and dose dependence of irradiation on the mitochondrial proteome, confluent (chapter 2.7.2) WI38 cells (CPD similar to that of long-term experiments) were exposed to X-rays (8 Gy or 16 Gy) and mitochondrial isolation was performed immediately after irradiation (approx. 2h later) and one week later. Medium changes were performed immediately after irradiation and 3 days after.

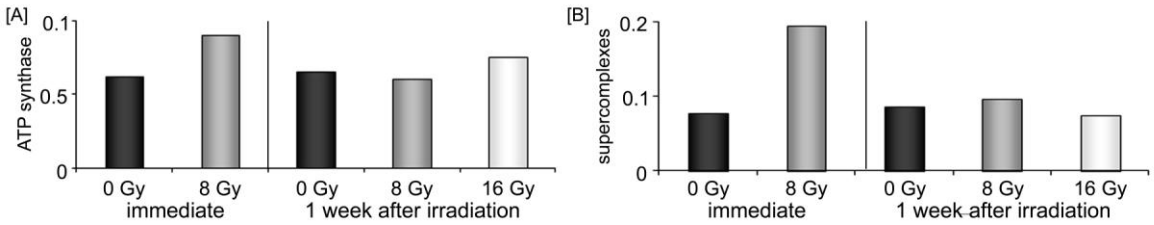

Fig. 4-48. Changes in the total amount of (A) ATP synthase (sum of monomer and dimer) and (B) of the sum of supercomplexes in progeny of non-irradiated (dark), and irradiated (8 Gy = gray, 16 Gy = white) WI38 cells immediate and one week after exposure to X-rays. Quantitation occurred in the first dimension after CBB G-250 staining of proteins.

The amount of ATP synthase was increased about 1.4-fold immediately after irradiation with a dose of 8 Gy but retired to the level of non-irradiated one week later (Fig. 4-48 A). The exposure to 16 Gy was followed by a slightly increased level of ATP synthase one week after irradiation. Also of respiratory chain supercomplexes larger abundances were found immediately after irradiation with 8 Gy (Fig. 4-48 B). One week later nearly the same protein level was present in irradiated and non-irradiated cells and there was no effect of the larger irradiation dose.

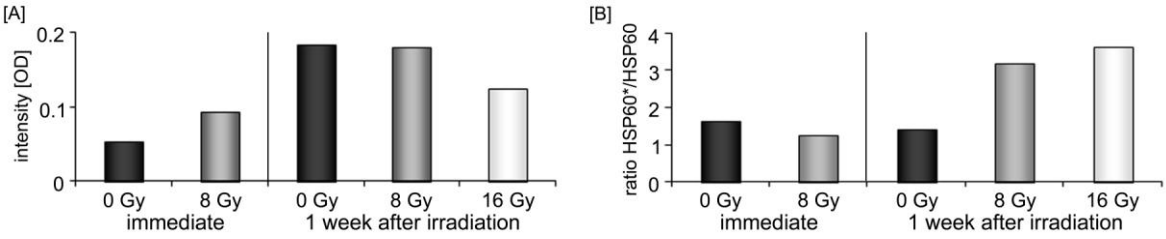

Fig. 4-49. Total amount of heat shock protein 60 (sum of both oligomeric forms) and (B) the ratio of HSP60* to HSP60 in progeny of non-irradiated (dark), and irradiated (8 Gy = gray, 16 Gy = white) WI38 cells immediate and one week after exposure to X-rays. Quantitation occurred in the first dimension after CBB G-250 staining of proteins.

Exposure to X-rays with a dose of 8 Gy was leading to an immediate 1.8-fold increase of mitochondrial HSP60 amount (Fig. 4-49 A). One week later, HSP60 abundances increased in all samples to a large extent. In cells irradiated with a dose of 16 Gy less HSP60 was present as compared to the ratio of 8 Gy and non-irradiated cells. The ratio of HSP60* to

HSP60 remained unchanged in non-irradiated cells immediately after irradiation and one week later. No immediate effect on the ratio of both HSP60 oligomeric occurred for the dose of 8 Gy. But one week later the proportion of HSP60* increased relatively to that of HSP60 to a large extent.

Summary

WI38 cells had already performed 37 cell population doublings at the beginning of the experiment. Compared to AG1522D (CPD 24) and NHDF (CPD 26) they were relatively progressed in age. The Hayflick limit of 50 cell population doublings was not reached for AG1522D cells in both experiments (Fig. 4-39). Cells entered phase III of cell growth characterized by reduced proliferation rate like NHDF cells as discussed in chapter 1354.4.1.1. Only WI38 cells entered senescence since no cell population doubling was detected like it is described for this state. Progeny of non-irradiated cells were already senescent at day 52, while progeny of irradiated cells entered senescence later at day 66. But also for these cells the Hayflick limit was not reached but with a CPD45 they were quite close, compared to NHDF and AG1522D. In line with NHDF, cellular ageing of AG1522D cells was accompanied by an increase of cells containing chromosomal damages accompanied by unchanged level of the number of aberrations per diploid cell (Fig. 4-41 A, B). Also the appearance of aberrant tetraploid AG1522D cells was comparable but contrary to NHDF, an age-associated increase of damages per cell was observed (Fig. 4-41 C). Same alterations occurred at the chromosomal level of WI38 cells except the fact that tetraploid cells were present already at day 1 (Fig. 4-40). These observations seem to be overall present in different cell lines independent of their origin. In both, NHDF and AG1522D, the number of aberrant cells with twice the set of chromosomes increased at a CPD of about 36. Only WI38 cells already passed nearly 47 cell population doublings before the age-associated increase of chromosomal damages. These cells seemed to be more protected against damages of the genome than the skin fibroblasts (AG1522D and NHDF).

Ionizing irradiation was increasing the amount of aberrant cells as well as the number of aberrations in diploid and tetraploid cells to the same extent independent from irradiation type (Fig. 4-41, Fig. 4-40, Fig. 4-27) in AG1522D, WI38 and NHDF. But in cells exposed to X-rays, chromosomal damages with maximal 2-3 aberrations per cell were detected until day 15, while at that time point after heavy ion irradiation the number of aberrant cells was already at the level of non-irradiated cells. Interestingly, the number of damages per cell was higher (3-4) in these cells (Fig. 4-41 A2, B2). Nevertheless, the recovery from irradiation was similar in both experiments. However, in contrast to cells irradiated with carbon ions showing growth behavior similar to non-irradiated cells, cell proliferation decelerated to a larger extent already at day 62 in progeny of cells exposed to X-rays (Fig. 4-39), although the number of aberrant cells and damages per cell (2n and 4n) comparable to that of high LET irradiation and non-irradiated cells. As described in chapter 1.2, for both densely and sparsely ionizing radiation the number of the most harmful double strand breaks is comparable (Heilmann et al., 1995), but successful double strand break repair is more likely after low LET than after

high LET exposure (Heilmann et al., 1996; Taucher-Scholz et al., 1996). The different distribution of ionizing events that is characteristic of each radiation type may have influenced the ability of the cell to repair chromosomal aberrations. If damages are unreparable, cells are undergoing apoptosis and are eliminated quickly, helping the rest of the cell culture to recover after irradiation. But if cells contain numerous DNA lesions not leading to cell death, the possibility that incorrect repair occurs is increased. Cell recovery may be prolonged and unrepaired damages may accumulate in cells over time leading to increased chromosomal instability and reduced lifespan or early senescence. This might explain, why progeny of X-ray irradiated cells entered the phase III of cell growth earlier than non-irradiated cells and those exposed to heavy ions.

The late effect of irradiation on chromosomes was visible for WI38 cells (Fig. 4-40). An increase of cells containing chromosomal aberrations occurred not only immediately after exposure to X-rays but also in senescent cells. The higher chromosomal instability may result from the fact that these cells passed already several cell population doublings when being irradiated. Another possibility is that lung cells (WI38) are more vulnerable to irradiation.

With minor exceptions, in all analyzed cell types (AG1522D, WI38 and NHDF) a senescence-associated decrease in the abundance of the ATP synthase, complex I, complex III_2, supercomplexes and mitochondrial HSP60 occurred in non-irradiated cells (Fig. 4-42, Fig. 4-43, Fig. 4-44, Fig. 4-45, Fig. 4-46, Fig. 4-47). The abundance decrease was sometimes different in extent and interrupted by a transient increase. Alterations in the mitochondrial proteome are therefore by trend similar to those in mitochondria of rat cortex and can be possibly correlated with the age-associated increase of the genomic instability (possibly of both mtDNA and nDNA).

In mitochondria of progeny of AG1522D cells irradiated with heavy ions, the same senescence-associated decline in protein abundance was also found (except complex III_2) and WI38 cells exposed to X-rays (except supercomplexes). Possibly all damaged cells of AG1522D were eliminated after heavy ion irradiation leading to a complete recovered cell culture with normal senescence-associated alterations in the mitochondrial proteome. After X-ray irradiation of AG1522D cells, most mitochondrial proteins analyzed were unchanged in the amount or even increased although cell proliferation declined. In conclusion, it seems that X-ray irradiation was leading to an earlier senescence although protein abundances of complex I, III_2, ATP synthase, respiratory chain supercomplexes as well as HSP60 were unchanged or even increased. This may be an indication for the presence of less active or possibly defect enzymes due to increased damages in the DNA. These aberrations may be less visible than the loss of a whole chromosome but manifested in the accumulation of small damages like simple base exchanges.

In all four analyzed cell lines (NHDF, HEK-(h)DAT, AG1522D and WI38) two oligomeric forms of mitochondrial HSP60 were found. It was demonstrated for NHDF cells that the senescence and irradiation induced shift towards the smaller form, HSP60*, can be

correlated with an increased level of apoptosis. Noteworthy, in AG1522D cells exposed to carbon ions the proportion of HSP60* was increased relatively to the large HSP60 form at day 6. In the same cell line after X-ray irradiation, this increase occurred decelerated at day 47 possibly since induction of apoptosis was also later since cells try to repair irradiation induced damages. Also in NHDF and WI38 the proportion of the smaller HSP60* form was still increased at day 14 and day 35 after exposure to X-rays, respectively.

Analysis of the immediate effect of X-ray exposure (~2h) on the mitochondrial proteome of WI38 cells showed that after irradiation with a dose of 8 Gy the abundance of the ATP synthase (1.4-fold), respiratory chain supercomplexes (2.5-fold) and HSP60 (1.8-fold) indicating a larger energy demand required. One week later the protein amount of the ATP synthase and of supercomplexes returned to the level of non-irradiated cells. A dose of 16 Gy, compared to non-irradiated cells and cells exposed to 8 Gy, resulted in only slightly increased level of the ATP synthase one week after irradiation and did not affect the level of supercomplexes. The amount of the mitochondrial HSP60 was dependent on the time cells remained in one culture flask without subcultivation or simply on the fact how long cells are confluent as assumed already in the present study in chapter 4.3.2 for HEK-(h)DAT cells. Also in WI38 cells the total HSP60 abundance (sum of both oligomeric forms) was increase after one week in non-irradiated cells and cells exposed to X-rays (both doses). Noteworthy, a dose of 16 Gy resulted in a slightly reduced increased. Noteworthy, while immediately after irradiation with X-rays no change in the ratio of HSP60* and HSP60 occurred, a pronounced shift towards the smaller HSP60* was present one week later in irradiated but not in non-irradiated cells. In conclusion, the amount of proteins involved in energy supply (ATP synthase and supercomplexes) was immediately increased after irradiation to provide the higher energy level required for damage repair. One week later, the major chromosomal damages are repaired. Cells that were unable to recover undergo apoptosis. In NHDF cells, the apoptotic level was still increased 17 days after exposure to X-rays (Fig. 4-28). Hence the increased level of HSP60* is indicating an increase of apoptotic cells in both 8 Gy and 16 Gy irradiated cells.

4.5 Characterization of functional molecular dynamics in cells under different ageing states using neutron scattering

To unravel, if alterations in cellular molecular dynamics can serve as biomarkers for apoptosis, the dynamical behavior of baby hamster kidney cells (BHK21) without and after induction of apoptosis was compared. The apoptosis represent an extreme morphologically different cellular state compared to healthy cells since the whole cell is destroyed in this process. These preliminary neutron scattering experiments, using extreme states, should reveal if differences in dynamical behavior can be detected and correlated with biological function or state of a cell.

Neutron scattering experiments were performed at the Institut Laue-Langevin (ILL) with the help of Thomas Hauss (Helmholtz-Zentrum Berlin für Materialien und Energie GmbH), Judith Peters (ILL), Andreas Stadler (ILL), Joseph Zaccai (ILL) and Marion Jasnin (ILL). I was mainly responsible for cell culturing, transport and sample preparation. Data evaluation and interpretation was made by Thomas Hauss (Helmholtz-Zentrum Berlin für Materialien und Energie GmbH) and Judith Peters (ILL).

In line with experiments performed previously on intact bacteria (Jasnin et al., 2008; Tehei et al., 2004), elastic temperature scans were performed for six temperatures between 5°C and 40°C. The temperature dependence of the atomic mean square displacement and a mean resilience value (Zaccai, 2000) was evaluated for cytoplasmic macromolecules in untreated and apoptotic cells. To induce apoptosis, confluent cells were treated 24 hours before exposure to neutrons with the peptide H-RCYVVM-OH (0.5 mM) and camptothecine (5 µM). As described in chapter 2.7.3, the peptide is an activator of the CD47 complex [Cluster of Differentiation 47 (Brown and Frazier, 2001)] while camptothecine prevents DNA re-ligation and therefore causes DNA damage by binding to the topoisomerase type I/DNA complex leading to DNA damage and apoptosis (Redinbo et al., 1998).

4.5.1 Comparison of healthy and apoptotic cells

For the first (15.-18.06.2009) experiment, cells were harvested and pelleted via centrifugation one or two days before the experiment at the Technische Universität Darmstadt (Germany) and stored at 4°C until final sample preparation. The cell survival after the transport to the ILL in Grenoble was controlled via replating the non-treated sample (Fig. 4-50). Non-treated and apoptotic cells were measured on the neutron spectrometer IN13 (ILL, Grenoble, France) performing temperature scans from 280 to 313 K in steps of 6 K. The data collection time varied from 3 to 5 hours and was increased with increasing temperature.

The method of inelastic neutron spectroscopy gives an average view on structural fluctuations. The values of mean square displacements $\langle u^2 \rangle$, describing the motion of ^1H atoms (Sears, 1992). The results depict in Fig. 4-50 gives a hint that the motions are slightly reduced in apoptotic cells compared to healthy.

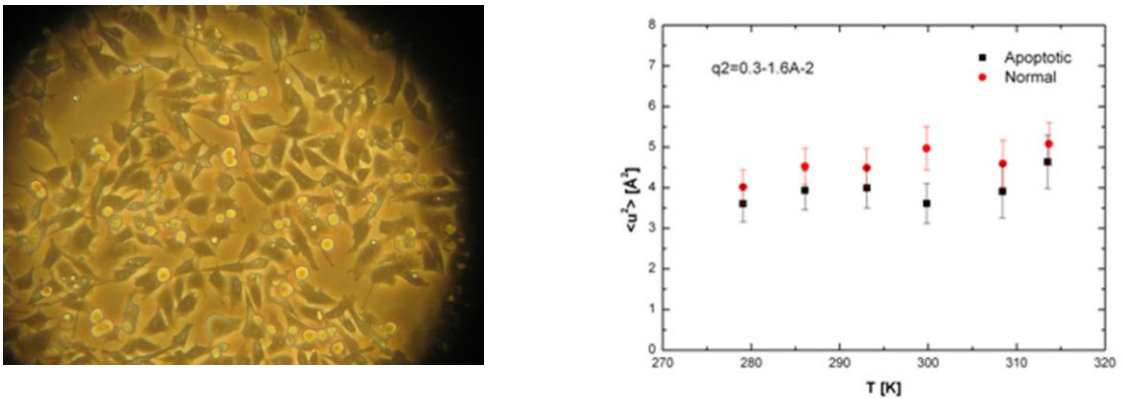

Fig. 4-50. Morphology of replated, non-treated cells before the experiment, after the transport in form of a cell sediment (left side, photo was made through the ocular of the microscope). The mean square displacements ($<u^2>$) extracted from the scattering data in the Q range 0.5 – 1.3 $Å^{-1}$ are plotted as a function of temperature (right side).

After the experiment, healthy cells were replated to check the survival, but no living cell was observed. The conditions during the measurement are extreme for living cells: tightly closed from air, without nutrition and packed as a dense cell paste. Further off-line tests showed that the cells were able to survive about 6 hours under such extreme conditions.

The experiment was repeated in September 2009 (26.08.-6.09.2009) by changing every 6 hours the samples to assure their survival. Cells were transported in cell culture flasks one week before the experiment to France and were harvested immediately before exposure to

Table 4-4. Cell survival of samples after each measurement. The respective amount [µg] of cells (after centrifugation at 800 g) is indicated.

SAMPLE	Measurement parameters	Cell amount used in the experiment	survival
Sample 1: control	4x 1h at 304K	600 µg	Cells survived the treatment, spreading and cell doubling after 21hs was observed
Sample 2: control	4x 1h at 280K/288K/296K	600 µg	Cells survived the treatment, spreading and cell doubling after 27hs was observed
Sample 3: Control	4x 1h at 315K	600 µg	No survival
Sample 4: Apoptosis	4x 1h at 304K	500 µg	Few single cells survived, no cell doubling, only spreading of some few cells
Sample 5: Control	4x 1h at 288K/296K/304K	600 µg	Few single cells survived, no cell doubling, only spreading of some few cells
Sample 6: Control	4x 1h at 304K repetition	600 µg	Few cells survived, no cell doubling, only spreading of some cells
Sample 7: Control	4x 1h at 300K	600 µg	After 14h most cells spread again and begin to proliferate
Sample 8: dead cells	4x 1h at 296K/304K/315K	700 µg	Cells died on purpose before starting the experiment
Sample 9: Control	4x 1h at 310K	600 µg	Cells survived the treatment, spreading and cell doubling after 21hs was observed
Sample 10: Apoptosis	4x 1h at 280K/288K/ 296K/304K/315K	600 µg	No cell survival

neutrons. The sample preparation was similar to the first experiment. Again apoptotic cells (apoptosis induced similar to the first experiment) were compared to healthy cells. Measurements were performed again temperatures of 280 to 315 K, but exchanging the samples every 6 hours for temperatures higher than 296 K. The data collection time varied from 4 to 5 hours per temperature point. Replating of the non-treated cells demonstrated that they survived at a high rate the experiment (Table 4-4). The fluctuation amplitudes were slightly reduced in apoptotic cells (Fig. 4-51). However, the absolute height of the MSD strongly depends on the sample preparation and even the two control samples do not give the same results for the MSD. The straight lines are so far simply a guidance for the eye, but they are related to the effective elastic force constants (proportional to the inverse of the slope of the MSD versus temperature dependence) (Zaccai, 2000). It seems that the effective force constants are very similar for the two control samples and softer than for the apoptotic and dead cells, which seems to be stiffer. The effect is rather surprising and should be confirmed in further experiments.

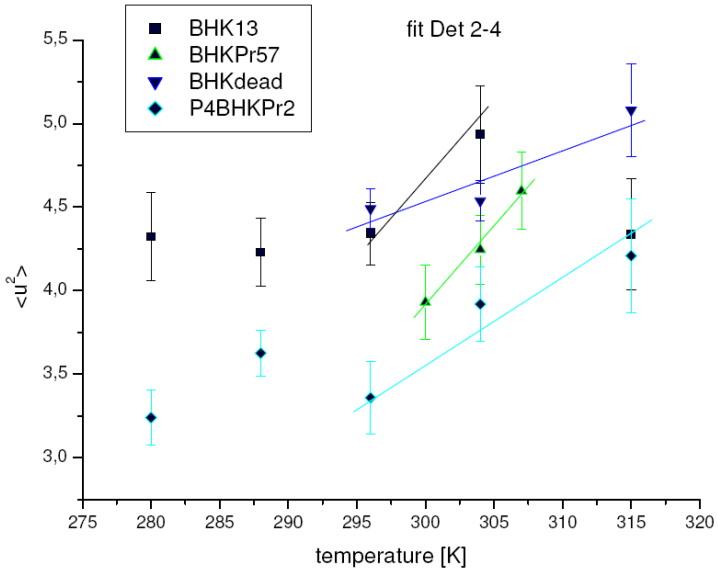

Fig. 4-51. The mean square displacements (<u^2>) extracted from the scattering data in the *Q* range 0.5 – 1.3 Å^{-1} are plotted as a function of temperature. MSD extracted for control (BHK13 = samples 1-3 and BHKPr57 = samples 5-7), apoptotic (P4BHKPr2 = sample 4 and 10) and dead cells (sample 8). The straight lines are guidance to the eye.

4.5.2 Summary

In the first experiment the motions seemed to be slightly reduced in apoptotic cells. This may be explained by the fact that when cells enter apoptosis the cell morphology and inner structure is changing. The cell cytoskeleton, a highly complex and highly structured construction, is destroyed. As consequence, cells are losing their shape and membranes form bulges outwards (Vermeulen et al., 2005). Cells begin to shrink in size and the nuclear as well as the DNA are fragmented.

Although from the second experiment opposite results were obtained and the background signal is pronounced, it seems that extreme physiological different states as healthy and dead or apoptotic cells can be distinguished in these neutron scattering experiments. The method has to be improved and many factors have to be changed or modulated. But thereafter neutron scattering experiments may be useful to analyze the physiological state of a cell population. A sample holder should be developed allowing measurements at physiological culture conditions (presence of medium, nutrition, oxygen, etc.). High temperatures (>40°C) will always remain a critical parameter for cell cultures.

5 List of abbreviations

1D	one dimensional
2D	two dimensional
9-me-BC	9-methyl-beta carboline
ACO2	mitochondrial aconitase 2
AP	alkaline phosphatase
APS	ammonium persulfate
ATP	adenosine triphosphate
BCIP	5-bromo-4-chloro-3-indolyl phosphate
BHM	bovine heart mitochondria
Bis-Tris	2-[Bis(2-hydroxyethyl)amino]-2-(hydroxymethyl)-1,3-propanediol
BN	Blue-native
BSA	bovine serum albumin
CBB	Coomassie Brilliant Blue
CoQ	coenzyme Q
CPD	cumulative population doubling
CR	caloric restriction
Cyt c	cytochrome c
Da	dalton
DAB	3,3'-Diaminobenzidine
DCDHF	2‘-7‘-Dichlorodihydrofluorescein diacetate
ΔpH	proton gradient
ΔΨ	membrane potential
Δ*p*	proton motive force
D_2O	heavy water
Dest. water	distilled water
DHE	dihydroethidium
DMF	N,N-dimethylformamide
DMSO	dimethylsulfoxid
DNA	deoxyribonucleic acid
DNP	2,4-dinitrophenylhydrazone
DNPH	2,4-dinitrophenylhydrazine
DTT	1,4-dithiotreitol
eV	electronvolt
$FADH_2$	flavin adenine dinucleotide
FCS	fetal bovine serum
GABA	gamma-aminobutyric acid
GSI	Gesellschaft für Schwerionenforschung
GU	Gray-units
Gy	gray
H_2O_2	hydrogen peroxide
HEK	baby hamster kidney cells
HEPES	4-(2-hydroxyethyl)-1-piperazineethanesulfonic acid
HMW	high molecular weight
HSP	heat shock protein
IgG	immunoglobulin G
ILL	Institut Laue-Langevin
J	joule
LET	Linear Energy Transfer
LMW	Low molecular weight
mA	Milliampere
MALDI	(Matrix Assisted Laser Desorption Ionization
MilliQ-Wasser	purified and deionized water to a high degree (typically 18.2 MΩ·cm), particle free up to 0,22 µm
M_R	molecular masse
MS	mass spectrometry
mt	mitochondrial
NAD	nicotinamide adenine dinucleotide
nDNA	nuclear DNA
NHDF	normal human dermal fibroblasts
O1/2	aged rats 1 and 2, 30 months, cortex mitochondria
OD	optical density

OxPhos	Oxidative Phosphorylation
PA	polyacrylamide gel
PAGE	polyacrylamide gel electrophoresis
PBS	phosphate buffered saline
PD	Parkinson's disease
PIC	protease-inhibitor-cocktail
PS	phosphatidylserine
PVDF	polyvinylidenfluorid
ROS	reactive oxygen species
rRNA	ribosomal ribonucleic acid
tRNA	transfer ribonucleic acid
RBE	relative biological effectiveness
RT	room temperature
ROS	reactive oxygen species
SDS	Sodium dodecyl sulfate
SOD	superoxide dismutase
SPF	specific pathogen-free
TBARS	ThioBarbituric acid reactive substances
TCA	trichloroacetic acid
TOF	Time-of-flight
Tricin	*N*-[2-Hydroxy-1,1-bis(hydroxymethyl)ethyl]glycine
Tris	Tris(hydroxymethyl)-aminomethan
TEMED	tetramethylethylenediamine
$<u^2>$	mean square displacement
(v/v)	volume per volume unit
V	voltage
(w/v)	weight per volume
Y1/2	young rats 5-months (cortex mitochondria)

6 References

Organisation Intergouvernementale de la convention du Mètre, 2006. The International system of Units (SI), Bureau International des Poids et Mesures, 8th edition ed.

Alberts, B., Johnson, A., Lewis, J., Raff, M., Roberts, K., Walter, P., 1994. Molecular Biology of the Cell. New York: Garland Publishing Inc.

Altman, J., Das, G.D., 1965. Autoradiographic and histological evidence of postnatal hippocampal neurogenesis in rats. J Comp Neurol 124, 319-335.

Anderson, R.E., Lefkovits, I., 1979. In vitro evaluation of radiation-induced augmentation of the immune response. Am J Pathol 97, 456-472.

Anderton, B.H., 2002. Ageing of the brain. Mech Ageing Dev 123, 811-817.

Andreyev, A.Y., Kushnareva, Y.E., Starkov, A.A., 2005. Mitochondrial metabolism of reactive oxygen species. Biochemistry (Mosc) 70, 200-214.

Angermuller, S., Fahimi, H.D., 1981. Selective cytochemical localization of peroxidase, cytochrome oxidase and catalase in rat liver with 3,3'-diaminobenzidine. Histochemistry 71, 33-44.

Aquilano, K., Vigilanza, P., Rotilio, G., Ciriolo, M.R., 2006. Mitochondrial damage due to SOD1 deficiency in SH-SY5Y neuroblastoma cells: a rationale for the redundancy of SOD1. FASEB J 20, 1683-1685.

Arivazhagan, P., Panneerselvam, C., 2004. Alpha-lipoic acid increases Na^+K^+ATPase activity and reduces lipofuscin accumulation in discrete brain regions of aged rats. Ann N Y Acad Sci 1019, 350-354.

Arya, R., Mallik, M., Lakhotia, S.C., 2007. Heat shock genes - integrating cell survival and death. J Biosci 32, 595-610.

Ashmore, L.J., Hrizo, S.L., Paul, S.M., Van Voorhies, W.A., Beitel, G.J., Palladino, M.J., 2009. Novel mutations affecting the Na, K ATPase alpha model complex neurological diseases and implicate the sodium pump in increased longevity. Hum Genet 126, 431-447.

Attwell, D., Laughlin, S.B., 2001. An energy budget for signaling in the grey matter of the brain. J Cereb Blood Flow Metab 21, 1133-1145.

Azevedo, F.A., Carvalho, L.R., Grinberg, L.T., Farfel, J.M., Ferretti, R.E., Leite, R.E., Jacob Filho, W., Lent, R., Herculano-Houzel, S., 2009. Equal numbers of neuronal and nonneuronal cells make the human brain an isometrically scaled-up primate brain. J Comp Neurol 513, 532-541.

Bayreuther, K., Rodemann, H.P., Hommel, R., Dittmann, K., Albiez, M., Francz, P.I., 1988. Human skin fibroblasts in vitro differentiate along a terminal cell lineage. Proc Natl Acad Sci U S A 85, 5112-5116.

Beal, M.F., Hyman, B.T., Koroshetz, W., 1993. Do defects in mitochondrial energy metabolism underlie the pathology of neurodegenerative diseases? Trends Neurosci 16, 125-131.

Beinert, H., Kennedy, M.C., 1993. Aconitase, a two-faced protein: enzyme and iron regulatory factor. FASEB J 7, 1442-1449.

Belanoff, J.K., Gross, K., Yager, A., Schatzberg, A.F., 2001. Corticosteroids and cognition. J Psychiatr Res 35, 127-145.

Bereiter-Hahn, J., Voth, M., 1994. Dynamics of mitochondria in living cells: shape changes, dislocations, fusion, and fission of mitochondria. Microsc Res Tech 27, 198-219.

Berry, E.A., Trumpower, B.L., 1985. Isolation of ubiquinol oxidase from Paracoccus denitrificans and resolution into cytochrome bc1 and cytochrome c-aa3 complexes. J Biol Chem 260, 2458-2467.

Beyer, C., 2007. Einfluss von Oxidantien, Antioxidantien und Reinigungsparametern auf Atmungskettenkomplexe der Rattenleber, Fachbereich Chemie. Technische Universität Darmstadt, Darmstadt.

Billard, J.M., 2006. Ageing, hippocampal synaptic activity and magnesium. Magnes Res 19, 199-215.

Bindokas, V.P., Jordan, J., Lee, C.C., Miller, R.J., 1996. Superoxide production in rat hippocampal neurons: selective imaging with hydroethidine. J Neurosci 16, 1324-1336.

Blakely, E.A., Kronenberg, A., 1998. Heavy-ion radiobiology: new approaches to delineate mechanisms underlying enhanced biological effectiveness. Radiat Res 150, S126-145.

Blanco, G., Mercer, R.W., 1998. Isozymes of the Na-K-ATPase: heterogeneity in structure, diversity in function. Am J Physiol 275, F633-650.

Blander, G., de Oliveira, R.M., Conboy, C.M., Haigis, M., Guarente, L., 2003. Superoxide dismutase 1 knock-down induces senescence in human fibroblasts. J Biol Chem 278, 38966-38969.

Blum, H., Beier, H., Gross, H.J., 1987. Improved silver staining of plant proteins, RNA and DNA in polyacrylamide gels. Electrophoresis 8, 93-99.

Bornhövd, C., Vogel, F., Neupert, W., Reichert, A.S., 2006. Mitochondrial membrane potential is dependent on the oligomeric state of F_1F_0-ATP synthase supracomplexes. J Biol Chem 281, 13990-13998.

Borras, C., Gil, P., Vina, J., 2010. Biogerontology in Spain: the most significant studies. Biogerontology 12, 77-81.

Bossi, O., Gartsbein, M., Leitges, M., Kuroki, T., Grossman, S., Tennenbaum, T., 2008. UV irradiation increases ROS production via PKCdelta signaling in primary murine fibroblasts. J Cell Biochem 105, 194-207.

Boveris, A., Oshino, N., Chance, B., 1972. The cellular production of hydrogen peroxide. Biochem J 128, 617-630.

Bradford, M.M., 1976. A rapid and sensitive method for the quantitation of microgram quantities of protein utilizing the principle of protein-dye binding. Anal Biochem 72, 248-254.

Bradley, T.J., Satir, P., 1981. 5-hydroxytryptamine-stimulated mitochondrial movement and microvillar growth in the lower malpighian tubule of the insect, Rhodnius prolixus. J Cell Sci 49, 139-161.

Brewer, G.J., Jones, T.T., Wallimann, T., Schlattner, U., 2004. Higher respiratory rates and improved creatine stimulation in brain mitochondria isolated with anti-oxidants. Mitochondrion 4, 49-57.

Brown, E.J., Frazier, W.A., 2001. Integrin-associated protein (CD47) and its ligands. Trends Cell Biol 11, 130-135.

Brys, K., Castelein, N., Matthijssens, F., Vanfleteren, J.R., Braeckman, B., 2010. Disruption of insulin signaling preserves bioenergetic competence of mitochondria in aging *Caenorhabditis elegans*. BMC Biol. 8:91.

Budd, S.L., Nicholls, D.G., 1998. Mitochondria in the life and death of neurons. Essays Biochem 33, 43-52.

Burger, C., 2010. Region-specific genetic alterations in the aging hippocampus: implications for cognitive aging. Front Aging Neurosci 2, 140.

Burnette, W.N., 1981. "Western blotting": electrophoretic transfer of proteins from sodium dodecyl sulfate--polyacrylamide gels to unmodified nitrocellulose and radiographic detection with antibody and radioiodinated protein A. Anal Biochem 112, 195-203.

Butte, A.J., Dzau, V.J., Glueck, S.B., 2001. Further defining housekeeping, or "maintenance," genes Focus on "A compendium of gene expression in normal human tissues". Physiol Genomics 7, 95-96.

Butterfield, D.A., Poon, H.F., St Clair, D., Keller, J.N., Pierce, W.M., Klein, J.B., Markesbery, W.R., 2006. Redox proteomics identification of oxidatively modified hippocampal proteins in mild cognitive impairment: insights into the development of Alzheimer's disease. Neurobiol Dis 22, 223-232.

Cai, T., Wang, H., Chen, Y., Liu, L., Gunning, W.T., Quintas, L.E., Xie, Z.J., 2008. Regulation of caveolin-1 membrane trafficking by the Na/K-ATPase. J Cell Biol 182, 1153-1169.

Cameron, H.A., Woolley, C.S., McEwen, B.S., Gould, E., 1993. Differentiation of newly born neurons and glia in the dentate gyrus of the adult rat. Neuroscience 56, 337-344.

Carney, J.M., Starke-Reed, P.E., Oliver, C.N., Landum, R.W., Cheng, M.S., Wu, J.F., Floyd, R.A., 1991. Reversal of age-related increase in brain protein oxidation, decrease in enzyme activity, and loss in temporal and spatial memory by chronic administration of the spin-trapping compound N-tert-butyl-alpha-phenylnitrone. Proc Natl Acad Sci U S A 88, 3633-3636.

Carreau, A., El Hafny-Rahbi, B., Matejuk, A., Grillon, C., Kieda, C., 2011. Why is the partial oxygen pressure of human tissues a crucial parameter?: Small molecules and hypoxia. J Cell Mol Med.

Cereijido, M., Contreras, R.G., Shoshani, L., Flores-Benitez, D., Larre, I., 2008. Tight junction and polarity interaction in the transporting epithelial phenotype. Biochim Biophys Acta 1778, 770-793.

Ceriani, R.L., Peterson, J.A., Blank, E.W., Chan, C.M., Cailleau, R., 1992. Development and characterization of breast carcinoma cell lines as in vitro and in vivo models for breast cancer diagnosis and therapy. In Vitro Cell Dev Biol 28A, 397-402.

Cerqueira, J.J., Mailliet, F., Almeida, O.F., Jay, T.M., Sousa, N., 2007. The prefrontal cortex as a key target of the maladaptive response to stress. J Neurosci 27, 2781-2787.

Chen, X.J., Butow, R.A., 2005. The organization and inheritance of the mitochondrial genome. Nat Rev Genet 6, 815-825.

Cheng, M.Y., Hartl, F.U., Horwich, A.L., 1990. The mitochondrial chaperonin hsp60 is required for its own assembly. Nature 348, 455-458.

Chew, B.P., Park, J.S., 2004. Carotenoid action on the immune response. J Nutr 134, 257S-261S.

Choi, D.W., 1996. Ischemia-induced neuronal apoptosis. Curr Opin Neurobiol 6, 667-672.

Chung, L., Ng, Y.C., 2006. Age-related alterations in expression of apoptosis regulatory proteins and heat shock proteins in rat skeletal muscle. Biochim Biophys Acta 1762, 103-109.

Colindres, M., Fournier, C., Ritter, S., Zahnreich, S., Decker, H., Dencher N., Frenzel M., 2008. Increase of oxidative stress in normal human fibroblasts after irradiation. GSI Scientific Report 2007, 356.

Colotti, C., Cavallini, G., Vitale, R.L., Donati, A., Maltinti, M., Del Ry, S., Bergamini, E., Giannessi, D., 2005. Effects of aging and anti-aging caloric restrictions on carbonyl and heat shock protein levels and expression. Biogerontology 6, 397-406.

Dani, D., Dencher, N.A., 2008. Native-DIGE: a new look at the mitochondrial membrane proteome. Biotechnol J 3, 817-822.

Dani, D., Shimokawa, I., Komatsu, T., Higami, Y., Warnken, U., Schokraie, E., Schnölzer, M., Krause, F., Sugawa, M.D., Dencher, N.A., 2009. Modulation of oxidative phosphorylation machinery signifies a prime mode of anti-ageing mechanism of calorie restriction in male rat liver mitochondria. Biogerontology, DOI 10.1007/s10522-10009-19254-y.

Daum, G., 1985. Lipids of mitochondria. Biochim Biophys Acta 822, 1-42.

Davis, B.J., 1964. Disc Electrophoresis. Ii. Method and Application to Human Serum Proteins. Ann N Y Acad Sci 121, 404-427.

Dencher, N.A., Frenzel, M., Reifschneider, N.H., Sugawa, M., Krause, F., 2007. Proteome alterations in rat mitochondria caused by aging. Ann N Y Acad Sci 1100, 291-298.

Di Felice, V., Ardizzone, N., Marciano, V., Bartolotta, T., Cappello, F., Farina, F., Zummo, G., 2005. Senescence-associated HSP60 expression in normal human skin fibroblasts. Anat Rec A Discov Mol Cell Evol Biol 284, 446-453.

DiMauro, S., 2004. Mitochondrial diseases. Biochim Biophys Acta 1658, 80-88.

Doster, W., Cusack, S., Petry, W., 1989. Dynamical transition of myoglobin revealed by inelastic neutron scattering. Nature 337, 754-756.

Driscoll, I., Sutherland, R.J., 2005. The aging hippocampus: navigating between rat and human experiments. Rev Neurosci 16, 87-121.

Dykens, J.A., 1994. Isolated cerebral and cerebellar mitochondria produce free radicals when exposed to elevated CA2+ and Na+: implications for neurodegeneration. J Neurochem 63, 584-591.

Eisenberg, E., Levanon, E.Y., 2003. Human housekeeping genes are compact. Trends Genet 19, 362-365.

Ekstrom, R., Liu, D.S., Richardson, A., 1980. Changes in brain protein synthesis during the life span of male Fischer rats. Gerontology 26, 121-128.

Erecinska, M., Dagani, F., 1990. Relationships between the neuronal sodium/potassium pump and energy metabolism. Effects of K+, Na+, and adenosine triphosphate in isolated brain synaptosomes. J Gen Physiol 95, 591-616.

Esteban, M.A., Maxwell, P.H., 2005. Manipulation of oxygen tensions for in vitro cell culture using a hypoxic workstation. Expert Rev Proteomics 2, 307-314.

Fazekas de St Groth, S., Webster, R.G., Datyner, A., 1963. Two new staining procedures for quantitative estimation of proteins on electrophoretic strips. Biochim Biophys Acta 71, 377-391.

Ferre, S., Lluis, C., Justinova, Z., Quiroz, C., Orru, M., Navarro, G., Canela, E.I., Franco, R., Goldberg, S.R., 2010. Adenosine-cannabinoid receptor interactions. Implications for striatal function. Br J Pharmacol 160, 443-453.

Ffrench-Constant, C., Mathews, G.A., 1994. Brain repair: lessons from developmental biology. J Neurol 242, S29-32.

Fornai, F., Schluter, O.M., Lenzi, P., Gesi, M., Ruffoli, R., Ferrucci, M., Lazzeri, G., Busceti, C.L., Pontarelli, F., Battaglia, G., Pellegrini, A., Nicoletti, F., Ruggieri, S., Paparelli, A., Sudhof, T.C., 2005. Parkinson-like syndrome induced by continuous MPTP infusion: convergent roles of the ubiquitin-proteasome system and alpha-synuclein. Proc Natl Acad Sci U S A 102, 3413-3418.

Fournier, C., Kraft-Weyrather, W., Kraft, G., 1998. Survival, differentiation and collagen secretion of human fibroblasts after irradiation with carbon ions and X-rays. Phys Med 14 Suppl 1, 44-47.

Fournier, C., Winter, M., Zahnreich, S., Nasonova, E., Melnikova, L., Ritter, S., 2007. Interrelation amongst differentiation, senescence and genetic instability in long-term cultures of fibroblasts exposed to different radiation qualities. Radiother Oncol 83, 277-282.

Frenzel, M., 2006. Altersabhängige Untersuchung des Proteoms von *Rattus norvegicus*, Fachbereich Chemie. Technische Universität Darmstadt, Darmstadt.

Frenzel, M., Durante, M., Fournier, C., Ritter, S., Dencher, N.A., 2010a. Interplay of irradiation and age on the mitoproteome of human cell cultures. GSI Scientific Report 2009, 497.

Frenzel, M., Rommelspacher, H., Sugawa, M.D., Dencher, N.A., 2010b. Ageing alters the supramolecular architecture of OxPhos complexes in rat brain cortex. Exp Gerontol 45, 563-572.

Galvan, V., Jin, K., 2007. Neurogenesis in the aging brain. Clin Interv Aging 2, 605-610.

Gavin, P.D., Prescott, M., Luff, S.E., Devenish, R.J., 2004. Cross-linking ATP synthase complexes in vivo eliminates mitochondrial cristae. J Cell Sci 117, 2333-2343.

Gems, D., Partridge, L., 2008. Stress-response hormesis and aging: "that which does not kill us makes us stronger". Cell Metab 7, 200-203.

Gilkerson, R.W., Selker, J.M., Capaldi, R.A., 2003. The cristal membrane of mitochondria is the principal site of oxidative phosphorylation. FEBS Lett 546, 355-358.

Giraud, M.F., Paumard, P., Soubannier, V., Vaillier, J., Arselin, G., Salin, B., Schaeffer, J., Brethes, D., di Rago, J.P., Velours, J., 2002. Is there a relationship between the supramolecular organization of the mitochondrial ATP synthase and the formation of cristae? Biochim Biophys Acta 1555, 174-180.

Gómez, L.A., Monette, J.S., Chavez, J.D., Maier, C.S., Hagen, T.M., 2009. Supercomplexes of the mitochondrial electron transport chain decline in the aging rat heart. Arch Biochem Biophys 490, 30-35.

Gorg, A., Postel, W., Westermeier, R., 1978. Ultrathin-layer isoelectric focusing in polyacrylamide gels on cellophane. Anal Biochem 89, 60-70.

Grandier-Vazeille, X., Guerin, M., 1996. Separation by blue native and colorless native polyacrylamide gel electrophoresis of the oxidative phosphorylation complexes of yeast mitochondria solubilized by different detergents: specific staining of the different complexes. Anal Biochem 242, 248-254.

Gredilla, R., Garm, C., Holm, R., Bohr, V.A., Stevnsner, T., 2008. Differential age-related changes in mitochondrial DNA repair activities in mouse brain regions. Neurobiol Aging.

Greenberg, D.A., Jin, K., 2006. Neurodegeneration and neurogenesis: focus on Alzheimer's disease. Curr Alzheimer Res 3, 25-28.

Grillner, S., Wallen, P., 2002. Cellular bases of a vertebrate locomotor system-steering, intersegmental and segmental co-ordination and sensory control. Brain Res Brain Res Rev 40, 92-106.

Groebe, K., Krause, F., Kunstmann, B., Unterluggauer, H., Reifschneider, N.H., Scheckhuber, C.Q., Sastri, C., Stegmann, W., Wozny, W., Schwall, G.P., Poznanovic, S., Dencher, N.A., Jansen-Dürr, P., Osiewacz, H.D., Schrattenholz, A., 2007. Differential proteomic profiling of mitochondria from *Podospora anserina*, rat and human reveals distinct patterns of age-related oxidative changes. Exp Gerontol 42, 887-898.

Guillon, G., Roy, C., Jard, S., 1978. A systematic study of effects of non-ionic detergens on solubilization and activity of pig kidney adenylate cyclase. Eur J Biochem 92, 341-348.

Gunter, T.E., Buntinas, L., Sparagna, G., Eliseev, R., Gunter, K., 2000. Mitochondrial calcium transport: mechanisms and functions. Cell Calcium 28, 285-296.

Haak, J.L., Buettner, G.R., Spitz, D.R., Kregel, K.C., 2009. Aging augments mitochondrial susceptibility to heat stress. Am J Physiol Regul Integr Comp Physiol 296, R812-820.

Hackenbrock, C.R., Chazotte, B., Gupte, S.S., 1986. The random collision model and a critical assessment of diffusion and collision in mitochondrial electron transport. J Bioenerg Biomembr 18, 331-368.

Hakim, J., 1993. Reactive oxygen species and inflammation. C.R. Seances Soc Biol Fil 187, 286-295.

Halliwell, B., Gutteridge, J.M.C., 2007. Free radicals in biology and medicine. Oxford Forth edition.

Haripriya, D., Devi, M.A., Kokilavani, V., Sangeetha, P., Panneerselvam, C., 2004. Age-dependent alterations in mitochondrial enzymes in cortex, striatum and hippocampus of rat brain -- potential role of L-Carnitine. Biogerontology 5, 355-364.

Harman, D., 1956. Aging: a theory based on free radical and radiation chemistry. J Gerontol 11, 298-300.

Harman, D., 1972. The biologic clock: the mitochondria? J Am Geriatr Soc 20, 145-147.

Harper, M.E., Monemdjou, S., Ramsey, J.J., Weindruch, R., 1998. Age-related increase in mitochondrial proton leak and decrease in ATP turnover reactions in mouse hepatocytes. Am J Physiol 275, E197-206.

Harvey, W.R., 1992. Physiology of V-ATPases. J Exp Biol 172, 1-17.

Hayflick, L., Moorhead, P.S., 1961. The serial cultivation of human diploid cell strains. Exp Cell Res 25, 585-621.

Hayflick, L., 1985. The cell biology of aging. Clin Geriatr Med 1, 15-27.

Hayflick, L., 1994. Trypsin in poliovaccine manufacture. Lancet 343, 611.

Haynes, V., Traaseth, N.J., Elfering, S., Fujisawa, Y., Giulivi, C., 2010. Nitration of specific tyrosines in FoF1 ATP synthase and activity loss in aging. Am J Physiol Endocrinol Metab 298, E978-987.

Hecker, H., Burri, P.H., Bohringer, S., 1973. Quantitative ultrastructural differences in the mitochondrium of pleomorphic bloodforms oF Trypanosoma brucei. Experientia 29, 901-903.

Heilmann, J., Taucher-Scholz, G., Kraft, G., 1995. Induction of DNA double-strand breaks in CHO-K1 cells by carbon ions. Int J Radiat Biol 68, 153-162.

Heilmann, J., Taucher-Scholz, G., Haberer, T., Scholz, M., Kraft, G., 1996. Measurement of intracellular dna double-strand break induction and rejoining along the track of carbon and neon particle beams in water. Int J Radiat Oncol Biol Phys 34, 599-608.

Henneberry, R.C., 1997. Excitotoxicity as a consequence of impairment of energy metabolism: the energy-linked excitotoxic hypothesis. In: Mitochondria and free radicals in neurodegenerative disease, in: Beal, M.F., Howell, N., Bodis-Wollner, I. (Eds.), 111–143, New York: Wiley-Liss.

Hoch, F.L., 1992. Cardiolipins and biomembrane function. Biochim Biophys Acta 1113, 71-133.

Hunzinger, C., Wozny, W., Schwall, G.P., Poznanovic, S., Stegmann, W., Zengerling, H., Schoepf, R., Groebe, K., Cahill, M.A., Osiewacz, H.D., Jagemann, N., Bloch, M., Dencher, N.A., Krause, F., Schrattenholz, A., 2006. Comparative profiling of the mammalian mitochondrial proteome: multiple aconitase-2 isoforms including N-formylkynurenine modifications as part of a protein biomarker signature for reactive oxidative species. J Proteome Res 5, 625-633.

Hutter, E., Skovbro, M., Lener, B., Prats, C., Rabol, R., Dela, F., Jansen-Durr, P., 2007. Oxidative stress and mitochondrial impairment can be separated from lipofuscin accumulation in aged human skeletal muscle. Aging Cell 6, 245-256.

Ina, Y., Sakai, K., 2004. Prolongation of life span associated with immunological modification by chronic low-dose-rate irradiation in MRL-lpr/lpr mice. Radiat Res 161, 168-173.

Ivanina, A.V., Sokolova, I.M., Sukhotin, A.A., 2008. Oxidative stress and expression of chaperones in aging mollusks. Comp Biochem Physiol B Biochem Mol Biol 150, 53-61.

Jacobs, H.T., 2003. The mitochondrial theory of aging: dead or alive? Aging Cell 2, 11-17.

Jasnin, M., Tehei, M., Moulin, M., Haertlein, M., Zaccai, G., 2008. Solvent isotope effect on macromolecular dynamics in E. coli. Eur Biophys J 37, 613-617.

John, G.B., Shang, Y., Li, L., Renken, C., Mannella, C.A., Selker, J.M., Rangell, L., Bennett, M.J., Zha, J., 2005. The mitochondrial inner membrane protein mitofilin controls cristae morphology. Mol Biol Cell 16, 1543-1554.

Kandel, E.R., Schwartz, J.H., M.Jessell, T., 2000. Principles of Neural Science Fourth Edition, in: McGraw-Hill., U.S.o.A. (Ed.), p. 324. .

Karthikeyan, G., Resnick, M.A., 2005. Impact of mitochondria on nuclear genome stability. DNA Repair (Amst) 4, 141-148.

Kaur, J., Sharma, D., Singh, R., 2001. Acetyl-L-carnitine enhances Na(+), K(+)-ATPase glutathione-S-transferase and multiple unit activity and reduces lipid peroxidation and lipofuscin concentration in aged rat brain regions. Neurosci Lett 301, 1-4.

Keeney, P.M., Xie, J., Capaldi, R.A., Bennett, J.P., Jr., 2006. Parkinson's disease brain mitochondrial complex I has oxidatively damaged subunits and is functionally impaired and misassembled. J Neurosci 26, 5256-5264.

Kim, G.J., Fiskum, G.M., Morgan, W.F., 2006. A role for mitochondrial dysfunction in perpetuating radiation-induced genomic instability. Cancer Res 66, 10377-10383.

Kloppel, C., Michels, C., Zimmer, J., Herrmann, J.M., Riemer, J., In yeast redistribution of Sod1 to the mitochondrial intermembrane space provides protection against respiration derived oxidative stress. Biochem Biophys Res Commun 403, 114-119.

Knab, B., 2009. Optimierung der ATP-Bestimmung in Zellen mittels Lumineszenz, Fachbereich Chemie. Technische Universität Darmstadt, Darmstadt.

Kraft, G., 1987. Radiobiological Effects of Very Heavy Ions: Inactivation, Induction of Chromosome Aberrations and Strand Breaks. Nucl. Sci. Appl. 3, 1-28.

Krajcovicova-Kudlackova, M., Valachovicova, M., Paukova, V., Dusinska, M., 2008. Effects of diet and age on oxidative damage products in healthy subjects. Physiol Res 57, 647-651.

Krause, F., 2004. Biochemische Charakterisierung der supramolekularen Organisation der mitochondrialen OXPHOS-Komplexe von Säugern, Pilzen und Pflanzen, Fachbereich Chemie. Technische Universität Darmstadt, Darmstadt.

Krause, F., Reifschneider, N.H., Vocke, D., Seelert, H., Rexroth, S., Dencher, N.A., 2004a. "Respirasome"-like supercomplexes in green leaf mitochondria of spinach. J Biol Chem 279, 48369-48375.

Krause, F., Scheckhuber, C.Q., Werner, A., Rexroth, S., Reifschneider, N.H., Dencher, N.A., Osiewacz, H.D., 2004b. Supramolecular organization of cytochrome c oxidase- and alternative oxidase-dependent respiratory chains in the filamentous fungus *Podospora anserina*. J Biol Chem 279, 26453-26461.

Krause, F., Reifschneider, N.H., Goto, S., Dencher, N.A., 2005. Active oligomeric ATP synthases in mammalian mitochondria. Biochem Biophys Res Commun 329, 583-590.

Krause, F., Seelert, H., 2008. Detection and analysis of protein-protein interactions of organellar and prokaryotic proteomes by blue native and colorless native gel electrophoresis. Curr Protoc Protein Sci Chapter 19, Unit 19 18.

Krause, F., Oxidative phosphorylation supercomplexes in various eukaryotes: A paradigm change gains critical momentum, in: Siso, M.I.G. (Ed.), 2007. Transworld Resarch Network, Kerala, India, pp. 179–213.

Krieger, H. (Ed.), 2007. Grundlagen der Strahlenphysik und des Strahlenschutzes. BG Teubner Verlag.

Kuhn, H.G., Dickinson-Anson, H., Gage, F.H., 1996. Neurogenesis in the dentate gyrus of the adult rat: age-related decrease of neuronal progenitor proliferation. J Neurosci 16, 2027-2033.

Kuonen, D.R., Roberts, P.J., Cottingham, I.R., 1986. Purification and analysis of mitochondrial membrane proteins on nondenaturing gradient polyacrylamide gels. Anal Biochem 153, 221-226.

Kuroiwa, T., 1982. Mitochondrial nuclei. Int Rev Cytol 75, 1-59.

Kwong, L.K., Sohal, R.S., 2000. Age-related changes in activities of mitochondrial electron transport complexes in various tissues of the mouse. Arch Biochem Biophys 373, 16-22.

Laemmli, U.K., 1970. Cleavage of structural proteins during the assembly of the head of bacteriophage T4. Nature 227, 680-685.

Langer, A.K., Poon, H.F., Munch, G., Lynn, B.C., Arendt, T., Butterfield, D.A., 2006. Identification of AGE-modified proteins in SH-SY5Y and OLN-93 cells. Neurotox Res 9, 255-268.

Laranjinha, J., Ledo, A., 2007. Coordination of physiologic and toxic pathways in hippocampus by nitric oxide and mitochondria. Front Biosci 12, 1094-1106.

Lavenex, P., Banta Lavenex, P., Amaral, D.G., 2007. Postnatal development of the primate hippocampal formation. Dev Neurosci 29, 179-192.

Lazarov, O., Mattson, M.P., Peterson, D.A., Pimplikar, S.W., van Praag, H., 2010. When neurogenesis encounters aging and disease. Trends Neurosci 33, 569-579.

Le Bourg, E., Rattan, S.I.S. (Eds.), 2008. Mild Stress and Healthy Aging: Applying hormesis in aging research and interventions. Springer.

Le Pécheur, M., Morrow, G., Kim, H.-J., Schäfer, E., Dencher, N., Tanguay, R.M., 2009. Characterization of OXPHOS complexes in long-lived flies overexpressing Hsp22. Mitochondria in ageing and age-related disease, MiMage final meeting (and LINK-AGE Topic Research) Group Meeting, abstract 16, p. 35.

Lee, C.F., Liu, C.Y., Hsieh, R.H., Wei, Y.H., 2005. Oxidative stress-induced depolymerization of microtubules and alteration of mitochondrial mass in human cells. Ann N Y Acad Sci 1042, 246-254.

Lee, Y.H., Govinda, B., Kim, J.C., Kim, T.I., Lee, N.H., Lee, J.C., Yi, H.K., Jhee, E.C., 2009. Oxidative stress resistance through blocking Hsp60 translocation followed by SAPK/JNK inhibition in aged human diploid fibroblasts. Cell Biochem Funct 27, 35-39.

Lee, Y.J., Ducoff, H.S., 1989. Radiation factors and their influence on induction of oxygen resistance. Radiat Res 117, 158-162.

Li, N., Ragheb, K., Lawler, G., Sturgis, J., Rajwa, B., Melendez, J.A., Robinson, J.P., 2003. Mitochondrial complex I inhibitor rotenone induces apoptosis through enhancing mitochondrial reactive oxygen species production. J Biol Chem 278, 8516-8525.

Li, Q., Vande Velde, C., Israelson, A., Xie, J., Bailey, A.O., Dong, M.Q., Chun, S.J., Roy, T., Winer, L., Yates, J.R., Capaldi, R.A., Cleveland, D.W., Miller, T.M., ALS-linked mutant superoxide dismutase 1 (SOD1) alters mitochondrial protein composition and decreases protein import. Proc Natl Acad Sci U S A 107, 21146-21151.

Limoli, C.L., Giedzinski, E., Morgan, W.F., Swarts, S.G., Jones, G.D., Hyun, W., 2003. Persistent oxidative stress in chromosomally unstable cells. Cancer Res 63, 3107-3111.

Liu, S.Z., Liu, W.H., Sun, J.B., 1987. Radiation hormesis: its expression in the immune system. Health Phys 52, 579-583.

Liu, S.Z., 1989. Radiation hormesis. A new concept in radiological science. Chin Med J (Engl) 102, 750-755.

Lombardi, A., Silvestri, E., Cioffi, F., Senese, R., Lanni, A., Goglia, F., de Lange, P., Moreno, M., 2009. Defining the transcriptomic and proteomic profiles of rat ageing skeletal muscle by the use of a cDNA array, 2D- and Blue native-PAGE approach. J Proteomics 72, 708-721.

Lorenz, E., Hollcroft, J.W., Miller, E., Congdon, C.C., Schweisthal, R., 1955. Long-term effects of acute and chronic irradiation in mice. I. Survival and tumor incidence following chronic irradiation of 0.11 r per day. J Natl Cancer Inst 15, 1049-1058.

Lottspeich, F., Engels, J.W., 2006. Bioanalytik. Spektrum Akademischer Verlag 2. Auflage.

Luckey, T.D., 1982. Physiological benefits from low levels of ionizing radiation. Health Phys 43, 771-789.

Lundin, A., Hasenson, M., Persson, J., Pousette, A., 1986. Estimation of biomass in growing cell lines by adenosine triphosphate assay. Methods Enzymol 133, 27-42.

Mattson, M.P., 1998. Modification of ion homeostasis by lipid peroxidation: roles in neuronal degeneration and adaptive plasticity. Trends Neurosci 21, 53-57.

McBride, H.M., Neuspiel, M., Wasiak, S., 2006. Mitochondria: more than just a powerhouse. Curr Biol 16, R551-560.

McIntyre, J.S., Craik, F.I., 1987. Age differences in memory for item and source information. Can J Psychol 41, 175-192.

Mehnati, P., Keshtkar, A., Mesbahi, A., Sasaki, H., 2006. Track detection on the cells exposed to high LET heavy-ions by CR-39 plastic and terminal deoxynucleotidyl transferase (TdT). Iranian Journal of Radiation Research 4, 137-141.

Meissner, C., Bruse, P., Oehmichen, M., 2006. Tissue-specific deletion patterns of the mitochondrial genome with advancing age. Exp Gerontol 41, 518-524.

Menzies, R.A., Gold, P.H., 1971. The turnover of mitochondria in a variety of tissues of young adult and aged rats. J Biol Chem 246, 2425-2429.

Merkwirth, C., Langer, T., 2009. Prohibitin function within mitochondria: essential roles for cell proliferation and cristae morphogenesis. Biochim Biophys Acta 1793, 27-32.

Miller, D.B., O'Callaghan, J.P., 2003. Effects of aging and stress on hippocampal structure and function. Metabolism 52, 17-21.

Miller, D.B., O'Callaghan, J.P., 2005. Aging, stress and the hippocampus. Ageing Res Rev 4, 123-140.

Minauro-Sanmiguel, F., Wilkens, S., Garcia, J.J., 2005. Structure of dimeric mitochondrial ATP synthase: novel F_0 bridging features and the structural basis of mitochondrial cristae biogenesis. Proc Natl Acad Sci U S A 102, 12356-12358.

Miwa, H., Kubo, T., Morita, S., Nakanishi, I., Kondo, T., 2004. Oxidative stress and microglial activation in substantia nigra following striatal MPP+. Neuroreport 15, 1039-1044.

Mizutani, T., Nakashima, S., Nozawa, Y., 1998. Changes in the expression of protein kinase C (PKC), phospholipases C (PLC) and D (PLD) isoforms in spleen, brain and kidney of the aged rat: RT-PCR and Western blot analysis. Mech Ageing Dev 105, 151-172.

Morgenstern, N.A., Lombardi, G., Schinder, A.F., 2008. Newborn granule cells in the ageing dentate gyrus. J Physiol 586, 3751-3757.

Moriyama, Y., Nelson, N., 1989a. H+-translocating ATPase in Golgi apparatus. Characterization as vacuolar H+-ATPase and its subunit structures. J Biol Chem 264, 18445-18450.

Moriyama, Y., Nelson, N., 1989b. Lysosomal H+-translocating ATPase has a similar subunit structure to chromaffin granule H+-ATPase complex. Biochim Biophys Acta 980, 241-247.

Moriyama, Y., Futai, M., 1990. H(+)-ATPase, a primary pump for accumulation of neurotransmitters, is a major constituent of brain synaptic vesicles. Biochem Biophys Res Commun 173, 443-448.

Moriyama, Y., Maeda, M., Futai, M., 1992. The role of V-ATPase in neuronal and endocrine systems. J Exp Biol 172, 171-178.

Mrak, R.E., Griffin, S.T., Graham, D.I., 1997. Aging-associated changes in human brain. J Neuropathol Exp Neurol 56, 1269-1275.

Munro, T.R., 1970. The relative radiosensitivity of the nucleus and cytoplasm of Chinese hamster fibroblasts. Radiat Res 42, 451-470.

Murphy, D.G., DeCarli, C., McIntosh, A.R., Daly, E., Mentis, M.J., Pietrini, P., Szczepanik, J., Schapiro, M.B., Grady, C.L., Horwitz, B., Rapoport, S.I., 1996. Sex differences in human brain morphometry and metabolism: an in vivo quantitative magnetic resonance imaging and positron emission tomography study on the effect of aging. Arch Gen Psychiatry 53, 585-594.

Navarro, A., Bandez, M.J., Lopez-Cepero, J.M., Gomez, C., Boveris, A.D., Cadenas, E., Boveris, A.A., High Doses of Vitamin E Improve Mitochondrial Dysfunction in Rat Hippocampus and Frontal Cortex Upon Aging. Am J Physiol Regul Integr Comp Physiol.

Neff, D., Dencher, N.A., 1999. Purification of multisubunit membrane protein complexes: isolation of chloroplast F_oF_1-ATP synthase, CF_o and CF_1 by blue native electrophoresis. Biochem Biophys Res Commun 259, 569-575.

Nicholls, D.G., Ferguson, S., 1992. Biogenetics. 2. Academic Press, London.

Nicholls, D.G., 2003. Bioenergetics and transmitter release in the isolated nerve terminal. Neurochem Res 28, 1433-1441.

Nicholson, D.A., Yoshida, R., Berry, R.W., Gallagher, M., Geinisman, Y., 2004. Reduction in size of perforated postsynaptic densities in hippocampal axospinous synapses and age-related spatial learning impairments. J Neurosci 24, 7648-7653.

Nicklas, W.J., Vyas, I., Heikkila, R.E., 1985. Inhibition of NADH-linked oxidation in brain mitochondria by 1-methyl-4-phenyl-pyridine, a metabolite of the neurotoxin, 1-methyl-4-phenyl-1,2,5,6-tetrahydropyridine. Life Sci 36, 2503-2508.

Nijtmans, L.G., de Jong, L., Artal Sanz, M., Coates, P.J., Berden, J.A., Back, J.W., Muijsers, A.O., van der Spek, H., Grivell, L.A., 2000. Prohibitins act as a membrane-bound chaperone for the stabilization of mitochondrial proteins. EMBO J 19, 2444-2451.

Nugent, S., Mothersill, C.E., Seymour, C., McClean, B., Lyng, F.M., Murphy, J.E., 2010. Altered mitochondrial function and genome frequency post exposure to γ-radiation and bystander factors. Int J Radiat Biol 86, 829-841.

Oliver, C.N., Ahn, B.W., Moerman, E.J., Goldstein, S., Stadtman, E.R., 1987. Age-related changes in oxidized proteins. J Biol Chem 262, 5488-5491.

Ornstein, L., 1964. Disc Electrophoresis. I. Background and Theory. Ann N Y Acad Sci 121, 321-349.

Owusu-Ansah, E., Yavari, A., Banerjee, U., 2008. A protocol for in vivo detection of reactive oxygen species Protocol Exchange doi:10.1038/nprot.2008.23.

Ozawa, T., 1997. Genetic and functional changes in mitochondria associated with aging. Physiol Rev 77, 425-464.

Pan, Y., Shadel, G.S., 2009. Extension of chronological life span by reduced TOR signaling requires down-regulation of Sch9p and involves increased mitochondrial OXPHOS complex density. Aging (Albany NY) 1, 131-145.

Parkes, T.L., Elia, A.J., Dickinson, D., Hilliker, A.J., Phillips, J.P., Boulianne, G.L., 1998. Extension of Drosophila lifespan by overexpression of human SOD1 in motorneurons. Nat Genet 19, 171-174.

Paumard, P., Vaillier, J., Coulary, B., Schaeffer, J., Soubannier, V., Mueller, D.M., Brethes, D., di Rago, J.P., Velours, J., 2002. The ATP synthase is involved in generating mitochondrial cristae morphology. EMBO J 21, 221-230.

Paxinos, G., Watson, C., 1998. The rat brain - in stereotaxic coordinates, Fourth edition ed. Academic Press.

Peters, A., 2007. Chapter 5: The Effects of Normal Aging on Nerve Fibers and Neuroglia in the Central Nervous System, in: Riddle, D. (Ed.), Brain Aging: Models, Methods, and Mechanisms, Bookshelf ID: NBK3873 PMID: 21204349.

Petin, V.G., Morozov, II, Kabakova, N.M., Gorshkova, T.A., 2003. [Some effects of radiation hormesis for bacterial and yeast cells]. Radiats Biol Radioecol 43, 176-178.

Petit-Paitel, A., Brau, F., Cazareth, J., Chabry, J., 2009. Involvment of cytosolic and mitochondrial GSK-3beta in mitochondrial dysfunction and neuronal cell death of MPTP/MPP-treated neurons. PLoS One 4, e5491.

Poon, H.F., Calabrese, V., Calvani, M., Butterfield, D.A., 2006a. Proteomics analyses of specific protein oxidation and protein expression in aged rat brain and its modulation by L-acetylcarnitine: insights into the mechanisms of action of this proposed therapeutic agent for CNS disorders associated with oxidative stress. Antioxid Redox Signal 8, 381-394.

Poon, H.F., Shepherd, H.M., Reed, T.T., Calabrese, V., Stella, A.M., Pennisi, G., Cai, J., Pierce, W.M., Klein, J.B., Butterfield, D.A., 2006b. Proteomics analysis provides insight into caloric restriction mediated oxidation and expression of brain proteins associated with age-related impaired cellular processes: Mitochondrial dysfunction, glutamate dysregulation and impaired protein synthesis. Neurobiol Aging 27, 1020-1034.

Poon, H.F., Vaishnav, R.A., Getchell, T.V., Getchell, M.L., Butterfield, D.A., 2006c. Quantitative proteomics analysis of differential protein expression and oxidative modification of specific proteins in the brains of old mice. Neurobiol Aging 27, 1010-1019.

Porter, N.M., Landfield, P.W., 1998. Stress hormones and brain aging: adding injury to insult? Nat Neurosci 1, 3-4.

Prachar, J., 2010. Mouse and human mitochondrial nucleoid--detailed structure in relation to function. Gen Physiol Biophys 29, 160-174.

Rao, G., Xia, E., Richardson, A., 1990. Effect of age on the expression of antioxidant enzymes in male Fischer F344 rats. Mech Ageing Dev 53, 49-60.

Rao, M.S., Hattiangady, B., Abdel-Rahman, A., Stanley, D.P., Shetty, A.K., 2005. Newly born cells in the ageing dentate gyrus display normal migration, survival and neuronal fate choice but endure retarded early maturation. Eur J Neurosci 21, 464-476.

Rattan, S.I., 2008. Hormesis in aging. Ageing Res Rev 7, 63-78.

Redinbo, M.R., Stewart, L., Kuhn, P., Champoux, J.J., Hol, W.G., 1998. Crystal structures of human topoisomerase I in covalent and noncovalent complexes with DNA. Science 279, 1504-1513.

Reifschneider, N., 2006. Elekrophoretische und massenspektrometrische Analyse des mitochondrial Proteoms von Eukaryoten, Fachbereich Chemie. Technische Universität Darmstadt, Darmstadt.

Reifschneider, N.H., Goto, S., Nakamoto, H., Takahashi, R., Sugawa, M., Dencher, N.A., Krause, F., 2006. Defining the mitochondrial proteomes from five rat organs in a physiologically significant context using 2D blue-native/SDS-PAGE. J Proteome Res 5, 1117-1132.

Renart, J., Reiser, J., Stark, G.R., 1979. Transfer of proteins from gels to diazobenzyloxymethyl-paper and detection with antisera: a method for studying antibody specificity and antigen structure. Proc Natl Acad Sci U S A 76, 3116-3120.

Rexroth, S., 2004. Struktur und Dynamik der Thylakoidmembran, Fachbereich Chemie. Technische Universität Darmstadt, Darmstadt.

Rickwood, D., Wilson, M.T., Darley-Usmar, V.M., 1987. Isolation and characteristics of intact mitochondria. In Mitochondria. (Hrsg.: Darley-Usmar, V.M., Rickwood, D., Wilson, M.T.R.), 1-16.

Rivera, A., Maxwell, S.A., 2005. The p53-induced gene-6 (proline oxidase) mediates apoptosis through a calcineurin-dependent pathway. J Biol Chem 280, 29346-29354.

Rothman, S.M., Mattson, M.P., Adverse stress, hippocampal networks, and Alzheimer's disease. Neuromolecular Med 12, 56-70.

Sastre, J., Pallardo, F.V., Vina, J., 2003. The role of mitochondrial oxidative stress in aging. Free Radic Biol Med 35, 1-8.

Schäfer, E., Seelert, H., Reifschneider, N.H., Krause, F., Dencher, N.A., Vonck, J., 2006. Architecture of active mammalian respiratory chain supercomplexes. J Biol Chem 281, 15370-15375.

Schäfer, E., Dencher, N.A., Vonck, J., Parcej, D.N., 2007. Three-dimensional structure of the respiratory chain supercomplex $I_1III_2IV_1$ from bovine heart mitochondria. Biochemistry 46, 12579-12585.

Schagger, H., von Jagow, G., 1987. Tricine-sodium dodecyl sulfate-polyacrylamide gel electrophoresis for the separation of proteins in the range from 1 to 100 kDa. Anal Biochem 166, 368-379.

Schagger, H., 1995. Quantification of oxidative phosphorylation enzymes after blue native electrophoresis and two-dimensional resolution: normal complex I protein amounts in Parkinson's disease conflict with reduced catalytic activities. Electrophoresis 16, 763-770.

Schägger, H., Pfeiffer, K., 2000. Supercomplexes in the respiratory chains of yeast and mammalian mitochondria. EMBO J 19, 1777-1783.

Schapira, A.H., Cooper, J.M., Dexter, D., Clark, J.B., Jenner, P., Marsden, C.D., 1990a. Mitochondrial complex I deficiency in Parkinson's disease. J Neurochem 54, 823-827.

Schapira, A.H., Mann, V.M., Cooper, J.M., Dexter, D., Daniel, S.E., Jenner, P., Clark, J.B., Marsden, C.D., 1990b. Anatomic and disease specificity of NADH CoQ1 reductase (complex I) deficiency in Parkinson's disease. J Neurochem 55, 2142-2145.

Scherer, E.B., Matte, C., Ferreira, A.G., Gomes, K.M., Comim, C.M., Mattos, C., Quevedo, J., Streck, E.L., Wyse, A.T., 2009. Methylphenidate treatment increases Na(+), K (+)-ATPase activity in the cerebrum of young and adult rats. J Neural Transm 116, 1681-1687.

Schon, E.A., Dencher, N.A., 2009. Heavy breathing: energy conversion by mitochondrial respiratory supercomplexes. Cell Metab 9, 1-3.

Schwassmann, H.J., Rexroth, S., Seelert, H., Dencher, N.A., 2007. Metabolism controls dimerization of the chloroplast F_oF_1 ATP synthase in *Chlamydomonas reinhardtii*. FEBS Lett 581, 1391-1396.

Sears, V.F., 1992. Neutron scattering lengths and cross sections. Neutron News 3, 26-37.

Seelert, H., Krause, F., 2008. Preparative isolation of protein complexes and other bioparticles by elution from polyacrylamide gels. Electrophoresis 29, 2617-2636.

Seelert, H., Dani, D.N., Dante, S., Hauss, T., Krause, F., Schäfer, E., Frenzel, M., Poetsch, A., Rexroth, S., Schwassmann, H.J., Suhai, T., Vonck, J., Dencher, N.A., 2009. From protons to OXPHOS supercomplexes and Alzheimer's disease: structure-dynamics-function relationships of energy-transducing membranes. Biochim Biophys Acta 1787, 657-671.

Seki, T., Arai, Y., 1995. Age-related production of new granule cells in the adult dentate gyrus. Neuroreport 6, 2479-2482.

Seluanov, A., Hine, C., Azpurua, J., Feigenson, M., Bozzella, M., Mao, Z., Catania, K.C., Gorbunova, V., 2009. Hypersensitivity to contact inhibition provides a clue to cancer resistance of naked mole-rat. Proc Natl Acad Sci U S A 106, 19352-19357.

Shankar, S.K., 2011. Biology of aging brain. Indian J Pathol Microbiol 53, 595-604.

Shepherd, G.M., 1994. Neurobiology. Oxford University Press.

Siegbahn, P.E., Blomberg, M.R., 2008. Proton pumping mechanism in cytochrome c oxidase. J Phys Chem A 112, 12772-12780.

Silvestri, E., Lombardi, A., Glinni, D., Senese, R., Cioffi, F., Lanni, A., Goglia, F., Moreno, M., de Lange, P., 2011. Mammalian mitochondrial proteome and its functions: current investigative techniques and future perspectives on ageing and diabetes. Journal of integrated omics 1, 17-27.

Sinclair, W.K., 1968. Cyclic x-ray responses in mammalian cells in vitro. Radiat Res 33, 620-643.

Skulachev, V.P., 1996. Role of uncoupled and non-coupled oxidations in maintenance of safely low levels of oxygen and its one-electron reductants. Q Rev Biophys 29, 169-202.

Smith, C.D., Carney, J.M., Starke-Reed, P.E., Oliver, C.N., Stadtman, E.R., Floyd, R.A., Markesbery, W.R., 1991. Excess brain protein oxidation and enzyme dysfunction in normal aging and in Alzheimer disease. Proc Natl Acad Sci U S A 88, 10540-10543.

Smith, D.E., Rapp, P.R., McKay, H.M., Roberts, J.A., Tuszynski, M.H., 2004. Memory impairment in aged primates is associated with focal death of cortical neurons and atrophy of subcortical neurons. J Neurosci 24, 4373-4381.

Smith, E.L., Pickels, E.G., 1940. Micelle Formation in Aqueous Solutions of Digitonin. Proc Natl Acad Sci U S A 26, 272-277.

Soehn, M., 2009. Untersuchung von Fluoreszenzfarbstoffen, Fachbereich Chemie. Technische Universität Darmstadt, Darmstadt.

Sohal, R.S., Sohal, B.H., 1991. Hydrogen peroxide release by mitochondria increases during aging. Mech Ageing Dev 57, 187-202.

Söhn, M., 2010. Der Einfluss von Altern und Kalorienreduktion auf das mitochondriale Proteom des Rattenhirns, Fachbereich Chemie. Technische Universität, Darmstadt.

Sonsalla, P.K., Wong, L.Y., Winnik, B., Buckley, B., 2010. The antiepileptic drug zonisamide inhibits MAO-B and attenuates MPTP toxicity in mice: clinical relevance. Exp Neurol 221, 329-334.

Sousa, N., Lukoyanov, N.V., Madeira, M.D., Almeida, O.F., Paula-Barbosa, M.M., 2000. Reorganization of the morphology of hippocampal neurites and synapses after stress-induced damage correlates with behavioral improvement. Neuroscience 97, 253-266.

Spencer, W.D., Raz, N., 1995. Differential effects of aging on memory for content and context: a meta-analysis. Psychol Aging 10, 527-539.

Spodnik, J.H., Wozniak, M., Budzko, D., Teranishi, M.A., Karbowski, M., Nishizawa, Y., Usukura, J., Wakabayashi, T., 2002. Mechanism of leflunomide-induced proliferation of mitochondria in mammalian cells. Mitochondrion 2, 163-179.

Stadtman, E.R., 2006. Protein oxidation and aging. Free Radic Res 40, 1250-1258.

Starke-Reed, P.E., Oliver, C.N., 1989. Protein oxidation and proteolysis during aging and oxidative stress. Arch Biochem Biophys 275, 559-567.

Stöckl, P., Hütter, E., Zwerschke, W., Jansen-Dürr, P., 2006. Sustained inhibition of oxidative phosphorylation impairs cell proliferation and induces premature senescence in human fibroblasts. Exp Gerontol 41, 674-682.

Stöckl, P., Zankl, C., Hütter, E., Unterluggauer, H., Laun, P., Heeren, G., Bogengruber, E., Herndler-Brandstetter, D., Breitenbach, M., Jansen-Dürr, P., 2007. Partial uncoupling of oxidative phosphorylation induces premature senescence in human fibroblasts and yeast mother cells. Free Radic Biol Med 43, 947-958.

Storch, A., Ludolph, A.C., Schwarz, J., 1999. HEK-293 cells expressing the human dopamine transporter are susceptible to low concentrations of 1-methyl-4-phenylpyridine (MPP+) via impairment of energy metabolism. Neurochem Int 35, 393-403.

Suhai, T., Dencher, N.A., Poetsch, A., Seelert, H., 2008. Remarkable stability of the proton translocating F1FO-ATP synthase from the thermophilic cyanobacterium Thermosynechococcus elongatus BP-1. Biochim Biophys Acta 1778, 1131-1140.

Sultana, R., Boyd-Kimball, D., Poon, H.F., Cai, J., Pierce, W.M., Klein, J.B., Markesbery, W.R., Zhou, X.Z., Lu, K.P., Butterfield, D.A., 2006a. Oxidative modification and down-

regulation of Pin1 in Alzheimer's disease hippocampus: A redox proteomics analysis. Neurobiol Aging 27, 918-925.

Sultana, R., Boyd-Kimball, D., Poon, H.F., Cai, J., Pierce, W.M., Klein, J.B., Merchant, M., Markesbery, W.R., Butterfield, D.A., 2006b. Redox proteomics identification of oxidized proteins in Alzheimer's disease hippocampus and cerebellum: an approach to understand pathological and biochemical alterations in AD. Neurobiol Aging 27, 1564-1576.

Suzui, N., Yoshimi, N., Kawabata, K., Mori, H., 1999. The telomerase activities in several organs and strains of rats with ageing. Lab Anim 33, 149-154.

Szabados, E., Fischer, G.M., Gallyas, F., Jr., Kispal, G., Sumegi, B., 1999. Enhanced ADP-ribosylation and its diminution by lipoamide after ischemia-reperfusion in perfused rat heart. Free Radic Biol Med 27, 1103-1113.

Taanman, J.W., 1999. The mitochondrial genome: structure, transcription, translation and replication. Biochim Biophys Acta 1410, 103-123.

Taucher-Scholz, G., Heilmann, J., Kraft, G., 1996. Induction and rejoining of DNA double-strand breaks in CHO cells after heavy ion irradiation. Adv Space Res 18, 83-92.

Tehei, M., Franzetti, B., Madern, D., Ginzburg, M., Ginzburg, B.Z., Giudici-Orticoni, M.T., Bruschi, M., Zaccai, G., 2004. Adaptation to extreme environments: macromolecular dynamics in bacteria compared in vivo by neutron scattering. EMBO Rep 5, 66-70.

Thilmany, S., 2008. Effekte des Alterns und der kurzzeitigen Kalorienrestriktion auf das mitochondriale Proteom der Rattenleber, Fachbereich Chemie. Technische Universität Darmstadt, Darmstadt.

Toescu, E.C., Myronova, N., Verkhratsky, A., 2000. Age-related structural and functional changes of brain mitochondria. Cell Calcium 28, 329-338.

Toescu, E.C., 2005. Normal brain ageing: models and mechanisms. Philos Trans R Soc Lond B Biol Sci 360, 2347-2354.

Towbin, H., Staehelin, T., Gordon, J., 1979. Electrophoretic transfer of proteins from polyacrylamide gels to nitrocellulose sheets: procedure and some applications. Proc Natl Acad Sci U S A 76, 4350-4354.

Tsujii, H., Tsuji, H., Okumura, T., 1994. [Progress in heavy particle radiotherapy]. Gan To Kagaku Ryoho 21, 929-935.

Veereshwarayya, V., Kumar, P., Rosen, K.M., Mestril, R., Querfurth, H.W., 2006. Differential effects of mitochondrial heat shock protein 60 and related molecular chaperones to prevent intracellular beta-amyloid-induced inhibition of complex IV and limit apoptosis. J Biol Chem 281, 29468-29478.

Vermeulen, K., Van Bockstaele, D.R., Berneman, Z.N., 2005. Apoptosis: mechanisms and relevance in cancer. Ann Hematol 84, 627-639.

Vina, J., Borras, C., Miquel, J., 2007. Theories of ageing. IUBMB Life 59, 249-254.

Virchow, R., 1854. Über das ausgebreitete Vorkommen einer dem Nervenmark analogen Substanz in den tierischen Geweben. Virchows Arch. Pathol. Anat. 6, 562–572.

Vladimir-Knezevic, S., Blazekovic, B., Stefan, M.B., Alegro, A., Koszegi, T., Petrik, J., 2011. Antioxidant activities and polyphenolic contents of three selected Micromeria species from Croatia. Molecules 16, 1454-1470.

Wachsberger, P., Burd, R., Dicker, A.P., 2003. Tumor response to ionizing radiation combined with antiangiogenesis or vascular targeting agents: exploring mechanisms of interaction. Clin Cancer Res 9, 1957-1971.

Wang, W., Yang, X., Lopez de Silanes, I., Carling, D., Gorospe, M., 2003. Increased AMP:ATP ratio and AMP-activated protein kinase activity during cellular senescence linked to reduced HuR function. J Biol Chem 278, 27016-27023.

Weber, U., 1996. Volumenkonforme Bestrahlung mit Kohlenstoff-Ionen zur Vorbereitung einer Strahlentherapie, Gesamthochschule Kassel.

Wechser, M.A., Bowman, B.J., 1995. Regulation of the expression of three housekeeping genes encoding subunits of the Neurospora crassa vacuolar ATPase. Mol Gen Genet 249, 317-327.

Weichselbaum, R.R., Rose, C.M., Ervin, T.J., Miller, D., 1983. Radiobiologic research for head and neck cancer therapy. Therapeutic implications. Arch Otolaryngol 109, 792-796.

Wendenburg, S., 2010. Aufbau einer Methode zur Messung der ATP-Konzentration mit Hilfe von Lumineszenz, Fachbereich Chemie. Technische Universität Darmstadt, Darmstadt.

Wernicke, C., Hellmann, J., Zięba, B., Kuter, K., Ossowska, K., Frenzel, M., Dencher, N.A., Gille, G., Rommelspacher, H., 2010. 9-Methyl-β-carboline has restorative effects in an animal model of Parkinson's disease. Pharmacological Reports 62, in press.

Wheelock, A.M., Morin, D., Bartosiewicz, M., Buckpitt, A., 2006. Use of a fluorescent internal protein standard to achieve quantitative two-dimensional gel electrophoresis. Proteomics 6, 1385-1398.

Winter, M., 2007. Zelluläre und molekularbiologische Grundlagen der vorzeitigen Alterung humaner Fibroblasten nach Bestrahlung mit Röntgenstrahlen oder Kohlenstoff-Ionen. Technische Universität Darmstadt, Darmstadt.

Wolff, S., 1998. The adaptive response in radiobiology: evolving insights and implications. Environ Health Perspect 106 Suppl 1, 277-283.

Yan, L.J., Levine, R.L., Sohal, R.S., 1997. Oxidative damage during aging targets mitochondrial aconitase. Proc Natl Acad Sci U S A 94, 11168-11172.

Yarian, C.S., Rebrin, I., Sohal, R.S., 2005. Aconitase and ATP synthase are targets of malondialdehyde modification and undergo an age-related decrease in activity in mouse heart mitochondria. Biochem Biophys Res Commun 330, 151-156.

Yarian, C.S., Sohal, R.S., 2005. In the aging housefly aconitase is the only citric acid cycle enzyme to decline significantly. J Bioenerg Biomembr 37, 91-96.

Yazdani, U., German, D.C., Liang, C.L., Manzino, L., Sonsalla, P.K., Zeevalk, G.D., 2006. Rat model of Parkinson's disease: chronic central delivery of 1-methyl-4-phenylpyridinium (MPP+). Exp Neurol 200, 172-183.

Yelnik, J., Francois, C., Percheron, G., 1997. Spatial relationships between striatal axonal endings and pallidal neurons in macaque monkeys. Adv Neurol 74, 45-56.

Yonezawa, M., Takeda, A., Misonoh, J., 1990. Acquired radioresistance after low dose X-irradiation in mice. J Radiat Res (Tokyo) 31, 256-262.

Yonezawa, M., Misonoh, J., Hosokawa, Y., 1996. Two types of X-ray-induced radioresistance in mice: presence of 4 dose ranges with distinct biological effects. Mutat Res 358, 237-243.

Yotnda, P., Wu, D., Swanson, A.M., 2010. Hypoxic tumors and their effect on immune cells and cancer therapy. Methods Mol Biol 651, 1-29.

Zaccai, G., 2000. How soft is a protein? A protein dynamics force constant measured by neutron scattering. Science 288, 1604-1607.

Zahnreich, S., Melnikova, L., Winter, M., Nasonova, E., Durante, M., Ritter, S., Fournier, C., 2010. Radiation-induced premature senescence is associated with specific cytogenetic changes. Mutat Res 701, 60-66.

Zahnreich, S., 2011. Untersuchungen zur genetischen Stabilität von normalen humanen Fibroblasten nach Einwirkung von dicht-ionisierender Strahlung. Doctorial Thesis, Technische Universität Darmstadt.

Zerbetto, E., Vergani, L., Dabbeni-Sala, F., 1997. Quantification of muscle mitochondrial oxidative phosphorylation enzymes via histochemical staining of blue native polyacrylamide gels. Electrophoresis 18, 2059-2064.

Zhao, H., Joseph, J., Fales, H.M., Sokoloski, E.A., Levine, R.L., Vasquez-Vivar, J., Kalyanaraman, B., 2005. Detection and characterization of the product of hydroethidine and intracellular superoxide by HPLC and limitations of fluorescence. Proc Natl Acad Sci U S A 102, 5727-5732.

Zick, M., Rabl, R., Reichert, A.S., 2009. Cristae formation-linking ultrastructure and function of mitochondria. Biochim Biophys Acta 1793, 5-19.

Zwerschke, W., Mazurek, S., Stöckl, P., Hütter, E., Eigenbrodt, E., Jansen-Dürr, P., 2003. Metabolic analysis of senescent human fibroblasts reveals a role for AMP in cellular senescence. Biochem J 376, 403-411.

7 Curriculum Vitae

Diplom-Biologin
Monika Frenzel

Zeisigstraße 6
63329 Egelsbach

Born 16.04.1982 in Königs Wusterhausen, Germany

DISSERTATION

10/2006 –04/2011	Doctoral thesis studies in the Physical Biochemistry group / Institute of Biochemistry at TU Darmstadt, Prof. Dr. N.A. Dencher Thesis: *"Mitochondrial ageing in rat brain areas and human fibroblasts"*

UNIVERSITY STUDIES

01/2001 – 09/2006	Diploma thesis studies in the Physical Biochemistry group / Institute of Biochemistry at TU Darmstadt, Thesis: "*Age-dependent alterations of the proteome of* Rattus norvegicus" Grade: Dipl.-Biol.
09/2003	Intermediate diploma
10/2001 – 09/2006	Course of study: Biology, TU Darmstadt

SCHOOL EDUCATION

1998 – 2001	Weibelfeld-Schule in Dreieich Sprendlingen, Grammar School Abitur (university entrance exam)
1992 – 1998	Heinrich-Heine-Schule in Dreieich Sprendlingen, Comprehensive school
1991 – 1992	Wilhelm-Leuschner-Schule in Egelsbach, Grade School
1990 – 1991	Robert-Biehl-Oberschule in Königs Wusterhausen, Grade School
1988 – 1990	Otto-Grabowski-Oberschule in Königs Wusterhausen, Grade School

Egelsbach, den 1. April 2011

(Monika Frenzel)

Monika Frenzel

Zeisigstraße 6

63329 Egelsbach

Egelsbach, 1. April 2011

Eidesstattliche Erklärung

Ich erkläre hiermit an Eides Statt, dass ich meine Dissertation selbständig und nur mit den angegebenen Hilfsmitteln angefertigt habe.

(Monika Frenzel)

Monika Frenzel
Zeisigstraße 6
63329 Egelsbach

Egelsbach, 1. April 2011

Erklärung

Ich erkläre hiermit, noch keinen Promotionsversuch unternommen zu haben.

(Monika Frenzel)